MASS DISTRIBUTION IN THERMAL NEUTRON FISSION OF Pu^{239}

by

D.A. MARSDEN

A thesis submitted to the Faculty of Graduate Studies and Research in partial fulfilment of the requirements for the degree of Doctor of Philosophy

Department of Chemistry,
McGill University,
Montreal, Que.

June 1963.

ACKNOWLEDGEMENTS

The author gratefully acknowledges his indebtedness to the following persons and institutions:

Professor L. Yaffe for his stimulating direction and constant encouragement throughout the course of this work.

Mr. S.K. Mukherji and other members of the Radiochemistry Laboratory for their help in innumerable ways.

My wife, Barbara, for her infinite patience and encouragement during the course of this work.

Mrs. C. Macfarlane for typing this thesis and her painstaking pursuit of grammatical errors.

The Chemistry Department of McGill University for Demonstratorships in 1958 - 1959 and 1960 - 1961.

The Canadian Industries Limited for C.I.L. Fellowships in 1959 - 1960 and 1961 - 1962.

The Graduate Faculty of McGill University for the Alexander McFee Fellowship in 1960 - 1961.

TABLE OF CONTENTS

INTRODUCTION

1. GENERAL

The main purpose of nuclear power reactors is the release of energy arising from the initiation and maintenance of the fission chain reaction in nuclear fuels. It was known that the U^{235} isotope, present in 0.72% abundance in natural uranium, was fissionable with thermal neutrons but that the U^{238} isotope present in 99.28% abundance could only be caused to fission with neutrons of higher energy. In addition, the U^{238} nucleus was capable of capturing thermal neutrons and would therefore act as a parasite in the nuclear chain reaction. This parasitic capture was soon recognized to lead to the formation of Pu^{239} in the following way. The uranium 238 nucleus captures a slow neutron to form U^{239}. This isotope decays by β^- emission with a half-life of 23 minutes to form neptunium 239. Np^{239} is also β^- active, decaying with a half-life of 2.3 days to form Pu^{239}.

$$_{92}U^{238} + {}_{0}n' \longrightarrow {}_{92}U^{239} \xrightarrow{23\ m.} {}_{93}Np^{239} \xrightarrow{2.3\ d.} {}_{94}Pu^{239}$$

Pu^{239} was found to have a half-life of 24,400[1] years. It decayed by alpha-particle emission. It undergoes the fission reaction with thermal neutrons with a cross section

of 742 barns* (2). The fission reaction is accompanied by an average release of about 3 neutrons per fission and an amount of energy equivalent to that released in U^{235} fission, so that it is eminently suitable as a reactor fuel. One other attractive feature for the use of Pu^{239} as reactor fuel is that it too can capture thermal neutrons parasitically, but this neutron capture reaction leads to the formation of Pu^{240} which is a fertile material like U^{238}. That is, Pu^{240} will capture a neutron to form Pu^{241} which is also fissile. The relationships involved are shown in Fig. 1(3).

In order to use Pu^{239}, it was necessary to produce it in quantity and to know what properties affect its use as a fuel.

Pu^{239} does not occur in Nature. It is made in 'breeder' reactors by the capture process already discussed. The separation of plutonium from the U^{238} matrix has been the subject of extensive research which has resulted in its production on a macro scale.

When Pu^{239} is used as a reactor fuel, there is a continuous build-up of fission products as the fuel becomes used up. These fission products are radioactive and are also

---

*The cross section is a measure of the probability of a reaction occurring and has dimensions of cm^2. The unit 1 barn is equal to 10^{-24} cm^2.

Figure 1

PLUTONIUM ISOTOPE CHAIN FROM

ESCHBACH AND GOLDSMITH(3)

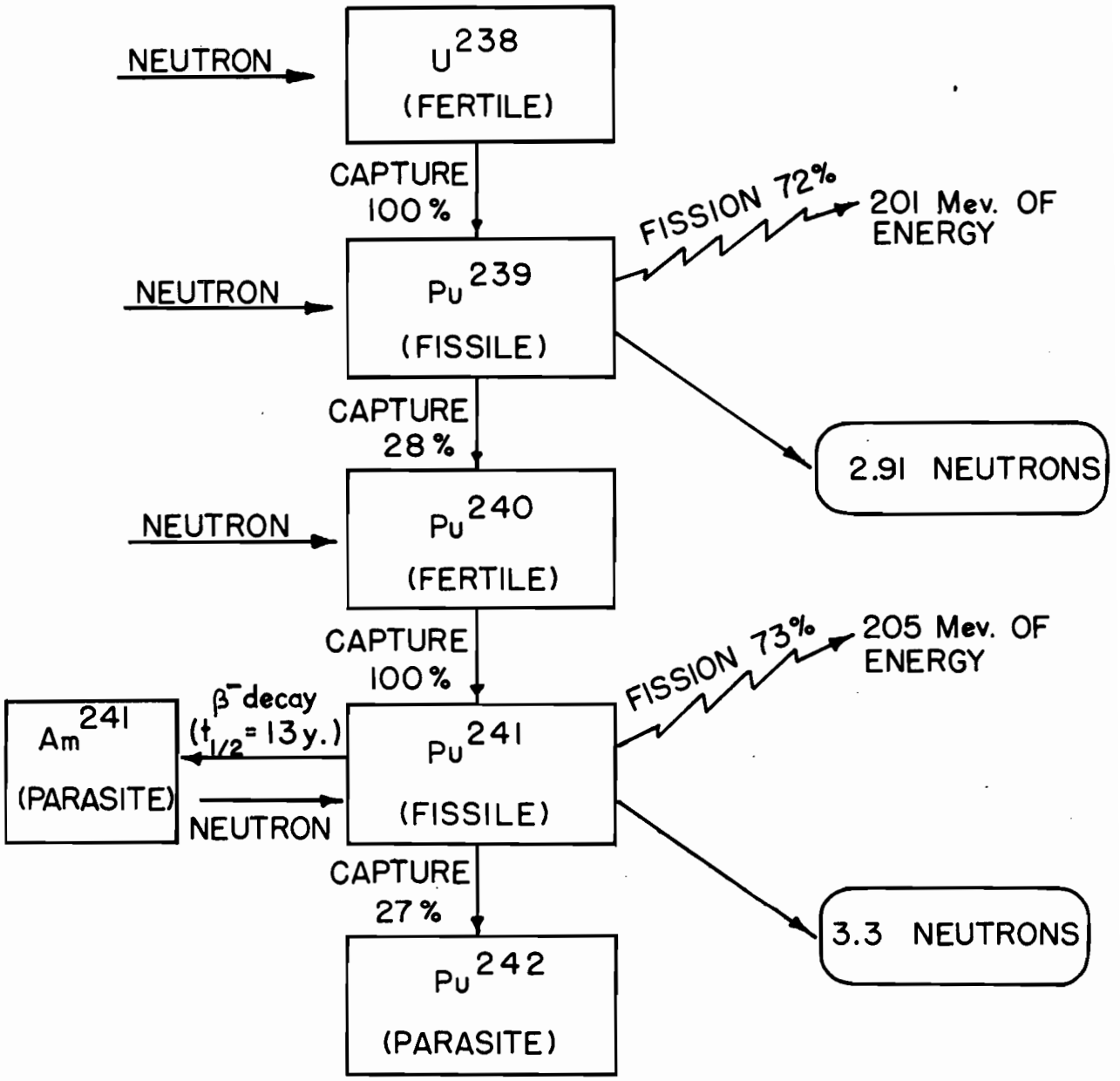
NEUTRON
U 238
(FERTILE)
CAPTURE
100 %
FISSION 72%
201 Mev. OF
ENERGY
NEUTRON
Pu 239
(FISSILE)
CAPTURE
28 %
2.91 NEUTRONS
NEUTRON
Pu 240
(FERTILE)
CAPTURE
100 %
FISSION 73%
205 Mev. OF
ENERGY
Am 241
(PARASITE)
β⁻ decay
(t1/2 = 13 y.)
Pu 241
(FISSILE)
NEUTRON
CAPTURE
27 %
3.3 NEUTRONS
Pu 242
(PARASITE)

capable of parasitic capture of thermal neutrons. It is therefore necessary to know accurately the yields of the various fission products in order to estimate the effects of fission product poisoning, to evaluate problems connected with chemical processing of the irradiated fuel and to calculate shielding requirements.

In addition to this, a great deal of interest in the yields of the various fission products exists because it is believed that from such a study may arise clues as to the nature of the fission process itself.

2. THE FISSION PROCESS

A predominant characteristic of low-energy fission is the splitting of the fissioning nucleus into two fragments. Divisions into more than two fragments have been observed[4] to occur but they are very rare. This investigation will consider only binary fission.

Thermal neutrons, that is, neutrons with energy of gas molecules at room temperature (0.025 ev) react with almost all nuclear species in one isotopic form or another[5]. By far the most common reaction is the neutron capture or (n, γ) reaction. A few exceptions are found among reactions with light nuclei in cases where the binding energy of a proton or an alpha particle is appreciably lower than that of a neutron. The reactions $B^{10}(n,p)Be^{10}$, $N^{14}(n,p)C^{14}$, $Cl^{35}(n,p)S^{35}$, $B^{10}(n,\alpha)Li^{7}$, and $Li^{6}(n,\alpha)H^{3}$ occur with

thermal neutrons. With the heavy elements, however, in particular those nuclides with an odd number of neutrons, the fission process or (n,f) reaction occurs with a higher probability than the (n, γ) reaction. From the point of view of the energetics of the reaction, this is a direct result of the additional excitation energy supplied by the pairing of the incoming neutron with the odd neutron of the target nucleus.

In the reaction with Pu^{239}, the neutron is captured to form a compound nucleus in an excited state, which then deexcites as follows:

$$ {}_{94}Pu^{239} + {}_{0}n^{1} \longrightarrow \left[{}_{94}Pu^{240*} \right] \begin{cases} \xrightarrow{(n,\gamma)} {}_{94}Pu^{240} \text{ (6580 years)} \\ \xrightarrow{(n,f)} {}_{Z_1}X_1^{A_1} + {}_{Z_2}X_2^{A_2} + \nu\, {}_{0}n^{1} + \gamma + Q \end{cases} $$

The (n, γ) reaction competes with the (n,f) reaction as a mode of deexcitation of the compound nucleus occurring with less than half the probability of the fission reaction[2]. In the above representation, ${}_{Z_1}X_1^{A_1}$ and ${}_{Z_2}X_2^{A_2}$ are the primary light and heavy fragments, respectively, formed in the fission process; ν is the total number of neutrons released; γ is the energy released as electromagnetic radiation at the instant of fission and Q is the kinetic energy of the fission fragments and fission neutrons.

Here, the laws of conservation of mass and charge must be satisfied. Consequently the sum of the mass numbers of the complementary fission fragments, plus the actual number (integral) of neutrons emitted, for any given pair, must be equal to the mass of the compound nucleus,

$$A_1 + A_2 + \nu = 240.$$

Also, the sum of the nuclear charges of complementary fission fragments must be equal to the nuclear charge of the fissioning nucleus,

$$Z_1 + Z_2 = 94.$$

3. MECHANISM OF FISSION

It is generally accepted that nuclear reactions occurring at low excitation energies (up to about 30 to 40 Mev) proceed mainly via a compound nucleus. This concept introduced by N. Bohr[6] postulates an actual coalescence of projectile and target nucleus, with a subsequent sharing of the incoming energy among all the nucleons. The lifetime of the compound nucleus is relatively long compared to the time required for a particle to traverse the nucleus. The compound nucleus, now in an excited state, breaks up into the reaction products in a manner which is completely independent of its mode of formation. Moreover, it may deexcite in several different ways, each mode of disintegration occurring

with a specific probability.

The extension of the compound nucleus concept to the fission reaction was proposed simultaneously by Bohr and Wheeler[7] and Frenkel[8]. This synthesis is achieved by comparing the nucleus to a liquid drop. The nucleus is considered to be an incompressible, densely packed system of nucleons, with the protons evenly distributed throughout the nuclear volume. The forces operating within this system are the short range 'exchange' forces between nucleons and the coulomb repulsive forces between protons. Because the nucleons at the surface of the nucleus have no neighbours on the outside, an unsaturation of the 'exchange' forces exists at the surface which is similar to the surface tension of a liquid drop. The shape of a nucleus is a result of the balance between its 'surface tension' and the coulomb forces. Just as a liquid drop assumes a spherical shape under the action of surface tension, so too the heavy nucleus assumes the most stable configuration, a sphere, because of the unsaturation of the nuclear forces at its surface.

Excitation of such a system through the formation of a compound nucleus leads to instability in the form of distortions of shape away from the spherical. These distortions lead to increases in the surface area, hence in the surface energy, and in the electrostatic repulsion. These changes oppose one another, the increase in surface

energy tending to return the nucleus to its original shape and the increased coulombic repulsion tending to increase the distortion. As long as the distortions remain small, a state of dynamic equilibrium can be imagined in which the compound nucleus alternates between the spherical and the distorted shapes. But, if at any time the distortions become severe, the coulomb repulsion predominates and the resulting imbalance is sufficient to cause the break-up of the compound nucleus.

Fig. 2 shows a diagrammatic representation of the splitting of the compound nucleus, together with the subsequent events which accompany the fission process. The compound nucleus splits into two fragments, forming the primary excited fission fragments. From these fragments prompt neutrons are evaporated, followed by the emission of photons, leaving as end products the nuclei A_3Z_3 and A_4Z_4 in their ground states. These nuclides have an excess of neutrons. They therefore decay to stability by a number of β^- emissions forming a series of isobaric decay chains. The members of these chains are called the fission products.

Since A_3Z_3 and A_4Z_4 appear in less than a millisecond after fission, the sequence of events is not known from direct observation but is based on the following:

(1) experiments which show that the neutrons are evaporated from the primary fission fragments

Figure 2

DIAGRAMMATIC REPRESENTATION OF

THE FISSION PROCESS

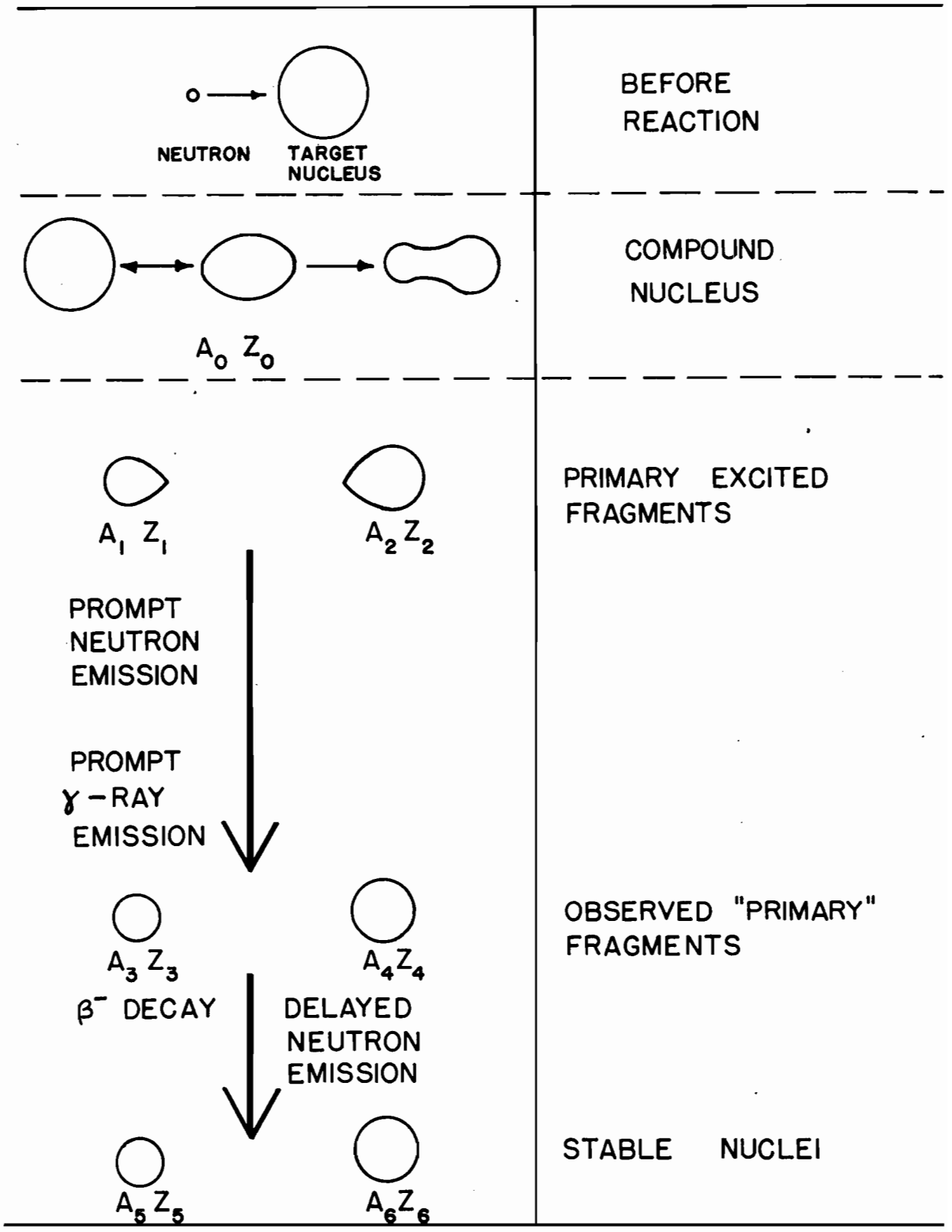
BEFORE REACTION
NEUTRON
TARGET NUCLEUS
COMPOUND NUCLEUS
$A_0 Z_0$
PRIMARY EXCITED FRAGMENTS
$A_1 Z_1$
$A_2 Z_2$
PROMPT NEUTRON EMISSION
PROMPT γ-RAY EMISSION
OBSERVED "PRIMARY" FRAGMENTS
$A_3 Z_3$
$A_4 Z_4$
β^- DECAY
DELAYED NEUTRON EMISSION
STABLE NUCLEI
$A_5 Z_5$
$A_6 Z_6$

before they come to rest[9].

(2) the fact that γ-ray emission is known to be a slower process than neutron emission, and

(3) the actual observations of the β^- decay chains.

4. FISSION PRODUCT DECAY CHAINS

The splitting of the compound nucleus may take place in a variety of ways, since fission products with atomic numbers from 30 to 66 and mass numbers from 72 to 166 have been observed. These nuclides are on the neutron-rich side of stability, which is to be expected, since the fissioning nucleus has a larger neutron-to-proton ratio than the stable nuclides in the region of the fission products. They therefore decay to stability by successive β^- emissions, forming a series of isobaric decay chains.

These decay chains exhibit all the characteristics of β^- decay. Straight chains result from successive direct parent-daughter decays. Chain branching occurs where isomeric metastable states with measurable half-lives exist. Chain continuity is then re-established by either (1) isomeric transition to the ground state, (2) β^- decay to a daughter metastable state or (3) β^- decay to an excited level or to the ground state of the daughter. Occasionally a member of a chain is formed with enough excitation energy to deexcite by neutron emission in addition to β^- decay[7]. This phenomenon occurs when the binding energy of the last neutron

is low and usually takes place in nuclides with a shell - plus - one, - three or - five[10,11] complement of neutrons. These are the well-known delayed neutron emitters. Finally, a few fission products, known as shielded nuclides, cannot be formed by β^- decay. In these cases the isobaric nuclides of one charge number lower, i.e. their 'would-be' parents, are stable. They can therefore only be formed independently in fission.

For any particular decay chain, the first member can only be formed independently. All the other members of the chain may be formed independently or as a result of decay of their precursors. This may be represented as follows:

$$A_o \longrightarrow B_o \longrightarrow C_o \longrightarrow D_o \quad \text{(stable)}$$

$$B_1 \longrightarrow C_1 \longrightarrow D_1 \quad \text{(stable}$$

$$C_2 \longrightarrow D_2 \quad \text{(stable)}$$

$$D_3 \quad \text{(stable)}$$

Here the letters represent the numbers of nuclei of each species formed. A measure of the amount of the individual members A_o, B_1, C_2 or D_3 would provide information on the <u>independent yield</u> of a particular member in an isobaric chain. A measure of the quantities

$$B_i = B_o + B_1 = A_o + B_1$$

$$\text{or} \quad C_i = C_o + C_1 + C_2 = A_o + B_1 + C_2$$

would be a measure of the cumulative yield of these intermediate members of the decay chain. Finally, it is seen that

$$D_i = D_o + D_1 + D_2 + D_3 = A_o + B_1 + C_2 + D_3$$

Thus a measure of the amount of D after all its radioactive precursors have died away will be a measure of the total chain yield for that particular mass number.

The concept of a fission yield, inherent in these three measurements, is defined as the percentage of the total fission acts leading directly or indirectly to the particular nuclide in question.

5. CHARGE DISTRIBUTION

Investigations of the distribution of nuclear charge in fission are concerned with establishing the most probable charge resulting from a particular fissioning mode and the distribution of charges, in an isobaric chain, about this most favoured charge.

Ideally, a measure of the yields of isobaric primary fission fragments would furnish a complete picture of charge distribution in fission. Unfortunately the primary fragments are formed so far removed from stability that their radioactive decay half-lives are prohibitively short. Information about charge distribution therefore has mainly come from measurements of the yields of 'shielded'

nuclides and from yields of nuclides which can be separated in a time which is short compared to the half-lives of their parents. In the latter case, corrections for growth from the parent can be made and the independent yields determined.

All the data, accumulated to the present time, indicate that for thermal neutron fission the postulate of 'Equal Charge Displacement'[12] holds.[4] This hypothesis states that for a given fission event, the two complementary fragments always have equal $Z_A - Z_P$ values. Here Z_A is the value of Z corresponding to the highest binding energy for a given mass number A and is obtained from an appropriate mass equation. Z_P is defined as the most probable charge for a primary fission fragment of mass number A. If on the average three neutrons are given off per fission in Pu^{239}, then the following relations hold,

$$(Z_A - Z_P)_{\text{light fragment}} = (Z_A^* - Z_P^*)_{\text{heavy fragment}}$$

or

$$Z_A - Z_P = Z_{237-A} - (94 - Z_P)$$

and, on solving for Z_P, the following equation is obtained

$$Z_P = 47 + \tfrac{1}{2}(Z_A - Z_{237-A}).$$

With the help of this equation and the calculated values for Z_A and Z_{237-A}, the most probable charge, Z_P, for any mass number A can be found. When the measured independent yields

are plotted against $Z - Z_p$, using the Z_p values calculated from the equation above, a probability distribution is obtained (Fig. 3)[10,12,13] which shows that about 50% of the total chain yield occurs for $Z = Z_p$, about 25% each for $Z = Z_p \pm 1$, about 2% for $Z = Z_p \pm 2$ and much less for other Z values. It is assumed in the treatment above that the distribution is valid for all the isobaric chains.

One consequence of this distribution is that the cumulative yield of a fission product, which is one or two charge units from stability, is very nearly the total chain yield for that mass number.

6. MASS DISTRIBUTION

The distribution of mass in fission has been determined in two ways. First, by radiochemical techniques the cumulative yields of radioactive nuclides near the end of the mass chains have been measured. Secondly, in mass spectrometer studies, using the isotope dilution technique[14], the yields of stable and long-lived members at the end of the mass chains have been determined.

If these yields are plotted against the respective mass numbers, a distribution is obtained which extends from mass number 72 to mass number 166. For Pu^{239}, the distribution is approximately symmetrical about a minimum at mass number 119 with two maxima, one at approximately mass number 99 and the other at approximately mass number 138. The

Figure 3

DISTRIBUTION OF NUCLEAR CHARGE

——— Glendenin, Coryell and Edwards[12]

- - - - Wahl et al.[13]

● Pappas[10]

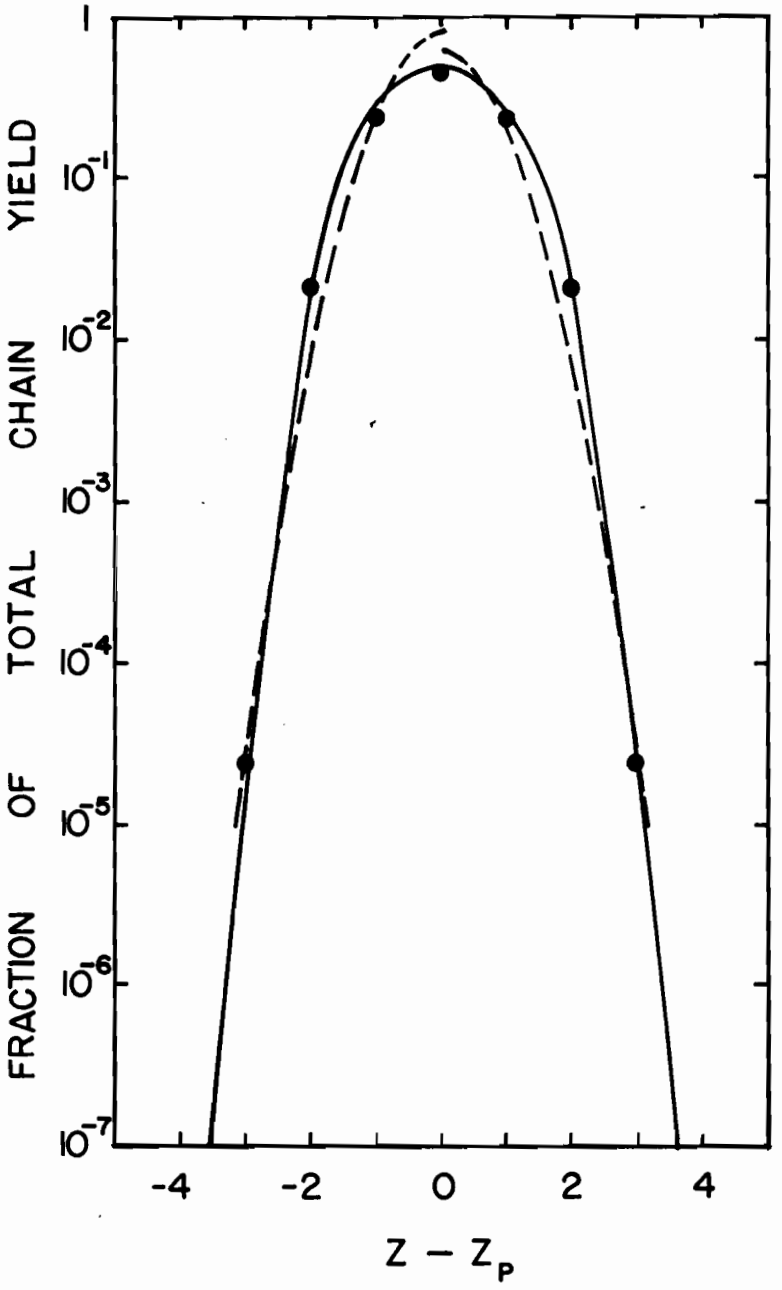
FRACTION OF TOTAL CHAIN YIELD
1
10^{-1}
10^{-2}
10^{-3}
10^{-4}
10^{-5}
10^{-6}
10^{-7}
-4
-2
0
2
4
$Z - Z_P$

width at half height for either peak is about 15 mass numbers. Spikes, the so-called 'fine structure', occur at the top of each peak.

This asymmetry in mass distribution is characteristic of thermal-neutron fission, since similar distributions have been found for U^{235} and U^{233}. A comparison of the three distributions is shown in Fig. 4[15]. It is seen that, while these distributions exhibit similarities in their gross structure, they differ in certain details. The maxima of the light mass peaks shift by about 5 mass numbers in going from U^{233} to Pu^{239}, while the heavy peak remains fixed. The Pu^{239} yield in the region of the valley is approximately four times that of U^{233} and U^{235} in the same region. The 'fine structure' at the top of the peaks is, in general, not the same for the three fissioning nuclei. Spikes occur at mass numbers 100 and 134 for Pu^{239} and U^{235}, but apart from these the peak structures are entirely different. This is seen clearly in Fig. 5[15], where the peak structures are shown in an enlarged view.

7. FISSION THEORY

A comprehensive theory does not yet exist which can explain all of the facts of the fission process. This is primarily a reflection of the complexity of the fission process itself for only now, after the collection and correlation of large amounts of experimental data, are the

Figure 4

MASS DISTRIBUTION IN THERMAL-NEUTRON FISSION FROM KATCOFF[15]

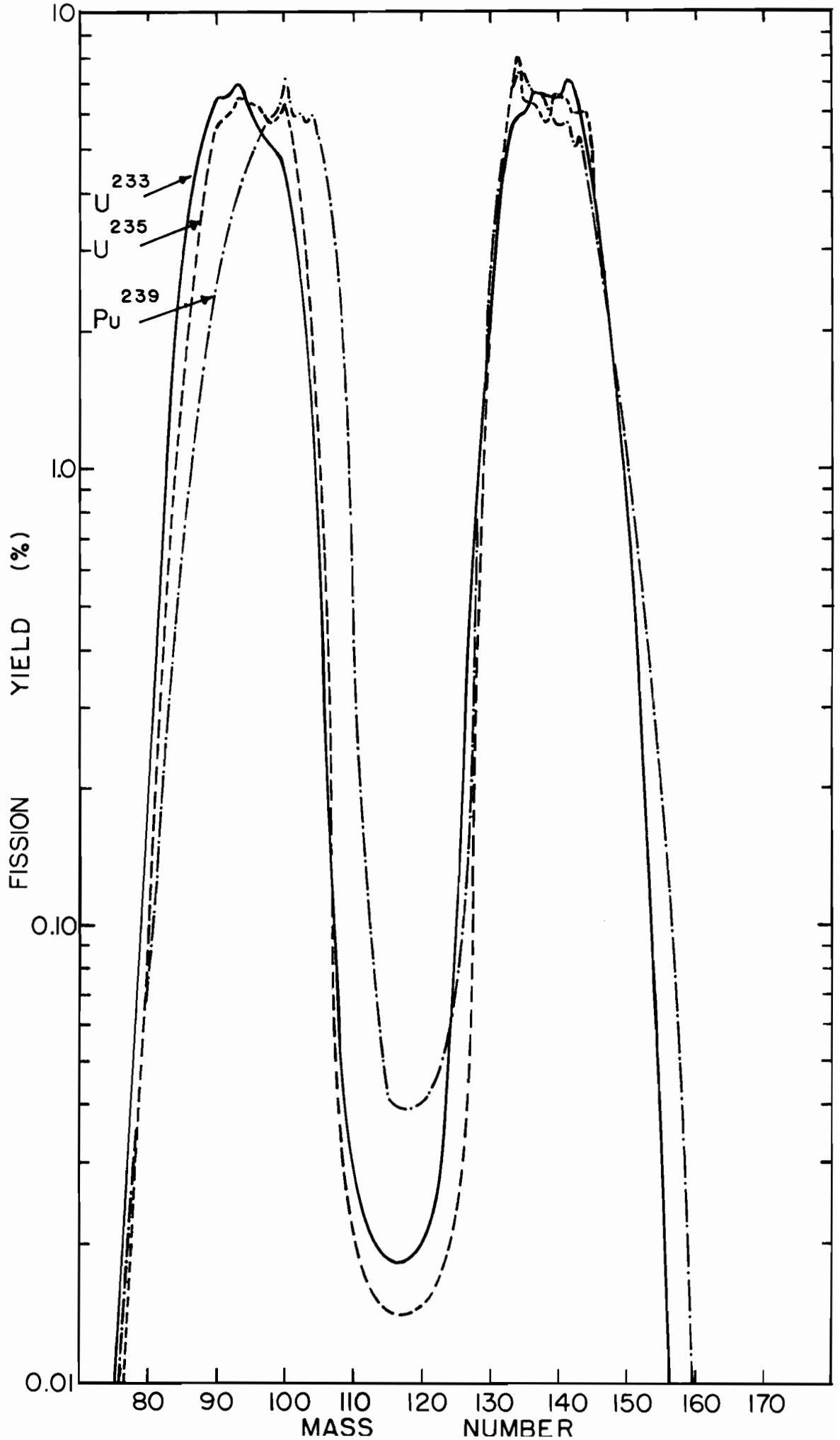
10
1.0
0.10
0.01
FISSION YIELD (%)
U^{233}
U^{235}
Pu^{239}
80
90
100
110
120
130
140
150
160
170
MASS NUMBER

Figure 5

ENLARGED VIEW OF PEAK STRUCTURES

IN THERMAL-NEUTRON FISSION

FROM KATCOFF[15]

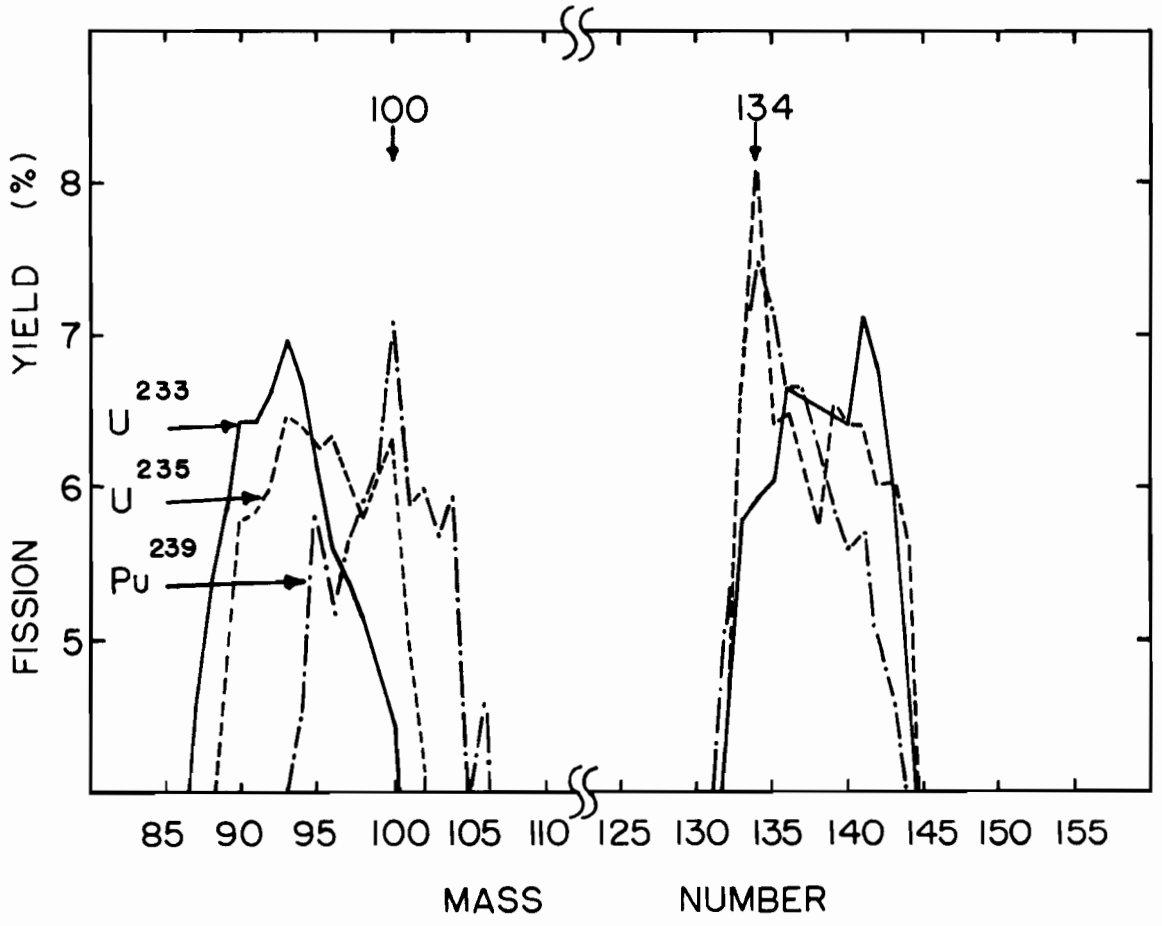
100
134
FISSION YIELD (%)
8
7
6
5
U^{233}
U^{235}
Pu^{239}
85 90 95 100 105 110 125 130 135 140 145 150 155
MASS NUMBER

actual details of the process discernible. Our knowledge of the fission process is based mainly on experimental observations, on the consideration of empirical prescriptions to fit the experimental data and on the consideration of nuclear models.

The knowledge obtained from the organization of data is seen, for example, in the distributions of mass and charge already discussed. No adequate theoretical explanation for either distribution exists. An empirical description of charge distribution - the ECD hypothesis (P.13) - is generally accepted to hold for low energy fission. But the prescriptions for determining Z_A and Z_P have been subject to much revision. In the original proposal of Glendenin et al.[12] Z_A values were calculated from the mass equation of Bohr and Wheeler[7]. These calculations showed Z_A, and hence Z_P, to be smooth continuous functions. Subsequently Pappas[10] showed that discontinuities in Z_A would arise in crossing closed neutron or proton shells, which had to be taken into account in calculating Z_P. He therefore modified the method for calculating Z_A, basing his calculations on the treatment of beta stability of Coryell et al.[16]. Kennett and Thode[17] were not able to fit data for I^{128} and I^{130} on the charge distribution curve. This led them to propose that discontinuities in Z_P itself had also to be taken into consideration. On account of these uncertainties

involved in calculating Z_p, Wahl and co-workers[13] adopted an empirical approach. Sufficient data for several independent yields for each of six mass chains from the thermal neutron fission of U^{235} had become available. From these data a charge dispersion curve was derived which best represented the data and which was gaussian in shape. This gaussian curve was represented by the formula

$$P(Z) = (C\pi)^{-\frac{1}{2}} e^{-\frac{(Z - Z_p)^2}{C}}$$

where P(Z) is the fractional independent yield of the fission product with atomic number Z,

C is a constant with a best-fitting value of 0.9.

It was assumed that this curve would be applicable to other chains for which fractional yields of only single members were known. Z_p values interpolated from the charge distribution curve were plotted against mass number and a smooth and continuous curve was drawn to fit the empirical values as well as possible. A comparison of the charge dispersion curves is shown in Fig. 3. The curve derived by Pappas[10] is not dissimilar from the original distribution of Glendenin et al.[12], but that of Wahl et al.[13] is narrower and rises to a higher maximum. Coryell et al.[18], in a reassessment of all the data for thermal neutron fission of U^{235} conclude that the ECD hypothesis is only a crude approximation of charge distribution. They maintain that the

experimental results show Z_p to be a single-valued function of the mass number A and that fine structure (sudden breaks or shifts) in a plot Z_p versus mass number A is a result of shell orienting effects in the nascent fragments just before scission.

The foregoing is by no means a theory of charge distribution but represents the present state of our knowledge of charge distribution. In other words, we are still in the data collection stage as far as the phenomena connected with fission are concerned. This is also seen from a consideration of nuclear models.

The liquid drop model[7] of the nucleus has provided much insight into the fission process. In particular, it defines the stability limits of heavy nuclei and has shown the probable mechanism of the splitting of a nucleus in fission. But it does not account for the details of the fission process. For example, it does not explain the asymmetric splitting of the mass of the fissioning nucleus. It is important to realize that this model treats the modes of motion of an idealized charged liquid drop and is only successful in so far as a heavy nucleus resembles such a model. This is true of all nuclear models. While the liquid drop model treats a nucleus as an assembly of particles all interacting strongly with one another, the shell model[19] of the nucleus considers the movement of single particles outside of a central core. The shell model of the nucleus arose from the fact that certain 'magic'

numbers of nucleons represented very stable structures. For example, if a nucleus contained 2, 8, 20, 28, 50, 82 or 126 neutrons, it was very stable, and similarly for protons. By analogy to atomic structure, where filled shells are spherically symmetric and have no spin or orbital angular momentum and no magnetic moment, it was argued that these magic numbers represented stable closed shells in the nucleus. The effect of shell structure in fission is seen in the fine structure of the mass distribuion curves. This phenomenon has been ascribed to

(1) the delayed neutron emitters[10] which decay by β^- emission to daughter products having a shell + 1 number of neutrons. This last neutron is loosely bound and is emitted instantaneously. The fission yield of the mass chain of the delayed neutron emitter is lowered and that of the chain of one mass number lower is increased.

(2) the prompt boil off of a neutron from primary fragments containing 51 and 83 neutrons[20]. It was also suggested that prompt neutron emission should be extended to the third, fifth, and seventh neutron outside of a closed shell[10].

(3) the preferential formation in the fission act of fragments with closed shell configurations, N = 82, 50, which is suggested by the complementarity of the spikes at masses 100 and 134[21].

The possibilities of other nuclear models have been explored with varying degrees of success. Among these may be mentioned the statistical model of Fong[22] which considered the densities of quantum states corresponding to the different fission modes just before separation of the fission fragments. Among other things, Fong was able to reproduce successfully the mass distribution curve for U^{235} fission.

The limited applicability of the various nuclear models towards a comprehensive fission theory has prompted Leachman[23] to adopt an entirely empirical approach. He argues that the collection and correlation of data about the fission phenomenon have established six characteristics of fission. These are:

(1) The asymmetry in mass distribution is always observed with the heavy peak of fragments 'fixed' in mass.

(2) Fragment excitation, as evidenced by neutron emission, increases above closed shells. This occurs in the valley of the fission yield curve, where symmetric fission is presumed to occur.

(3) There is a decrease in kinetic energy of repulsion of the fragments for symmetric fission which compensates for fact (2) above.

(4) Charge distribution in fission results in the lighter of the heavy fission fragment group being proton-rich

and the heavier being proton-deficient. The complementary trend for the light fragment group is the same.

(5) There is a coulomb dependence (with a fixed breaking distance for a given compound nucleus) of fission fragment energies as a function of nuclear size, which is determined from mass number and nuclear charge.

(6) The apparent tendency for the symmetric fission mode yield to increase with excitation energy to a yield exceeding the asymmetric fission yield.

From these facts a model for asymmetric fission is proposed having a 50-neutron-shell light fragment and a 50-proton-shell heavy fragment. This represents an 82 mass light fragment core and a 126 mass heavy fragment core. These cores are joined by a neck consisting of about 28 nucleons, of which 10 are protons and about 18 are neutrons.

8. FISSION PRODUCT YIELDS

Pu^{239} fission product yields have not been extensively studied radiochemically. The results of investigations undertaken in the Manhattan Project were reported in 1951 by Steinberg and Freedman[24] and included as part of a review of all radiochemical data by Steinberg and Glendenin in 1955[25]. The investigators had used Geiger-Müller counters for activity measurements. The number of

fission events were not determined directly in each experiment, the yields being often expressed relative to an internal standard - usually Ba^{140}. The estimated accuracy was 10 - 20%[25]. In 1958 Bunney et al.[26] reported fission product yields of the heavy rare earths which had been determined radiochemically. The yields obtained were calculated relative to those of Mo^{99}. The value adopted for this standard was 6.1% taken from Steinberg and Glendenin's report[25]. A side window gas flow proportional counter was used in this work. The authors claimed an accuracy of better than 10% in their reported values. Using improved radiochemical techniques, Bartholomew et al.[27] in 1959 determined yields for Sr^{89}, Sr^{91}, Ba^{139}, Ba^{140}, and La^{141}. These yields were calculated relative to the Ba^{140} yield, 5.68%, this value being taken from a review by Katcoff in 1958[28]. These investigators had used a $4\pi\beta$ proportional counter. The reliability of their results was claimed to be comparable to that obtained using mass spectrometric techniques. Other radiochemically determined yields reported are for I^{136}, by Stanley and Katcoff[29] and for several fission products in the valley of the mass distribution by Ford et al.[30].

Mass spectrometric studies, using isotope dilution techniques, have also been used to determine Pu^{239} fission product yields. By this technique Wiles et al.[31] determined the relative yields of 16 isotopes of cesium,

cerium, neodymium and samarium. These relative yields, together with yields of four xenon isotopes obtained by Fleming and Thode[32] and interpolated yields from a smooth mass-yield curve, were normalized to total 100% and reported as absolute yields. The xenon yields reported by Fleming and Thode[32] were for masses 131, 132, 134, and 136, and were normalized to the data of Wiles et al.[31] through the mass 133 chain. The yields obtained by the latter researchers, however, were thought to be invalidated by fractionation of the fission products, in particular the cesium and neodymium fractions, into the quartz irradiation container. On this account Fritze et al.[33] determined the absolute yield of Xe^{131}, renormalized the yields of Fleming and Thode[32] through this value and reported absolute yields for these isotopes, together with yields for krypton isotopes of masses 83, 84, 85, and 86. Bidinosti et al.[34], in a study of fission product poisons, reported absolute yields for Cs^{133}, Xe^{135}, Nd^{143}, Sm^{149}, and Sm^{151}. Fickel and Tomlinson[35,36] in an investigation similar to that of Wiles et al.[31], redetermined absolute yields for 17 mass fragments in the heavy peak and measured the relative yields of 19 mass fragments in the light peak. Absolute yields for the light mass peak were calculated relative to the Cs^{133} yield, 6.90%, from Fickel and Tomlinson[36]. The yields obtained for the heavy mass peak showed that fractionation had indeed taken

place in the work of Wiles et al.[31] The mass-spectrometric method has been shown to be very precise in determining relative isotopic ratios - reproducibilities of 1 - 2% have been obtained. The accuracy of the reported absolute yields is of the order of 3 - 5%[25,35,36].

Mass-spectrometric studies have also been carried out by Russian researchers on mass chains 133 - 153 in the heavy peak and Sr^{88}, Sr^{90} in the light peak. A summary of the results obtained was reported by Anikina et al.[37].

Evaluation of all published fission yield data was undertaken by Katcoff in 1958[28] and in 1960[16]. In the latter publication, preference is given to the work of Fickel and Tomlinson[35,36] for Pu^{239} thermal neutron fission yields.

9. PRESENT WORK

From a consideration of charge distribution in thermal neutron fission, it is seen that in any isobaric decay chain the cumulative yield of a nuclide that is one or two charge units away from stability represents almost the total chain yield. Radiochemical techniques then are ideally suitable for a study of mass distribution in fission.

In this technique, a specific fission product is separated chemically from the bulk of the fission products using the standard chemical techniques of specific precipitations, ion exchange separations, or solvent extractions. The radioactive atoms thus separated are

measured on a radiation measuring device to determine the number of atoms present. Since the amount of radioactive material formed is small, a known amount of the element to be separated is added to act as a carrier for the radioactive species. Care is taken that exchange between inactive carrier and radioactive atoms takes place. When the element in question exists in only one valence state, this is brought about by simply mixing the solutions carefully. Where several valence states exist, both species must at some time be in the same valence state. This is brought about by performing a series of oxidation-reduction stages. Since chemical separations are not always quantitative, the carrier recovered is analysed to determine the chemical yield. This yield also corresponds to the amount of radioactivity recovered.

The factor, which has most affected the accuracy of the yield values, has been the method of radioactivity assay. As improved techniques have been developed, the accuracy in reported yields has improved from 10 - 20%[25] for the earliest work to within 3 - 5%[27] for the latest. The work of Pate and Yaffe[38,39,40,41,42] and Yaffe and Fishman[43] on $4\pi\beta$ counting has afforded an easily applied and relatively accurate technique for the determination of disintegration rates of beta-emitting nuclides.

It is the purpose of this investigation to determine

the absolute yields of fission products, produced in the thermal neutron fission of Pu^{239}, one or two charge units away from stability using radiochemical techniques, in particular the $4\pi\beta$ radioactivity measurement technique developed by Pate and Yaffe.

DETERMINATION OF ABSOLUTE FISSION YIELDS

1. DEFINITION OF ABSOLUTE FISSION YIELD

The total or cumulative fission yield of a given fission product has been defined (P.12) as the percentage of the fission acts leading to the nuclide in question through direct formation and through decay of its precursors. The mass distribution curve defines the fission yield (total chain yield) for any given mass as a function of the mass number A. It has been seen that once a fission fragment has been formed, and the prompt neutrons have been emitted, there is no change in mass number - except for small effects due to delayed neutron emission. Thus the number of fissions leading to a given mass number as a function of mass is independent of time. Therefore the absolute cumulative yield, y, of a fission product is given by

$$y(\%) = \frac{\text{number of atoms formed directly} + \text{number of atoms formed by decay}}{\text{total number of fissions}} \times 100$$

In order to determine absolute fission yields therefore, it is required to know

(1) the disintegration rates of the fission products in the irradiated sample at 'saturation activity' (to be discussed), and

(2) the number of fissions occurring in the irradiated sample per unit time.

If a sample of fissile material is irradiated with neutrons in a nuclear reactor for a period of time T, during which the pile power is constant, then the disintegration rate, $N\lambda$ disintegrations per second, of a nuclide produced in fission, at the end of the irradiation is given by

$$N\lambda = Ry(1 - e^{-\lambda T}) = Ry(1 - e^{-0.693 \frac{T}{t_{\frac{1}{2}}}}) \quad \ldots\ldots\ldots (1)$$

since $\lambda = \ln 2/t_{\frac{1}{2}}$

where R = fission rate

y = fission yield of the nuclide

λ = disintegration constant of the nuclide

$t_{\frac{1}{2}}$ = half-life of the nuclide.

The product, Ry, represents the rate of formation of the nuclide. If T is increased, becoming large compared to $t_{\frac{1}{2}}$, the disintegration rate approaches a maximum value, $(N\lambda)_{max}$ say, which is given by

$$(N\lambda)_{max} = \frac{N\lambda}{1 - e^{-\lambda T}} = Ry \quad \ldots\ldots\ldots\ldots (2)$$

$(N\lambda)_{max}$ is called the 'saturation activity'. It represents an equilibrium between the rate of formation and the rate of decay of the nuclide in question. The various fission nuclides formed can therefore be compared at 'saturation activity'.

2. EQUATIONS USED

A. Growth and Decay equations*

The decay of all radioactive species is governed by the relationship that the rate of decay is proportional to the number of radioactive atoms present at any time. Thus, if there are N radioactive atoms present, this gives

$$-\frac{dN}{dt} = \lambda N \quad \ldots\ldots\ldots\ldots\ldots\ldots\ldots\ldots \quad (3)$$

where λ is the proportionality constant (usually called the disintegration constant). This expression, on integration, gives the relationship

$$N = N^{o}\, e^{-\lambda t} \quad \ldots\ldots\ldots\ldots\ldots\ldots\ldots \quad (4)$$

where N^{o} represents the number of atoms present at time t = o. Consider now N_1 radioactive atoms which decay to give N_2 daughter atoms which are also radioactive. The decay of N_1 is given by equation (4) above, that is

$$N_1 = N_1^{o}\, e^{-\lambda_1 t} \quad \ldots\ldots\ldots\ldots\ldots\ldots\ldots \quad (5)$$

The daughter atoms are formed at the rate at which the parent atoms decay, and themselves decay at the rate $\lambda_2 N_2$.

Thus
$$-\frac{dN_2}{dt} = -\lambda_1 N_1 + \lambda_2 N_2 \quad \ldots\ldots\ldots\ldots\ldots\ldots \quad (6)$$

---

*The following relations are excerpted from Friedlander and and Kennedy[44].

which on substituting for N_1 from equation (5) above and on rearranging gives

$$\frac{dN_2}{dt} + \lambda_2 N_2 - \lambda_1 N_1^o e^{-\lambda_1 t} = 0 \quad \ldots\ldots\ldots \quad (7)$$

This is a linear differential equation of first order. It is easily solved for N_2 giving,

$$N_2 = \frac{\lambda_1}{\lambda_2 - \lambda_1} N_1^o (e^{-\lambda_1 t} - e^{-\lambda_2 t}) + N_2^o e^{-\lambda_2 t} \quad \ldots\ldots \quad (8)$$

The first term on the right represents the growth and decay of the daughter atoms formed from the parent. The last term represents the decay of the daughter atoms present initially.

The extension of this treatment to decay chains of more than two members proceeds in a manner similar to the above, but the differential equations to be solved become more complicated. Bateman[45] provides solutions for n-membered chains if at t = o the parent substance alone is present.

B. Disintegration rate - fission yield relations

Consider a decay chain

$$A \longrightarrow B \longrightarrow C$$

The yield of A will be defined by equation (1) that is,

$$N_A \lambda_A = Ry_A (1 - e^{-\lambda_A T}) \quad \ldots\ldots\ldots\ldots \quad (9)$$

Since A is assumed to be the first member of the chain, the yield y_A represents the independent as well as total yield of nuclide A. The total yield of nuclide B is given by

$$y_B = y_A + (y_i)_B$$

where $(y_i)_B$ is the independent yield of B. The disintegration rate of B due to independent formation is given by an equation similar to (9) that is,

$$(N\lambda)^i_B = R(y_i)_B (1 - e^{-\lambda_B T}) \quad \ldots\ldots\ldots\ldots (10)$$

Nuclide B also grows from A during the irradiation. The number of atoms of B formed in this way is given by the solution of equation (6) which, in this case, is

$$-\frac{d(N)^A_B}{dt} = -N_A \lambda_A + (N\lambda)^A_B \quad \ldots\ldots\ldots\ldots (11)$$

Substituting for $N_A \lambda_A$ from equation (9) gives

$$-\frac{d(N)^A_B}{dt} = -Ry_A(1 - e^{-\lambda_A T}) + (N\lambda)^A_B \quad \ldots\ldots (12)$$

the solution of which is

$$(N)^A_B = \frac{Ry_A}{\lambda_B}\left[1 + \frac{\lambda_B e^{-\lambda_A T} - \lambda_A e^{-\lambda_B T}}{\lambda_A - \lambda_B}\right] \quad \ldots\ldots (13)$$

from which the disintegration rate of B formed from A during the irradiation is

$$(N\lambda)_B^A = Ry_A \left[1 + \frac{\lambda_B e^{-\lambda_A T} - \lambda_A e^{-\lambda_B T}}{\lambda_A - \lambda_B} \right] \quad .. (14)$$

At a time t after the irradiation $(N\lambda)_B^i$ and $(N\lambda)_B^A$ have decayed exponentially, so that

$$(N\lambda)_B^i \text{ at } t = (N\lambda)_B^i e^{-\lambda_B t} \quad ..... (15)$$

$$(N\lambda)_B^A \text{ at } t = (N\lambda)_B^A e^{-\lambda_B t} \quad ..... (16)$$

During the time, t, B continues to grow from A. The number of atoms of B formed in this way is given by applying equation (8) thus

$$(N)_B^{A'} = \frac{\lambda_A}{\lambda_B - \lambda_A} N_A (e^{-\lambda_A t} - e^{-\lambda_B t}) \quad ..... (17)$$

Substituting $N_A \lambda_A = Ry_A(1 - e^{-\lambda_A T})$ from equation (9)

gives $$(N)_B^{A'} = \frac{Ry_A(1 - e^{-\lambda_A T})(e^{-\lambda_A t} - e^{-\lambda_B t})}{\lambda_B - \lambda_A} \quad ..... (18)$$

from which the disintegration rate of B formed in this way is

$$(N\lambda)_B^{A'} = \frac{\lambda_B}{\lambda_B - \lambda_A} Ry_A(1 - e^{-\lambda_A T})(e^{-\lambda_A t} - e^{-\lambda_B t}) \quad ...(19)$$

The total disintegration rate of B after an irradiation time, T, and a decay time, t, is the sum of equations (15),(16), and (19), thus

$$(N\lambda)_B = (N\lambda)_B^i e^{-\lambda_B t} + (N\lambda)_B^A e^{-\lambda_B t} + (N\lambda)_B^{A'} \quad \ldots\ldots\ldots (20)$$

Substituting for $(N\lambda)_B^i$ from equation (10), $(N\lambda)_B^A$ from equation (14) and $(N\lambda)_B^{A'}$ from equation (19) gives

$$(N\lambda)_B = R(y_i)_B(1 - e^{-\lambda_B T})e^{-\lambda_B t} + Ry_A \left[1 + \frac{\lambda_B e^{-\lambda_A T} - \lambda_A e^{-\lambda_B T}}{\lambda_A - \lambda_B}\right] e^{-\lambda_B t} + \frac{Ry_A \lambda_B}{\lambda_B - \lambda_A}(1 - e^{-\lambda_A T})(e^{-\lambda_A t} - e^{-\lambda_B t}) \quad \ldots\ldots (21)$$

Simplifying equation (21) gives

$$(N\lambda)_B = R(y_i)_B(1 - e^{-\lambda_B T})e^{-\lambda_B t} + \frac{Ry_A}{\lambda_A - \lambda_B}\left[\lambda_A(1 - e^{-\lambda_B T})e^{-\lambda_B t} - \lambda_B(1 - e^{-\lambda_A T})e^{-\lambda_A t}\right] \quad ..(22)$$

In applying equation (22), two cases may be considered which are pertiment to this work.

(1) $\lambda_A \gg \lambda_B$:

In this case, if the disintegration rate of B is determined when nuclide A has decayed away completely, equation (21) becomes

$$(N\lambda)_B = R\left[y_A + (y_i)_B\right](1 - e^{-\lambda_B T})e^{-\lambda_B t} \quad \ldots\ldots\ldots (23)$$

$$= Ry_B(1 - e^{-\lambda_B T})e^{-\lambda_B t} \quad \ldots\ldots\ldots\ldots\ldots (24)$$

since $y_B = y_A + (y_i)_B$.

From this equation and the measured disintegration rate $(N\lambda)_B$, the total cumulative yield of nuclide B is determined.

(2) $\lambda_A < \lambda_B$:

In this case, if the disintegration rate of nuclide B is determined when the independently formed B has decayed away, equation (21) becomes

$$(N\lambda)_B = Ry_A \frac{\lambda_B}{\lambda_B - \lambda_A}(1 - e^{-\lambda_A T})e^{-\lambda_A t} \quad \ldots\ldots\ldots (25)$$

from which the total yield of the parent nuclide, A, can be calculated.

All the relationships discussed so far have been developed assuming that nuclide A was the first member of the decay chain. But the result obtained in case (1) above shows

them to be equally applicable to any parent-daughter pair along a decay chain as long as the precursors of the parent are sufficiently short lived to fulfil the condition in case (1).

C. Equations used in determining the fission rate

If a sample of fissile material is irradiated in a nuclear reactor while the pile power is kept constant the rate R, at which fission occurs in the material, is given by

$$R = N I \sigma_f \quad \ldots\ldots\ldots\ldots\ldots\ldots \quad (26)$$

where N = number of atoms in the sample of fissile material,

I = neutron flux expressed as neutrons per cm^2 per second,

σ_f = fission cross section expressed in cm^2.

If the sample is irradiated in such a position in the reactor that the contribution, to the neutron flux, of neutrons of epithermal energies is negligible, then I represents the thermal neutron flux and σ_f is the thermal neutron fission cross section. The value of σ_f for thermal neutron fission of Pu^{239} is well known(2). It therefore remains to determine I.

In order to do this, use is made of the reaction $Co^{59}(n,\gamma)Co^{60}$. Natural cobalt is monoisotopic, mass 59 occurring in 100% abundance, so that the only reaction which takes place when it is irradiated with thermal neutrons is the neutron capture reaction. The disintegration rate of Co^{60} measured after an irradiation of Co^{59} for a time, T, and after

a decay time, t, is given by

$$(N\lambda)_{Co^{60}} = N_{Co^{59}} I \sigma_c (1 - e^{-\lambda T}) e^{-\lambda t} \quad \ldots\ldots (27)$$

where $N_{Co^{59}}$ = number of Co^{59} atoms irradiated,

σ_c = thermal neutron caputre cross section for Co^{59},

λ = disintegration constant for Co^{60}.

The thermal neutron capture cross section for Co^{59} is well known[46] as is the half-life, hence the disintegration constant, of Co^{60} [47]. The thermal neutron flux can therefore be calculated from the measured disintegration rate for Co^{60} and the use of equation (27).

The fissile material and cobalt monitor are irradiated at the same time and in close proximity to one another. It is therefore assumed that the neutron flux 'seen' by both is the same. However, on account of the finite size of a sample, the intensity of the neutron flux at the surface will differ from that at any point inside the sample. It is necessary then to correct for this attenuation, both in the fissile material and in the monitor. In general the neutron attenuation is given by

$$I/I_o = e^{-(\frac{N\rho}{A}\sigma d)} \quad \ldots\ldots\ldots\ldots\ldots (28)$$

where I = neutron intensity inside the sample,

I_o = neutron intensity at the surface of the sample,

N = Avogadro's number, 6.023×10^{23},

ρ = density of the sample,

A = atomic weight of neutron absorbing material,

σ = total neutron cross section of the neutron absorbing material,

d = thickness of the sample.

For the non-directional flux of a nuclear reactor, the attenuation is usually calculated for half the sample thickness.

3. EXPERIMENTAL PROCEDURES

A. Target Preparation and Irradiation

The target material was a Plutonium-Aluminium alloy* in the form of turnings. It contained 3.81% of Pu^{239}. A quantity of this material, equivalent to about 1 mg of plutonium, was accurately weighed on a microbalance, then sealed in a quartz tube. The cobalt monitor was 'spec-pure' cobalt wire+, .0050" in diameter. A length of this wire, usually between 0.5 and 1 cm, was accurately weighed and also sealed in a quartz tube. Both tubes were wrapped in aluminun foil and sealed in an aluminum irradiation container. The container was placed in a No. 1 self-serve position in

---

*This material was obtained on loan from Atomic Energy of Canada Limited, Chalk River, Ontario.

+Obtained from Johnson Matthey & Mallory Co., Limited, Montreal.

the NRX reactor of Atomic Energy of Canada Limited, Chalk River, where the target was irradiated for a period of 48 hours.

B. Chemical Procedures

(i) Dissolution of fissile material:

On account of the low concentration of Pu^{239} in the Pu - Al alloy, ~ 0.5 atom %, recoil losses of fission products into the quartz tube were expected to be small. The quartz tube was covered with concentrated HCl in a 50 ml centrifuge tube, to which was added 1 ml of a solution containing 1 μg each of Cs^{+}, Ba^{++}, La^{+++}, and I^{-}. These ions were added to reduce adsorption losses of activities on the surface of the glassware. The quartz capsule was crushed and the Pu - Al alloy allowed to dissolve. When bromine or iodine were to be estimated, the dissolution was carried out in the cold by immersing the centrifuge tube in ice-water. Otherwise the dissolution was allowed to proceed at room temperature. After the sample had dissolved, the solution was transferred to a volumetric flask. The crushed pieces of the quartz vial were washed several times with small portions of concentrated HCl, the washings being transferred each time to the volumetric flask. Several washings with small volumes of distilled water were done in a similar manner. The solution in the volumetric flask was then made up to volume with distilled water. The final concentration of HCl in the fission product solution was ~ 9 M.

(ii) Dissolution of monitor:

The quartz capsule was broken and the cobalt wire transferred to a volumetric flask. The broken capsule was now crushed and repeatedly boiled with small volumes of dilute nitric acid, the solution being transferred to the volumetric flask after each boiling. After the cobalt wire had dissolved, the solution was made up to volume with distilled water. From this solution measured aliquots were removed and used to determine the Co^{60} disintegration rate.

(iii) Chemical separations:

The object of a chemical separation procedure is to obtain the nuclide of interest in a radiochemically pure form free from contaminating activities. Since the amount of a particular radioactive nuclide formed in fission is small, a known amount of the inactive element is added as a carrier for the radioactive species. Exchange between carrier atoms and active atoms is ensured either by mixing or by performing a series of oxidation-reduction cycles. The element of interest is now isolated by specific precipitations, solvent extraction or ion-exchange separations. To ensure removal of contaminating activities, repeated cycles of these operations are performed in the presence of 'hold-back' carriers for the suspected contaminants, interspersed with scavenging precipitations. The 'hold-back' carriers act as inactive diluents for the contaminating radioactivities. The

scavengers form precipitates which co-precipitate with or adsorb the contaminants. Finally, the element of interest is brought into solution and made up to a known volume. The detailed procedures used are given in the discussion of activities isolated (to follow).

(iv) Chemical yield determinations:

Since the separation procedures used were seldom quantitative, it was necessary to determine the amount of inactive carrier recovered, and hence the amount of radioactivity recovered. The amount of carrier added was equivalent to either 5 or 10 milligrams of inactive ions. The amount of carrier recovered was seldom more than 50 - 60% of the amount added - sometimes much less. Sensitive methods for determining the concentrations of the solutions were therefore necessary. Spectrophotometric procedures were used wherever feasible - a Beckman DU spectrophotometer being used for transmittance measurements. Standard methods, as given by Sandell[48], were generally employed. For cases where spectrophotometric methods did not exist or were not sufficiently accurate, titrations with EDTA (ethylene diamine tetra acetic acid)[49] were used. Quantitative precipitations were employed as a last resort. The particular method used for a given element is described in the discussion of activities isolated (to follow).

4. ACTIVITY MEASUREMENTS

A. Preparation of Sources

The technique described by Pate and Yaffe[38] was used for the preparation of films on which active sources were mounted for β -disintegration rate measurements. These films are made of VYNS resin (a copolymer of polyvinyl chloride and polyvinyl acetate) and possess excellent chemical resistance and mechanical strength. The films were rendered conducting by evaporating gold on to them while they were under high vacuum. The films used had a superficial density of between 10 - 15 μgm per cm^2, while the gold layer deposited was between 5 - 10 μgm per cm^2 thick. Just before use, the centre portion of the film was treated with a dilute solution of insulin to make it hydrophilic. The bulk of the insulin was removed before pipetting on to the film a measured aliquot of a fission product solution. The size of an aliquot was so chosen as to give an adequate counting rate. Several sources for each fission product were prepared at the same time and dried under an infra-red lamp. When the bulk of the solution had evaporated, the sources were rotated by hand under the lamp so that the whole area of the source remained wet up to the end of the evaporation.

Sources for measuring gamma radiations were prepared by pipetting 2 ml aliquots of the fission product solutions

into small glass vials which were then sealed.

B. Radiations Emitted

As discussed before, the fission products decay by the emission of β^- particles as a result of the excess neutrons that these nuclides possess due to their mode of formation. A free neutron is known to decay into a proton with the emission of a β^- particle and a neutrino, thus

$$ {}_0n^1 \longrightarrow {}_1p^1 + {}_{-1}\beta^0 + \nu $$

In a parallel manner, in β^- decay, the proton number is increased by one, the mass number remains constant, and a neutrino is also emitted

$$ {}_Z X^A \longrightarrow {}_{Z+1}X^A + {}_{-1}\beta^0 + \nu . $$

β^- decay may lead to a nucleus in an excited state or in its ground state. The excited nucleus deexcites to its ground state by emission of gamma rays, which may proceed directly or through intermediate excited levels. Thus one or more gamma rays may be emitted which are identified with the β^- decay process. The excited states usually have a very short lifetime and the gamma rays are then said to be in coincidence with the β^- emission. Excited states with measurable half-lives exist however. These are called nuclear isomers, since they have the same atomic number and mass number as the ground states but differ in their radioactive properties. Gamma-ray

emission to the ground state, called isomeric transition, is then neither in coincidence with the β ray emission nor with the other gamma rays. An alternative to gamma-ray emission is internal conversion. In this process an extranuclear electron is emitted with an energy equal to the difference between the gamma-ray energy and the binding energy of the electron in the atom.

The disintegration rates of fission products decaying by β^- emission or conversion electron emission were measured on a 4π proportional counter. Gamma rays were measured on a scintillation spectrometer.

C. 4π Counting

The main advantage in using a 4π counter is its high geometrical efficiency and insensitivity to scattering effects. The counter is insensitive to ionizing events, other than the initial one, which occur within the resolving time of the counter and electronic circuitry. This means that the counter will respond only once when a beta particle passes through the counting gas. Other accompanying phenomena, such as coincident gamma radiation, scattered radiation in the counter and secondary radiation, all cause ionization which occurs within the resolving time of the counter. Gamma transitions leading to isomeric states, however, give rise to delayed gamma rays and conversion electrons which will be recorded as separate events. In

this case, data from decay schemes will be required to calculate the number of these extra events occurring per primary disintegration.

To calculate disintegration rates from the 4 π counter data, the following have to be taken into account:

(a) failure of the counter to respond once to every beta disintegration,

(b) corrections for absorption in the source mount,

(c) corrections for absorption in the source material itself, and

(d) statistical counting errors.

(i) Equipment:

The 4 π counting equipment used is similar to that described by Pate and Yaffe[39]. The counting chamber is shown in Fig. 6. It consists of a cathode made of two brass hemispheres, 7 cm in diameter, and two anodes in the form of loops of 1 mil tungsten wire connected to thicker copper leads. The anodes are insulated from the cathode by large cylindrical stepped teflon insulators. The two halves of the cathode are machined to fit snugly when placed together and to allow the positioning of an aluminum film mount at exactly midway between the two anodes. In addition, gas inlet and outlet holes are provided. A block diagram of the 4 π counter and associated electronics is shown in Fig. 7. The positive anode voltage is supplied by a Nichols high voltage supply (AEP 1007B), while the cathode is kept at ground

Figure 6

4 π COUNTING CHAMBER

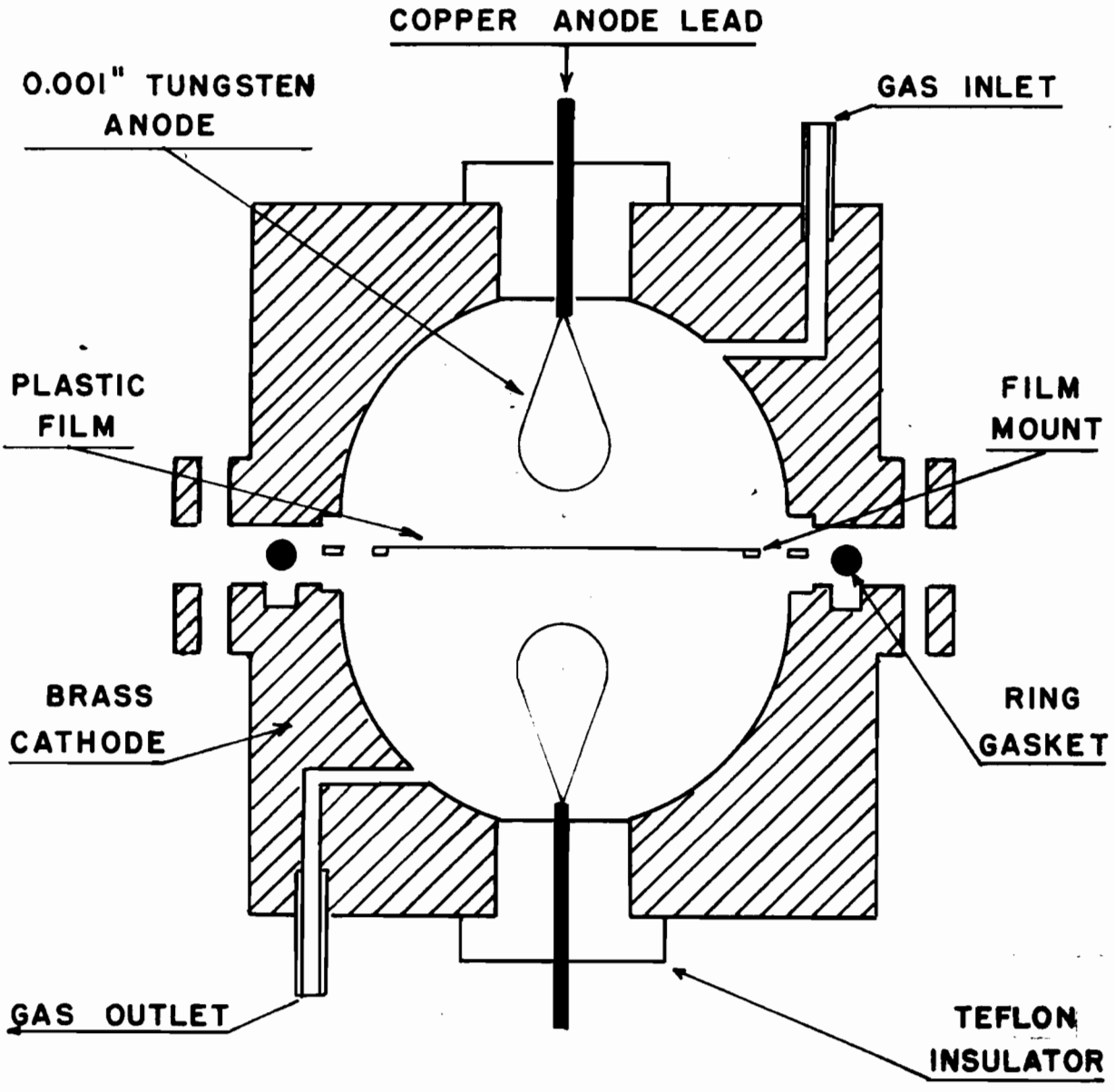
COPPER ANODE LEAD
0.001" TUNGSTEN ANODE
GAS INLET
PLASTIC FILM
FILM MOUNT
BRASS CATHODE
RING GASKET
GAS OUTLET
TEFLON INSULATOR

Figure 7

BLOCK DIAGRAM OF 4 π

COUNTING EQUIPMENT

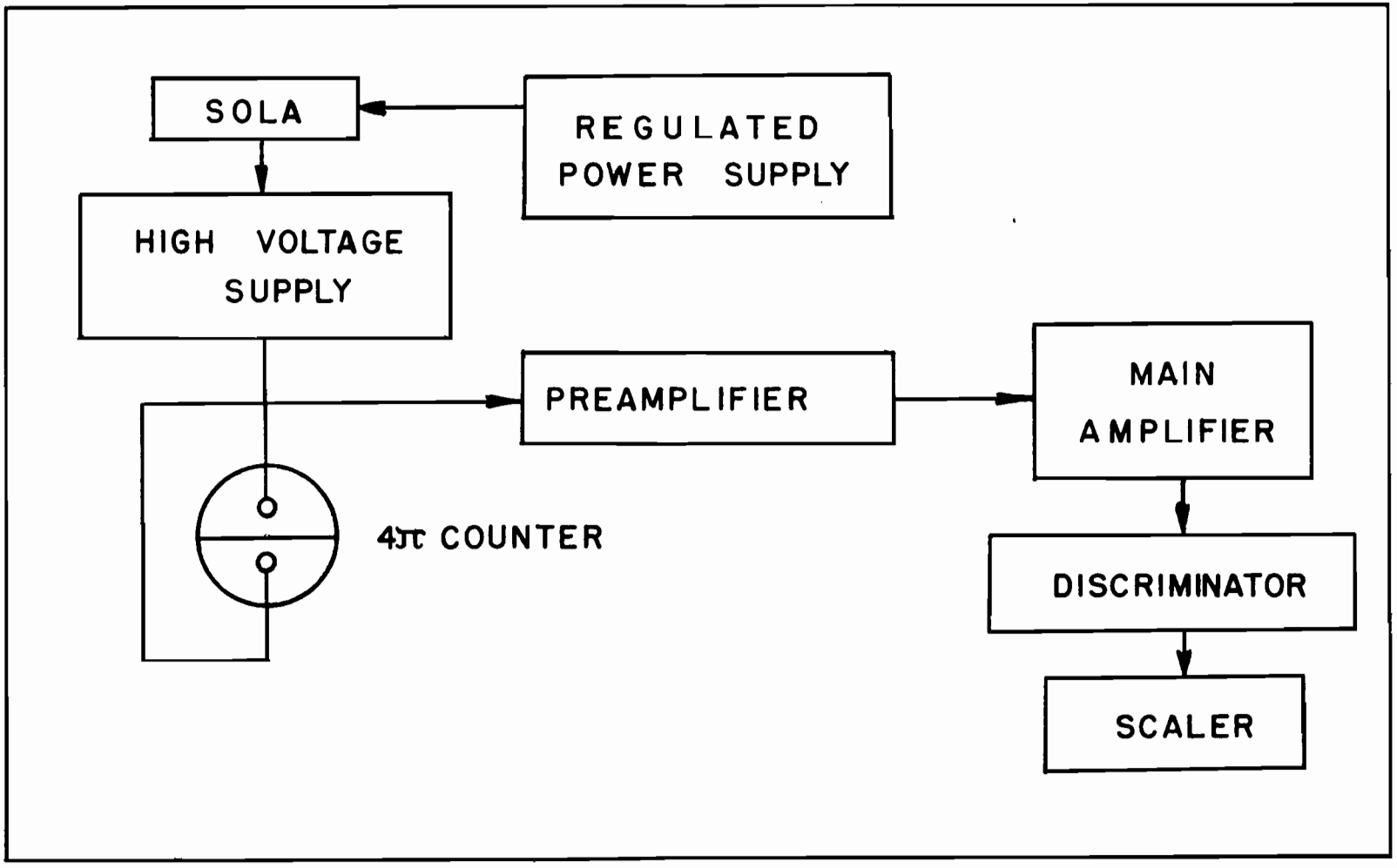
SOLA
REGULATED
POWER SUPPLY
HIGH VOLTAGE
SUPPLY
PREAMPLIFIER
MAIN
AMPLIFIER
4π COUNTER
DISCRIMINATOR
SCALER

potential. The anodes are connected in parallel to a pre-amplifier (Atomic Instrument 205-B), from which the output is fed into an Atomic Energy of Canada Limited amplifier-discriminator (AEP 1448). Counting rates were recorded on a Marconi scaling unit (AEP 908). Power is supplied to the pre-amplifier by a Lambda regulated power supply (model 28) and to the other units from a line voltage regulated power supply through a Sola constant voltage transformer.

(ii) Counter characteristics:

The counter was operated in the proportional region at atmospheric pressure with C.P. methane as the counting gas. A gas flow-rate of approximately 0.5 ml per second was maintained during measurements. The counter was flushed for several minutes after inserting a sample before counting began. The high voltage characteristics of the counter for radioactivities of varying maximum β^- ray energies are shown in Fig. 8. Fig. 9 illustrates the effect of varying the bias setting on the high voltage characteristics of the counter. Pate and Yaffe[39] have stated that if an increase of 200 volts in polarization potential or a 10 v decrease in discriminator bias causes no change in the counting rate observed, then the 4π counter is responding with maximum efficiency. On this account, a polarization potential of 2700 volts and a discriminator bias setting of 15 were chosen as the operating conditions for the counter.

Figure 8

4 π COUNTER HIGH VOLTAGE CHARACTERISTICS

● - Ra D + E (Bi^{210}) 1.17 Mev 100%

■ - Mo^{99}

450	kev	14%
870	"	~ 1%
1,230	"	85%

○ - I^{131}

250	kev	2.8%
330	"	9.3%
608	"	87.2%
810	"	0.7%

□ - Co^{60} 313 kev 100%

△ - Ba^{140}

480	kev	25%
600	"	10%
900	"	5%
1,010	"	60%

\+ La^{140}

830	kev	12%
1,100	"	26%
1,380	"	45%
1,710	"	10%
2,200	"	7%

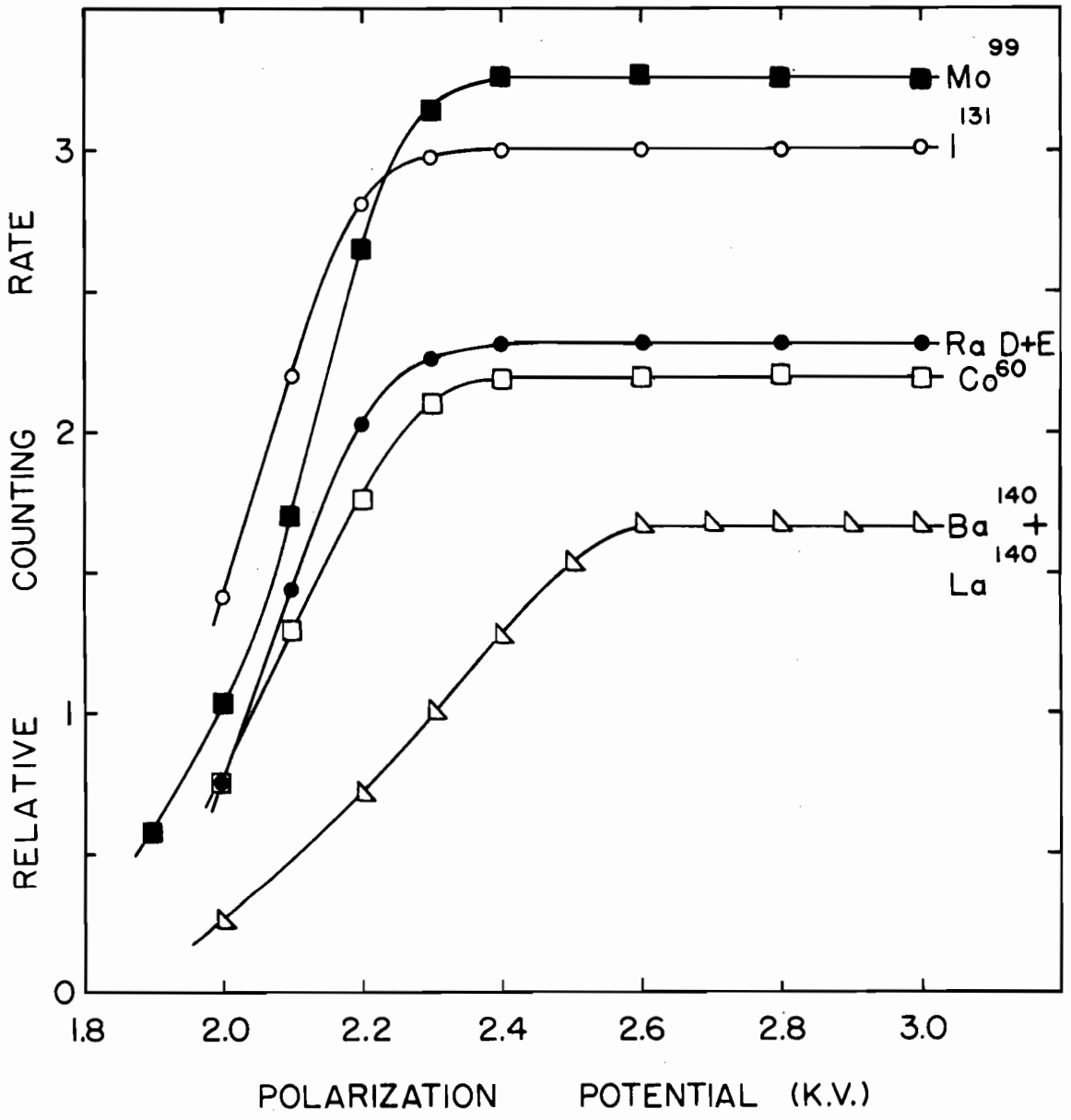
99
Mo
131
I
Ra D+E
Co60
140
Ba +
140
La
RELATIVE COUNTING RATE
0
1
2
3
1.8
2.0
2.2
2.4
2.6
2.8
3.0
POLARIZATION POTENTIAL (K.V.)

Figure 9

EFFECT OF VARYING THE BIAS SETTING
ON THE HIGH VOLTAGE CHARACTERISTICS
OF THE 4 π COUNTER

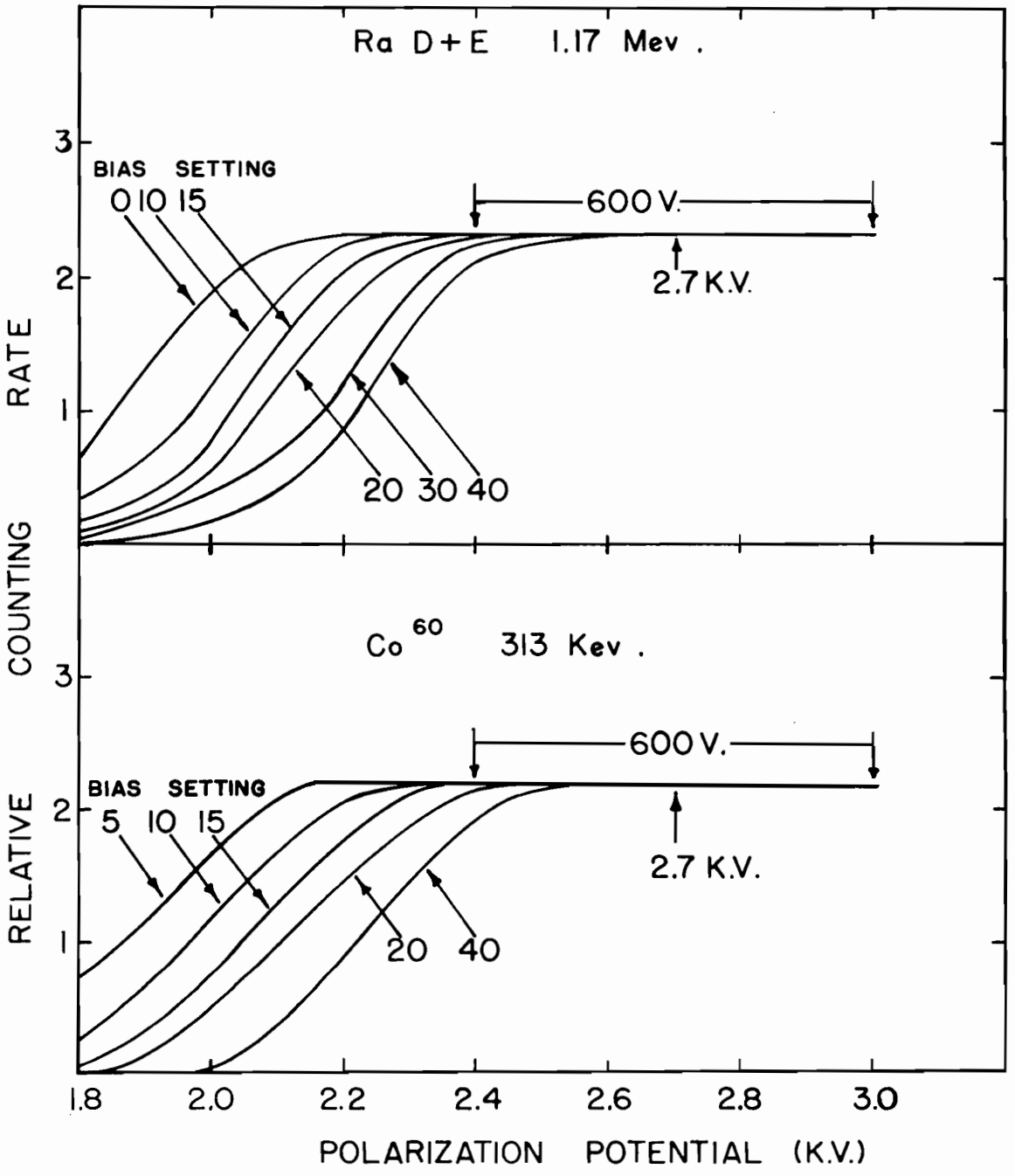
Ra D+E 1.17 Mev.
BIAS SETTING
0 10 15
600 V.
2.7 K.V.
20 30 40
COUNTING RATE
Co 60 313 Kev.
600 V.
BIAS SETTING
5 10 15
2.7 K.V.
20 40
RELATIVE
1.8 2.0 2.2 2.4 2.6 2.8 3.0
POLARIZATION POTENTIAL (K.V.)

(iii) Counting corrections:

(a) Resolution losses:

Counters operated in the proportional region have smaller resolving times than those operated in the Geiger region. Consequently, higher counting rates can be tolerated. But, resolution losses occur due in large part to losses in the associated electronics of the counting system, and to a lesser extent for reasons connected with the discharge mechanism in the counter. Pate and Yaffe[39] have suggested that resolution losses are best determined empirically. The method consists in preparing a series of P^{32} sources of increasing strengths, starting with counting rates at which resolution losses are known to be insignificant. The activity of these sources is measured, then secondary sources prepared from these by lamination. The activities of the laminated sources are determined and resolution losses obtained from the difference between the observed counting rates of the laminated sources and the sum of the individual counting rates. By repeating this process, a series of values for resolution loss at increasing observed counting rates is obtained. Fig. 10 shows a log-log plot of resolution losses vs. observed counting rates obtained with the counter used. At a counting rate of 1×10^5 counts per minute, the resolution loss is 1.8%. Losses due to absorption in the laminated films and self-absorption were assumed to be negligible because of the high energy of the P^{32} β^- rays -

Figure 10

RESOLUTION LOSS CORRECTION FOR THE

4 π COUNTER

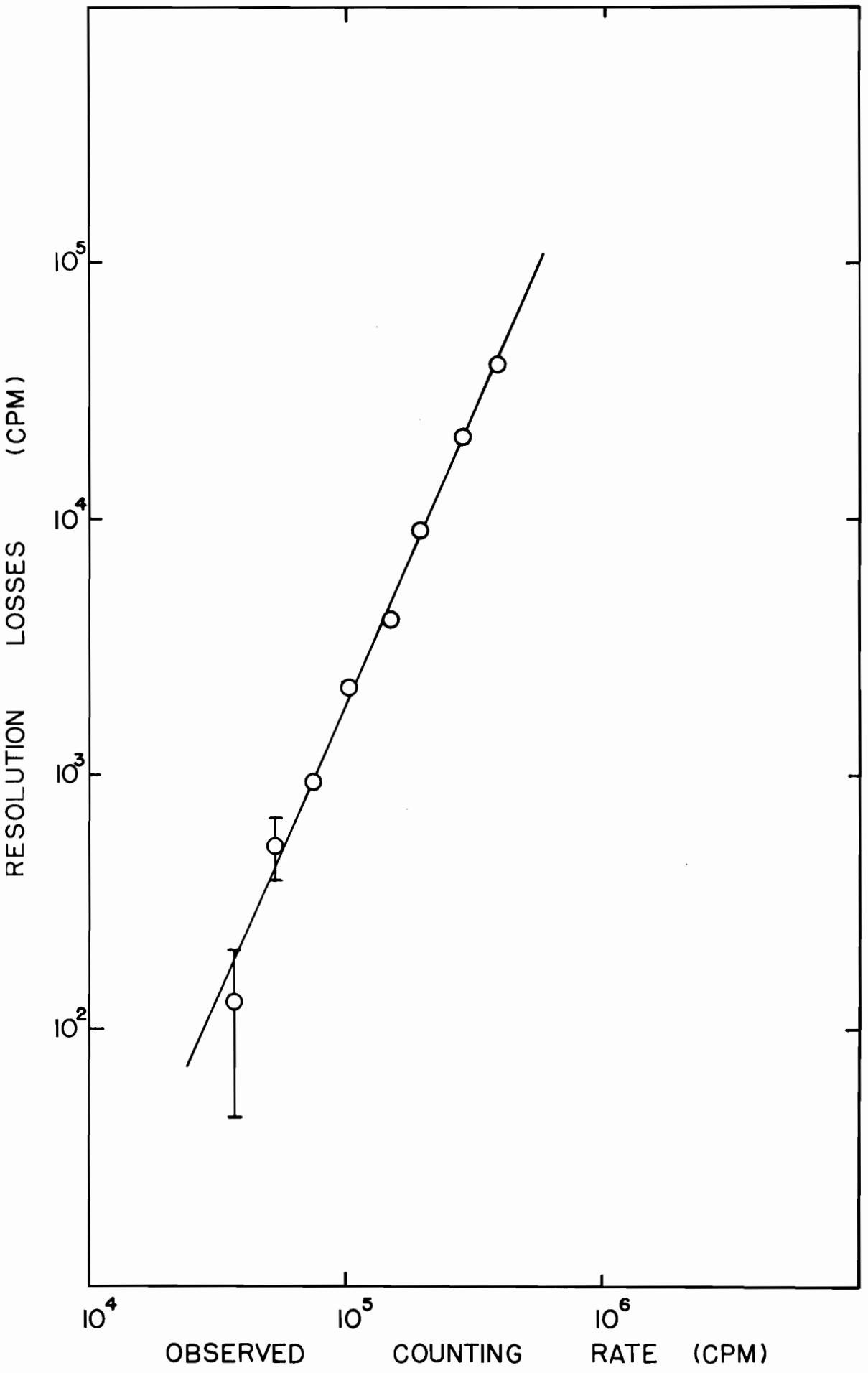
RESOLUTION LOSSES (CPM)
10^5
10^4
10^3
10^2
10^4
10^5
10^6
OBSERVED COUNTING RATE (CPM)

1.71 Mev, because of the high specific activity of the P^{32} solution and because very thin films were used.

(b) Source-mount absorption:

The energy spectrum of a β ray forms a continuous distribution of particle energies with average energy one-third the maximum energy. The softer components of this energy spectrum will be absorbed in the film mount. Thus the fraction of particles absorbed becomes larger for β rays of decreasing maximum energies. Pate and Yaffe[40] have developed an 'absorption curve method' for correcting for absorption in the source mount. In this method a source is prepared on a film of known thickness and the counting rate measured. The counting rate is again measured after laminating on to the back of the original mount a film of known superficial density. By repeating this procedure, the counting rate is determined as a function of increasing mount superficial densities. Extrapolation back to zero thickness gives the disintegration rate of the source. A series of curves are prepared in this way for β emitters of increasing maximum energies. These curves are reproduced in Fig. 11 where the transmission, that is the ratio of the observed counting rate to the disintegration rate, is plotted as a function of increasing beta maximum energies for source mounts of increasing superficial densities. Interpolations from these curves were used to determine source-mount absorption corrections in this work. The total superficial

Figure 11

SOURCE-MOUNT ABSORPTION CORRECTION

FOR A 4 π PROPORTIONAL COUNTER

Pate and Yaffe[40]

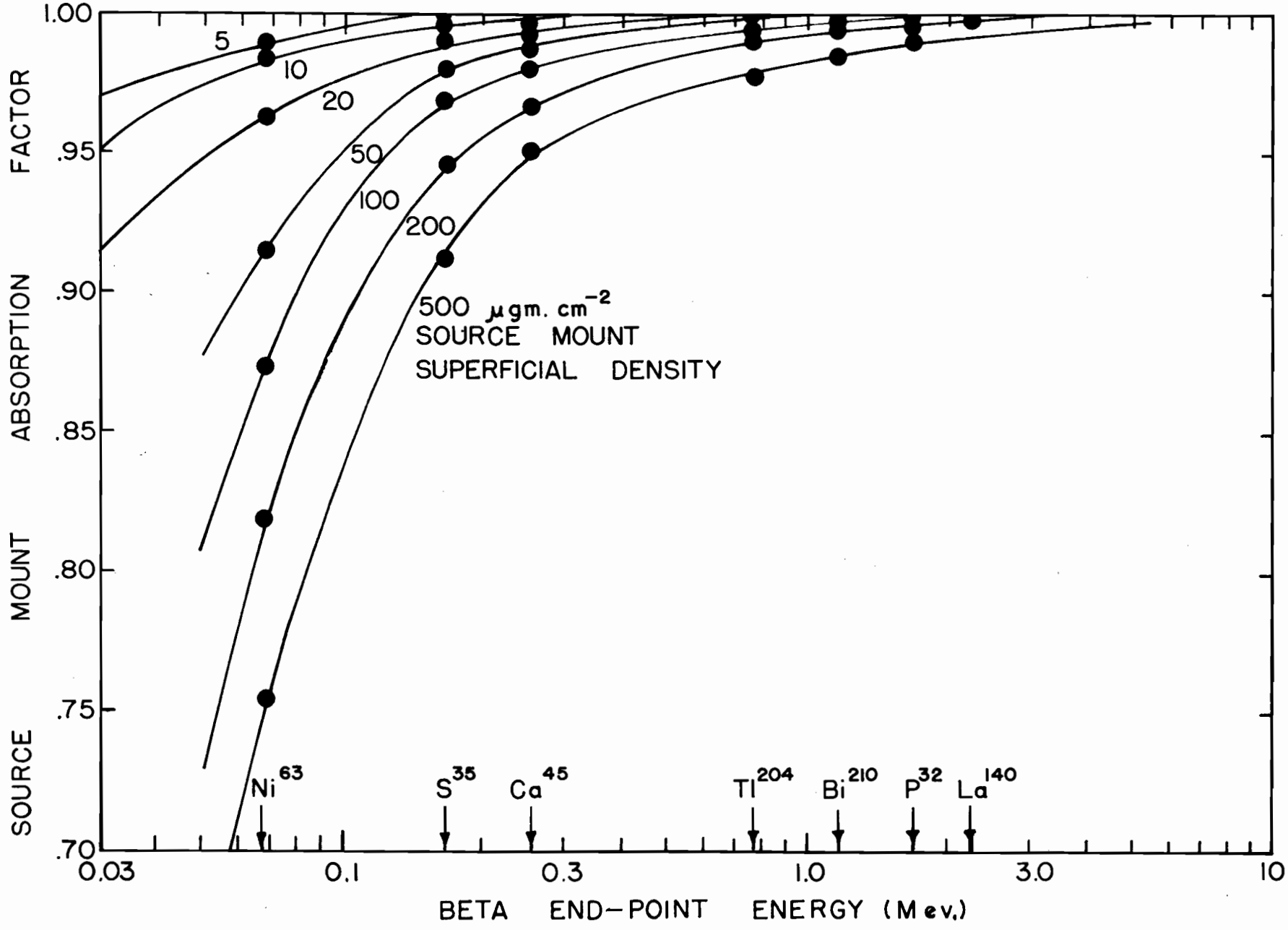
SOURCE MOUNT ABSORPTION FACTOR
1.00
.95
.90
.85
.80
.75
.70
5
10
20
50
100
200
500 μgm. cm⁻²
SOURCE MOUNT
SUPERFICIAL DENSITY
Ni 63
S 35
Ca 45
Tl 204
Bi 210
P 32
La 140
0.03
0.1
0.3
1.0
3.0
10
BETA END-POINT ENERGY (Mev.)

densities of the gold-coated VYNS films used in this work was between 15 and 25 μg per cm^2.

(c) Self-absorption:

Pate and Yaffe[42] and Yaffe and Fishman[50] have studied the self-absorption of β-emitting nuclides of increasing maximum beta energies. Their method was based on the preparation and measurement of radioactive sources of increasing source superficial densities. The sources were prepared by distilling an organic compound of the radioactive element of interest on to thin gold-coated VYNS films, under high vacuum. The apparent relative specific activity of each source is obtained by relating its specific activity to the extrapolated specific activity at zero source superficial density. Curves were then drawn of the apparent relative specific activities vs. β end-point energy at varying source superficial densities. These curves, reproduced from Yaffe and Fishman[50], are shown in Figs. 12 and 13. Corrections for self-absorption used in this work were interpolated from these curves. Since the nuclides investigated in this work generally decayed by the emission of more than one β-ray, the correction for each beta ray was weighted according to its percentage abundance and the sum of these weighted values used as the correction factor.

(d) Statistical counting errors:

Since the emission of radiation is a random phenomenon, the measurement of emission rates is governed by

Figure 12

SELF-ABSORPTION CORRECTION FOR A

4 π PROPORTIONAL COUNTER

Pate and Yaffe[42]

Yaffe and Fishman[50]

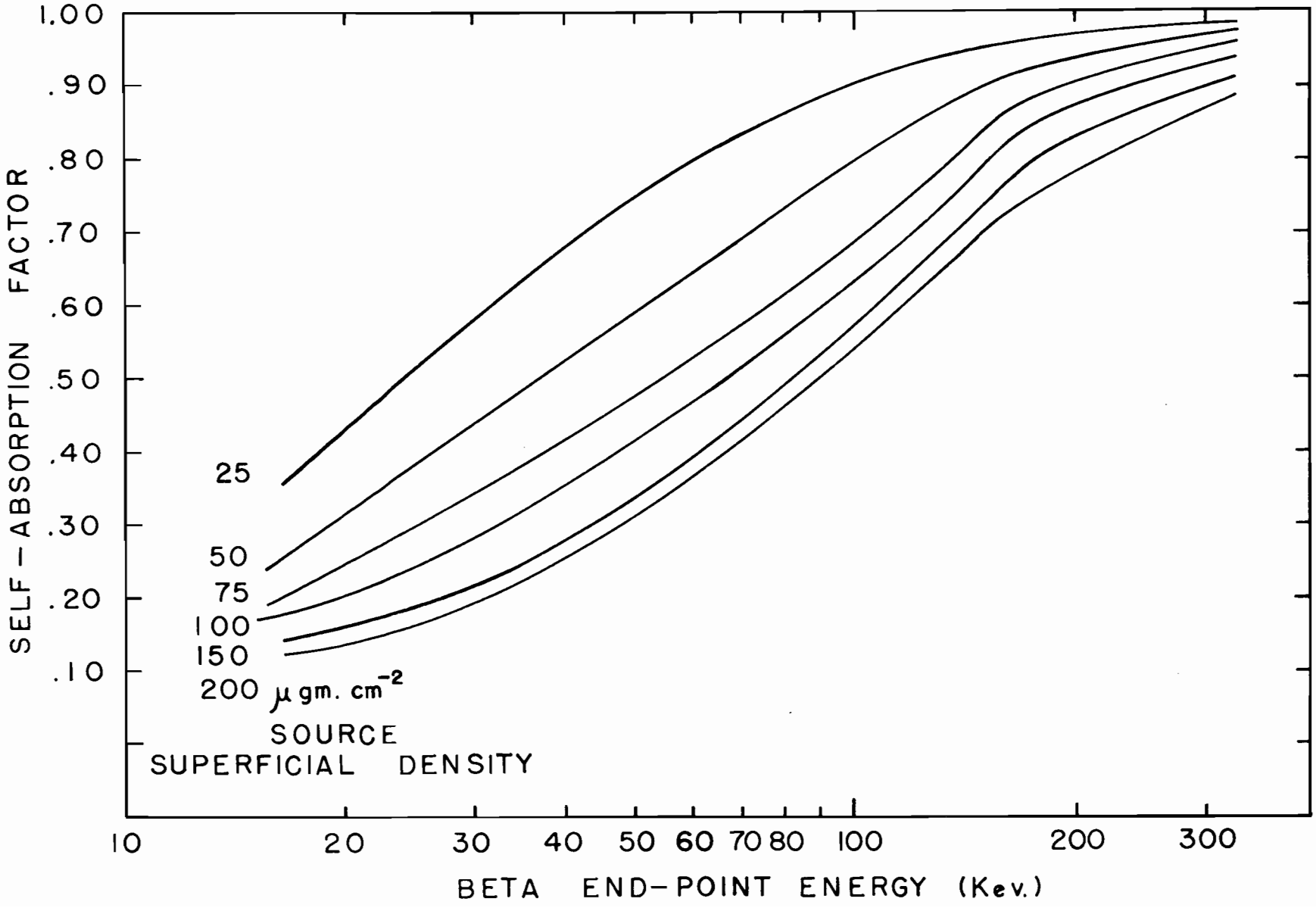
1.00
.90
.80
.70
.60
.50
.40
.30
.20
.10
SELF-ABSORPTION FACTOR
25
50
75
100
150
200 μ gm. cm⁻²
SOURCE
SUPERFICIAL DENSITY
10
20
30
40
50
60
70
80
100
200
300
BETA END-POINT ENERGY (Kev.)

Figure 13

SELF-ABSORPTION CORRECTION FOR A

4 π PROPORTIONAL COUNTER

Pate and Yaffe[42]

Yaffe and Fishman[50]

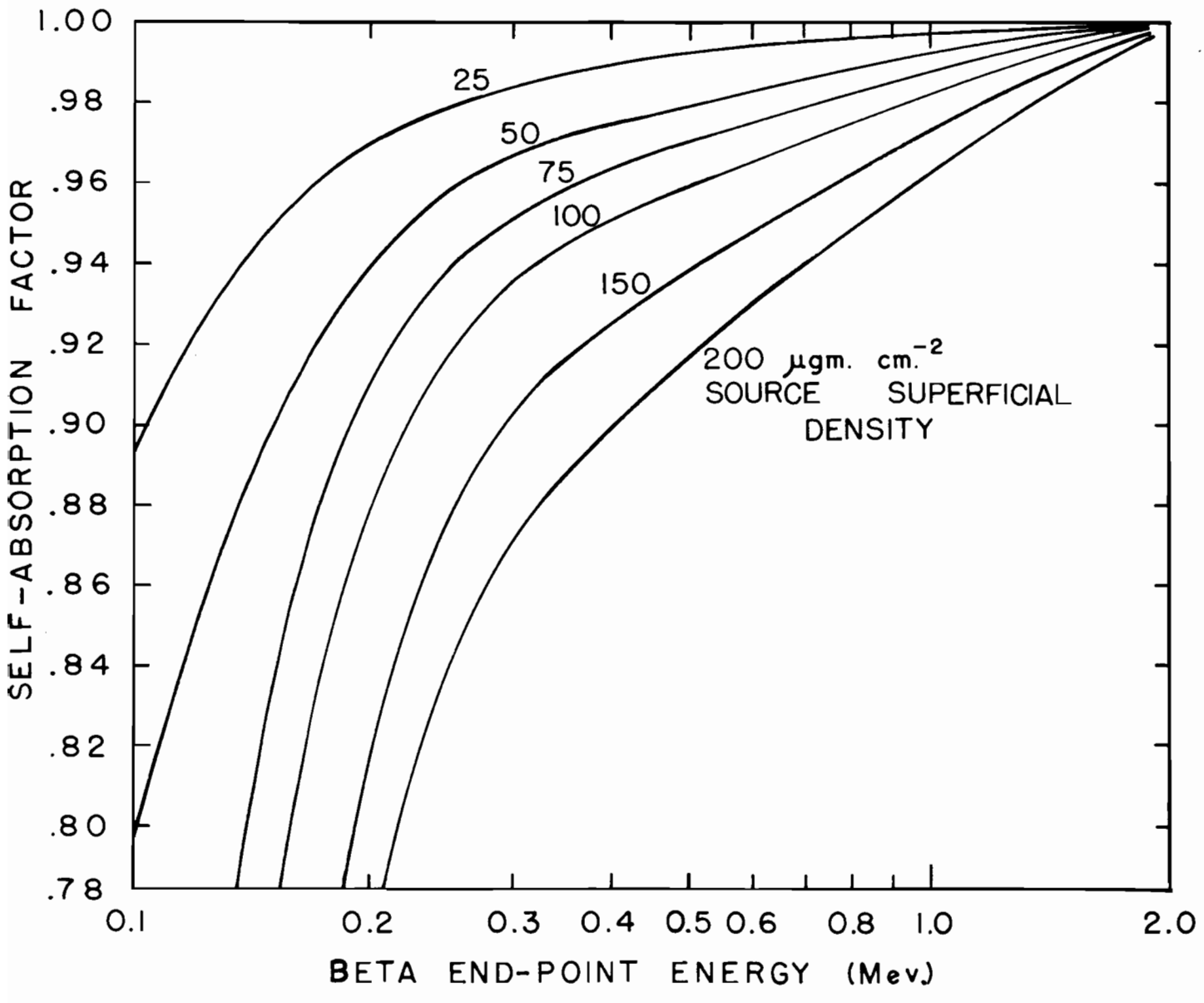
1.00
.98
.96
.94
.92
.90
.88
.86
.84
.82
.80
.78
SELF-ABSORPTION FACTOR
25
50
75
100
150
200 µgm. cm.⁻²
SOURCE SUPERFICIAL
DENSITY
0.1
0.2
0.3
0.4
0.5
0.6
0.8
1.0
2.0
BETA END-POINT ENERGY (Mev.)

statistical laws. If the duration of a measurement is small compared to the half-life of the radioactivity measured, then the rate of emission is given by

$$R \pm \sigma_R = \frac{m \pm \sqrt{m}}{t}$$

where R = rate per unit time,

σ_R = standard deviation,

m = total counts registered,

t = duration of measurement.

In this work a ratio $\pm \sqrt{m}/m \leq .01$ was maintained. Thus, by registering at least 10,000 counts during a counting period, the standard deviations of the counting rates were kept $\leq \pm$ 1%.

D. Scintillation counting

(i) Equipment:

Gamma rays were measured on a scintillation spectrometer which is shown diagrammatically in Fig. 14. The detector is a hermetically sealed unit supplied by the Harshaw Chemical Company consisting of a 3" x 3" sodium iodide crystal, activated with about 0.1% thallium iodide, optically coupled to a Du Mont 6363 photomultiplier tube. The latter was operated at a voltage of 1100 volts obtained from a Baird Atomic (model 318) high voltage supply. The ouput pulses from the photomultiplier tube are fed through a Hamner Electronics Co. preamplifier (model N-351) to a variable gain liner amplifier (Baird Atomic, model 215).

Figure 14

BLOCK DIAGRAM OF THE

SCINTILLATION SPECTROMETER

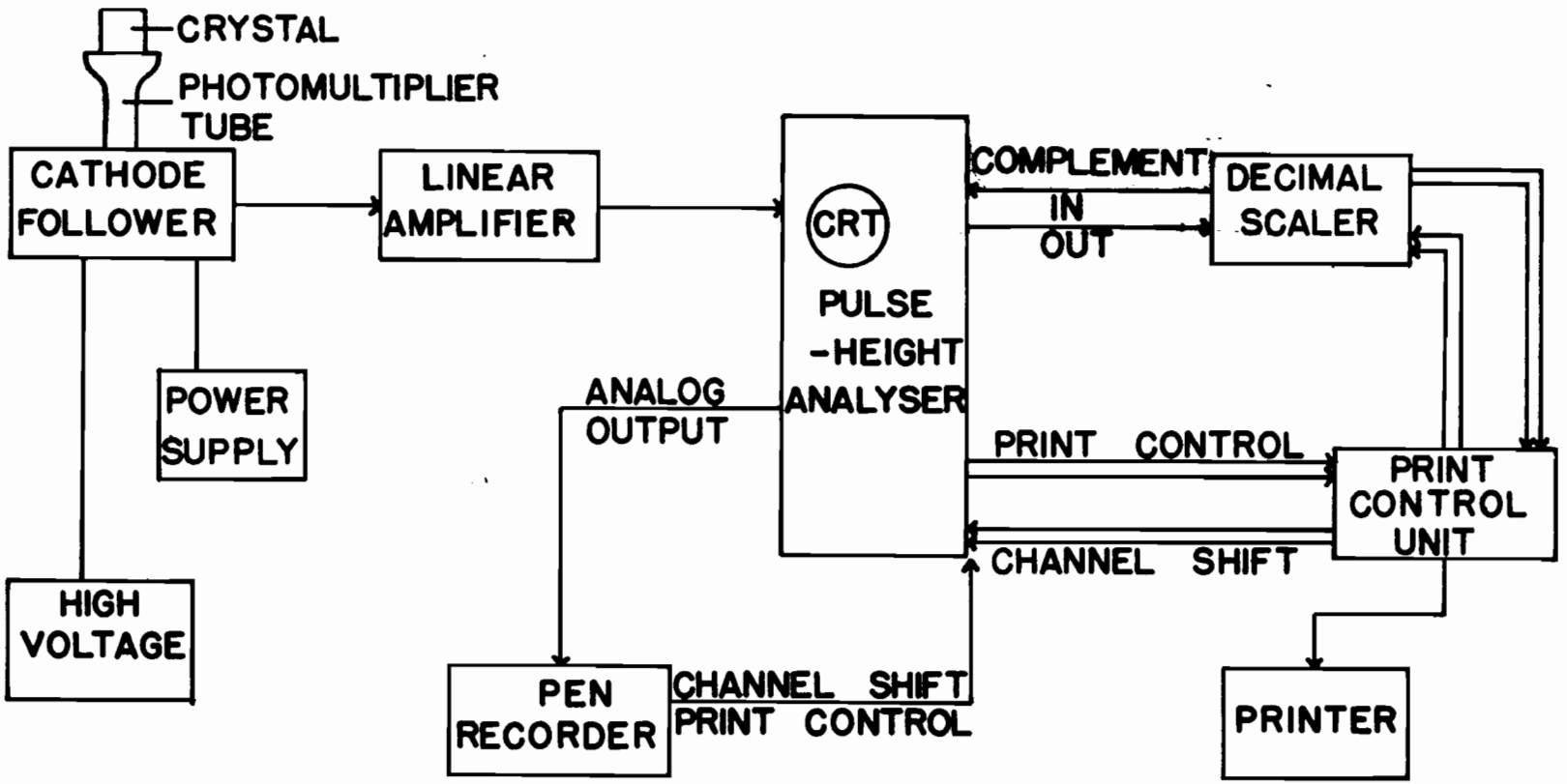
CRYSTAL
PHOTOMULTIPLIER TUBE
CATHODE FOLLOWER
LINEAR AMPLIFIER
CRT
PULSE -HEIGHT ANALYSER
COMPLEMENT
IN
OUT
DECIMAL SCALER
POWER SUPPLY
ANALOG OUTPUT
PRINT CONTROL
PRINT CONTROL UNIT
CHANNEL SHIFT
HIGH VOLTAGE
PEN RECORDER
CHANNEL SHIFT
PRINT CONTROL
PRINTER

The amplifier is coupled to a 100 channel pulse height analyser (Computing Devices of Canada Limited, type AEP-2230) through a cathode follower. The data collected by the pulse height analyser can be viewed on a cathode ray tube or can be recorded on a Westronics recorder (model 2705) which accepts analog signals. Also, after the analog signals are converted to decimal form by means of a decimal scaler (C.D.C., type 450), the data can be printed on a Victor digitmatic printer programmed by a print control unit (C.D.C., type 460). The analyser is provided with a microammeter on which resolution losses during measurement are indicated. These losses are due to the dead time of the analyser which lies between 35 and 135 μsec., depending on the pulse height. Resolution losses do not cause distortion in the gamma-ray spectrum but cause a reduction in its overall height.

(ii) Measurement of gamma rays:

Gamma rays interact with matter in the following ways:

(1) the Photoelectric effect - the energy of a gamma-ray photon is transferred to an electron of an atom or molecule which is then ejected with a kinetic energy equal to the difference between the photon energy and the binding energy of the electron.

(2) the Compton effect - the photon collides with an electron, transferring only part of its energy to the electron, and is itself scattered in the process.

The electrons ejected thus have a variety of energies up to a maximum known as the Compton Edge.

(3) Pair production - If the photon energy is greater than 1.02 Mev, the photon may be totally converted into a positron-electron pair. The positron is soon annihilated with the emission of two gamma rays, each of 511 kev energy, which in turn may interact by processes (1) and (2) above.

All of the three processes described may result from the interaction of a high energy gamma ray with matter. But the photoelectric effect is the primary mode of interaction of low energy gamma rays, whereas the Compton effect occurs primarily with gamma rays of medium energy.

When a gamma ray strikes the NaI(Tl) crystal of the spectrometer, free electrons are liberated as a result of the processes described. The energy of these electrons is expended in the formation of light photons in the crystal - about two light photons are emitted for every 100 electron volts of energy. These light photons are reflected by the housing of the crystal until they strike the cathode of the photomultiplier tube, causing a number of photoelectrons proportional to the number of light photons to be ejected. The number of these electrons is multiplied many times by the dynodes of the photomultiplier tube, resulting in an output voltage pulse which is proportional to the energy of the incident gamma ray. However, on account of the statistical

nature of the production of photoelectrons at the cathode of the photomultiplier tube, the output of this tube will be a statistical distribution of pulses. The photoelectric effect then results in a broad photopeak with the energy of the apex of the peak representing the incident gamma-ray energy. The Compton effect results in a continuum of energies ending at an energy somewhat lower than the photo-peak energies. In the case of pair production, if both the positron and the electron are stopped in the crystal, a photopeak will appear at an energy equal to the gamma-ray energy minus 1.02 Mev. If one or both of the annihilation gamma quanta are stopped photoelectrically in the crystal, peaks will appear at 511 kev or 1.02 Mev. On the other hand, if the annihilation quanta interact by the Compton effect, their continua will be added on to that of the original gamma ray.

The 100 channel pulse height analyser sorts the amplified output pulses of the detector according to their amplitudes into one or more of its 100 channels, counting and storing the number of pulses in each channel. The output data of the analyser is thus a reproduction of the gamma-ray spectrum, as seen by the detector, from which the energy of a gamma ray can be obtained from the channel number of the apex of the photopeak and the observed counting rate from the sum of the counting rates in each channel under the photopeak.

In this work the measured gamma-ray spectra were

used to identify the energies of the gamma rays emitted by a separated fission product and to plot peak height counting rates vs. decay time to give a qualitative measure of the half-life of a particular gamma ray. The data obtained in this way were compared with published values serving as a check on the identification of a particular fission product and of the radioactive purity of a chemical separation.

ACTIVITIES ISOLATED AND RESULTS

1. FLUX DETERMINATIONS

All irradiations were done in a No. 1 self-serve position in the NRX reactor at Chalk River. Since in this position the contribution to the neutron flux of epithermal neutrons is small, it was assumed that the samples were subjected to a wholly thermal neutron flux. The flux values, given in Table I, were calculated from equation (27), P. 39.

$$(N\lambda)_{Co^{60}} = N_{Co^{59}} I \sigma_c (1 - e^{-\lambda T}) e^{-\lambda t} \times \frac{1}{\text{attenuation}}$$

The half-life of Co^{60} was taken as 5.26 years[47]. The neutron flux is attenuated to 0.979 of its initial value by the 0.005" diameter cobalt wire. This value was calculated from equation (28), P. 39, and is identical to the value quoted by Santry[51] and agrees well with an experimentally determined value, 0.97, of Eastwood and Werner[52]. The thermal neutron capture cross section used for Co^{59} was 37.3 barns[46].

2. FISSION RATE DETERMINATIONS

The Pu^{239} was in the form of turnings of a plutonium-aluminium alloy containing 3.81% by weight of Pu^{239}. The atom concentration of Pu^{239} in the alloy was therefore $\sim 0.5\%$. It was assumed that the attenuation of the neutron

Table I

FISSION RATE DETERMINATIONS

Irradiation	Thermal neutron flux Units of 10^{12} neutrons cm^{-2} sec^{-1}	Weight of Pu^{239} (mg)	Fission rate Units of 10^{9} fissions sec^{-1}
A	1.880	1.015	3.569
B	2.527	1.334	6.300
C	1.292	0.345	0.834
D	1.425	0.730	1.943
E	1.557	0.744	2.163
F	1.195	0.430	0.961
G	1.319	1.357	3.345
H	1.150	1.328	2.854
J	1.087	1.833	3.724
KA	1.231	1.433	3.297
KB	1.231	0.555	1.277
LA	2.363	1.015	4.483
LB	2.363	1.049	4.631

flux in the sample of fissile material would be relatively small. The fission rates, given in Table I, for the plutonium samples were calculated from equation (26), P. 38.

$$R = N_{Pu^{239}} I \sigma_f$$

The thermal neutron fission cross section used for Pu^{239} was 742 barns[2].

3. FISSION PRODUCT ACTIVITIES

(a) Bromine

Bromine was separated by the method of Glendenin et al.[53]. Bromate and iodate carriers were added to an aliquot of the fission product solution, which was then treated with H_2S to ensure exchange between active bromine and the carrier. After oxidation to Br_2 with $KMnO_4$ and extraction with CCl_4, several oxidation-reduction cycles were performed together with extractions into and out of carbon tetrachloride to purify the bromine. Finally, the bromine was reduced to Br^- by a water solution of SO_2, warmed to remove excess SO_2 and then neutralized with dilute lithium hydroxide solution. The active solution was made up to a volume of 10 mls. Chemical yield was determined according to Volhard's method.

The gross beta decay curve, shown in Fig. 15, was resolved into a 37-d. component, a 4.2-d. component and a 34-hour component. Since the only bromine activity expected

Figure 15

β^- DECAY OF BROMINE FRACTION

O - Experimental points

x - Long-lived activity subtracted

● - 4.1-d. activity subtracted

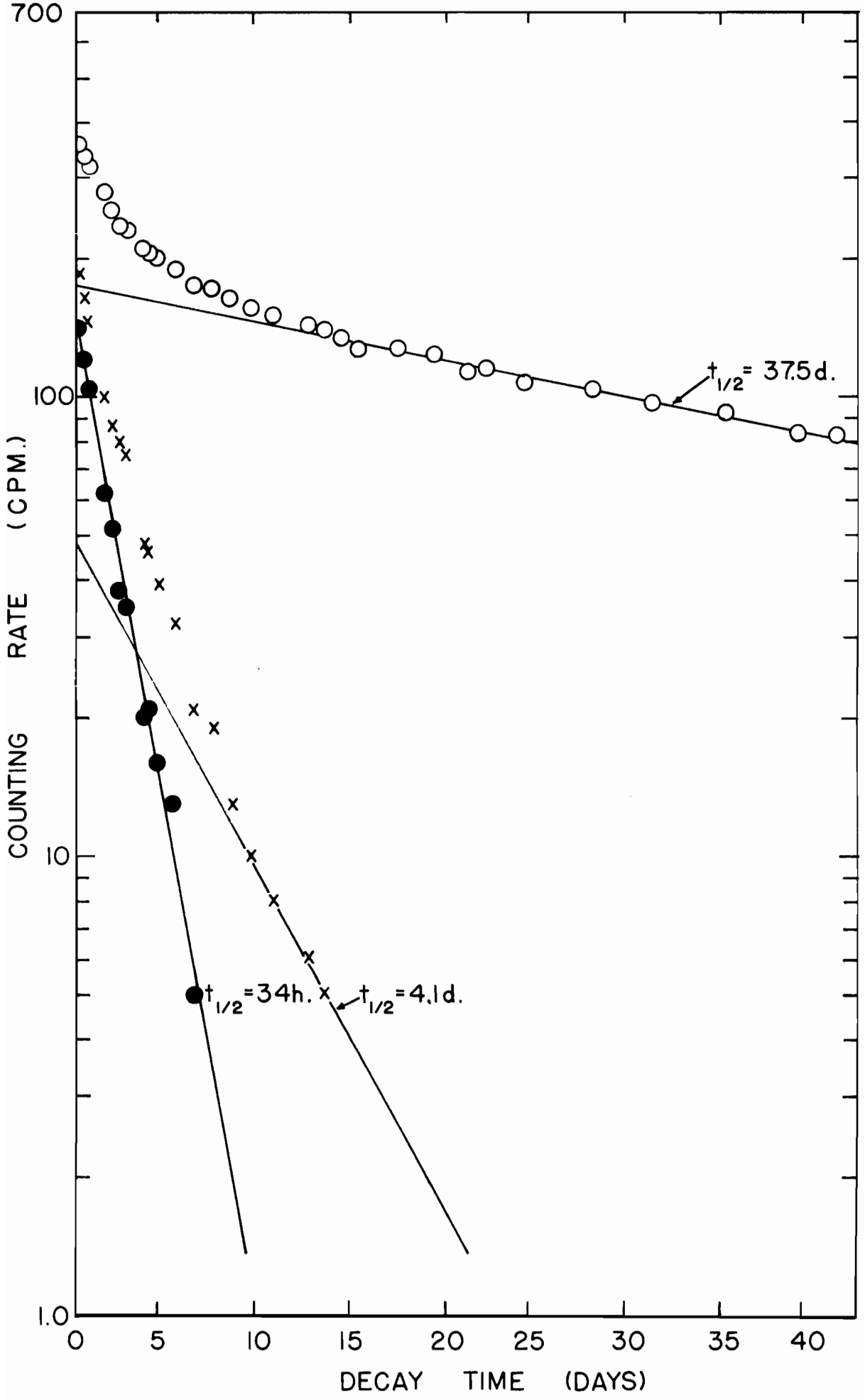
700
100
10
1.0
COUNTING RATE (CPM.)
0
5
10
15
20
25
30
35
40
DECAY TIME (DAYS)
$t_{1/2}$= 37.5d.
$t_{1/2}$=34h.
$t_{1/2}$=4.1d.

to be present was Br^{82} which has a half-life of 36 hours[54], gamma spectra were taken to try and identify the contaminating activities. It was not possible to identify either of the longer-lived activities. Br^{82} is a shielded nuclide and therefore occurs in very low yield. It decays by the emission of a 440 kev (100%) beta ray to an excited level of Kr^{82}. Coincident gamma rays have energies of 554, 619, 698, 777, 827, 1044, 1317, and 1475 kev respectively. The calculated fission yield is given in Table II.

Table II

FISSION YIELD DATA FOR Br^{82} (34 HOURS)

Irradiation	H
Observed activity	147 c/m
Source-mount absorption factor	.997
Self-absorption factor	.992
Aliquot factor	500
Chemical yield	77.24%
Time after irradiation	2.878 d.
Decay factor	0.2431
Time in reactor	2.133 d.
Saturation factor	0.6495
Saturation activity	1.015×10^{5} d/s
Fission rate	2.854×10^{9} f/s
Fission yield	3.56×10^{-3} %

(b) Strontium

The method of Glendenin[55] was used to separate strontium. Barium and strontium carriers were added to an aliquot of the fission product solution and their mixed nitrates were precipitated with fuming nitric acid. Barium was removed as $BaCrO_4$ from the mixed nitrates, after they had been dissolved in water, leaving the strontium behind in solution. The strontium was purified by precipitating the oxalate from ammoniacal solution, dissolving the oxalate precipitate in dilute nitric acid and again precipitating the nitrate. After being washed with ethyl alcohol, the nitrate was dissolved in water, was then transferred to a volumetric flask and made up to volume. Aliquots were removed from this solution for 4π β^- and γ-ray measurements. The chemical yield was determined by titration with EDTA in a 50% alcoholic solution, using phthalein complexone as indicator[49].

The gross decay curve was resolved into two components (Fig. 16). The long-lived component was assumed to be Sr^{90} - Y^{90} in equilibrium and the 50-d. component to be Sr^{89} which has a reported half-life of 50.4 days[56]. The strontium activities expected to be present as fission products occur in the following decay chains:

$$\text{short lived} \longrightarrow {}_{37}Rb^{89} \xrightarrow{15.4\ m.} {}_{38}Sr^{89} \xrightarrow{50.5\ d.} {}_{39}Y^{89}\ (\text{stable})$$

Figure 16

β^- DECAY OF STRONTIUM ACTIVITIES

● - Long-lived activity subtracted

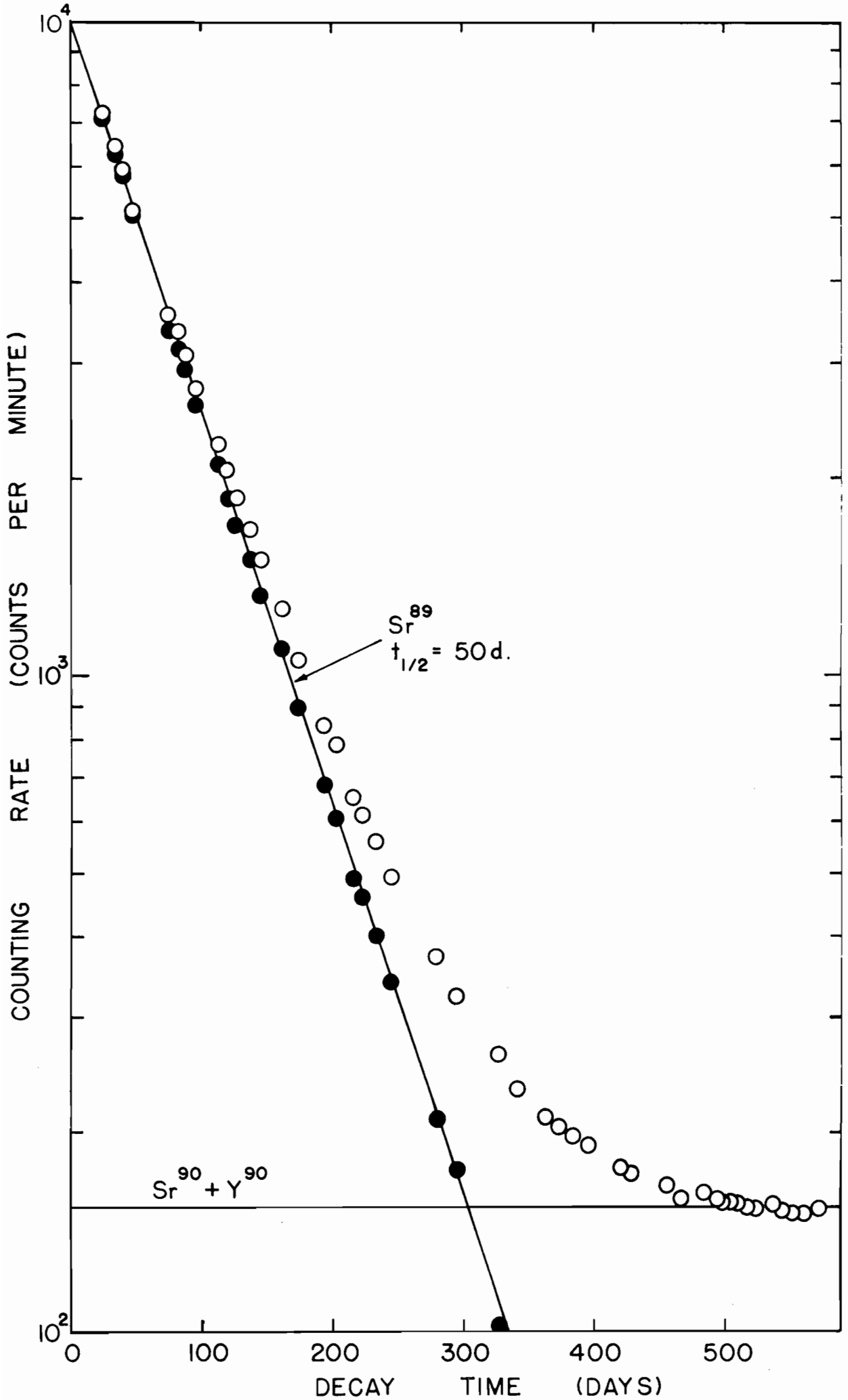
10^4
10^3
10^2
COUNTING RATE (COUNTS PER MINUTE)
Sr^{89}
$t_{1/2}$ = 50 d.
$Sr^{90} + Y^{90}$
0
100
200
300
400
500
DECAY TIME (DAYS)

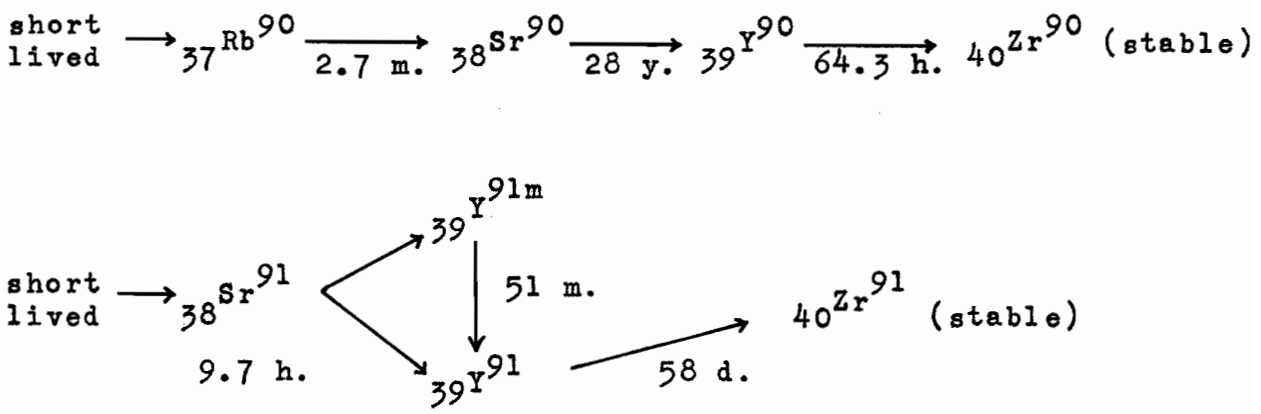

The elapsed time between the end of bombardment and the time of separation was such that all of the Sr^{91} had decayed away when Sr was isolated. Sr^{89} decays by β^- emission of maximum energy 1.46 Mev (100%) to stable Y^{89}. Sr^{90}, which has a reported half-life of 27.7 years[57], emits a 0.54 Mev β^- to form Y^{90} which itself decays by β^- emission with a half-life of 64 hours. No gamma rays were therefore expected in the Sr fraction and none was found. Since the Sr^{90} half-life is so much longer than its Y^{90} daughter, at equilibrium the disintegration rates of parent and daughter are equal. On this account half the counting rate of the long-lived activity was assumed to be due to Sr^{90} and the fission yield was calculated therefrom. Fission yield values for Sr^{89} are given in Table III and for Sr^{90} in Table IV.

(c) Yttrium

Yttrium was separated from an aliquot of the fission product solution by the method of Ballou[58]. Carriers for cerium, yttrium, lanthanum and zirconium were

Table III

FISSION YIELD DATA FOR Sr^{89} (50 DAYS)

Irradiation	B	C	D
Observed activity	9.90×10^3 c/m	1.98×10^4 c/m	1.29×10^4 c/m
Source-mount absorption factor	1.00	1.00	1.00
Self-absorption factor	1.00	0.991	0.995
Aliquot factor	2000	125	500
Chemical yield	14.44%	50.65%	67.27%
Time after irradiation	17.954 d.	113.406 d.	125.379 d.
Decay factor	0.7812	0.2033	0.1784
Time in reactor	2.005 d.	1.993 d.	1.994 d.
Saturation factor	0.0272	0.0270	0.0271
Activity at saturation	1.076×10^8 d/s	1.496×10^7 d/s	3.328×10^7 d/s
Fission rate	6.300×10^9 f/s	8.3364×10^8 f/s	1.9431×10^9 f/s
Fission yield	1.71%	1.79%	1.71%

Table IV

FISSION YIELD DATA FOR Sr^{90} (27.7 YEARS)

Irradiation	B	C	D
Observed activity	77 c/m	525 c/m	425 c/m
Source-mount absorption factor	0.996	0.996	0.996
Self-absorption factor	0.999	0.956	0.971
Aliquot factor	2000	125	500
Chemical yield	14.44%	50.65%	67.27%
Time after irradiation	17.954 d.	113.406 d.	125.379 d.
Decay factor	0.9988	0.9922	0.9914
Time in reactor	2.005 d.	1.993 d.	1.994 d.
Saturation factor	1.374×10^{-4}	1.366×10^{-4}	1.367×10^{-4}
Activity at saturation	1.301×10^{8} d/s	1.673×10^{7} d/s	4.018×10^{7} d/s
Fission rate	6.300×10^{9} f/s	8.3364×10^{8} f/s	1.9431×10^{9} f/s
Fission yield	2.07%	2.01%	2.07%

added to the solution from which yttrium and the Rare Earths were precipitated as fluorides. After the fluorides were dissolved in a boric acid - nitric acid mixture, cerium was removed, as recommended by Boldridge and Hume[59], by oxidation with sodium bromate and precipitation of the iodate. The rare earths were removed from the supernate by precipitating the potassium - rare earth carbonates. The yttrium, left in solution, was precipitated as the hydroxide, dissolved in dilute hydrochloric acid and made up to a volume of 10 ml. Chemical yields were determined spectrophotometrically using the sodium alizarin sulphonate method[48]. The standard curve obtained is given in Fig. 17.

Aliquots of the yttrium solution were mounted on VYNS films and measured in the $4\pi\beta$ proportional counter. A half-life of 59 days (Fig. 18) was obtained (measured over five half-lives) which corresponded to Y^{91} with an adopted half-life value of 59 days[54]. Y^{91} decays to Zr^{91} by β^- emission with maximum energies of 0.33 Mev (0.03%) and 1.54 Mev (99.7%). The decay chains for yttrium activities expected are

$$\text{short lived} \longrightarrow Sr^{90} \xrightarrow[28\ y.]{} Y^{90} \xrightarrow[64\ h.]{} Zr^{90}\ (\text{stable})$$

$$\text{short lived} \begin{cases} \nearrow Y^{91m} \xrightarrow{51\ m.} Y^{91} \\ \searrow Y^{91} \end{cases} \xrightarrow[58\ d.]{} Zr^{91}\ (\text{stable})$$

Figure 17

STANDARD CURVE FOR YTTRIUM

SODIUM ALIZARIN SULPHONATE METHOD[48]

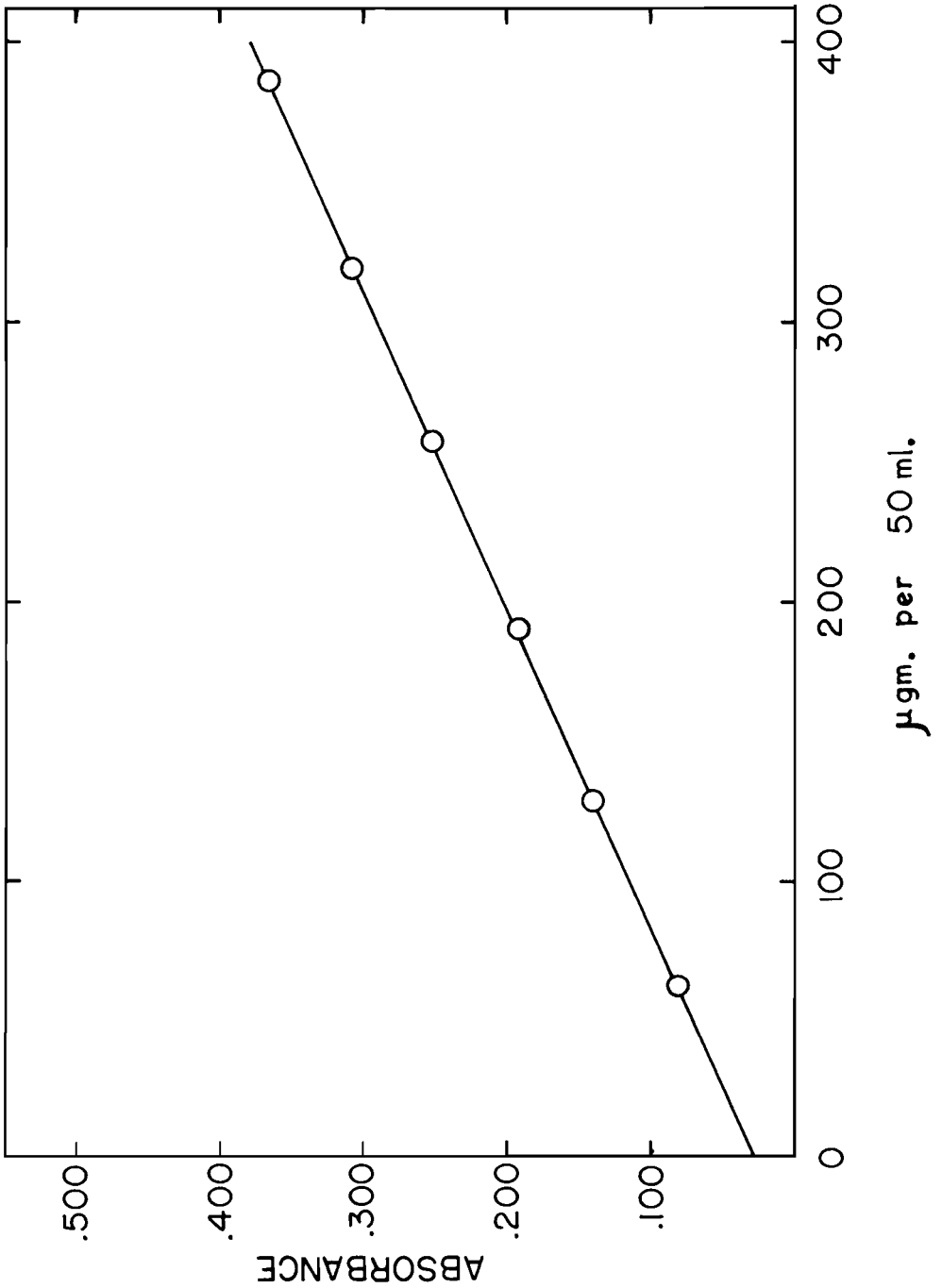
ABSORBANCE
.500
.400
.300
.200
.100
0
100
200
300
400
µgm. per 50 ml.

Figure 18

β^- DECAY OF Y^{91}

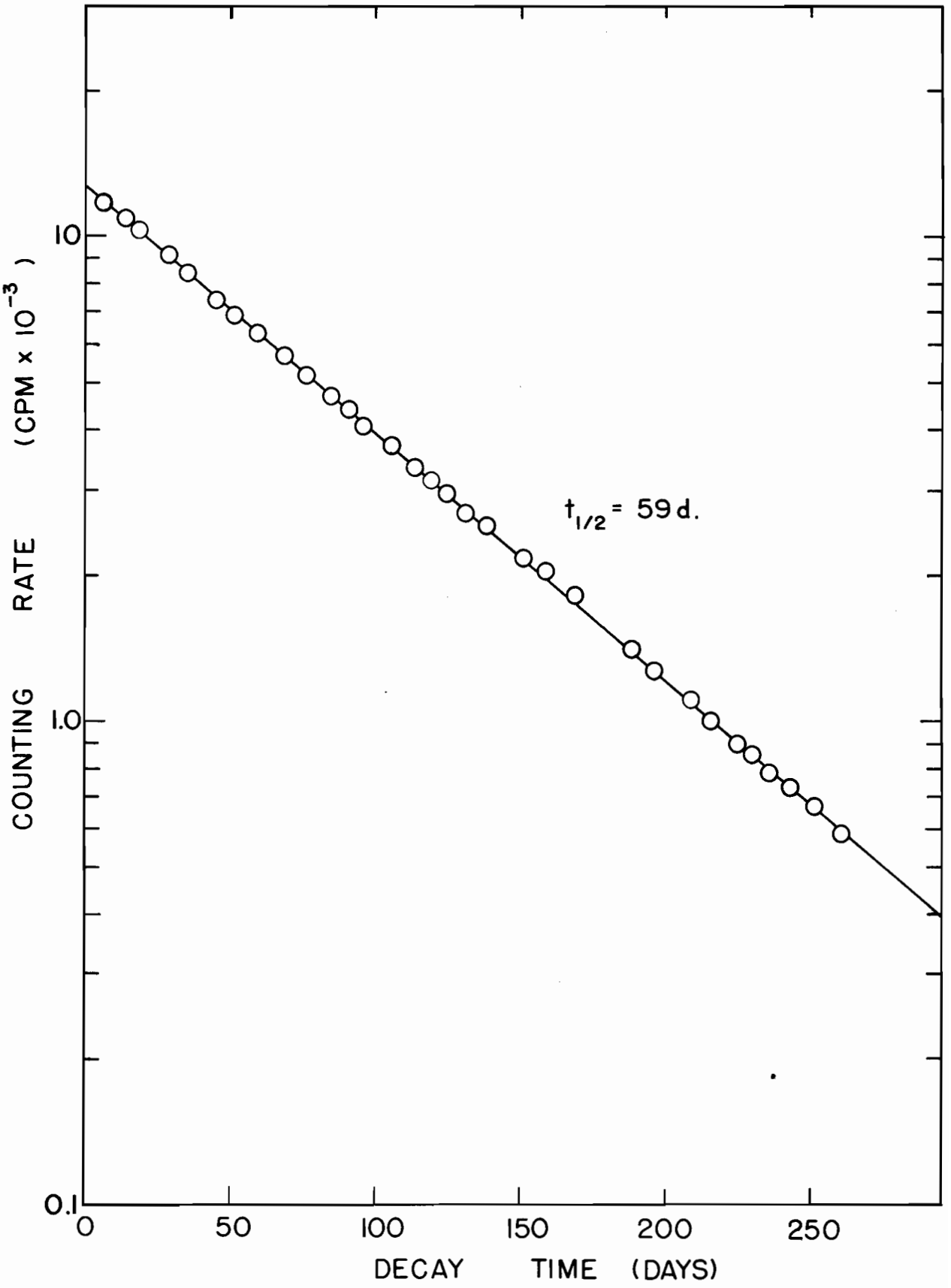
COUNTING RATE (CPM x 10^{-3})
10
1.0
0.1
$t_{1/2}$ = 59 d.
0
50
100
150
200
250
DECAY TIME (DAYS)

Since 4π counting was done several days after separation, the Y^{91m} (51 m.) and Y^{90} (64 h.) had decayed away. An aliquot of the yttrium solution showed no gamma spectrum when analysed on the scintillation spectrometer. The data for the yield determinations of Y^{91} are given in Table V.

Table V

FISSION YIELD DATA FOR Y^{91} (59 DAYS)

Irradiation	G	J
Observed activity	1.28×10^4 c/m	7.30×10^4 c/m
Source-mount absorption factor	1.00	1.00
Self-absorption factor	1.00	1.00
Aliquot factor	500	1000
Chemical yield	16.6%	57.1%
Time after irradiation	92.656 d.	3.944 d.
Decay factor	0.3368	0.9548
Time in reactor	2.136 d.	2.056 d.
Saturation factor	0.0248	0.0239
Activity at saturation	7.693×10^7 d/s	9.338×10^7 d/s
Fission rate	3.345×10^9 f/s	3.724×10^9 f/s
Fission yield	2.30%	2.51%

(d) Zirconium

With slight modifications, a solvent extraction method due to Moore[60], which made use of the solubility of zirconium - TTA (2-thenoyltrifluoroacetone) complexes in xylene was used to separate zirconium. A preliminary separation of barium fluozirconate[61] was necessary since plutonium is extracted along with zirconium in this method. Zirconium was recovered from the $BaZrF_6$ precipitate by dissolving it in dilute H_3BO_3-HNO_3 mixture, removing the barium as $BaSO_4$ and precipitating zirconium hydroxide. The hydroxide was dissolved in dilute HNO_3 and extracted into a xylene solution of TTA. The organic phase was scrubbed with 1 M HNO_3 and the zirconium removed with 0.25 M HF. Barium fluozirconate was again precipitated and the zirconium recovered as before. The precipitate was dissolved in dilute HNO_3 and made up to a volume of 10 mls. Chemical yield was determined by developing the coloured zirconium - 'Thoron' [1 - (0 - arsonophenylazo) - 2 naphthol - 3,6 disulphonic acid] complex[62]. The standard curve obtained is given in Fig. 19.

The gross β^- decay curve, shown in Fig. 20, was observed to increase to a maximum at about thirty days then to decrease into a long-lived tail. The amount of this background activity was estimated and subtracted from the gross counting rates to give the curve shown in Fig. 21, where the zirconium activity is seen to die away with a

Figure 19

STANDARD ABSORBANCE CURVE FOR ZIRCONIUM

('THORON' COMPLEX)

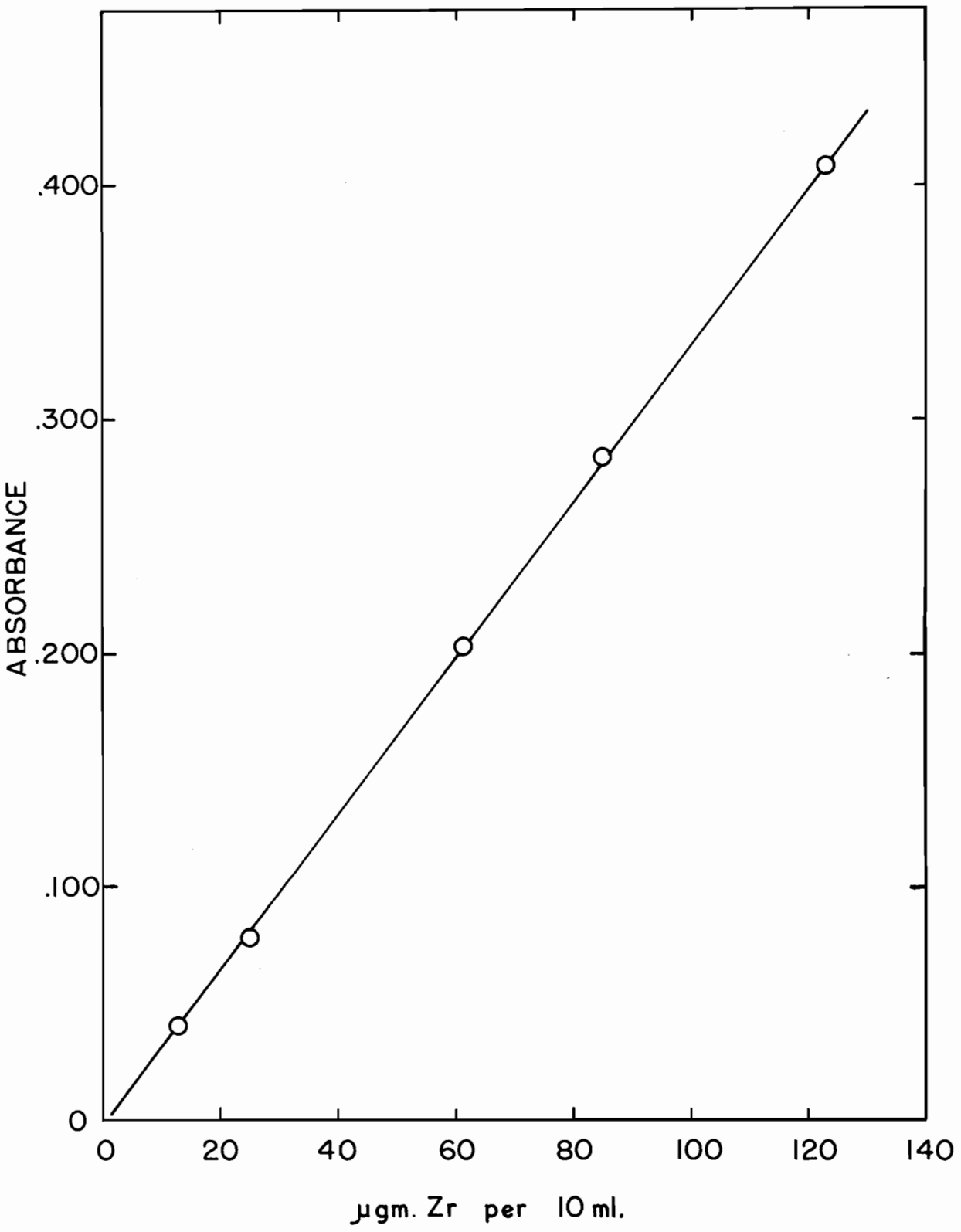
.400
.300
.200
.100
0
ABSORBANCE
0
20
40
60
80
100
120
140
µgm. Zr per 10 ml.

Figure 20

β^- DECAY OF ZIRCONIUM FRACTION

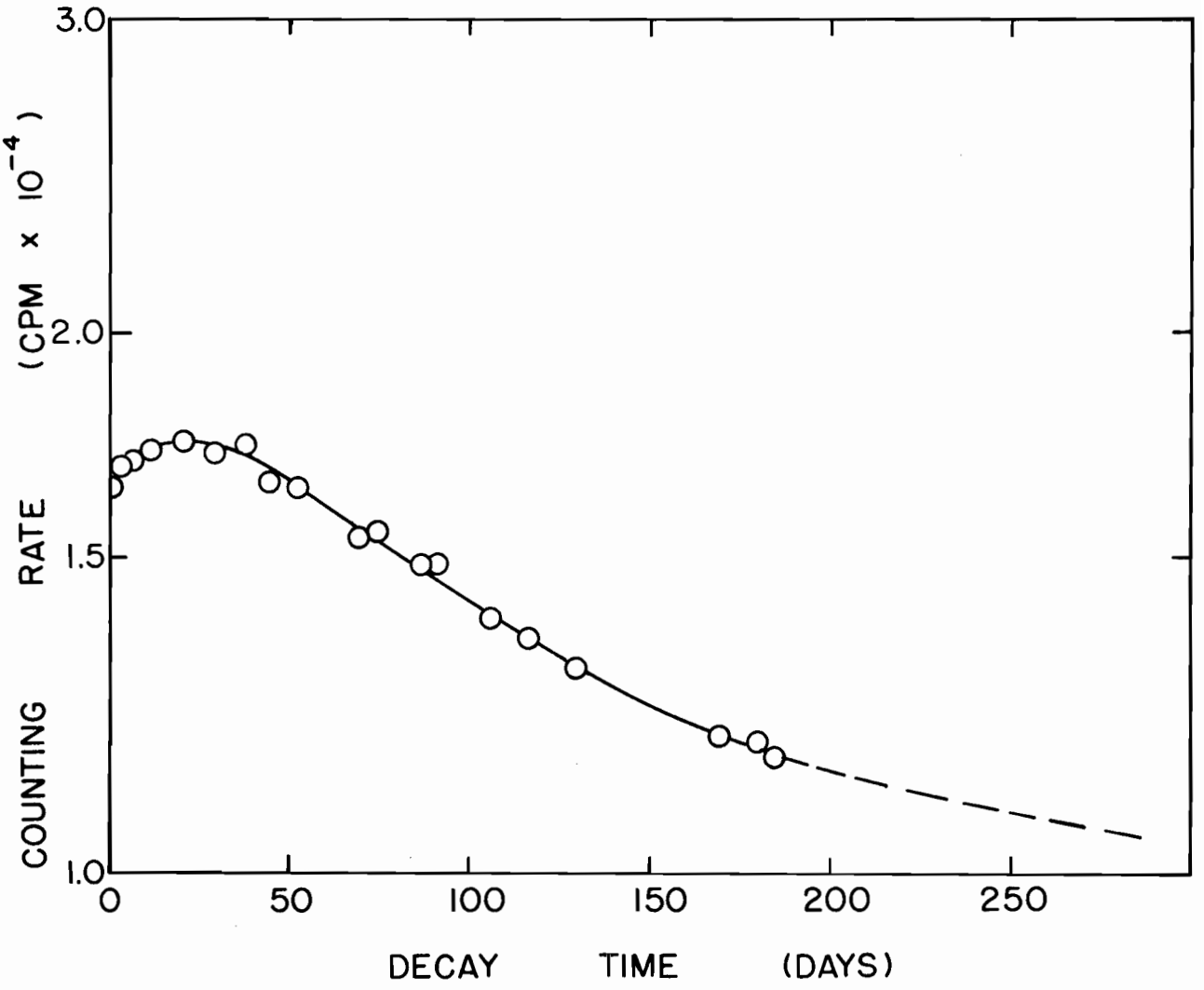
3.0
2.0
1.5
1.0
COUNTING RATE (CPM x 10^{-4})
0
50
100
150
200
250
DECAY TIME (DAYS)

Figure 21

β^- DECAY OF Zr^{95} ACTIVITY

(long-lived activity subtracted)

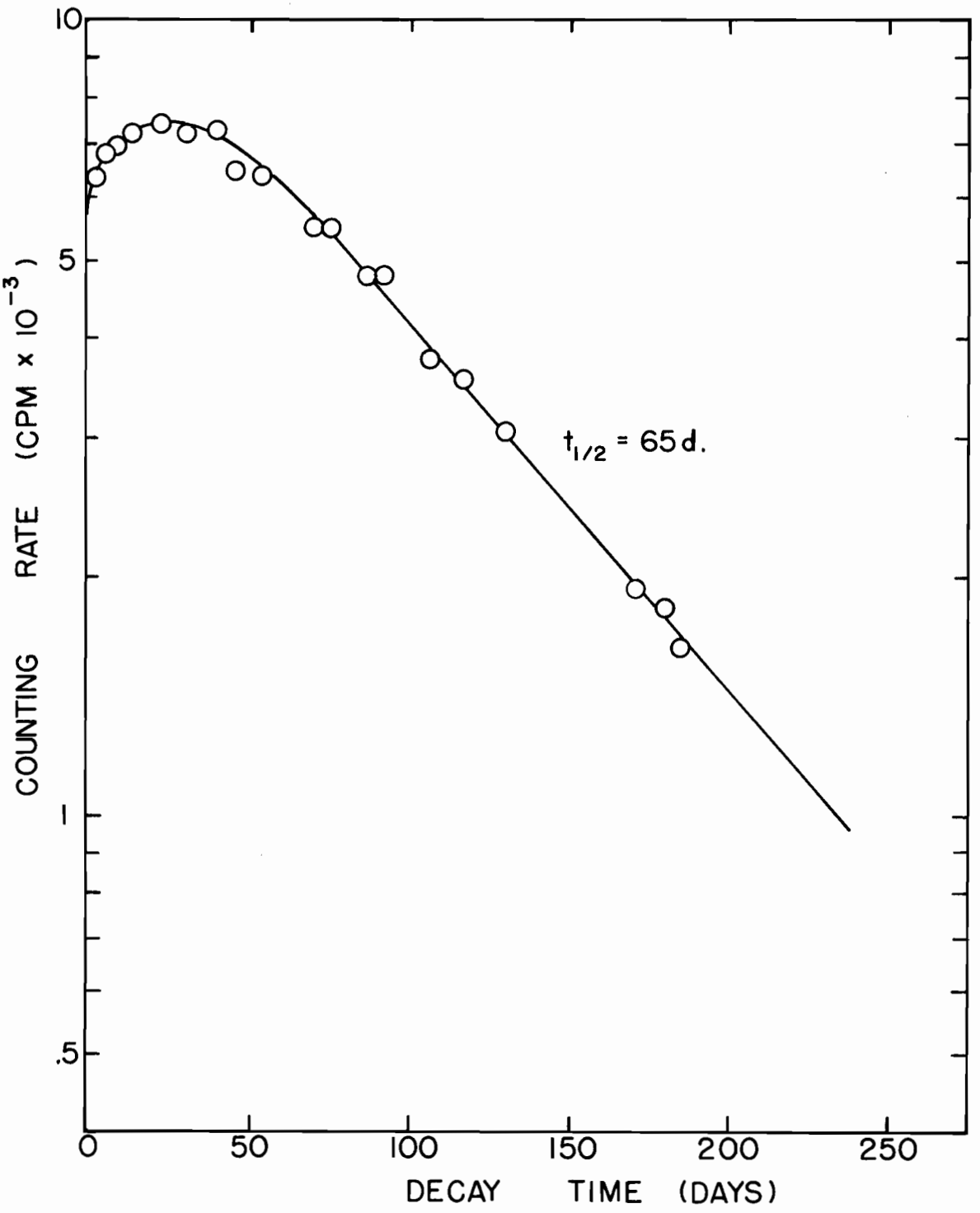
10
5
1
.5
COUNTING RATE (CPM x 10^{-3})
$t_{1/2}$ = 65 d.
0
50
100
150
200
250
DECAY TIME (DAYS)

half-life of 65 days. Zr^{95} arising from the following decay chain

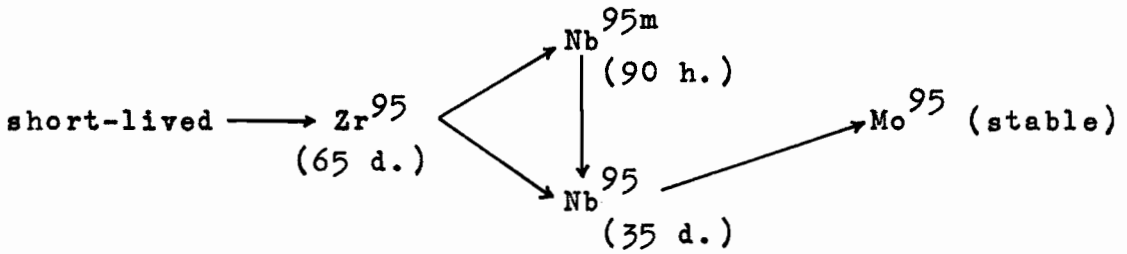

was the only zirconium activity expected to be detected in the fission product mixture. A gamma-ray spectrum of the zirconium fraction (Fig. 22) showed a prominent photopeak at 728 kev which shifted to 767 kev as the decay was followed. The decay of this gamma peak, shown in Fig. 23, also increased to a maximum then died away with a 65-day half-life. The contaminating long-lived activity was not identified.

Zr^{95} decays with a half-life of 65 days[54] by emission of β^- particles with maximum energies of 360 kev (43%), 396 kev (55%), 885 kev (2%), and 1.13 Mev (0.4%). Coincident gamma rays have energies of 760 and 726 kev. The Nb^{95} daughter decays by β^- emission of 160 kev (99%) and 930 kev (1%) maximum energies, with a 768 kev gamma ray in coincidence with the former. Disintegration rates to determine fission yields, given in Table VI, were obtained by extrapolating back to the time of separation where the Nb^{95} daughter activity was nil.

Figure 22

GAMMA-RAY SPECTRUM OF ZIRCONIUM FRACTION

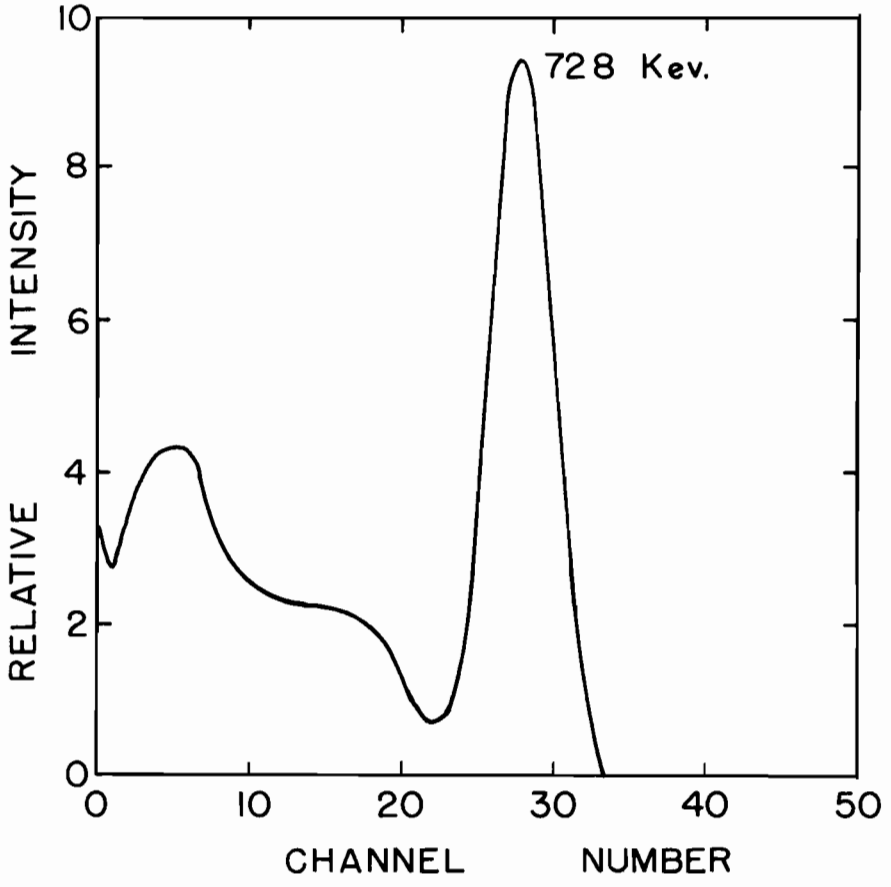
728 Kev.
RELATIVE INTENSITY
0
2
4
6
8
10
0
10
20
30
40
50
CHANNEL NUMBER

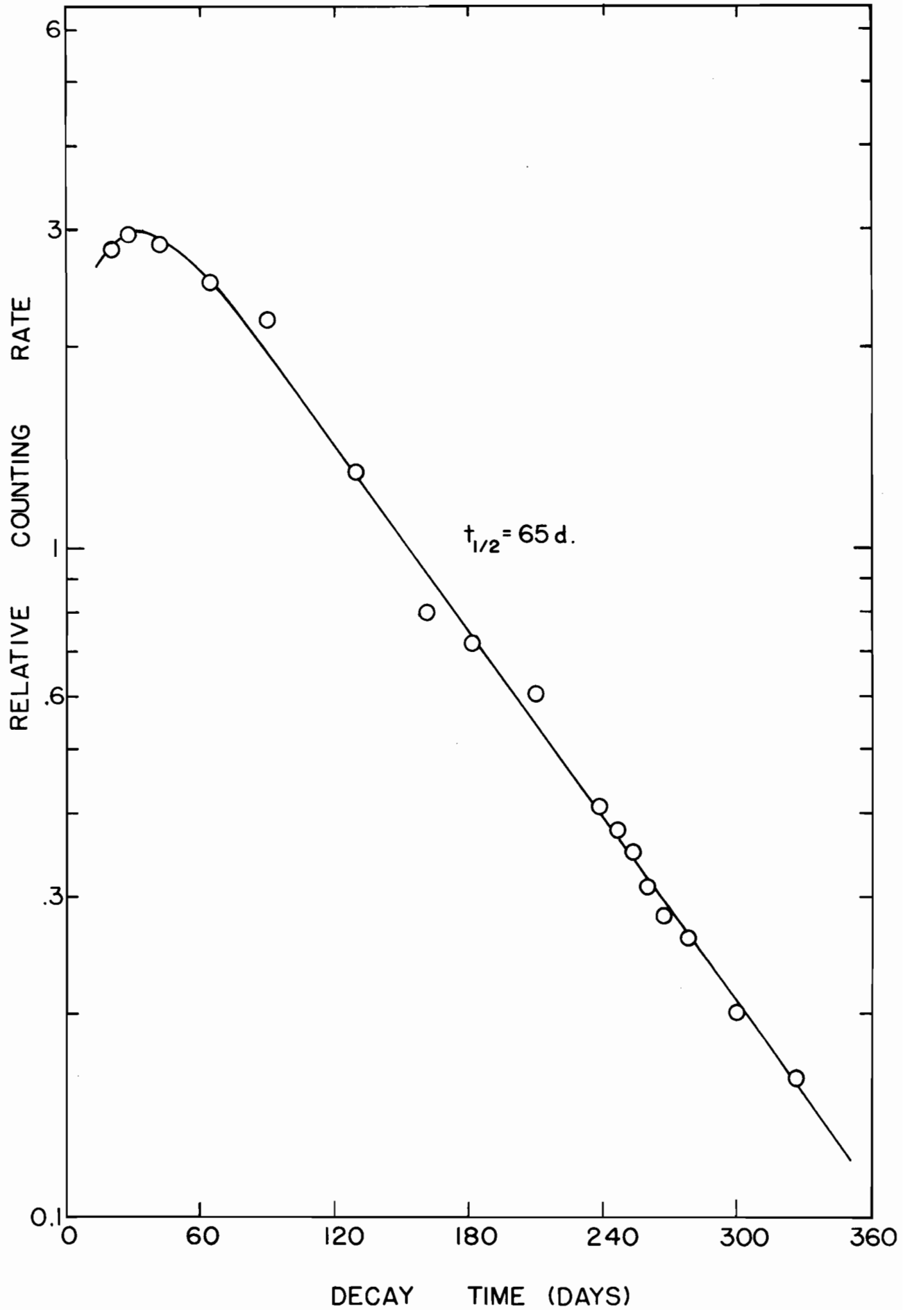
RELATIVE COUNTING RATE
6
3
1
.6
.3
0.1
$t_{1/2}$ = 65 d.
0
60
120
180
240
300
360
DECAY TIME (DAYS)

Table VI

FISSION YIELD DATA FOR Zr^{95} (65 DAYS)

Irradiation	F	G
Observed activity	6.20×10^3 c/m	1.20×10^4 c/m
Source-mount absorption factor	0.996	0.996
Self-absorption factor	0.970	0.995
Aliquot factor	285.7	1563
Chemical yield	45.28%	35.96%
Time after irradiation	251.656 d.	139.825 d.
Decay factor	0.0684	0.2252
Time in Reactor	1.998 d.	2.136 d.
Saturation factor	0.0211	0.0225
Activity at saturation	4.675×10^7 d/s	1.733×10^8 d/s
Fission rate	9.610×10^8 f/s	3.345×10^9 f/s
Fission yield	4.86%	5.18%

(e) Niobium

Niobium was separated by a method due to Glendenin[63] in which Nb_2O_5 was precipitated from an oxalic acid solution with chloric acid. Purification from zirconium was achieved by adding Zr hold-back carrier in repeated precipitations of the Nb_2O_5. The final precipitate was dissolved in saturated oxalic acid solution and made up to a volume of 10 mls. Chemical yields were determined on the spectrophotometer by the thiocyanate method[48] in which the yellow niobium thiocyanate complexes are extracted into peroxide-free ethyl ether (standard curve, Fig. 24).

The β^- decay curve, shown in Fig. 25, consisted of a single component which decayed with a half-life of 36.5 days measured over six half-lives. The gamma-ray spectrum contained one very prominent 758 kev photopeak (Fig. 26) which was seen to decay with a 34.2-day half-life (Fig. 27). The decay chain for the niobium activities expected in fission is

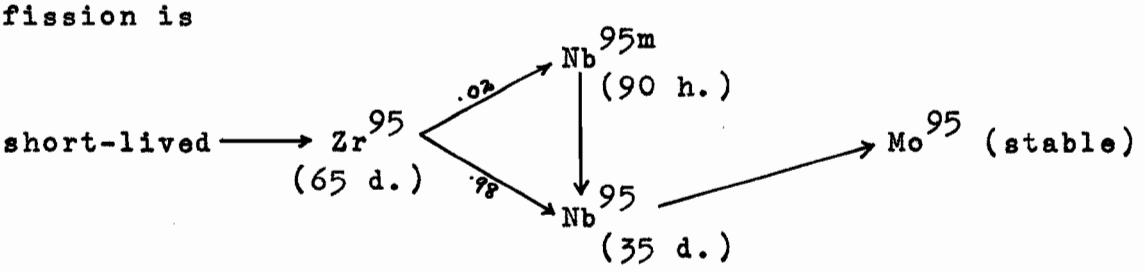

The 90-hour Nb^{95m} was not detected. The niobium activity was separated at a time when any independently formed Nb^{95m} would have decayed away. Any Nb^{95m} activity present would have come from the decay of Zr^{95} in the amount of 2% of its

Figure 24

STANDARD ABSORBANCE CURVE FOR

NIOBIUM-THIOCYANATE COMPLEXES

IN DIETHYL ETHER

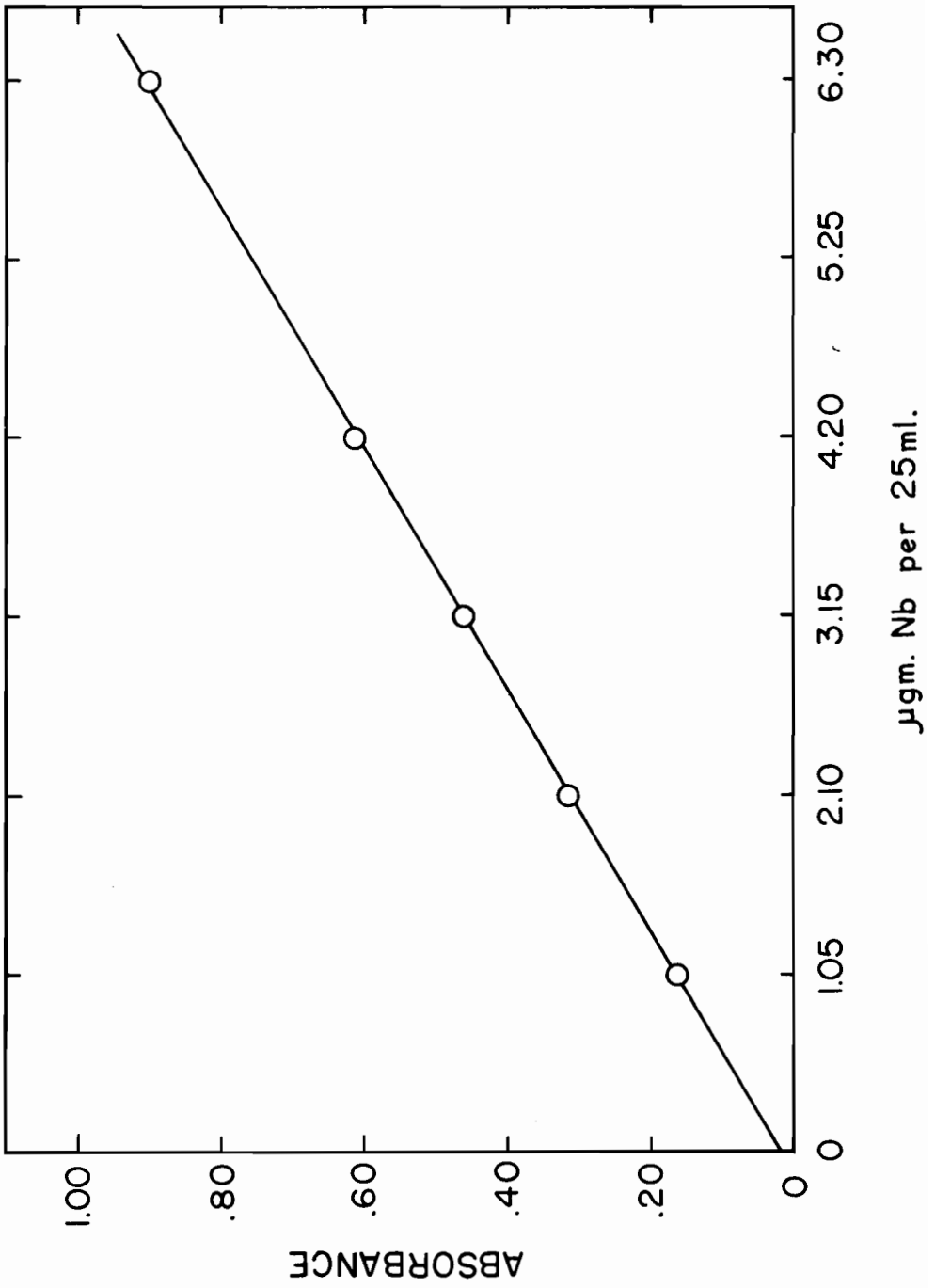
ABSORBANCE
1.00
.80
.60
.40
.20
0
0
1.05
2.10
3.15
4.20
5.25
6.30
µgm. Nb per 25ml.

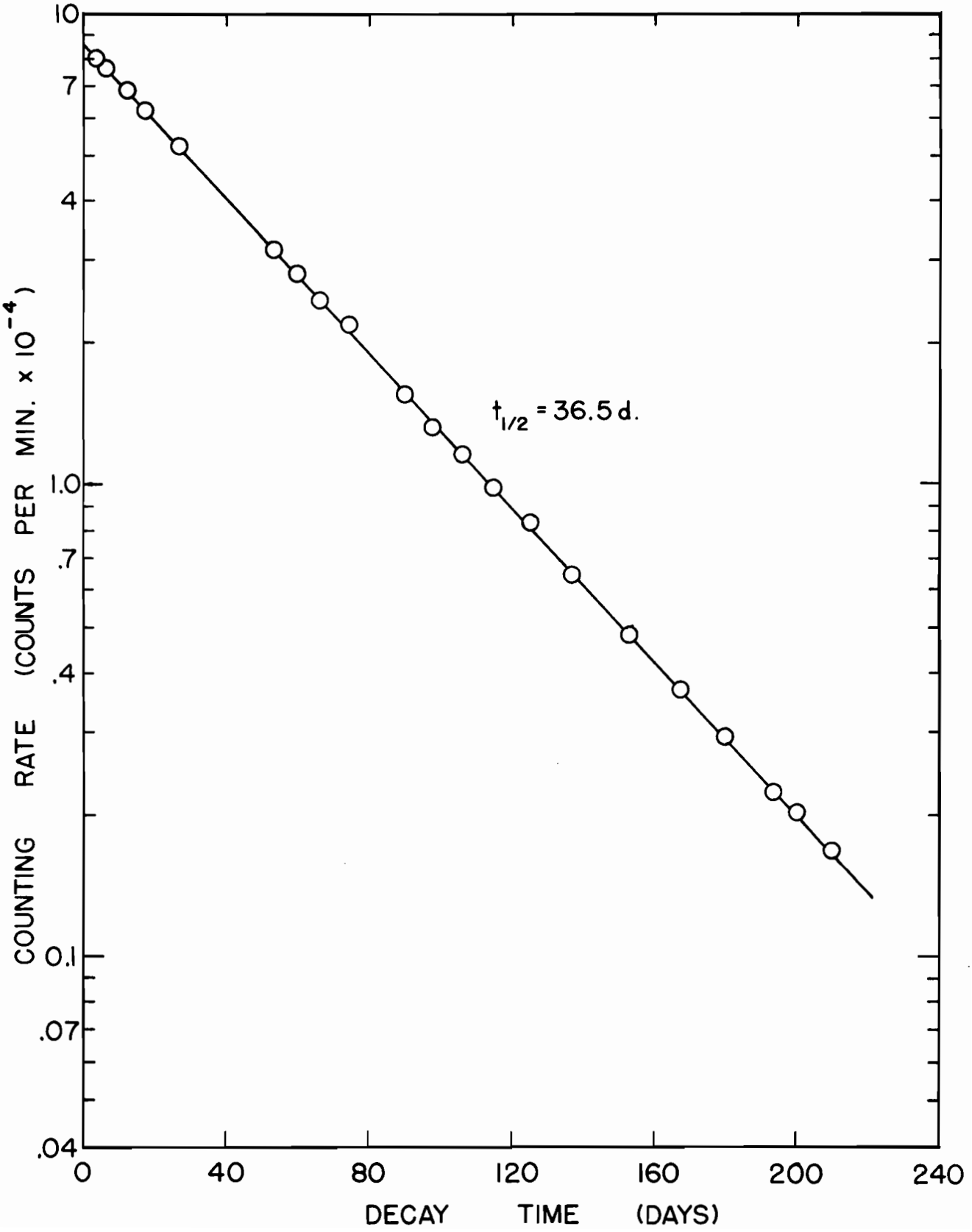
10
7
4
1.0
.7
.4
0.1
.07
.04
COUNTING RATE (COUNTS PER MIN. x 10^{-4})
$t_{1/2}$ = 36.5 d.
0
40
80
120
160
200
240
DECAY TIME (DAYS)

Figure 26

Nb^{95} GAMMA SPECTRUM

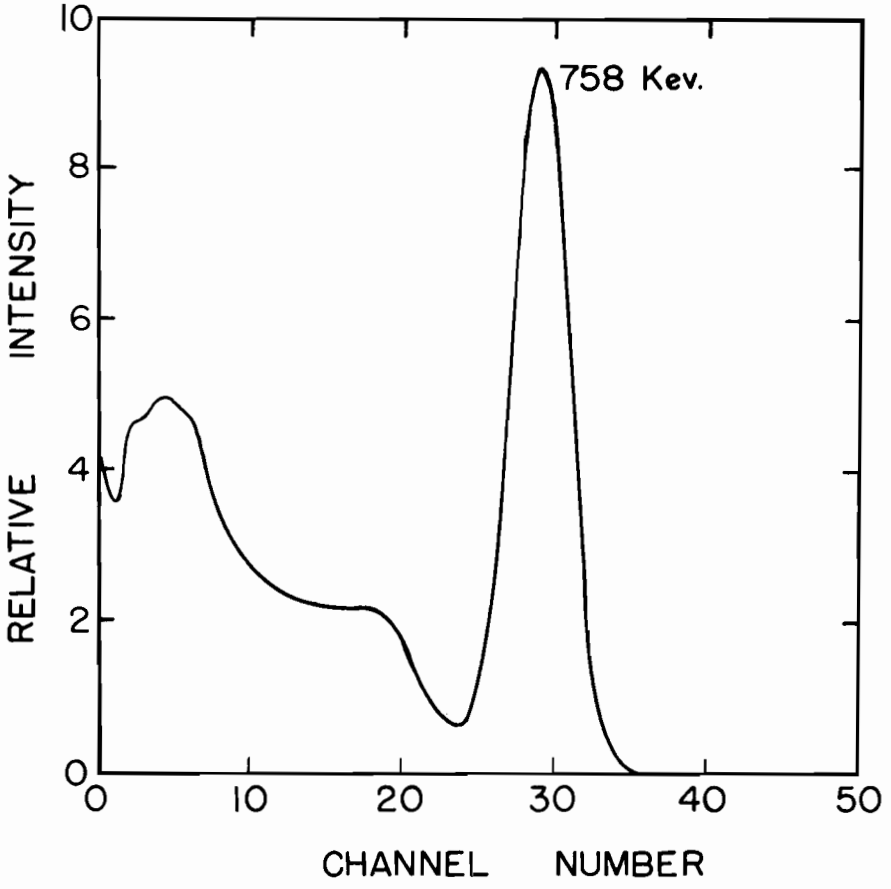
758 Kev.
RELATIVE INTENSITY
CHANNEL NUMBER
0
2
4
6
8
10
0
10
20
30
40
50

Figure 27

DECAY OF 758 KEV GAMMA RAY OF Nb^{95}

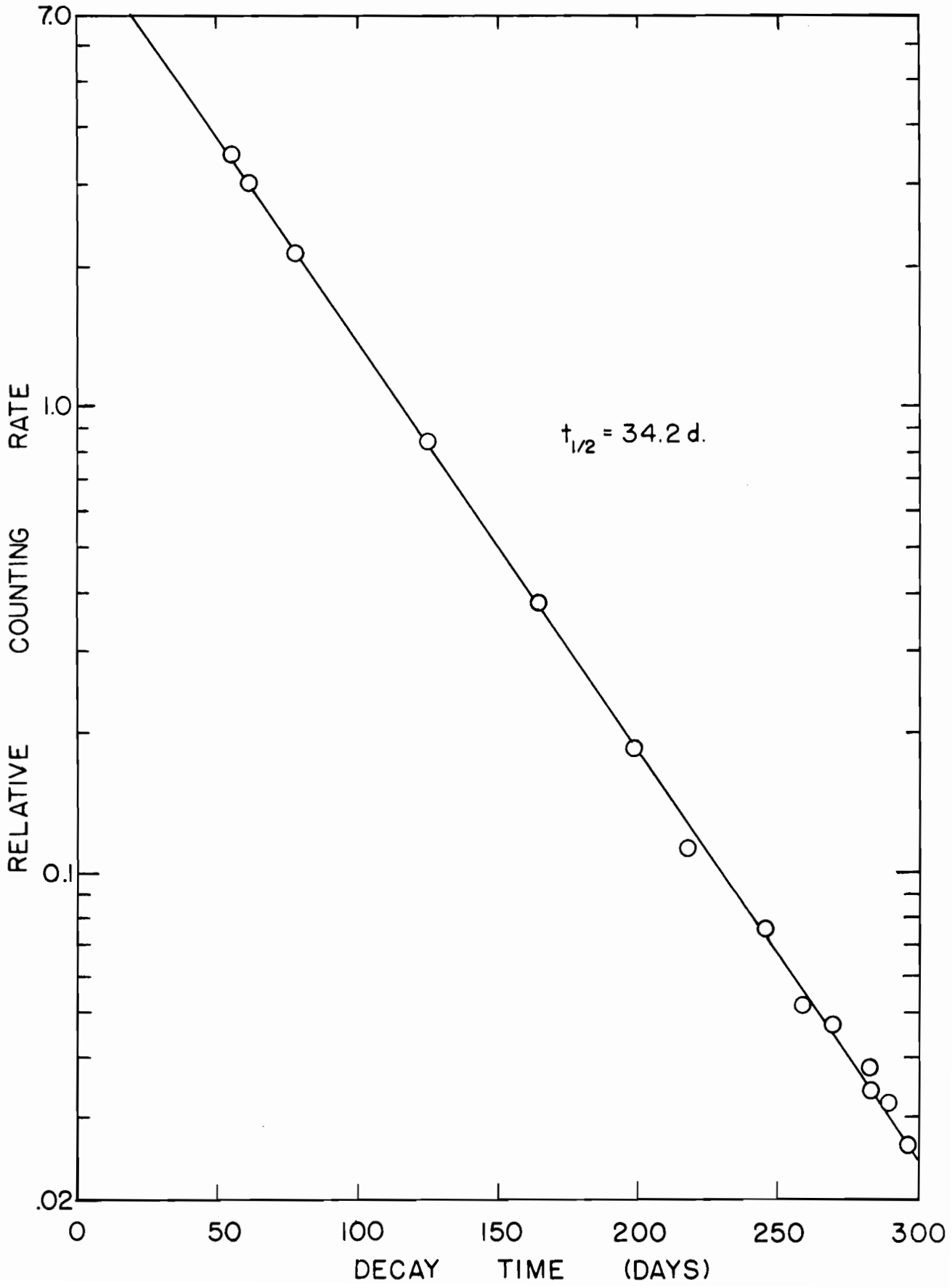
7.0
1.0
0.1
.02
RELATIVE COUNTING RATE
$t_{1/2}$ = 34.2 d.
0
50
100
150
200
250
300
DECAY TIME (DAYS)

disintegrations. Nb^{95} decays with a half-life of 35 days[54] by the emission of 160 kev (99%) and 930 kev (1%) beta rays. A 768 kev gamma ray is in coincidence with the 160 β^- ray.

In the β^- disintegration measurements for Nb^{95}, very large absorption corrections had to be applied because of the amount of oxalic acid necessary to keep the Nb_2O_5 in solution and because of the low energy of the 99% abundant β^- ray. Since Nb^{95} is only one charge unit away from stability, its independent yield will be extremely small and all the niobium activity results from decay of the zirconium parent during and after the irradiation up to the time of separation. Further, since $\lambda_{Zr^{95}} < \lambda_{Nb^{95}}$, equation (22) (P. 36) will apply with the term for the independent yield omitted, that is

$$(N\lambda)_{Nb^{95}} = \frac{Ry_{Zr^{95}}}{\lambda_{Zr^{95}} - \lambda_{Nb^{95}}} \left[\lambda_{Zr^{95}}(1 - e^{-\lambda_{Nb^{95}}T})e^{-\lambda_{Nb^{95}}t} - \lambda_{Nb^{95}}(1 - e^{-\lambda_{Zr^{95}}T})e^{-\lambda_{Zr^{95}}t} \right]$$

where T = the irradiation time.

t = time from end of bombardment to separation of Nb^{95}.

R = fission rate.

$y_{Zr^{95}}$ = fission yield for Zr^{95}.

The yields for zirconium were calculated in this way and are given in Table VII, in which the above equation is expressed as

$$(N\lambda)_{Nb^{95}} = Ry_{Zr^{95}} \times \text{correction factor}$$

Table VII

FISSION YIELD DATA FOR Zr^{95} (65 DAYS) CALCULATED FROM Nb^{95} (35 DAYS) DISINTEGRATION RATES

Irradiation	B	C	D
Observed counting rate	8.60×10^4 c/m	7.30×10^3 c/m	1.70×10^4 c/m
Aliquot factor	1000	500	1000
Chemical yield	63.2%	43.3%	40.5%
Self-absorption	0.811	0.608	0.719
Source-mount absorption	0.987	0.987	0.987
Nb^{95} disintegration rate	2.832×10^6 d/s	2.344×10^5 d/s	9.857×10^5 d/s
Time after irradiation	41.027 d.	188.334 d.	63.176 d.
Time in reactor	2.005 d.	1.993 d.	1.994 d.
Correction factor	9.44×10^{-3}	5.05×10^{-3}	1.034×10^{-2}
Fission rate	6.30×10^9 f/s	8.3364×10^8 f/s	1.9431×10^9 f/s
Zr^{95} fission yield	4.76%	5.57%	4.91%

(f) Molybdenum

The method of Scadden[64] was employed to separate molybdenum from the other fission products. Molybdenum carrier was added to an aliquot of the fission product mixture. The acidity was adjusted to $\sim$1 M and molybdenum precipitated with α-benzoinoxime in ethanol. The precipitate was dissolved in fuming nitric acid and the molybdenum reprecipitated as before, after diluting and partially neutralizing the acid solution. The α-benzoinoxime was destroyed by dissolving the precipitate in fuming nitric acid, adding perchloric acid and boiling down to $HClO_4$ fumes. After a ferric hydroxide scavenge was made, the molybdenum was precipitated as lead molybdate from the buffered solution. The precipitate was dissolved in dilute nitric acid and made up to 10 mls. Chemical yields were determined spectrophotometrically on the coloured molybdenum thiocyanate complex extracted with a carbon tetrachloride-n-amyl alcohol mixture[48]. The standard curve obtained is shown in Fig. 28.

Aliquots of the active solution, on being measured in the beta proportional counter, indicated an initial growth followed by decay with an average half-life of 68.2 hours lasting for about six half-lives (Fig. 29). Thereafter the decay curve began tailing off, indicating the presence of a long-lived activity. The gamma-ray spectrum of an aliquot of the active solution showed gamma peaks at 110, 351, 763,

Figure 28

STANDARD ABSORBANCE CURVE FOR

MOLYBDENUM THIOCYANATE COMPLEX

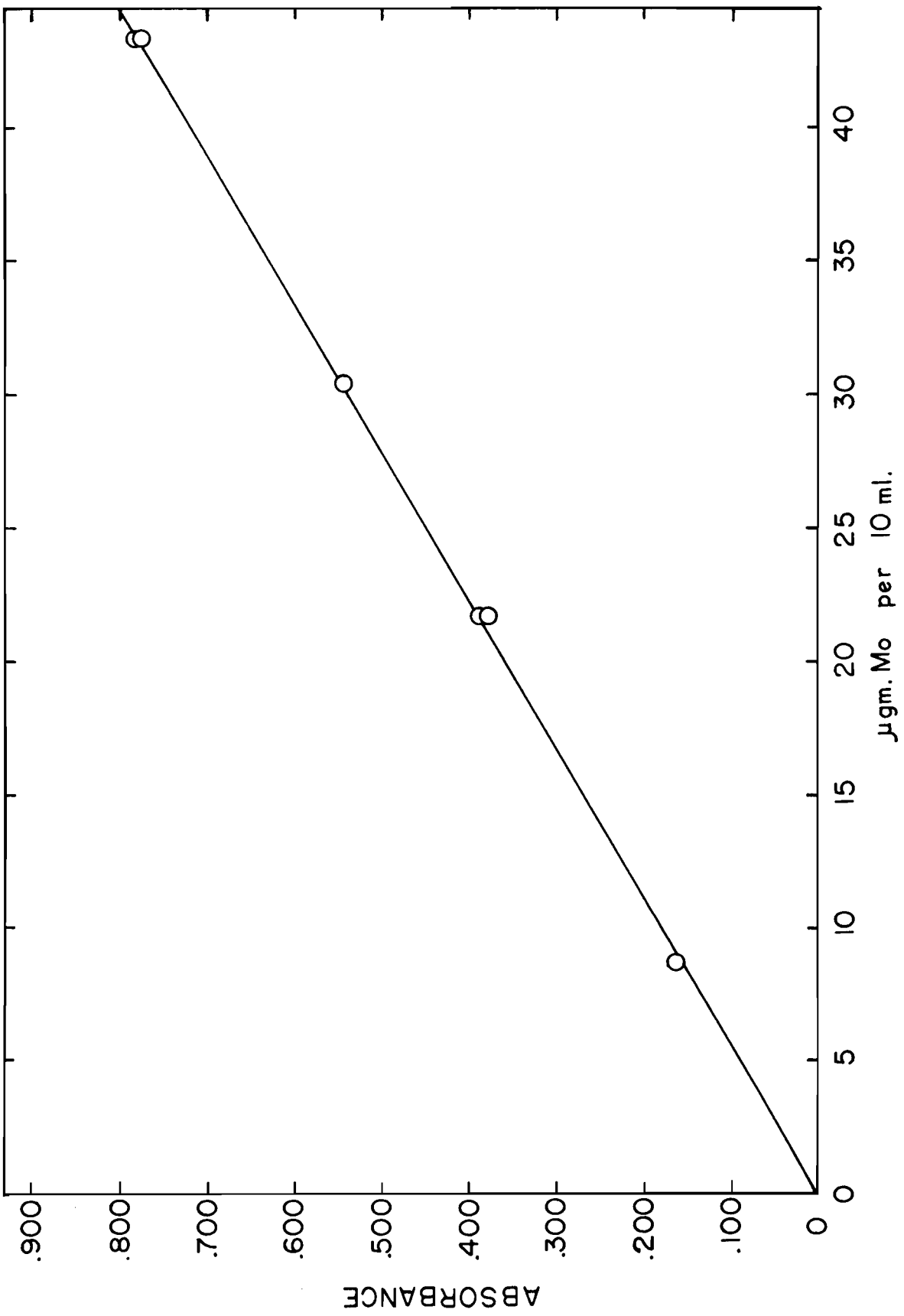
ABSORBANCE
.900
.800
.700
.600
.500
.400
.300
.200
.100
0
0
5
10
15
20
25
30
35
40
µgm. Mo per 10 ml.

Figure 29

DECAY OF MOLYBDENUM ACTIVITY

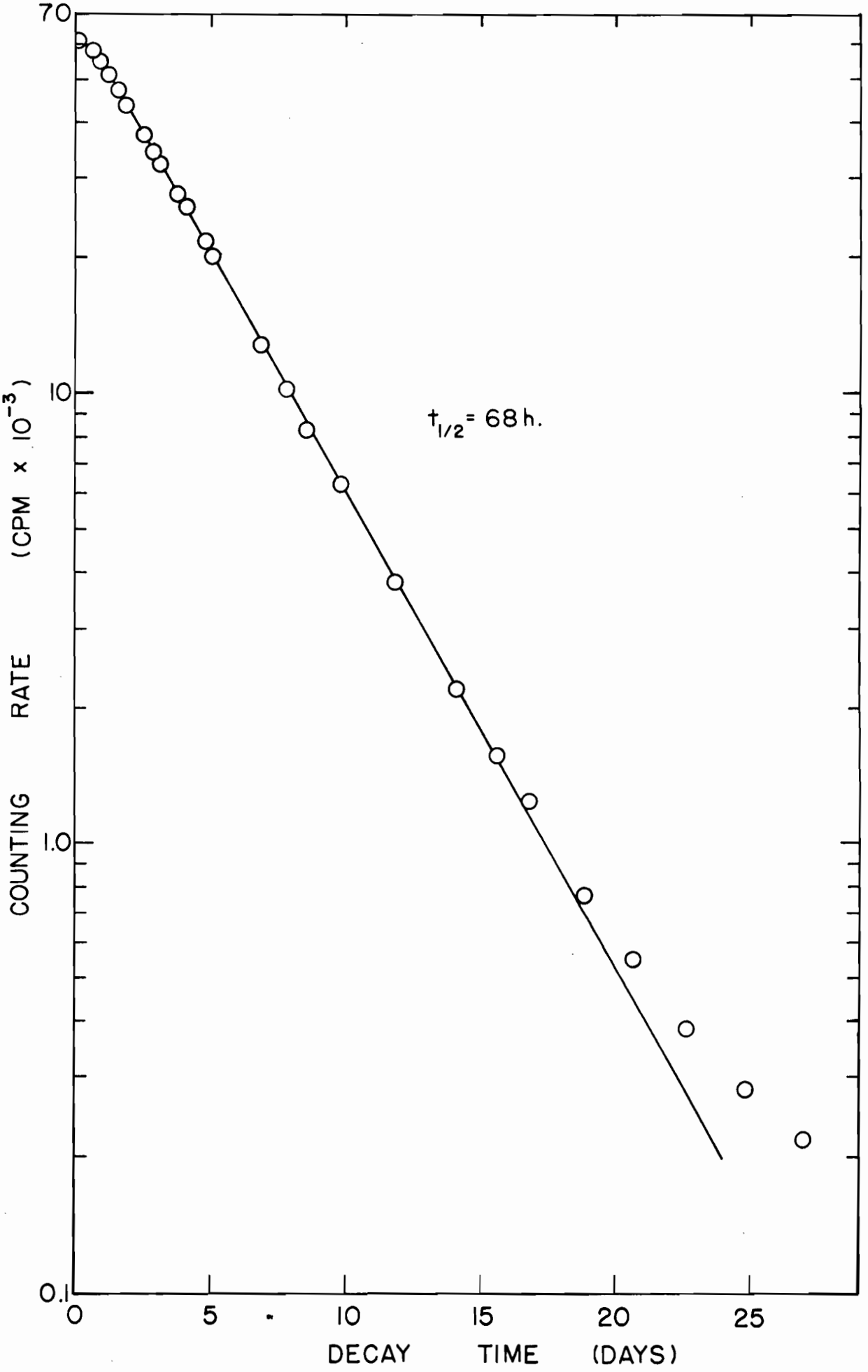
70
10
1.0
0.1
COUNTING RATE (CPM x 10^{-3})
$t_{1/2}$ = 68 h.
0
5
10
15
20
25
DECAY TIME (DAYS)

and 920 kev (Fig. 30). The peaks at 351 and 763 kev decayed with a half-life of 67.8 hours, whereas the 110 kev peak showed an initial growth then decayed with a similar half-life (Fig. 31). Mo^{99} has a reported half-life of 67 hours[54]. It decays by β^- emission with maximum energies of 0.45 (14%), 0.87 ($\sim$ 1%) and 1.23 Mev (85%) to a 6-hour metastable state of Tc^{99} which in turn decays by isomeric transitions to Tc^{99} (2.1×10^5 years). Gamma rays reported have energies of 2, 40, 140, 142, 181, 376, 741, 780, and 950 kev respectively. The 2, 140, and 142 kev gamma rays are associated with the Tc^{99m} transitions. A gamma-ray spectrum given by Heath[65] of an equilibrium mixture of Mo^{99} and Tc^{99m} shows gamma peaks at 0.04, 0.14 - 0.18, 0.36, and 0.75 Mev.

The decay chain involving Mo^{99} is

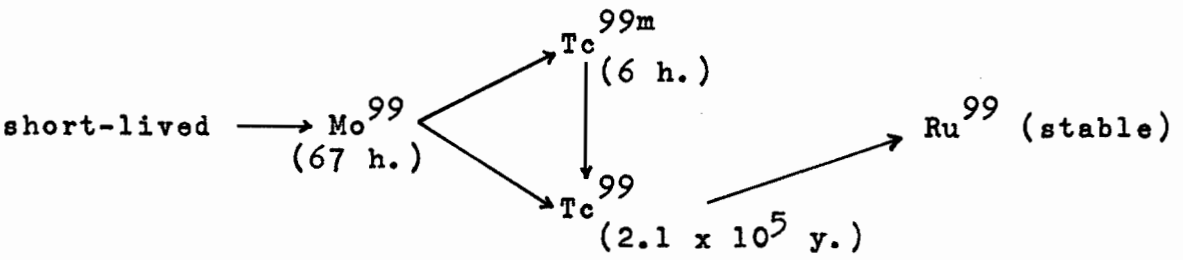

It would be expected that conversion electrons from the Tc^{99m} transitions would contribute to the observed counting rate. Since the complexity of the decay scheme did not allow calculation of this contribution, in order to obtain the Mo^{99} counting rate at separation time, the earlier part of the decay curve was extrapolated back to zero time, as shown in Fig. 32. Fission yield data for Mo^{99} are given in Table VIII.

Figure 30

Mo^{99} GAMMA SPECTRUM

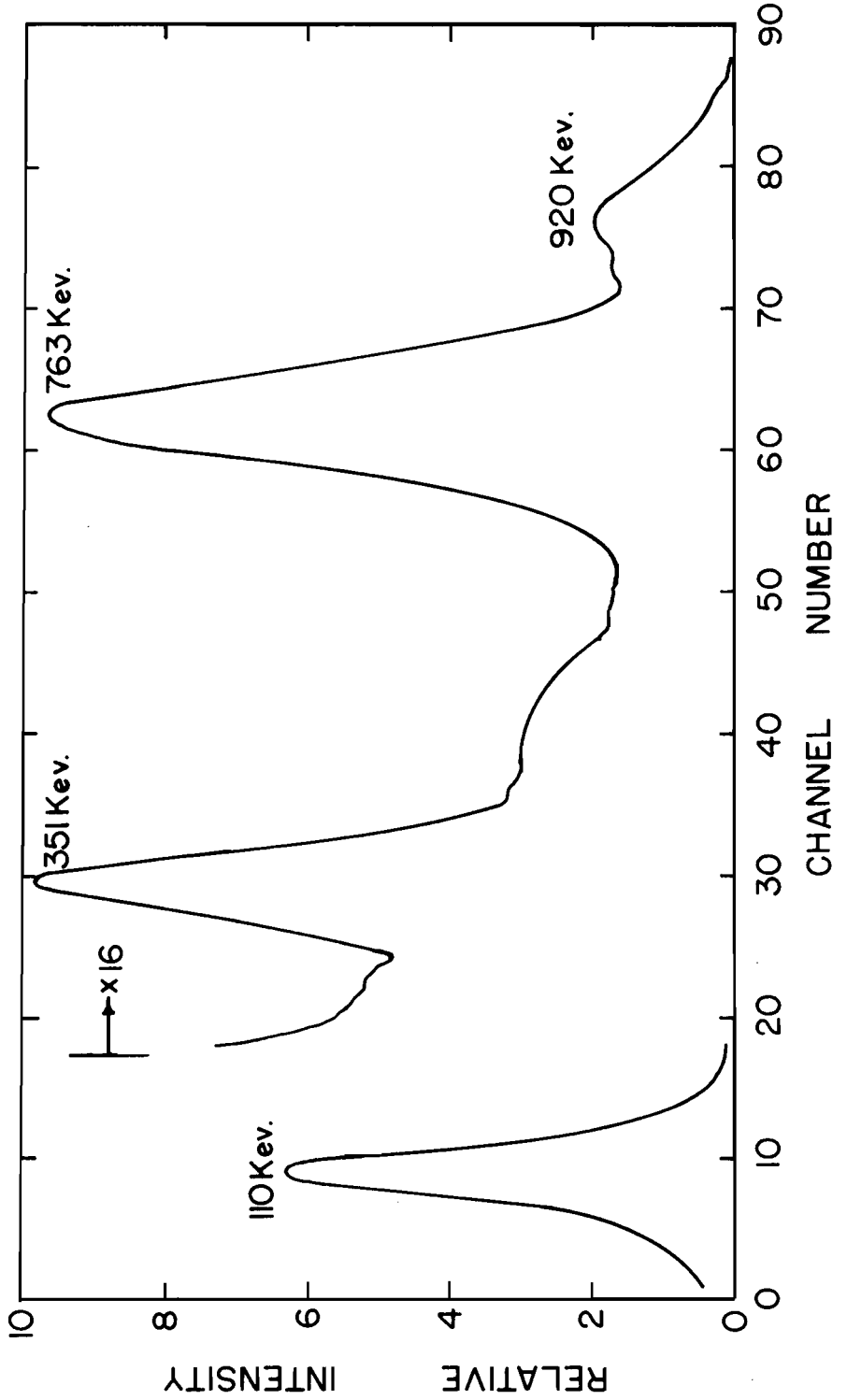
RELATIVE INTENSITY
CHANNEL NUMBER
0
2
4
6
8
10
0
10
20
30
40
50
60
70
80
90
110 Kev.
351 Kev.
763 Kev.
920 Kev.
x16

Figure 31

DECAY OF GAMMA RAYS FROM

MOLYBDENUM FRACTION

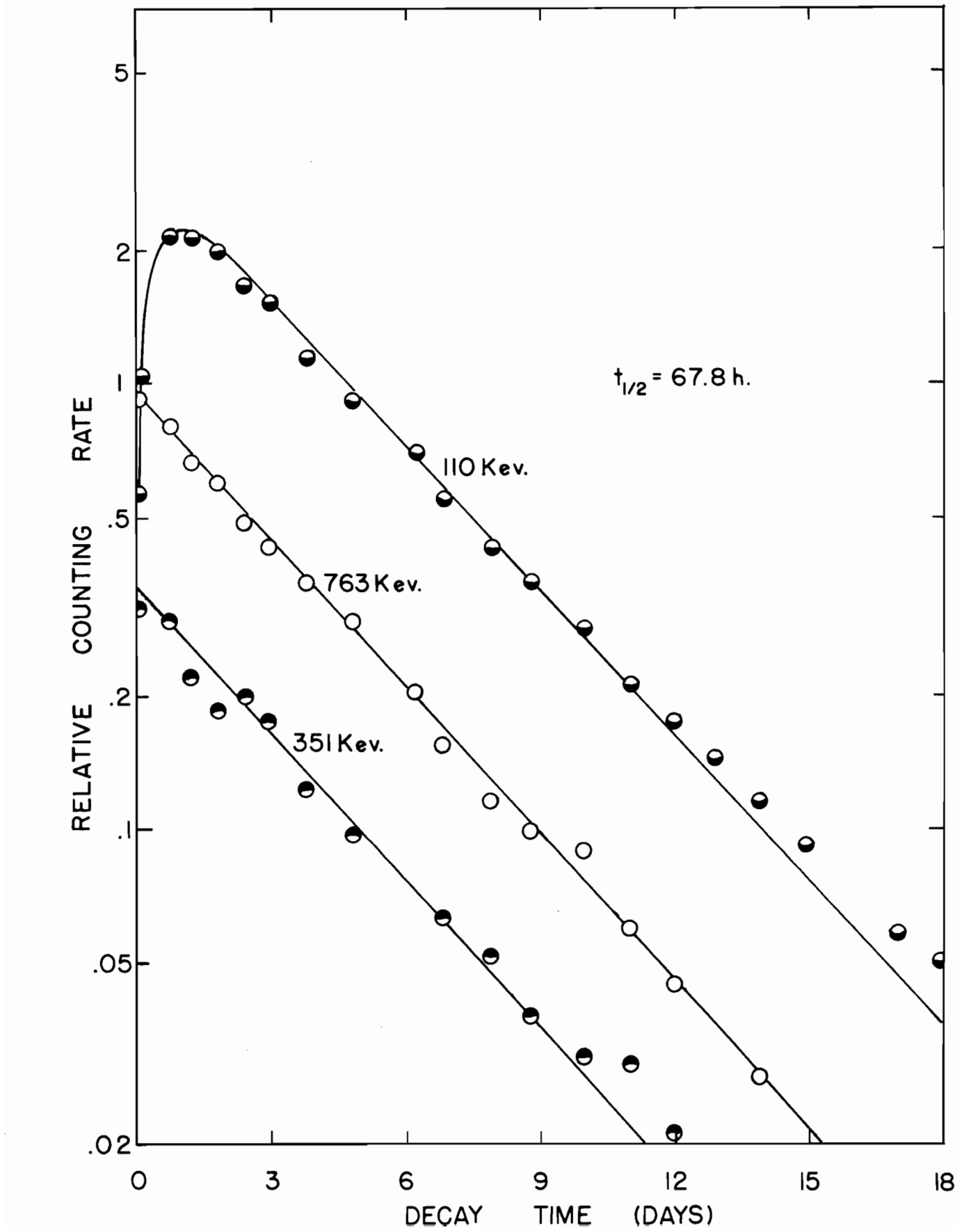
5
2
1
.5
.2
.1
.05
.02
RELATIVE COUNTING RATE
$t_{1/2}$ = 67.8 h.
110 Kev.
763 Kev.
351 Kev.
0
3
6
9
12
15
18
DECAY TIME (DAYS)

Figure 32

INITIAL PORTION OF Mo^{99} DECAY CURVE

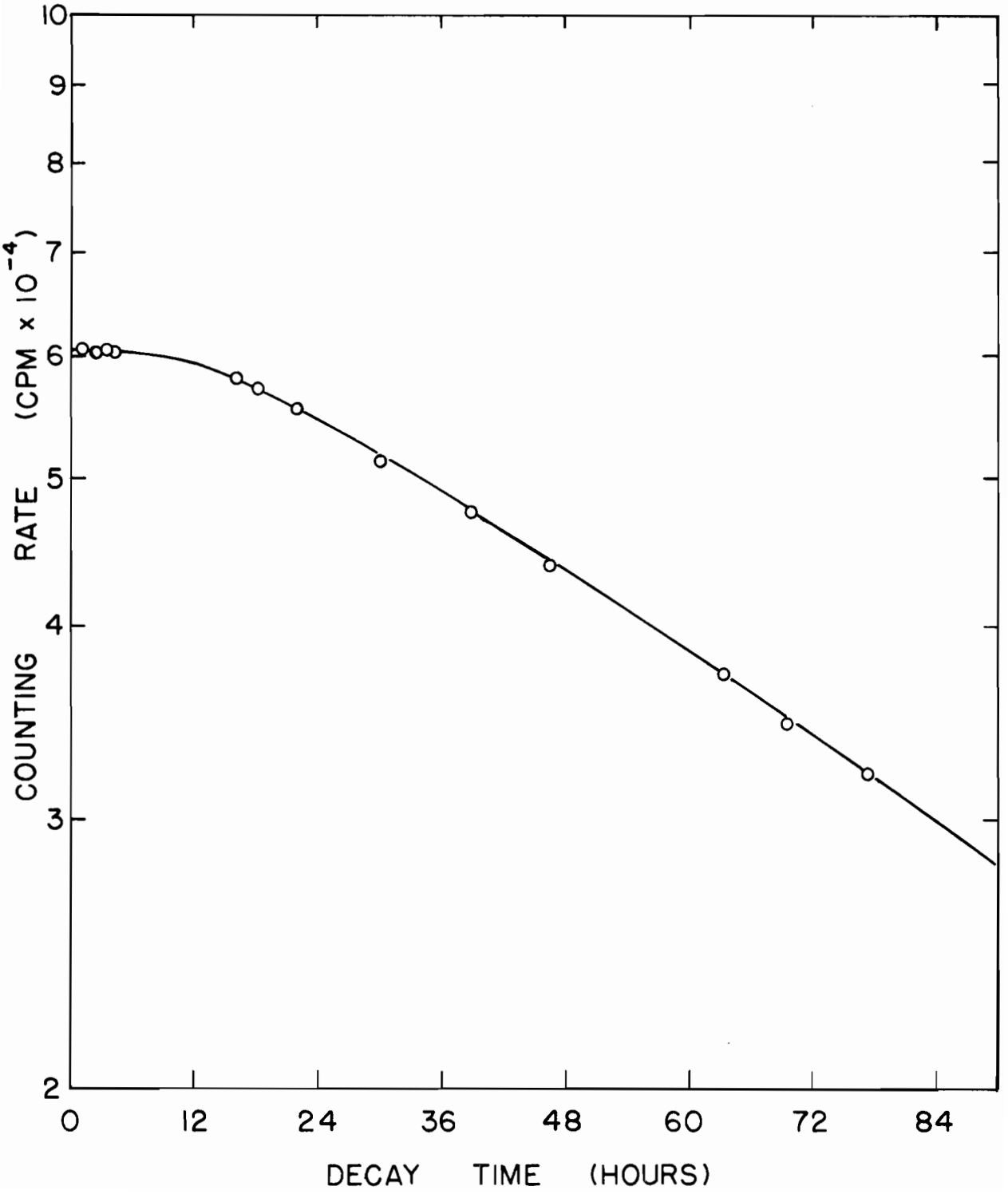
10
9
8
7
6
5
4
3
2
COUNTING RATE (CPM x 10^{-4})
0
12
24
36
48
60
72
84
DECAY TIME (HOURS)

Table VIII

FISSION YIELD DATA FOR Mo^{99} (68 HOURS)

Irradiation	B	C	E	H	J
Observed activity (c/m)	2.73×10^5	3.64×10^3	7.246×10^4	6.05×10^4	4.73×10^4
Source-mount absorption factor	1.00	1.00	1.00	1.00	1.00
Self-absorption factor	1.00	1.00	1.00	1.00	1.00
Aliquot factor	5000	500	1000	1000	1000
Chemical yield (%)	48.5	16.1	25.34	13.2	6.5
Time after irradiation (days)	4.752	18.435	9.359	8.690	7.897
Decay factor	0.3144	0.0112	0.1024	0.1205	0.1462
Time in reactor (days)	2.005	1.993	2.007	2.133	2.056
Saturation factor	0.3863	0.3845	0.3866	0.4051	0.3939
Activity at saturation (d/s)	3.862×10^8	$4.368 \times 10^{*1}$	1.2038×10^8	1.5648×10^8	2.1060×10^8
Fission rate (f/s)	6.300×10^9	8.3364×10^8	2.1633×10^9	2.854×10^9	3.724×10^9
Fission yield (%)	6.13	5.24	5.56	5.48	5.66

(g) Ruthenium

Ruthenium was separated from the other fission products by distilling off the volatile ruthenium oxide, RuO_4[66]. Ruthenium (+ 3), iodide and bromide carriers were added and ruthenium oxidized to volatile RuO_4 with sodium bismuthate and perchloric acid. The ruthenium oxide was then distilled into a sodium hydroxide solution from which it was precipitated by adding ethanol. Further purification was obtained by repeated precipitations of the RuO_4 from alkaline solution with ethanol. The final precipitate was dissolved in 6 M HCl and made up to 10 mls. Chemical yields were determined by developing the strongly coloured ruthenium-thiourea complex[48]. The standardization curve is shown in Fig. 33.

The gross decay curve obtained from 4 π counting was resolved graphically into two components, one with a 1.01-year half-life and the other with a 38-day half-life (Fig. 34). A gamma spectrum of the ruthenium fraction showed a very prominent 508 kev gamma peak (Fig. 35). The decay of this gamma peak, shown in Fig. 36, could be resolved into a 1.0-year half-life and a 37-day half-life. The decay chains of the ruthenium activities expected to be present are

short-lived $Ru^{103} \xrightarrow[39\ d.]{} Rh^{103m} \xrightarrow{57\ m.} Rh^{103}$ (stable

$Ru^{106} \xrightarrow[1.0\ y.]{} Rh^{106} \xrightarrow[30\ s.]{} Pd^{106}$ (stable)

Figure 33

STANDARD ABSORBANCE CURVE FOR

RUTHENIUM-THIOUREA COMPLEX

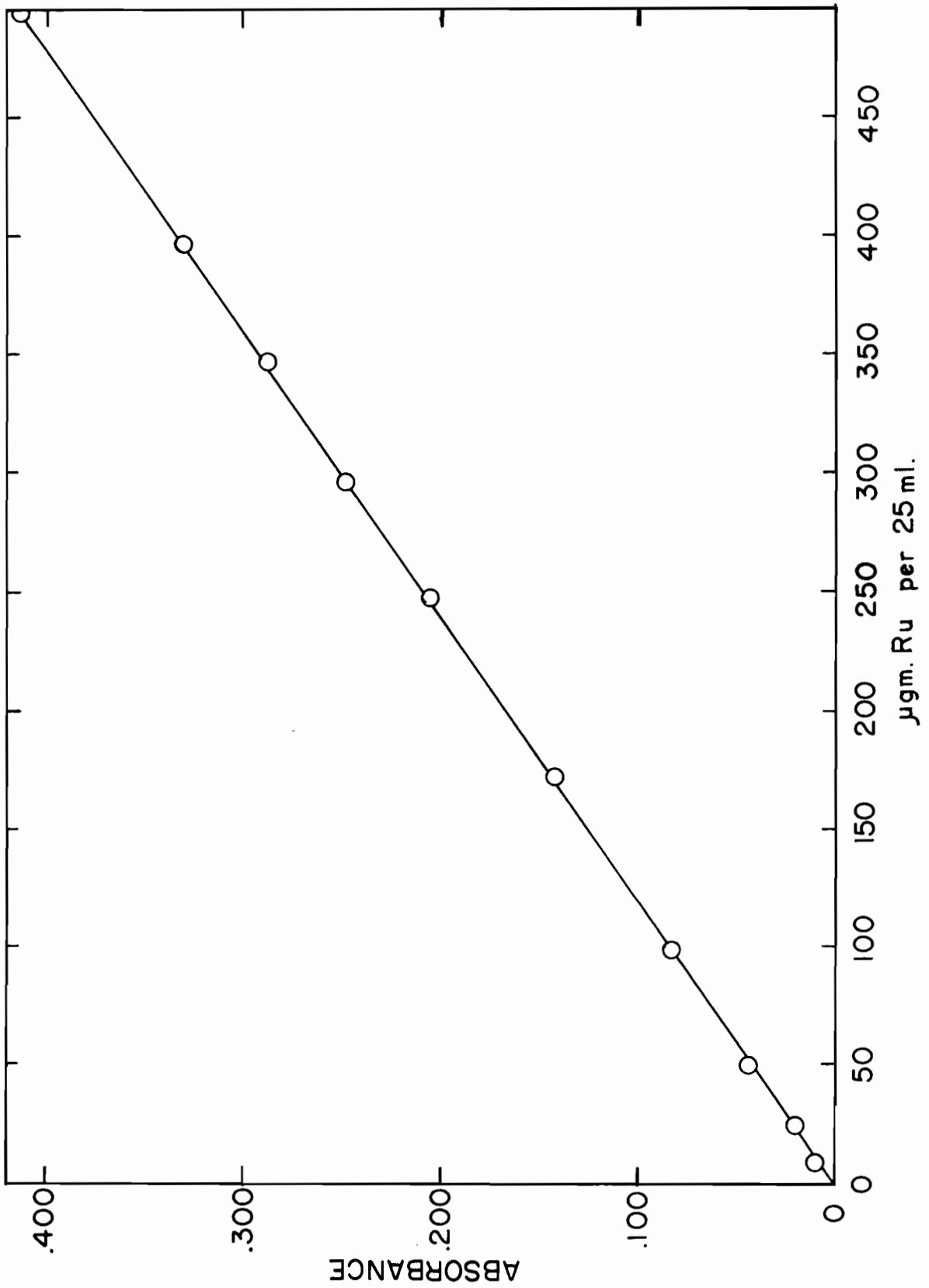
ABSORBANCE
.400
.300
.200
.100
0
0
50
100
150
200
250
300
350
400
450
µgm. Ru per 25 ml.

Figure 34

β^- DECAY OF RUTHENIUM FRACTION

O - Experimental points

● - Long-lived activity subtracted

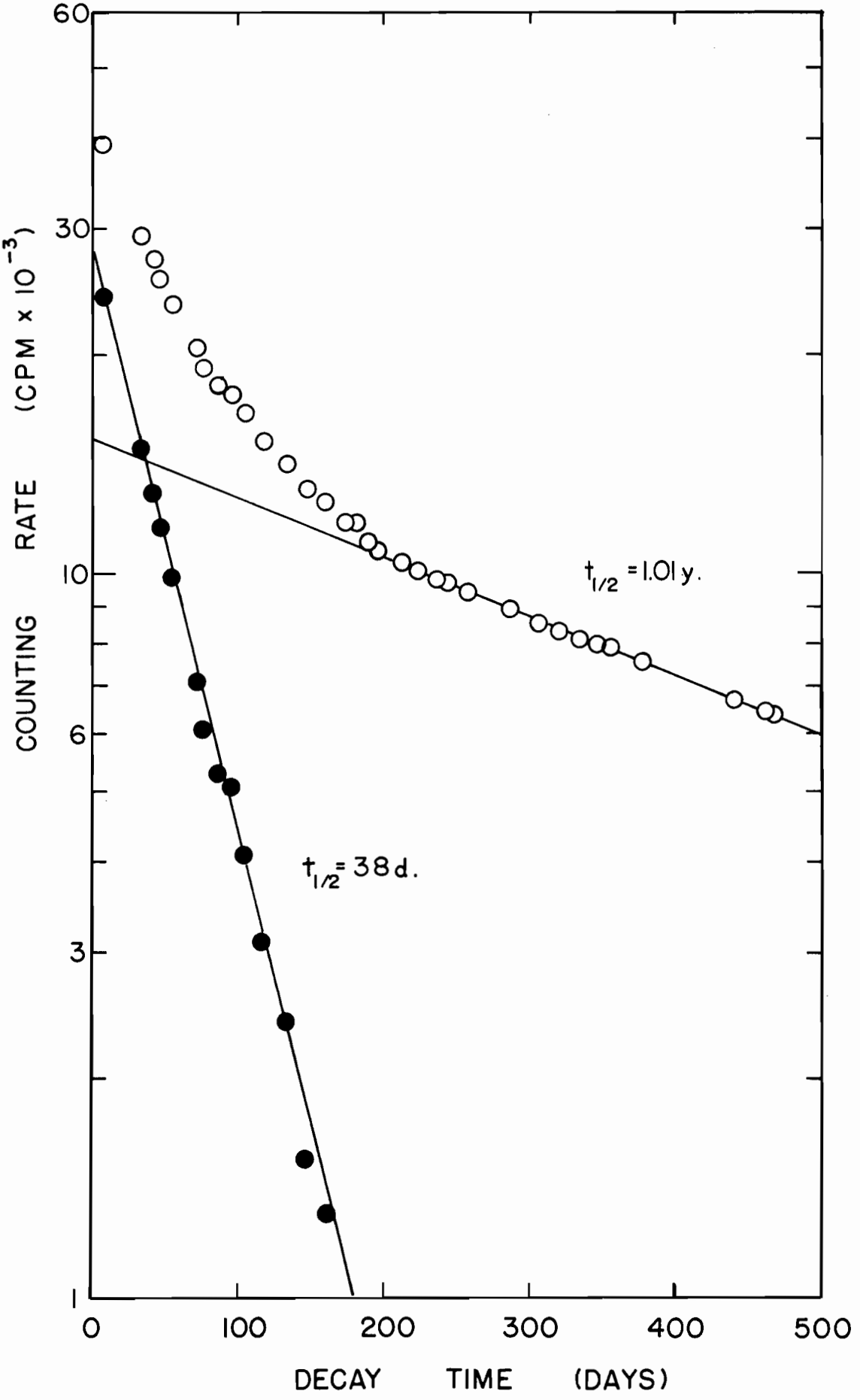
60
30
10
6
3
1
COUNTING RATE (CPM x 10^{-3})
$t_{1/2}$ = 1.01 y.
$t_{1/2}$ = 38 d.
0
100
200
300
400
500
DECAY TIME (DAYS)

Figure 35

GAMMA-RAY SPECTRUM OF THE RUTHENIUM FRACTION

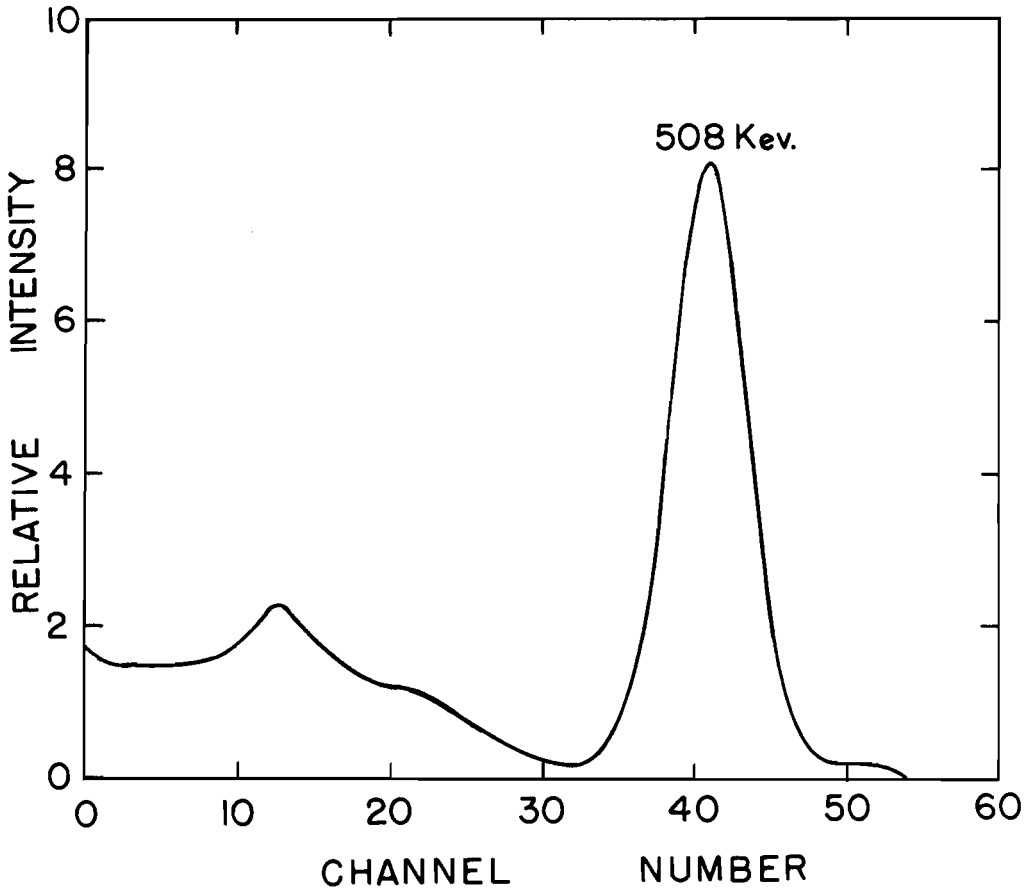
10
8
6
4
2
0
RELATIVE INTENSITY
508 Kev.
0
10
20
30
40
50
60
CHANNEL NUMBER

Figure 36

DECAY OF 508 KEV GAMMA RAY OF

RUTHENIUM FRACTION

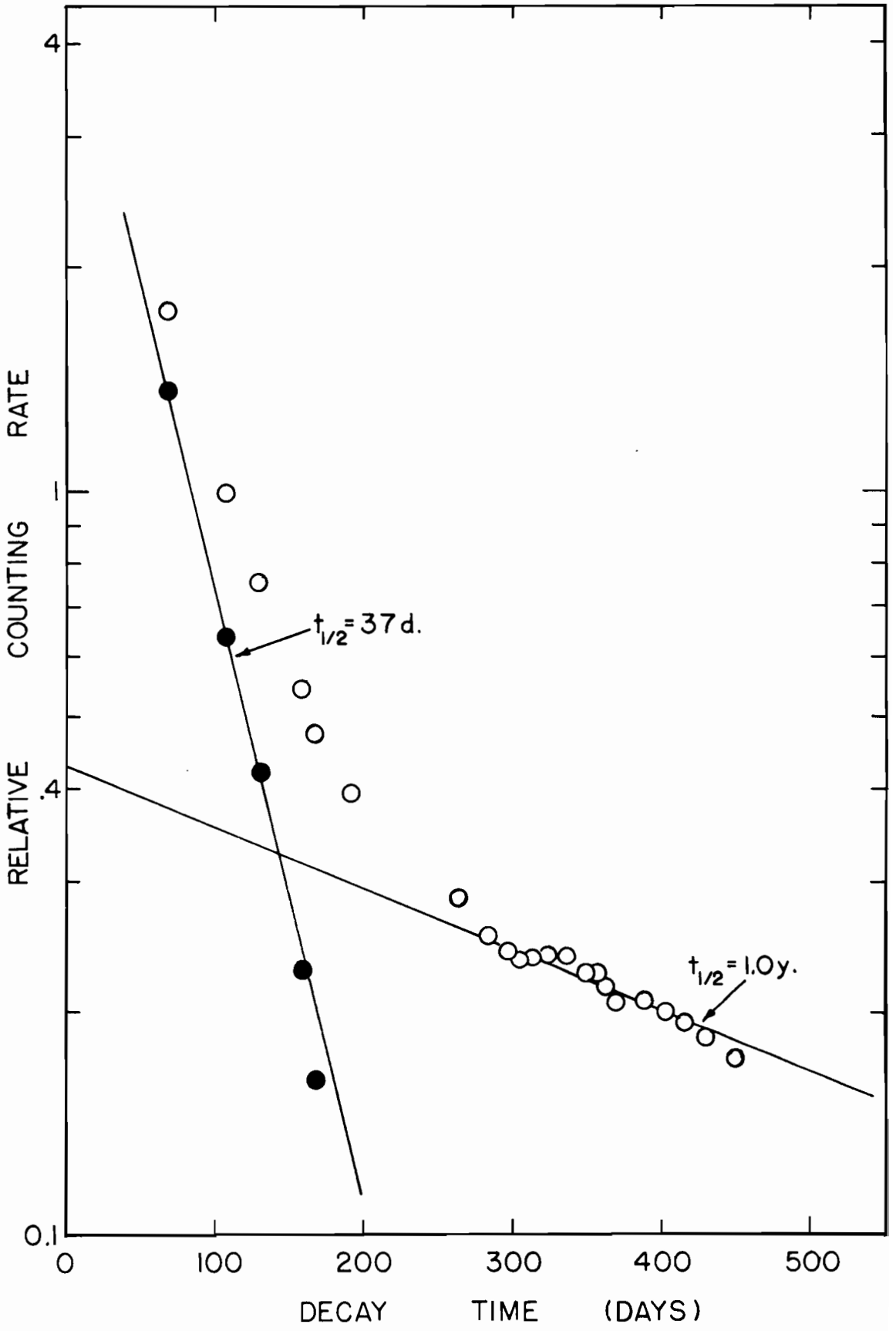
4
1
.4
0.1
RELATIVE COUNTING RATE
$t_{1/2}$ = 37 d.
$t_{1/2}$ = 1.0 y.
0
100
200
300
400
500
DECAY TIME (DAYS)

Ru^{103} has a reported half-life of 39.4 days[67] and decays to Rh^{103m} by beta emission with maximum energies of 100 (7%), 212 (89%), and 710 ($\sim$3%) kev. The 212 kev beta ray is in coincidence with a 498 kev gamma ray which has an equivalent abundance. Rh^{103m} decays to stable Rh^{103} with a half-life of 57 minutes by emitting a 40 kev gamma ray. Ru^{106} decays to Rh^{106} with a half-life of 1.0 year[54] by emitting a 39.2 kev beta particle. Rh^{106} is also beta active, having a half-life of 30 seconds and maximum beta energies of 2.0 (3%), 2.4 (12%), 3.1 (11%), and 3.53 (68%) Mev. Its most intense gamma ray has an energy of 513 kev.

To determine the disintegration rate of Ru^{103}, it is necessary to consider the conversion electron emission from Rh^{103m} (57 m.) which would be detected by the 4π counter. The number of extra events counted per β^- disintegration of Ru^{103} is given by

$$N_{e^-} = \underbrace{\left(\frac{\alpha_T}{1+\alpha_T} \times \text{B.R.}\right)}_{\text{conversion electrons}} + \underbrace{\left(e \times \frac{1}{1+\alpha_T} \times \text{B.R.}\right)}_{\text{unconverted gamma rays}}$$

where α_T = total internal conversion coefficient.

e = efficiency for detecting the unconverted gamma rays.

B.R. = branching ratio.

α_T is calculated to be 484 from the following data $\alpha_K = 40$

and $\alpha_K / \alpha_L = 0.09$[68]. α_K and α_L are the conversion coefficients for the K and L shells respectively. The efficiency for detecting the unconverted 40 kev gamma rays is less than 0.14%[69] so that the second term can be neglected. Therefore

$$N_{e^-} = \left(\frac{484}{485} \times .995\right) = .993.$$

The energies of these conversion electrons are given by

$$E_{e^-} = E_\gamma - B.E.$$

the difference between the gamma-ray energy and the binding energy of the electron in the K or L shell. Strominger et al.[70] give 23.2 and 3.4 kev for the K and L electron binding energies respectively. This results in 9% of the conversion electrons having energies of 17 kev and 91% having 37 kev energy. Since these conversion electrons are monoenergetic, they will be absorbed to a different extent in the source mount and in the source itself than β^- rays of the same maximum energies. It was assumed that the absorption of conversion electrons was equivalent to the absorption of β^- rays having maximum energies of twice the energy of the conversion electrons[71]. If Ru^{103} and Rh^{103m} are represented by subscripts 1 and 2 respectively, then since $\lambda_1 \ll \lambda_2$, at equilibrium

$$N_1 \lambda_1 + N_2 \lambda_2 = N_1 \lambda_1 (1.993)$$

that is

$$N_2 \lambda_2 = 0.993\, N_1 \lambda_1 .$$

Putting $A_1 = c_1 N_1 \lambda_1$ and $A_2 = c_2 N_2 \lambda_2$, where A_1 and A_2 are the observed counting rates of Ru^{103} and Rh^{103m} and c_1, c_2 are detection efficiencies given by the product of the self-absorption factor and the source-mount absorption factor,

$$\text{then} \quad \frac{A_1 + A_2}{A_1} = \frac{c_1 N_1 \lambda_1 + c_2 N_2 \lambda_2}{c_1 N_1 \lambda_1}$$

$$= \frac{c_1 N_1 \lambda_1 + 0.993\ c_2 N_1 \lambda_1}{c_1 N_1 \quad 1}$$

$$= 1 + 0.993 \frac{c_2}{c_1}$$

$$\text{and} \qquad A_1 = \frac{A_1 + A_2}{1 + 0.993 \frac{c_2}{c_1}}$$

that is the counting rate of Ru^{103} is given by dividing the observed counting rate of $Ru^{103} + Rh^{103m}$ by the factor $1 + 0.993 \frac{c_2}{c_1}$. From this $N_1 \lambda_1$, the disintegration rate, for Ru^{103} is given by

$$N_1 \lambda_1 = \frac{A_1}{c_1} = \frac{A_1 + A_2}{c_1 + 0.993\ c_2}$$

Disintegration rates for Ru^{103} were calculated in this way and fission yields computed as shown in Table IX. Using a similar computation, where now subscripts 1 and 2 refer to

Table IX

FISSION YIELD DATA FOR Ru^{103} (38 DAYS)

Irradiation	A	B	C	D
Observed counting rate (c/m)	2.58×10^4	7.62×10^4	1.52×10^4	7.35×10^4
Correction factor	1.658	1.898	1.764	1.864
Correeted counting rate (c/m)	1.556×10^4	4.015×10^4	8.617×10^3	3.943×10^4
Source-mount absorption factor	0.966	0.966	0.966	0.966
Self-absorption factor	0.909	0.976	0.951	0.968
Aliquot factor	2000	4000	500	2000
Chemical yield (%)	80.0	61.0	39.8	84.6
Time after irradiation (days)	129.715	60.985	117.184	49.186
Decay factor	0.1039	0.3449	0.1293	0.4238
Time in reactor (days)	2.033	2.005	1.993	1.994
Saturation factor	0.0349	0.0344	0.0342	0.0342
Activity at saturation (d/s)	2.035×10^8	3.922×10^8	4.440×10^7	1.1463×10^8
Fission rate (f/s)	3.5669×10^9	6.300×10^9	8.3364×10^8	1.9431×10^9
Fission yield (%)	5.71	6.23	5.33	5.90

Ru^{106} (1 yr.) and Rh^{106} (30 sec.), gives the following

$$\frac{A_1 + A_2}{A_1} = \frac{c_1 N_1 \lambda_1 + c_2 N_2 \lambda_2}{c_1 N_1 \lambda_1}$$

In this case, at equilibrium, since $\lambda_1 \ll \lambda_2$,

$$N_1 \lambda_1 = N_2 \lambda_2$$

therefore $$\frac{A_1 + A_2}{A_1} = \frac{c_1 N_1 \lambda_1 + c_2 N_1 \lambda_1}{c_1 N_1 \lambda_1} = 1 + \frac{c_2}{c_1}$$

The β^- rays of Rh^{106} all have energies > 2 Mev and would therefore be absorbed to a negligible extent. Thus $c_2 = 1$ and

$$\frac{A_1 + A_2}{A_1} = 1 + \frac{1}{c_1}$$

and $$N_1 \lambda_1 = \frac{A_1}{c_1} = \frac{A_1 + A_2}{1 + c_1}$$

The disintegration rate for Ru^{106} is therefore given by dividing the observed counting rate of $Ru^{106} + Rh^{106}$ by the factor $1 + c_1$. Fission yield data for Ru^{106} are given in Table X.

Table X

FISSION YIELD DATA FOR Ru^{106} (1.01 YEARS)

Irradiation	A	B	C	D
Observed counting rate (c/m)	1.535×10^4	1.43×10^4	6.98×10^3	1.05×10^4
Correction factor	3.433	2.312	2.912	2.527
Corrected counting rate (c/m)	4.471×10^3	6.185×10^4	2.397×10^3	4.155×10^3
Source-mount absorption factor	0.934	0.934	0.934	0.934
Self-absorption factor	0.440	0.816	0.540	0.700
Aliquot factor	2000	4000	500	2000
Chemical yield (%)	80.0	61.0	39.8	84.6
Time after irradiation (days)	129.715	60.985	117.184	49.186
Decay factor	0.7836	0.8917	0.8023	0.9117
Time in reactor (days)	2.033	2.005	1.993	1.994
Saturation factor	0.00382	0.00376	0.00375	0.00375
Activity at saturation (d/s)	1.514×10^8	2.647×10^8	3.310×10^7	7.312×10^7
Fission rate (f/s)	3.5669×10^9	6.300×10^9	8.3364×10^8	1.9431×10^9
Fission yield (%)	4.24	4.20	3.97	3.76

(h) Rhodium

Following a method due to Ballou[72] the pyridine complex of rhodium was extracted into pyridine from a strongly alkaline solution to separate rhodium from a fission product aliquot. Decontamination from tellurium is achieved by adding $Te^{(IV)}$ hold-back carrier along with Rh^{+3} carrier before the extraction. The rhodium was recovered from the pyridine layer by precipitating Rh_2S_3 with H_2S. The precipitate was dissolved in aqua regia, ruthenium was removed by adding Ru^{+3} carrier and distilling the ruthenium by fuming with $HClO_4$ and finally halogens were removed by adding I^- carrier and again fuming with $HClO_4$. Rh_2S_3 was again precipitated, dissolved in a minimum of aqua regia and made up to volume. Chemical yields were determined spectrophotometrically by the stannous chloride method[73] which gave a standard curve as shown in Fig. 37.

The β^- decay of the rhodium activity measured on the 4 π counter showed a single component with a half-life of 36 hours (Fig. 38) measured over seven half-lives. The gamma spectrum contained one photopeak at 315 kev (Fig. 39) which decayed with a half-life of 36 hours (Fig. 40). The rhodium activity expected to be present was Rh^{105}, a member of the decay chain

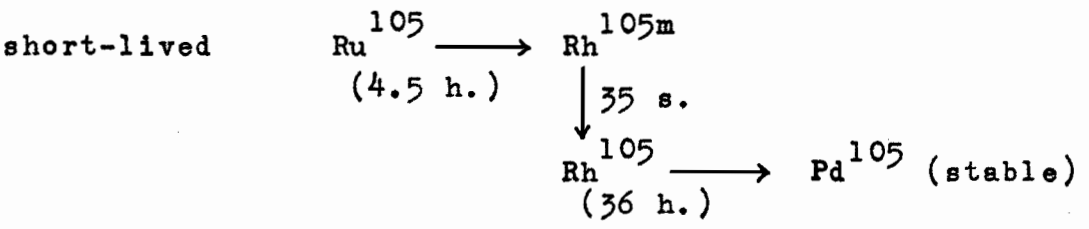

Figure 37

RHODIUM STANDARD ABSORBANCE CURVE

STANNOUS CHLORIDE METHOD(73)

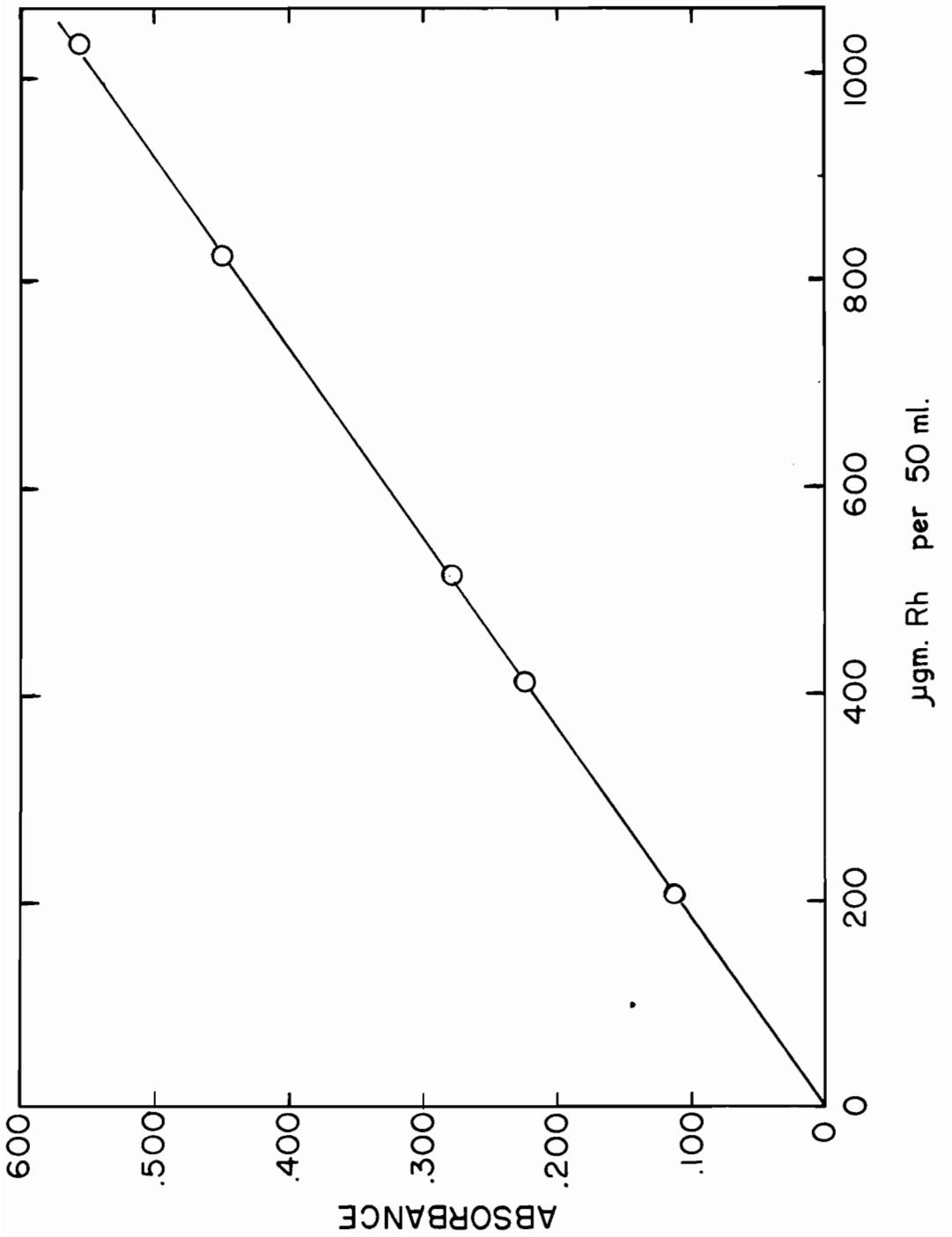
ABSORBANCE
.600
.500
.400
.300
.200
.100
0
0
200
400
600
800
1000
µgm. Rh per 50 ml.

Figure 38

β^- DECAY OF Rh^{105}

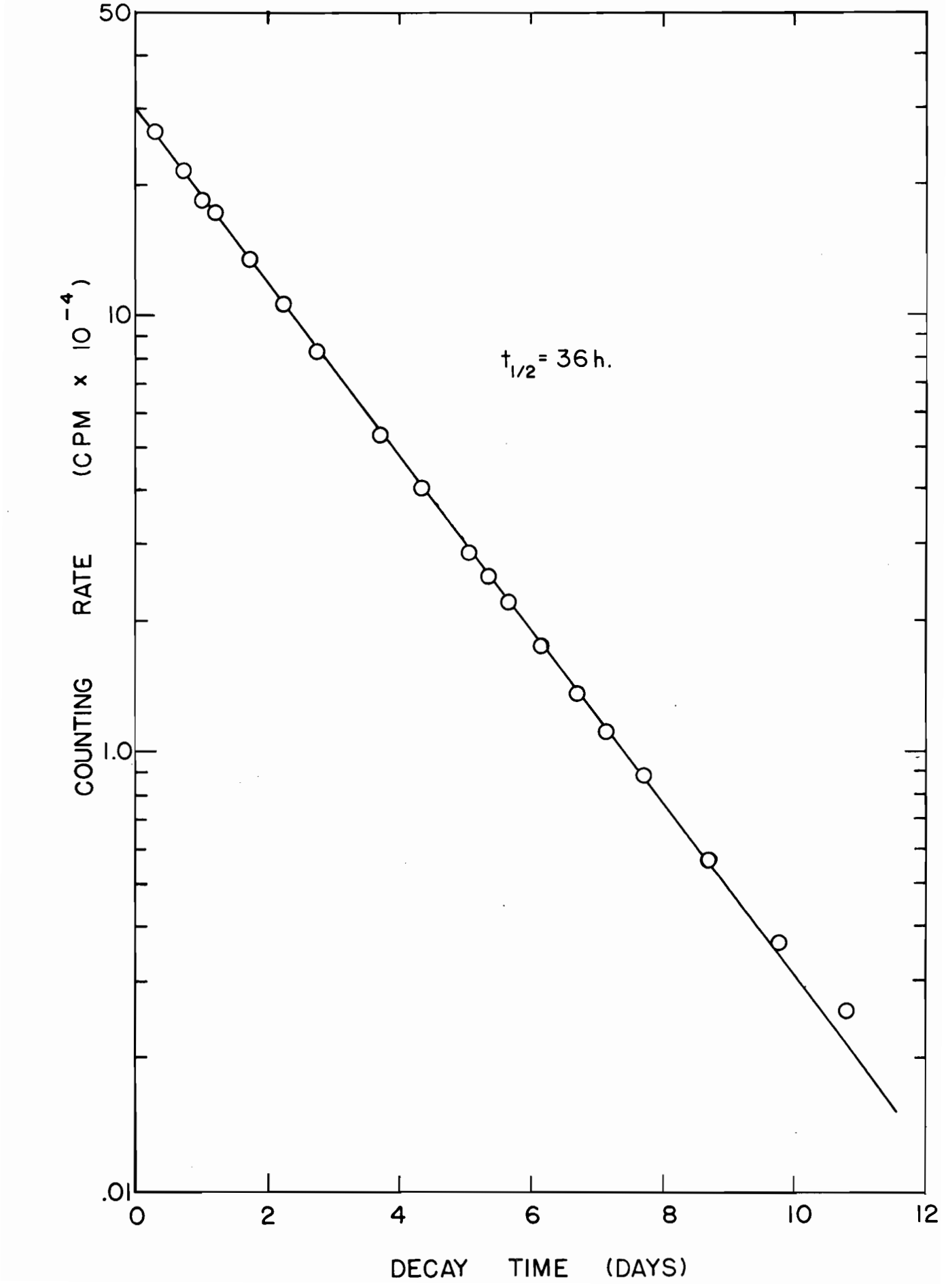
50
10
1.0
.01
COUNTING RATE (CPM x 10^{-4})
$t_{1/2}$ = 36 h.
0
2
4
6
8
10
12
DECAY TIME (DAYS)

Figure 39

GAMMA-RAY SPECTRUM OF Rh^{105}

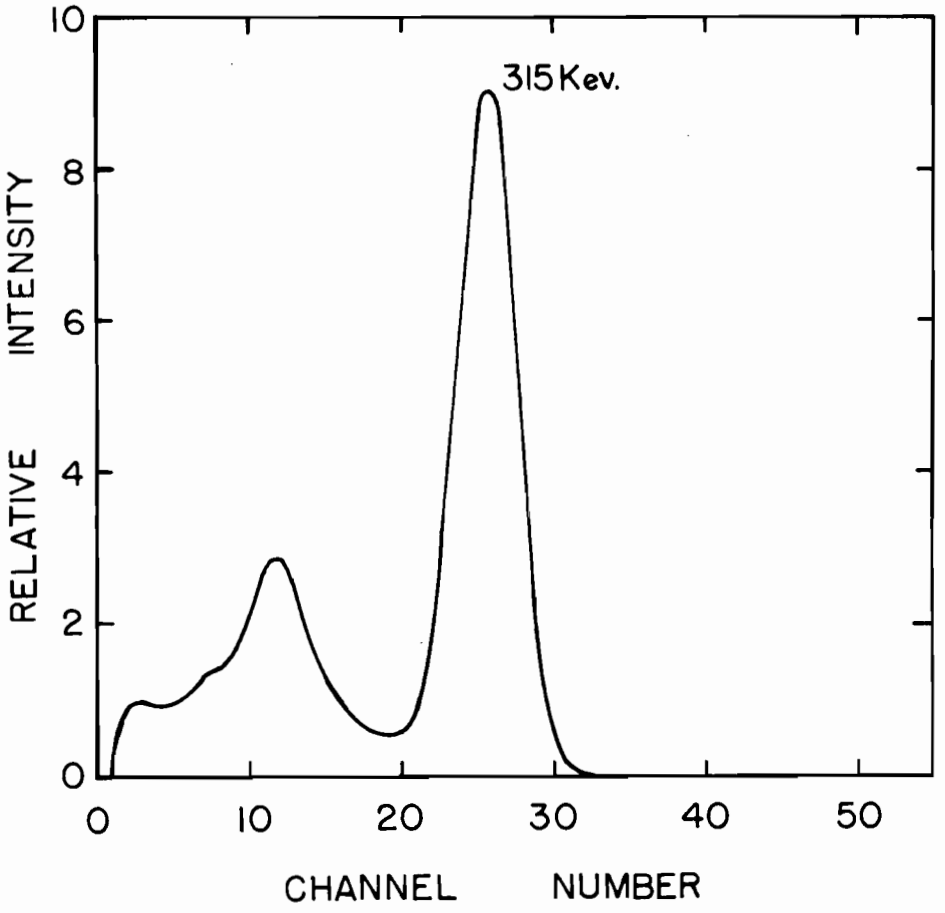
315 Kev.
RELATIVE INTENSITY
0
2
4
6
8
10
0
10
20
30
40
50
CHANNEL NUMBER

Figure 40

DECAY OF 315 KEV GAMMA RAY OF

RHODIUM ACTIVITY

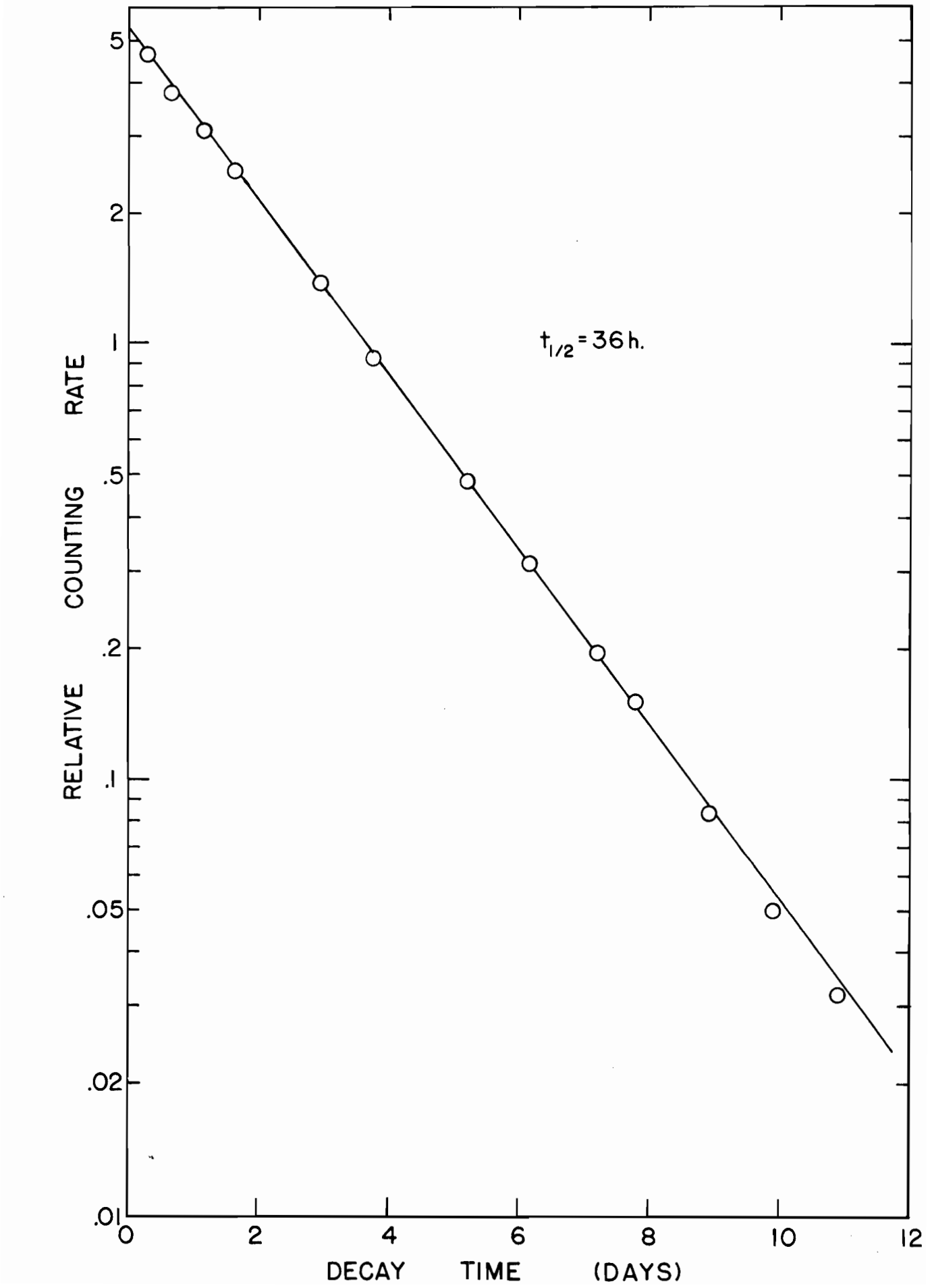
RELATIVE COUNTING RATE
5
2
1
.5
.2
.1
.05
.02
.01
$t_{1/2}$ = 36 h.
0
2
4
6
8
10
12
DECAY TIME (DAYS)

Rh^{105} has a half-life of 36 hours[54] and decays by the emission of 250 kev (10%) and 565 kev (90%) β^- rays. A 319 kev gamma ray is in coincidence with the 250 kev β^- ray. Fission yield data for rhodium are given in Table XI.

Table XI

FISSION YIELD DATA FOR Rh^{105} (36 HOURS)

Irradiation	H	J
Observed activity	1.10×10^5 c/m	3.00×10^5 c/m
Source-mount absortpion factor	0.997	0.997
Self-absorption factor	0.993	1.00
Aliquot factor	1000	2500
Chemical yield	38.44%	37.00%
Time after irradiation	6.543 d.	2.800 d.
Decay factor	0.0487	0.2743
Time in reactor	2.133 d.	2.056 d.
Saturation factor	0.6279	0.6132
Activity at saturation	1.575×10^8 d/s	2.014×10^8 d/s
Fission rate	2.854×10^9 f/s	3.724×10^9 f/s
Fission yield	5.52%	5.41%

(i) Silver

The method of Glendenin[74] was used to separate silver. Silver chloride was precipitated by adding silver carrier to an aliquot of the fission product solution which had been diluted so that the concentration of HCl was $\sim$ 0.3 M. Exchange between the carrier and any silver activity was ensured by gentle boiling and brisk stirring. After the AgCl was dissolved in ammonium hydroxide, purification was achieved by performing two cycles of ferric hydroxide scavenging followed by precipitation of Ag_2S, the silver sulphide being dissolved in nitric acid in between cycles. Silver is finally precipitated as AgCl which is dissolved in ammonium hydroxide and made up to a volume of 10 mls. Chemical yields were determined by titrating with EDTA the Ni^{+2} liberated on reacting Ag^{+} with tetracyanonickelate ion, $[Ni(CN)_4]^{-2}$, in ammoniacal solution, murexide being used as indicator[49]. The gross β^- decay curve was resolved into a 7.5-day component (Fig. 41) and a 3.14-hour component (Fig. 42). The gamma spectrum observed showed gamma peaks at 230, 340, and 625 kev (Fig. 43). The 340 kev gamma ray was seen to decay with a half-life of 7.5 days (Fig. 44) while the 625 kev gamma ray decayed with a half-life of 3.2 hours (Fig. 45). The silver activities expected to be present occur in the following decay chains

$$\text{short-lived} \longrightarrow Ag^{111}\ 7.5\ \text{d.} \longrightarrow Cd^{111}\ \text{(stable)}.$$

$$21\text{-h. } Pd^{112} \longrightarrow 3.2\text{-h. } Ag^{112} \longrightarrow Cd^{112}\ \text{(stable)}.$$

Figure 41

β^- DECAY OF Ag^{111}

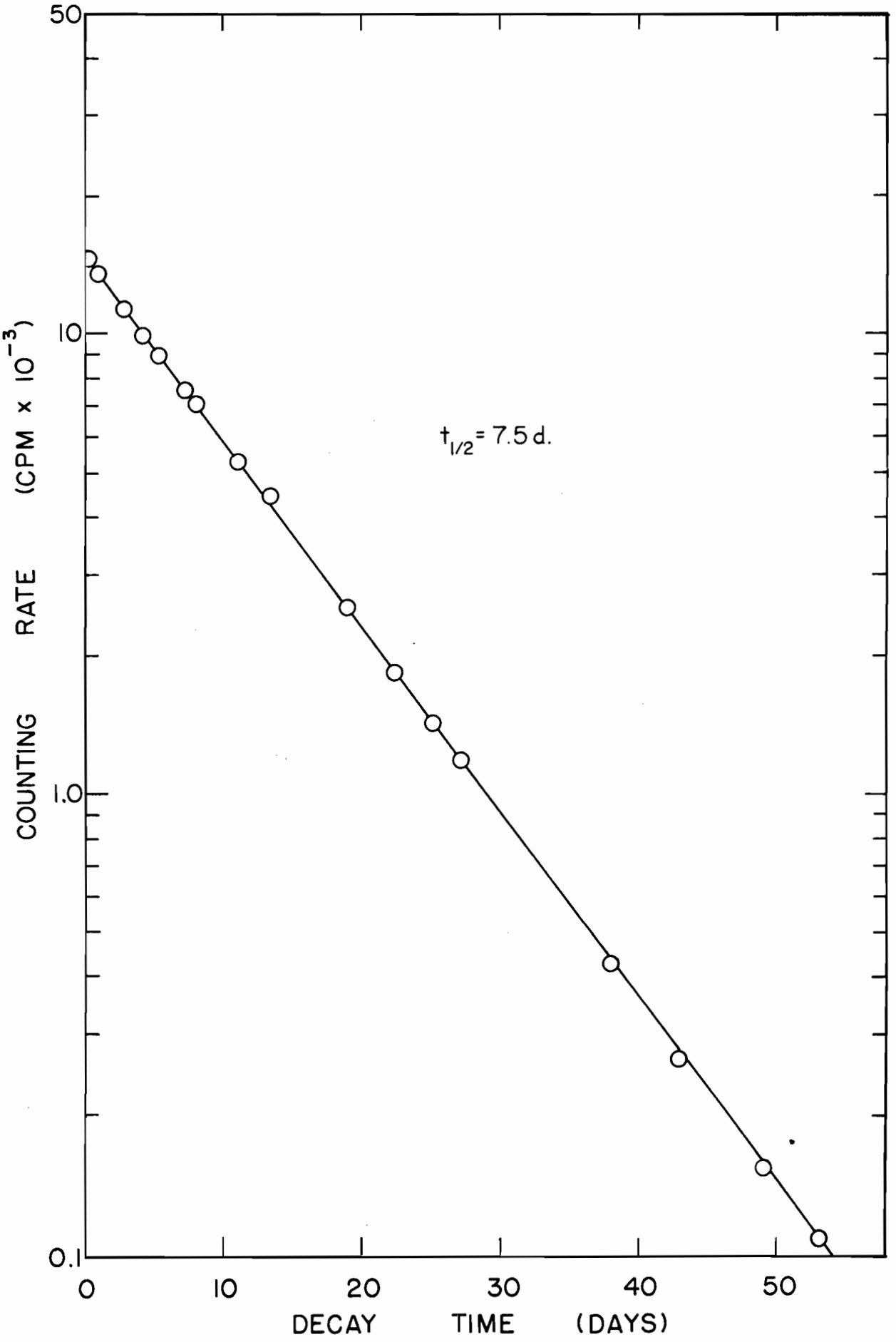
50
10
1.0
0.1
COUNTING RATE (CPM x 10^{-3})
$t_{1/2}$ = 7.5 d.
0
10
20
30
40
50
DECAY TIME (DAYS)

Figure 42

β^- DECAY OF Ag^{112}

O Experimental points

● 7.5-day activity subtracted

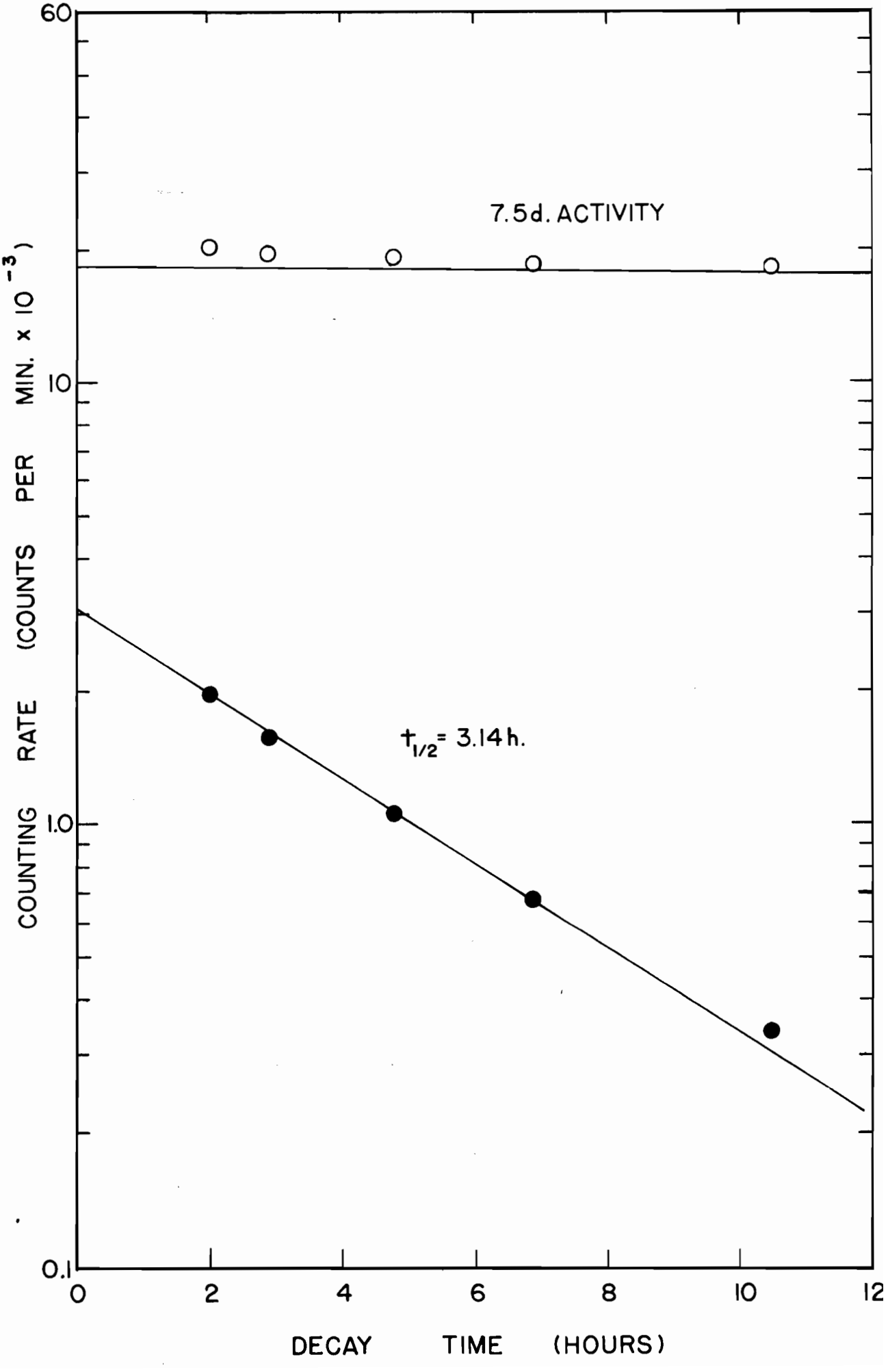
60
10
1.0
0.1
7.5d. ACTIVITY
$t_{1/2}$= 3.14h.
COUNTING RATE (COUNTS PER MIN. x 10^{-3})
0
2
4
6
8
10
12
DECAY TIME (HOURS)

Figure 43

GAMMA-RAY SPECTRUM OF SILVER FRACTION

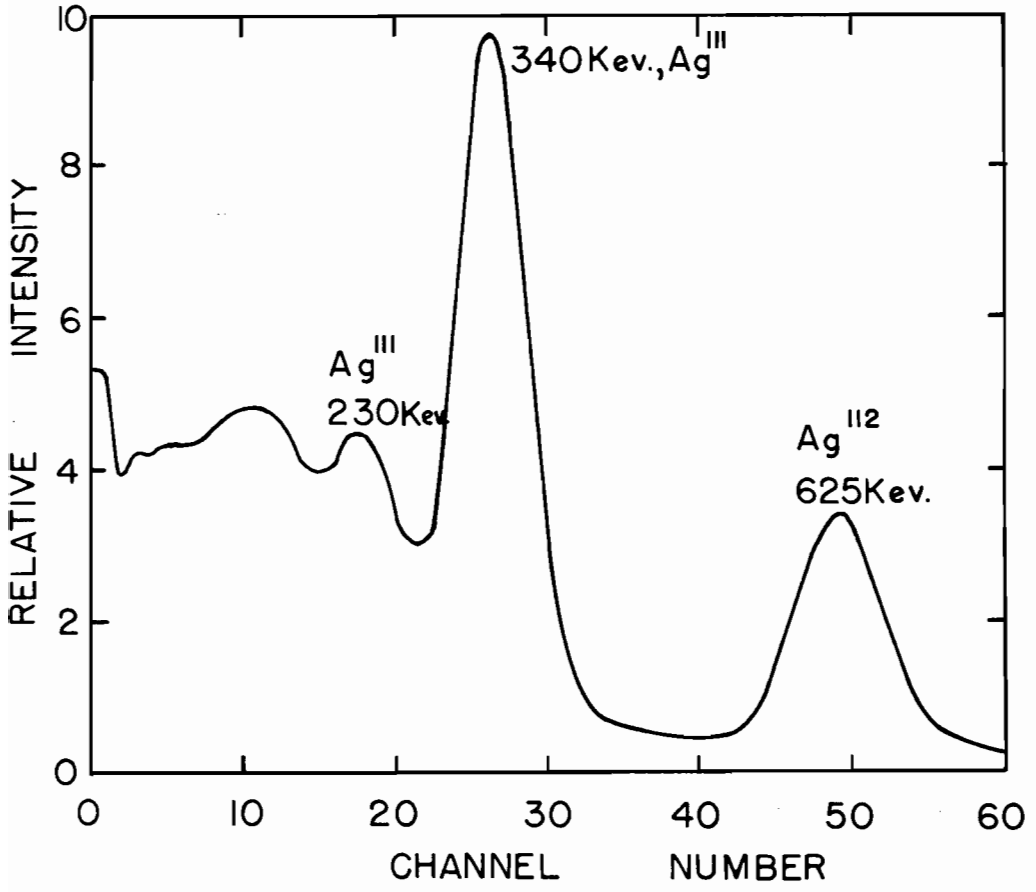
340Kev., Ag111
Ag111
230Kev.
Ag112
625Kev.
RELATIVE INTENSITY
CHANNEL NUMBER
0
2
4
6
8
10
0
10
20
30
40
50
60

Figure 44

DECAY OF 340 KEV GAMMA RAY OF

SILVER FRACTION

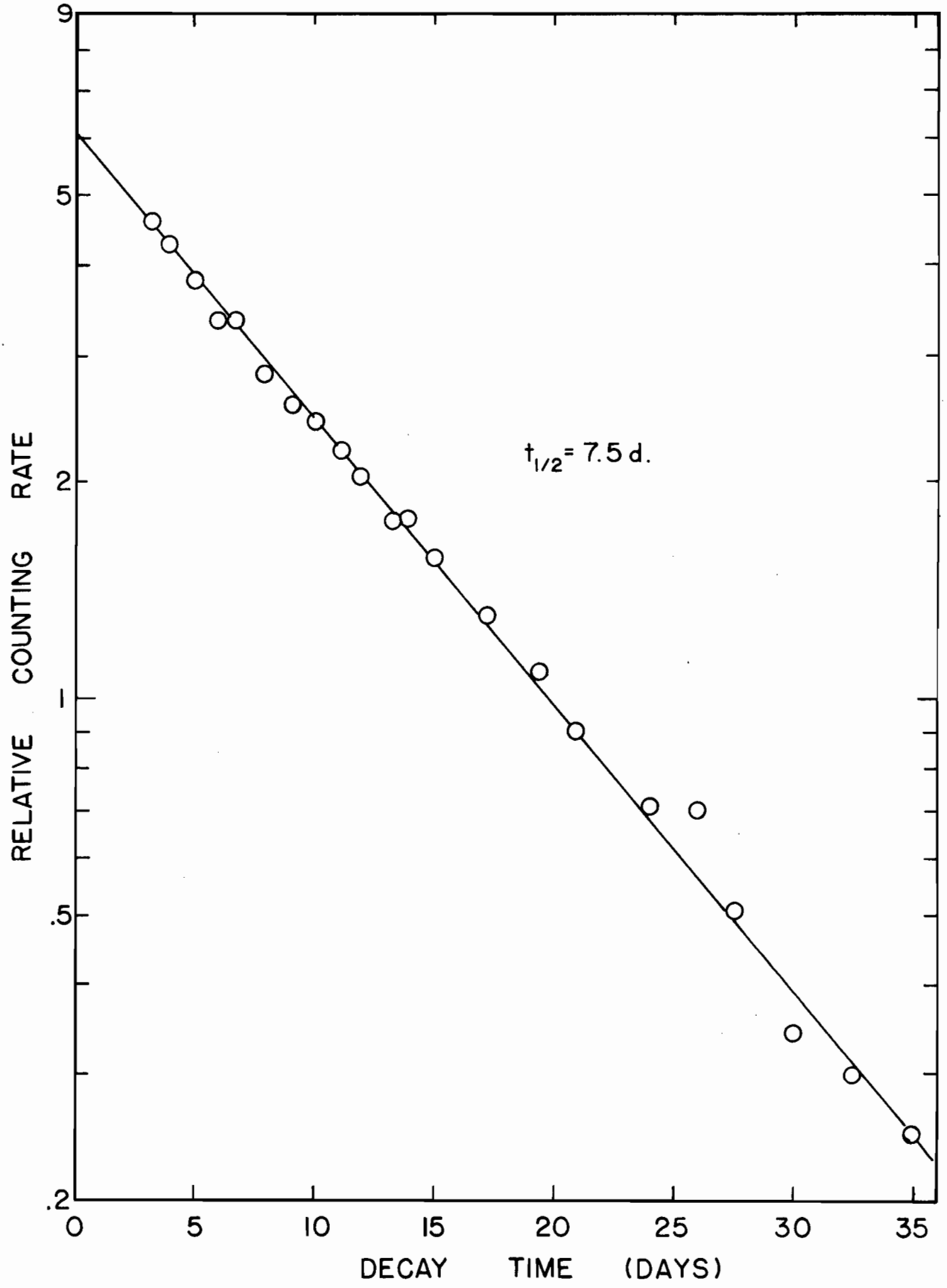
9
5
2
1
.5
.2
RELATIVE COUNTING RATE
$t_{1/2}$= 7.5 d.
0
5
10
15
20
25
30
35
DECAY TIME (DAYS)

Figure 45

DECAY OF 625 KEV GAMMA RAY OF

SILVER FRACTION

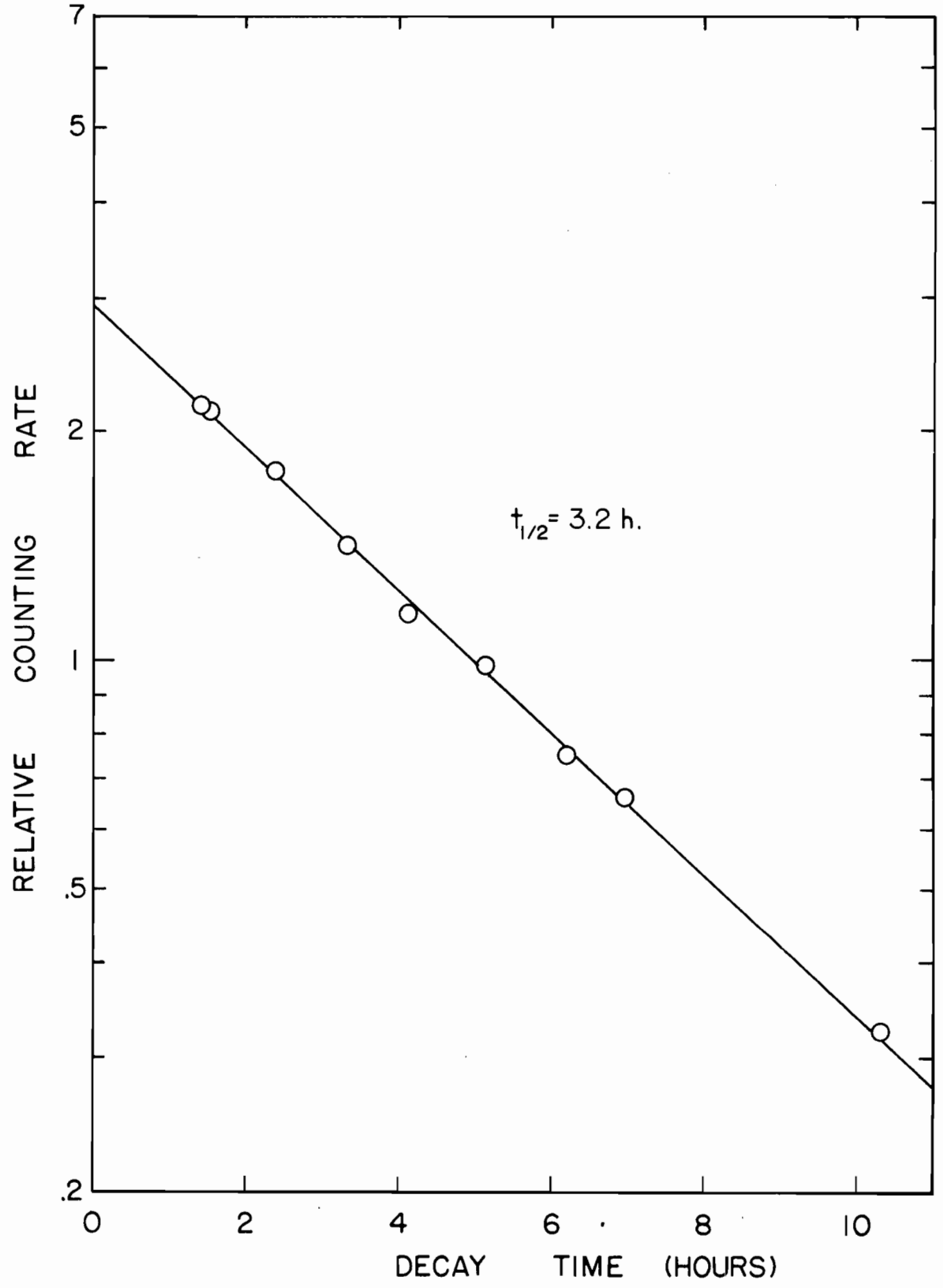
7
5
2
1
.5
.2
RELATIVE COUNTING RATE
$t_{1/2}$= 3.2 h.
0
2
4
6
8
10
DECAY TIME (HOURS)

Ag^{111} decays with a half-life of 7.5 days[54] by β^- emission with maximum energies of 0.69 (6.2%), 0.79 (1.1%), and 1.05 (92.7%) Mev. Gamma rays in coincidence with β^- emission have energies of 0.095, 0.247, and 0.342 Mev. Ag^{112} decays with a half-life of 3.2 hours[54]. The decay of Ag^{112} takes place through the emission of 15 beta rays of which the most abundant have maximum energies of 3.42 (18%) and 4.04 (56%) Mev. Reported gamma rays are as numerous, but the most intense has an energy of 615 kev.

Fission yield data for Ag^{111} are given in Table XII. Since the separation of silver had taken place when all the independently formed Ag^{112} had already decayed, the Ag^{112} activity results from the decay of 21-hour Pd^{112}. The fission yield of Pd^{112} was therefore calculated from the Ag^{112} disintegration rate by applying equation (25) P. 37, and is reported with the Pd^{112} data.

(j) Palladium

A method due to Seiler[75] was used to separate palladium from the other fission products. In this separation palladium dimethylglyoxime was precipitated from acid solution. Repeated scavenging with lanthanum and zirconium hydroxides and silver chloride provided further purification. The final dimethylglyoxime precipitate was dissolved by boiling with a small amount of aqua regia, which served to destroy the dimethylglyoxime, and made up to a volume of 10 mls. Chemical yields were determined in a procedure similar to that used for

Table XII

FISSION YIELD DATA FOR Ag^{111} (7.5 DAYS)

Irradiation	F	H_1	H_2
Observed activity	1.50×10^4 c/m	1.84×10^4 c/m	1.20×10^4 c/m
Source-mount absorption factor	1.00	1.00	1.00
Self-absorption factor	.989	1.00	1.00
Aliquot factor	500	1000	1000
Chemical yield	62.50%	30.50%	22.09%
Time after irradiation	10.378 d.	3.467 d.	3.467 d.
Decay factor	0.3833	0.7259	0.7259
Time in reactor	1.998 d.	2.133 d.	2.133 d.
Saturation factor	0.1686	0.1789	0.1789
Activity at saturation	3.1292×10^6 d/s	7.7426×10^6 d/s	6.9715×10^6 d/s
Fission rate	9.6100×10^8 f/s	2.854×10^9 f/s	2.854×10^9 f/s
Fission yield	0.32_6 %	0.27_1 %	0.24_4 %

silver[49].

The gross β^- decay curve was resolved into a 21-hour component and a 12-hour component (Fig. 46). The early portion of the decay due to the 21-hour component was calculated assuming that the later section of the decay represented an equilibrium mixture of Pd^{112} (21 hours) and Ag^{112} (3.2 hours). A gamma-ray spectrum of the palladium fraction (Fig. 47) showed gamma peaks at 20, 90, and 626 kev. The decay of the 626 kev peak [Fig. 48(a)] showed an initial growth, then fell away with a 21-hour half-life. The decay of the 20 kev peak [Fig. 48(b)] could be resolved into a 21-hour and a 12.5-hour component, while the 90 kev peak decayed with a half-life of 12.8 hours [Fig. 48(a)]. The mass chains for the palladium activities are:

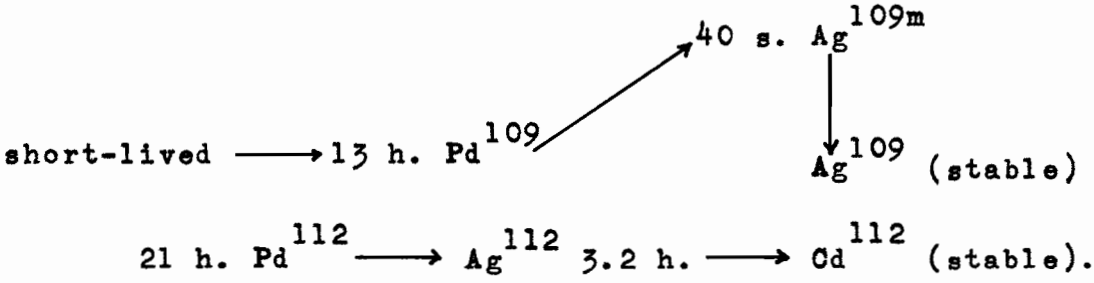

The half-life reported for Pd^{109} varies from 12.7 hours to 14.1 hours[54]. It decays to 40-second Ag^{109m} by emitting a 1.025 Mev (~100%) maximum energy beta ray. Ag^{109m} decays by isomeric transition of 88 kev to Ag^{109} (stable). This gamma ray is highly converted which results in the emission of 20 kev Ag X-rays. Pd^{112} has a reported half-life of 21 hours[54]. It decays to Ag^{112} (3.2 hours) by the

Figure 46

β^- DECAY OF PALLADIUM ACTIVITIES

○ - Experimental points

● - 21-hour activity subtracted

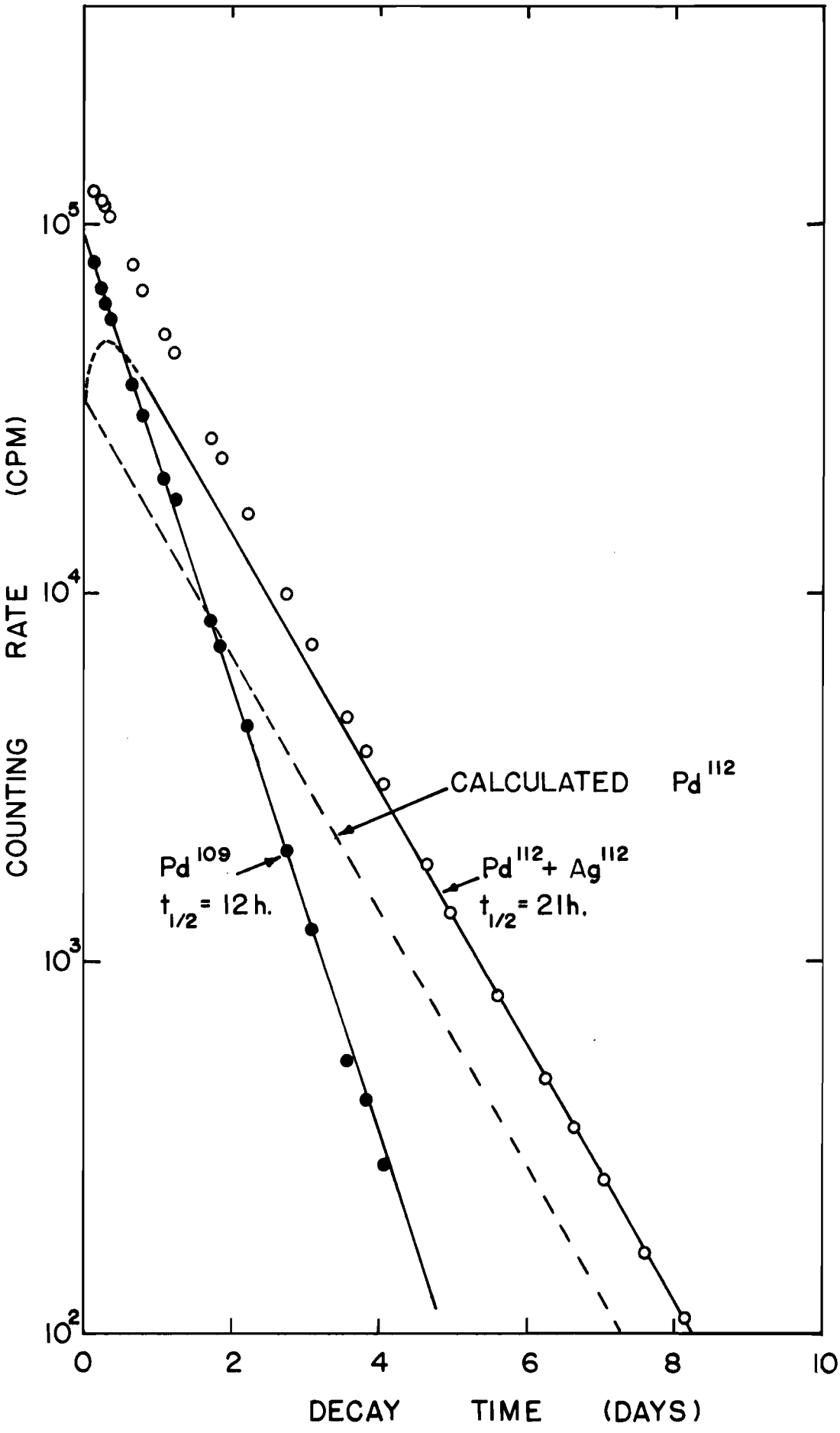
COUNTING RATE (CPM)
10^5
10^4
10^3
10^2
0
2
4
6
8
10
DECAY TIME (DAYS)
CALCULATED Pd^{112}
Pd^{109}
$t_{1/2}$ = 12 h.
Pd^{112} + Ag^{112}
$t_{1/2}$ = 21 h.

Figure 47

GAMMA SPECTRUM OF PALLADIUM ACTIVITIES

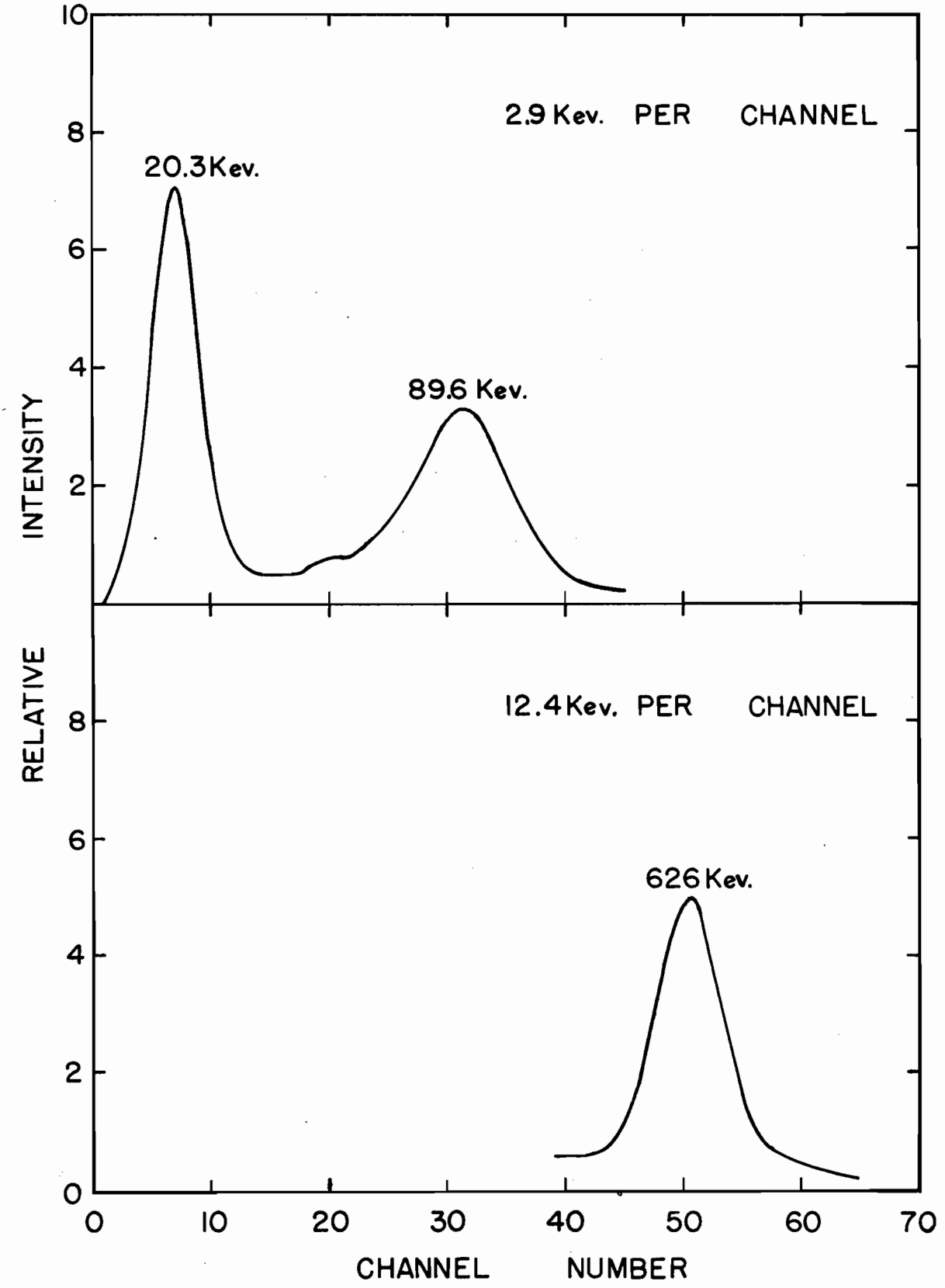
2.9 Kev. PER CHANNEL
20.3Kev.
89.6 Kev.
INTENSITY
12.4Kev. PER CHANNEL
626 Kev.
RELATIVE
0
2
4
6
8
10
0
10
20
30
40
50
60
70
CHANNEL NUMBER

Figure 48

DECAY OF PALLADIUM ACTIVITY

GAMMA RAYS

(a) Decay of 625 and 90 kev gamma peaks

(b) Decay of 20 kev gamma peak

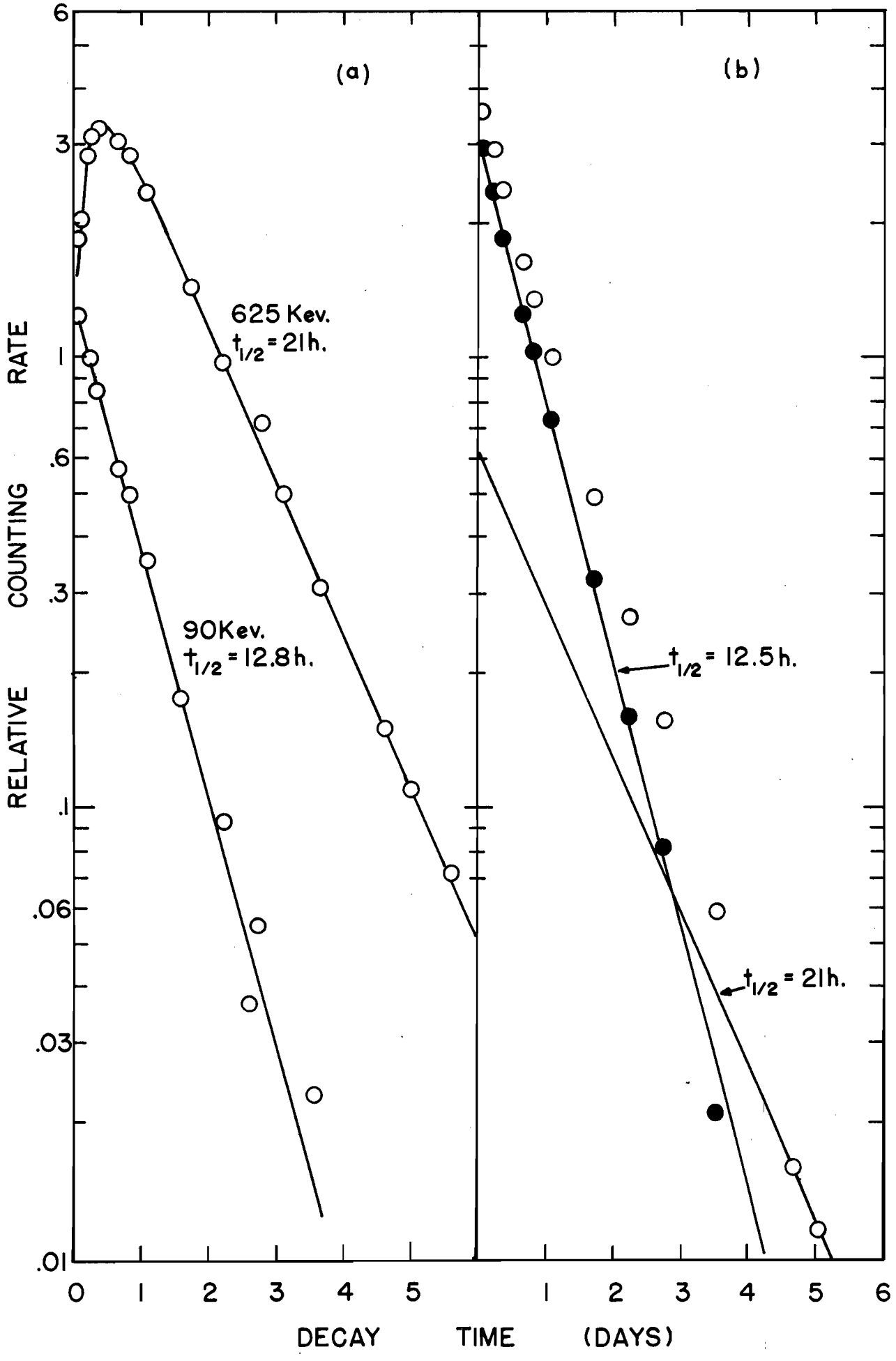
(a)
(b)
625 Kev.
$t_{1/2}$ = 21h.
90Kev.
$t_{1/2}$ = 12.8h.
$t_{1/2}$ = 12.5h.
$t_{1/2}$ = 21h.
RELATIVE COUNTING RATE
6
3
1
.6
.3
.1
.06
.03
.01
0 1 2 3 4 5
1 2 3 4 5 6
DECAY TIME (DAYS)

emission of a beta ray of maximum energy 280 kev in coincidence with an 18 kev gamma ray. As mentioned before (P. 120) the most intense gamma ray exhibited by Ag^{112} has an energy of 615 kev.

In determining the disintegration rate of Pd^{109}, it was necessary to take into account the conversion electrons emitted by Ag^{109m}. From the K-shell conversion coefficient 10.3, and the K/LM ratio 0.84 for the 88 kev gamma ray(54), the total conversion coefficient, α_T, is calculated to be 22.6 which gives a value of 0.958 for the number of conversion electrons emitted per beta disintegration:

$$N_{e^-} = \frac{\alpha_T}{1 + \alpha_T} = 0.958.$$

The detection efficiency for the 88 kev unconverted gamma rays is less than 0.1%(69). The energy of these conversion electrons is the difference between the gamma-ray energy and the electron binding energy. Strominger et al.(70) list the following for Ag: K electron binding energy 25.5 kev, L_1 and and M_1 electron binding energy 3.8 and 0.7 kev respectively. Therefore 44% of the conversion electrons have energies of $\sim$62 kev and 56% of $\sim$84 kev. The absorption determined as being equivalent to β^- rays with maximum energies of double the conversion electron energies gives a detection efficiency of 0.964 for the Ag^{109m} disintegrations while the Pd^{109} 1.025 Mev β^- ray is negligibly absorbed.

So that

$$\frac{\text{observed counting rate}}{Pd^{109}\text{ counting rate}} = 1 + (0.958 \times 0.964)$$

$$= 1.924.$$

Fission yield data for Pd^{109} are given in Table XIII. For Pd^{112} it was necessary to consider the growth of Ag^{112} which contributes to the equilibrium counting rate. At equilibrium the ratio of the disintegration rates is given by

$$\frac{N\lambda_{Ag^{112}}}{N\lambda_{Pd^{112}}} = \frac{\lambda_{Ag^{112}}}{\lambda_{Ag^{112}} - \lambda_{Pd^{112}}}$$

using the relation $\lambda = 0.693/t_{\frac{1}{2}}$ and substituting the values for the half-lives gives

$$\frac{N\lambda_{Ag^{112}}}{N\lambda_{Pd^{112}}} = 1.180.$$

Now putting $A = cN\lambda$, where A is the observed activity and c is the detection efficiency,

$$\frac{A_{Ag^{112}} + A_{Pd^{112}}}{A_{Pd^{112}}} = \frac{c_{Ag^{112}}N\lambda_{Ag^{112}} + c_{Pd^{112}}N\lambda_{Pd^{112}}}{c_{Pd^{112}}N\lambda_{Pd^{112}}}$$

$$= 1 + \frac{c_{Ag^{112}}}{c_{Pd^{112}}} \frac{N\lambda_{Ag^{112}}}{N\lambda_{Pd^{112}}}$$

$$= 1 + 1.180 \frac{c_{Ag^{112}}}{c_{Pd^{112}}}$$

Since the efficiency for detecting Ag^{112} is 1.00 and for Pd^{112} is 0.991,

$$A_{Pd^{112}} = \frac{\text{observed counting rate}}{2.191}$$

Fission yield data for Pd^{112} are given in Table XIV.

Table XIII

FISSION YIELD DATA FOR Pd^{109} (12 HOURS)

Irradiation	LA
Observed activity	4.73×10^4 c/m
Source-mount absorption factor	1.00
Self-absorption factor	1.00
Aliquot factor	50
Chemical yield	18.2%
Time after irradiation	3.848 d.
Decay factor	0.00483
Time in reactor	1.590 d.
Saturation factor	0.8896
Activity at saturation	5.052×10^7 d/s
Fission rate	4.483×10^9 f/s
Fission yield	1.13%

Table XIV

FISSION YIELD DATA FOR Pd^{112} (21 HOURS)

CALCULATED FROM Ag^{112} DAUGHTER

Irradiation	LA	H_1	H_2
Observed activity	3.28×10^4 c/m	2.614×10^3 c/m	1.630×10^3 c/m
Source-mount absorption factor	0.999	1.00	1.00
Self-absorption factor	0.992	1.00	1.00
Aliquot factor	50	1000	1000
Chemical yield	18.16%	30.50%	22.09%
Time after irradiation	3.848 d.	3.467 d.	3.467 d.
Decay factor	0.0475	0.0639	0.0639
Time in reactor	1.590 d.	2.133 d.	2.133 d.
Saturation factor	0.7161	0.8157	0.8157
Activity at saturation	4.425×10^6 d/s	2.740×10^6 d/s	2.360×10^6 d/s
Fission rate	4.483×10^9 f/s	2.854×10^9 f/s	2.854×10^9 f/s
Fission yield	0.099%	0.096%	0.083%

(k) Cadmium

Cadmium was separated from an aliquot of the fission product solution by the method of Glendenin[76]. This consisted of repeated precipitations of cadmium sulphide interspersed with ferric hydroxide and palladium sulphide scavenging precipitations. The final CdS precipitate was dissolved in a small amount of dilute hydrochloric acid which, after boiling to remove H_2S, was transferred to a volumetric flask. The solution was then made up to volume from which aliquots were removed for disintegration rate determinations and gamma-ray measurements. Chemical yield determinations were made by titrating aliquots of the solution with EDTA using Eriochrome Black T (+ methyl red) as an indicator[49].

The gross beta-decay curve was resolved graphically into a 43-day component (Fig. 49) and a 53.4-hour component (Fig. 50). The cadmium activities expected to be present occur in the following decay chain:

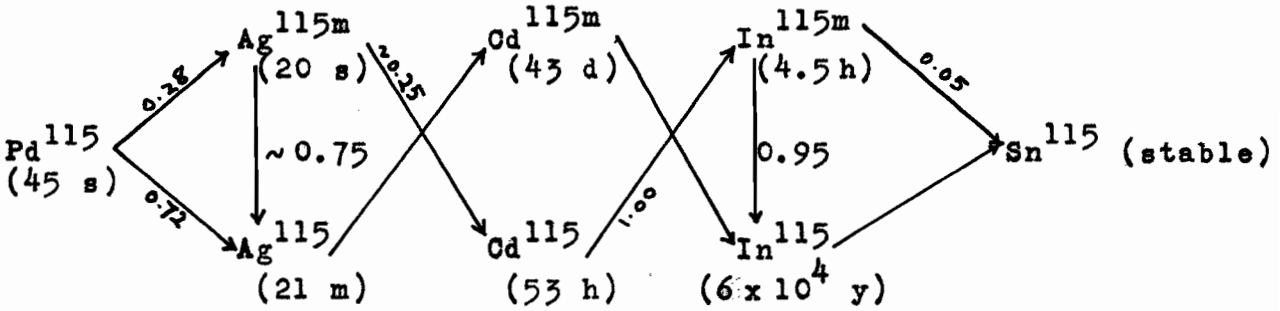

The half-lives for Cd^{115m} and Cd^{115g} have been reported as

Figure 49

BETA-DECAY CURVE FOR A SEPARATED CADMIUM SAMPLE

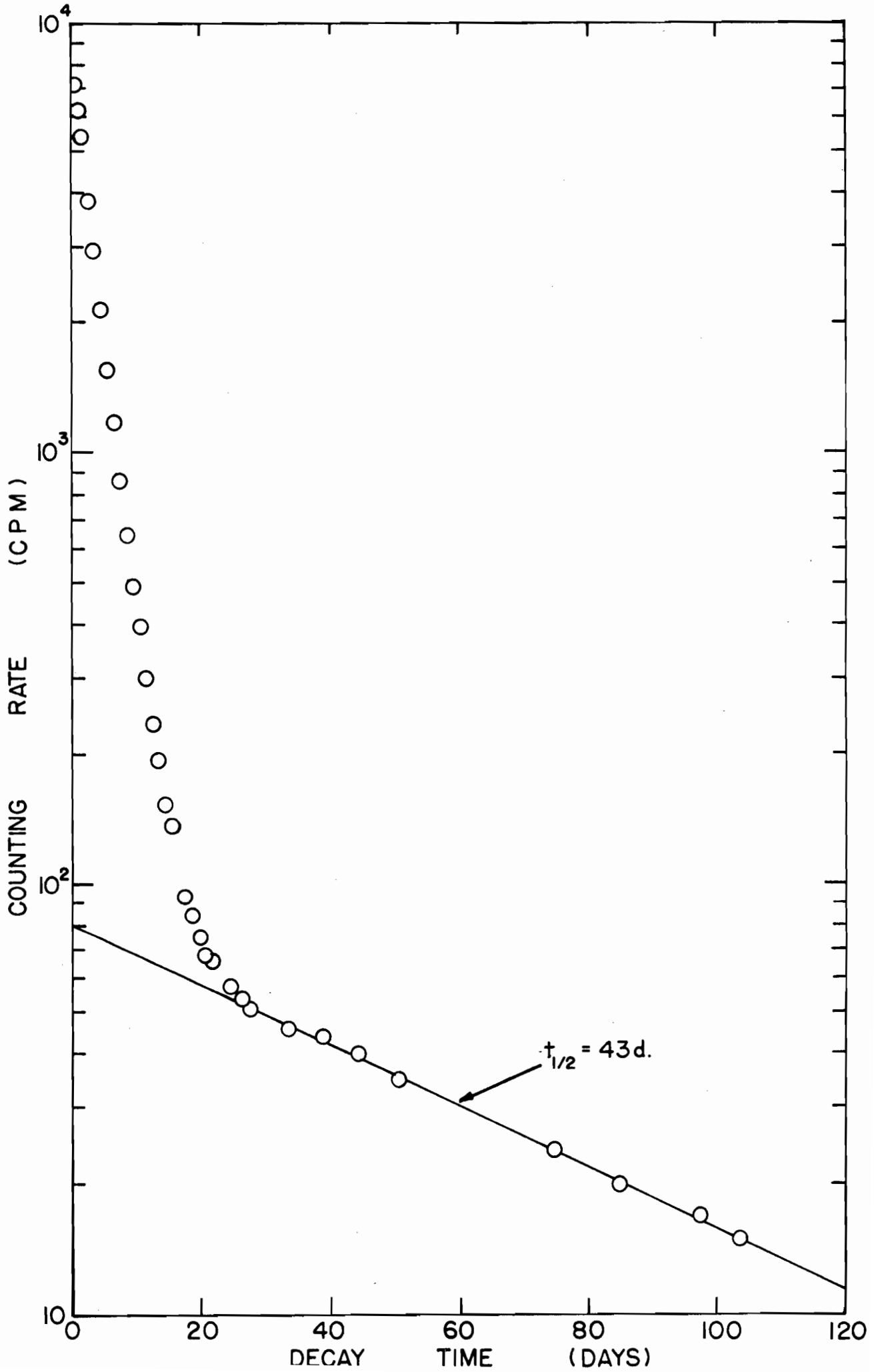
10^4
10^3
10^2
10
COUNTING RATE (CPM)
$t_{1/2}$ = 43d.
0
20
40
60
80
100
120
DECAY TIME (DAYS)

Figure 50

ANALYSIS OF EARLY PORTION OF

CADMIUM BETA-DECAY CURVE

O - Experimental points

● - Long-lived activity subtracted

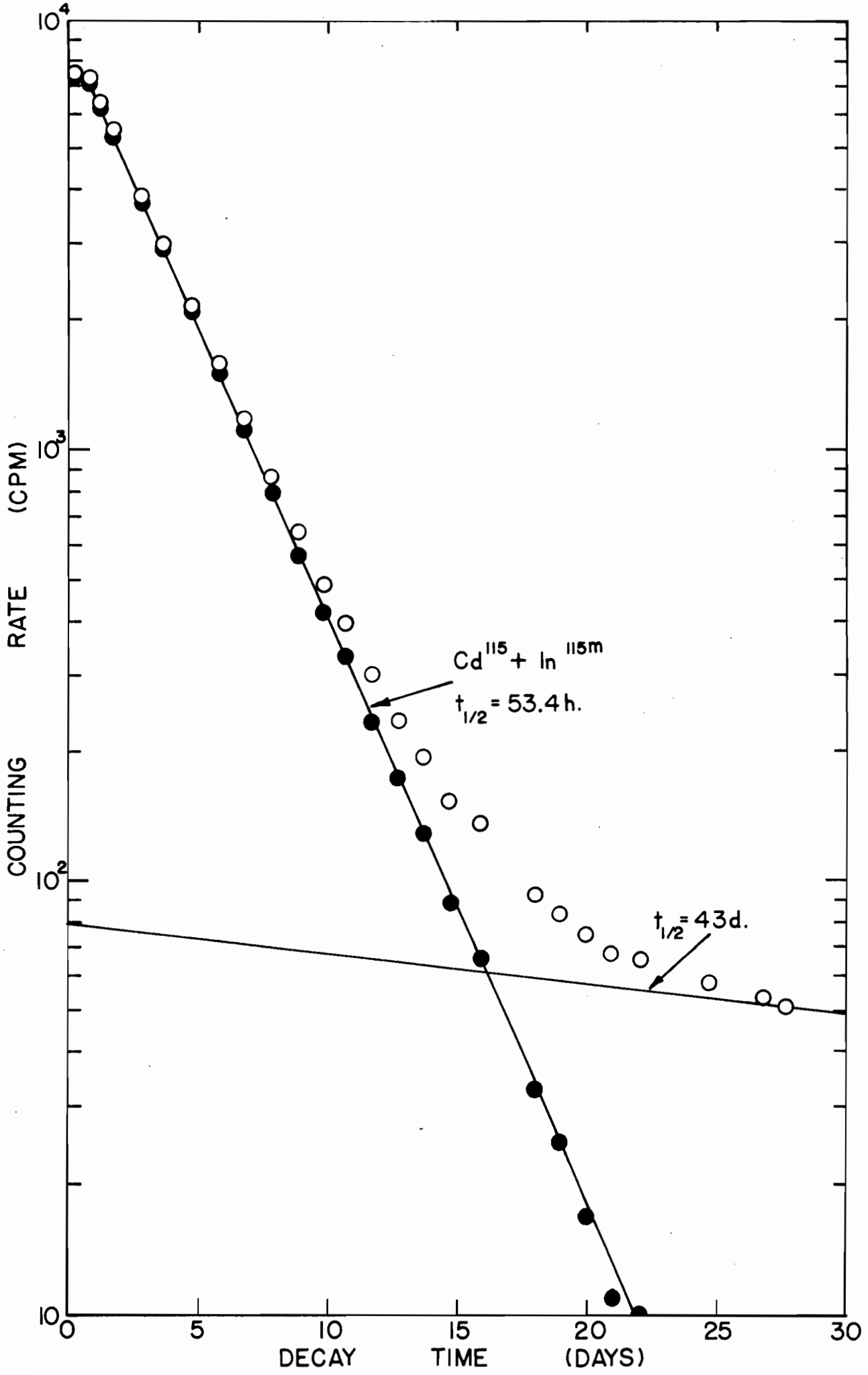
10^4
10^3
10^2
10
COUNTING RATE (CPM)
$Cd^{115} + In^{115m}$
$t_{1/2} = 53.4$ h.
$t_{1/2} = 43$ d.
0
5
10
15
20
25
30
DECAY TIME (DAYS)

43 days and 2.3 days (55.2 hours) respectively[54]. A gamma-ray spectrum (Fig. 51) taken several hours after the separation showed an X-ray to be present, together with gamma rays of energies 255, 333, and 527 kev. This was almost identical to a gamma spectrum for 54-hour Cd^{115} - 4.5 hour In^{115} (in equilibrium) given by Heath[65] and compared well with gamma rays for Cd^{115} listed in the Nuclear Data Sheets[54]. The 333 kev gamma ray was observed to grow and then to decay with a half-life of 54 hours, while the 527 kev gamma ray decayed with a similar half-life (Fig. 52). The absence of gamma rays characteristic of Cd^{115m} was due to the very small amount of this activity present in the sample and to the fact that about 97% of the beta disintegrations[54] lead directly to the ground state of In^{115}.

Yield determinations for Cd^{115m} are straightforward and are given in Table XV. Since Cd^{115g} decays to metastable In^{115m} (4.5 hours), the measured disintegration rate had to be corrected for the additional counts registered as a result of conversion electron emission. From the data $\alpha_K = 0.83$, $K/L_1M = 3.85$[77], the total internal conversion coefficient, α_T, is calculated to be 1.05. From this the number of conversion electrons is given by

$$N_{e^-} = \frac{\alpha_T}{1 + \alpha_T} = 0.512,$$

and the number of unconverted gamma rays is therefore 0.488.

Figure 51

GAMMA SPECTRUM OF A SEPARATED CADMIUM FRACTION

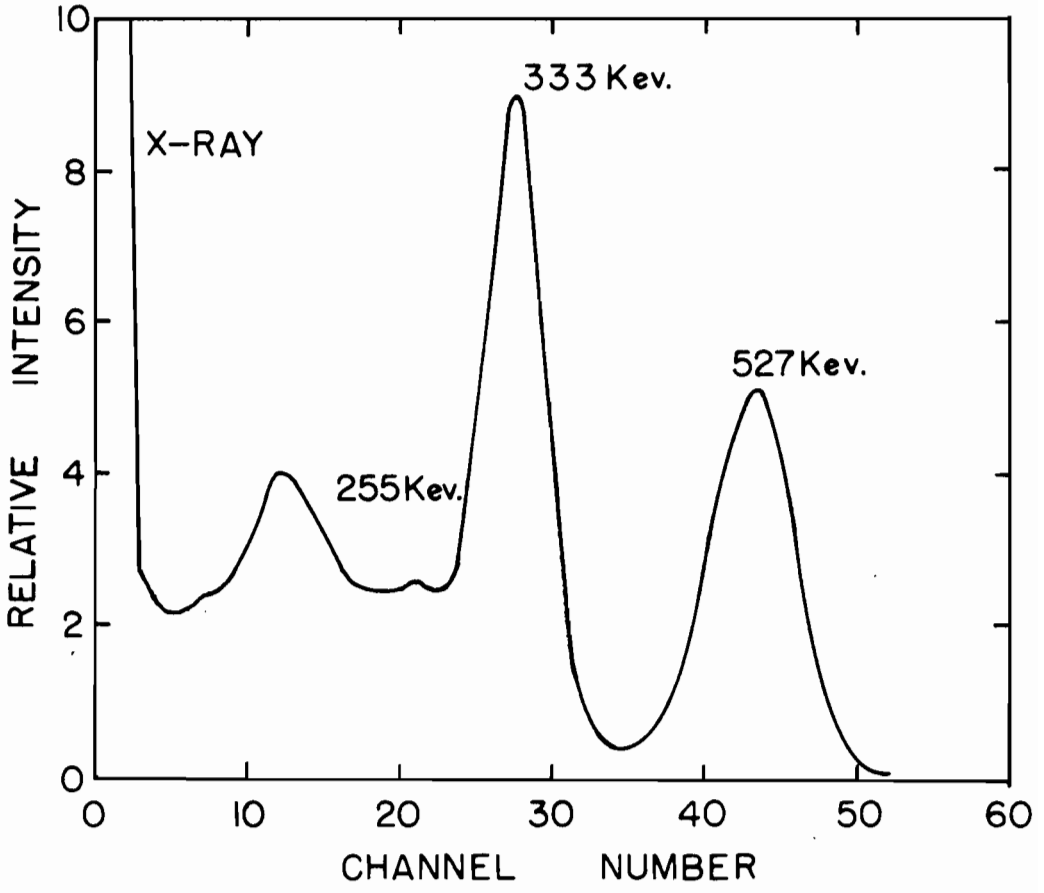
10
8
6
4
2
0
RELATIVE INTENSITY
X-RAY
333 Kev.
527 Kev.
255 Kev.
0
10
20
30
40
50
60
CHANNEL NUMBER

Figure 52

GAMMA DECAY CURVES FOR THE

SEPARATED CADMIUM FRACTION

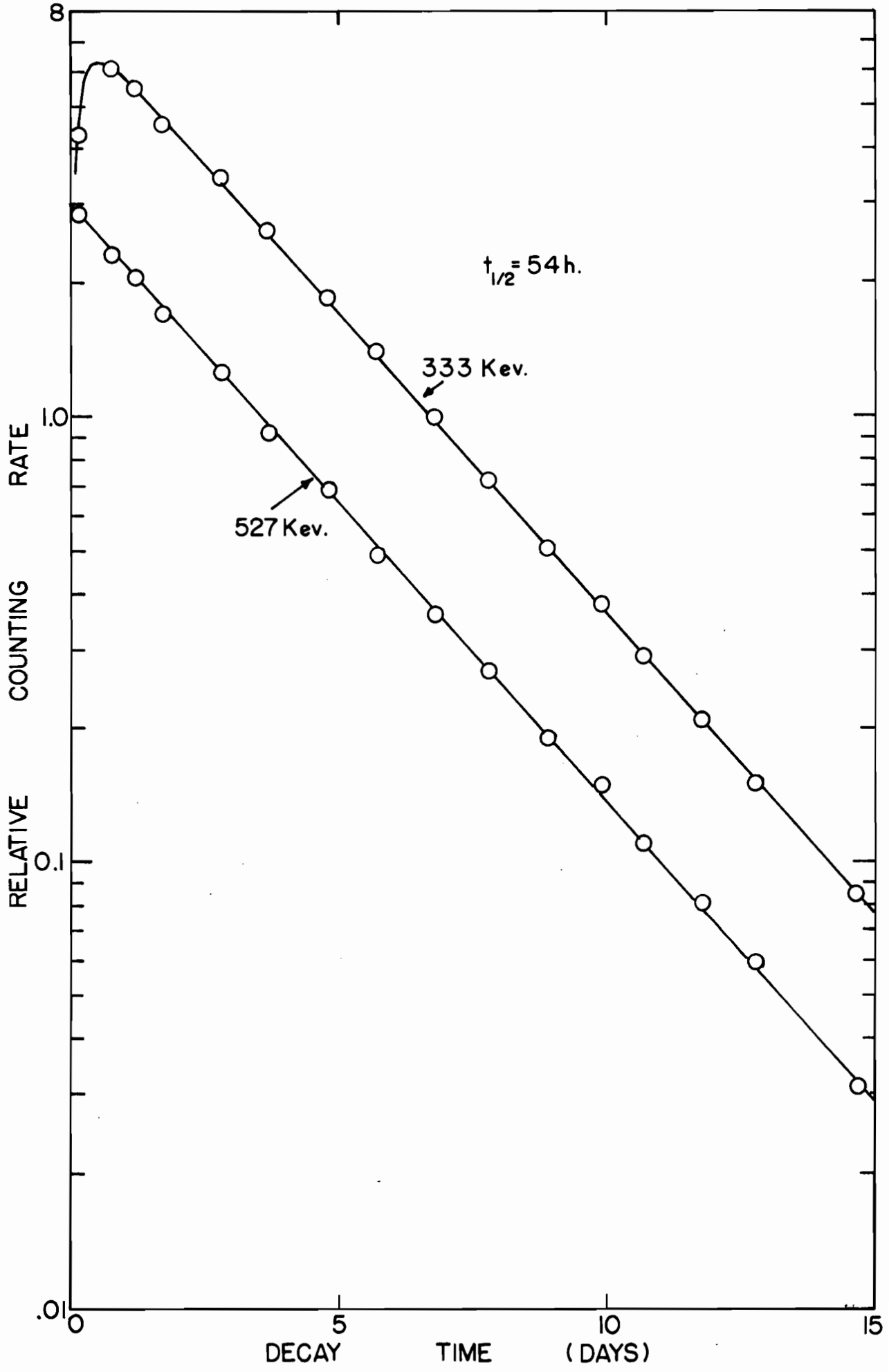
8
1.0
0.1
.01
RELATIVE COUNTING RATE
$t_{1/2}$ = 54 h.
333 Kev.
527 Kev.
0
5
10
15
DECAY TIME (DAYS)

Table XV

FISSION YIELD DATA FOR Cd^{115m} (43 DAYS)

Irradiation	KA_1	KA_2
Observed activity	80 c/m	117 c/m
Source-mount absorption factor	1.00	1.00
Self-absorption factor	1.00	1.00
Aliquot factor	500	500
Chemical yield	24.1%	24.2%
Time after irradiation	3.29 d.	3.29 d.
Decay factor	0.9484	0.9484
Time in reactor	2.07 d.	2.07 d.
Saturation factor	0.0329	0.0329
Activity at saturation	8.8765×10^4 d/s	1.2896×10^5 d/s
Fission rate	3.297×10^9 f/s	3.297×10^9 f/s
Fission yield	2.69×10^{-3} %	3.91×10^{-3} %

Since In^{115m} decays 94.5% by isomeric transition to In^{115} and 5.5% by 840 kev β^- emission to Sn^{115}, the observed β^- disintegration rate is related to the Cd^{115} disintegration rate by

$$\text{Observed D.R.} = Cd^{115}\ \text{D.R.}\left[1 + (0.512 \times 0.945) + 0.055\right]$$

Therefore

$$Cd^{115}\ \text{D.R.} + In^{115m}\ \text{D.R.} = Cd^{115}\ \text{D.R.}(1.539)$$

The efficiency of the 4 π counter for the 335 kev unconverted gamma rays is less then 0.14%[69] and the contribution due to these may therefore be neglected. At equilibrium, the disintegration rates of Cd^{115} and In^{115m} are related by

$$\frac{N_2 \lambda_2}{N_1 \lambda_1} = \frac{\lambda_2}{\lambda_2 - \lambda_1} = 1.093$$

Here the subscripts 1 and 2 refer to Cd^{115} and In^{115m} respectively. Putting $A = cN\lambda$, where A is the observed counting rate and c is the detection efficiency

$$\frac{A_1 + A_2}{A_1} = \frac{c_1 N_1 \lambda_1 + c_2 N_2 \lambda_2}{c_1 N_1 \lambda_1}$$

$$= 1 + \frac{c_2}{c_1} \times \frac{N_2 \lambda_2}{N_1 \lambda_1}$$

$$= 1 + \frac{c_2}{c_1} \quad \frac{\lambda_2}{\lambda_2 - \lambda_1}$$

c_1 is 1.00 and c_2 is given by the product of the factor 0.539, calculated above, and the absorption factor of the conversion electrons which was estimated to be 0.996. Therefore

$$\frac{A_1 + A_2}{A_1} = 1 + (0.539 \times 0.996 \times 1.093)$$

$$= 1.587$$

The observed counting rate for $Cd^{115} + In^{115m}$ was divided by this factor to give the Cd^{115} counting rate. Fission yield data for Cd^{115} are given in Table XVI.

Table XVI

FISSION YIELD DATA FOR Cd^{115g} (53.4 HOURS)

Irradiation	KA_1	KA_2
Observed activity	5.7×10^3 c/m	5.1×10^3 c/m
Source-mount absorption factor	1.00	1.00
Self-absorption factor	1.00	1.00
Aliquot factor	500	500
Chemical yield	24.1%	24.2%
Time after irradiation	3.29 d.	3.29 d.
Decay factor	0.3648	0.3648
Time in reactor	2.07 d.	2.07 d.
Saturation factor	0.4714	0.4714
Activity at saturation	1.1468×10^6 d/s	1.0200×10^6 d/s
Fission rate	3.297×10^9 f/s	3.297×10^9 f/s
Fission yield	3.48×10^{-2} %	3.09×10^{-2} %

(1) Antimony

The separation of antimony was achieved by precipitating metallic antimony with chromous chloride ($CrCl_2$)[78]. Exchange between carrier and the antimony activity was assured by adding Sb^{+3} carrier to an aliquot of the fission product solution, oxidizing Sb^{+3} to Sb^{+5} with bromine water then precipitating metallic antimony. Further purification was obtained after dissolving the precipitate in aqua regia by precipitating the sulphide with H_2S. The final precipitate was dissolved in a minimum of HCl, boiled to remove excess H_2S, then made up to volume. Chemical yields were determined by precipitating metallic antimony with chromous chloride and weighing.

The gross β^- decay curve was resolved graphically (Figs. 53 and 54) into the following components:

(1) a long-lived activity considerably above the background counting rate,

(2) a 61-day activity assigned to Sb^{124},

(3) a 12.8-day activity assumed to be Sb^{124}, and

(4) a 3.73-day activity assumed to be Sb^{127}.

The isobaric decay chains for these masses are

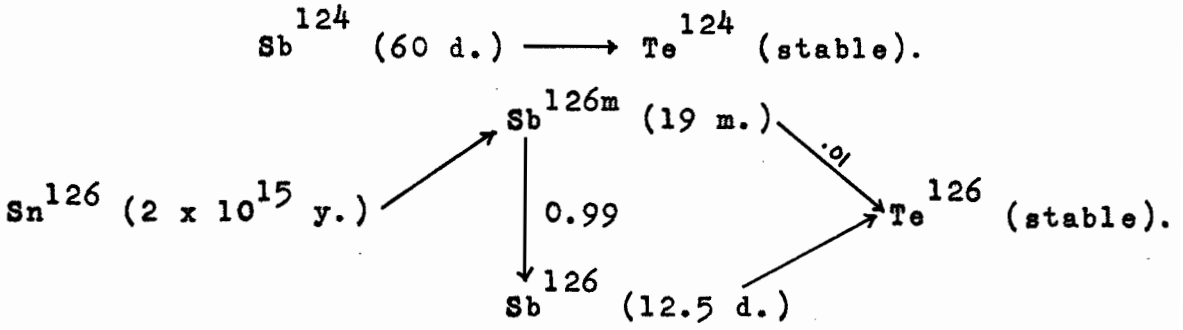

Figure 53

GROSS β^- DECAY CURVES FOR

ANTIMONY ACTIVITIES

O - Experimental points

● - Long-lived activity subtracted

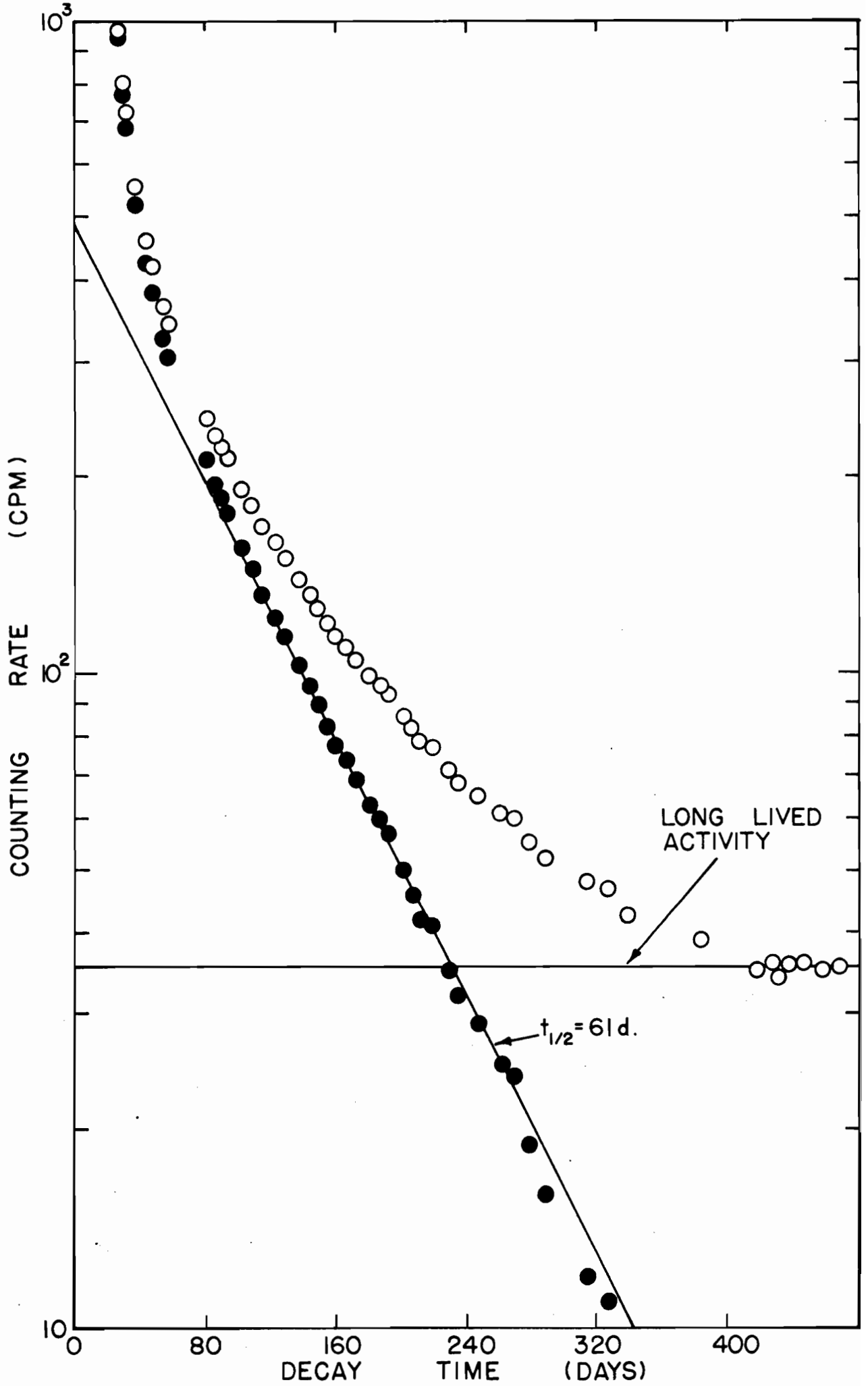
10^3
10^2
10
COUNTING RATE (CPM)
LONG LIVED ACTIVITY
$t_{1/2}$ = 61 d.
0
80
160
240
320
400
DECAY TIME (DAYS)

Figure 54

ANALYSIS OF β^- DECAY OF

ANTIMONY ACTIVITIES

x - Experimental points

O - Long-lived activity subtracted

● - 61-day activity subtracted

◐ - 12.8-day activity subtracted

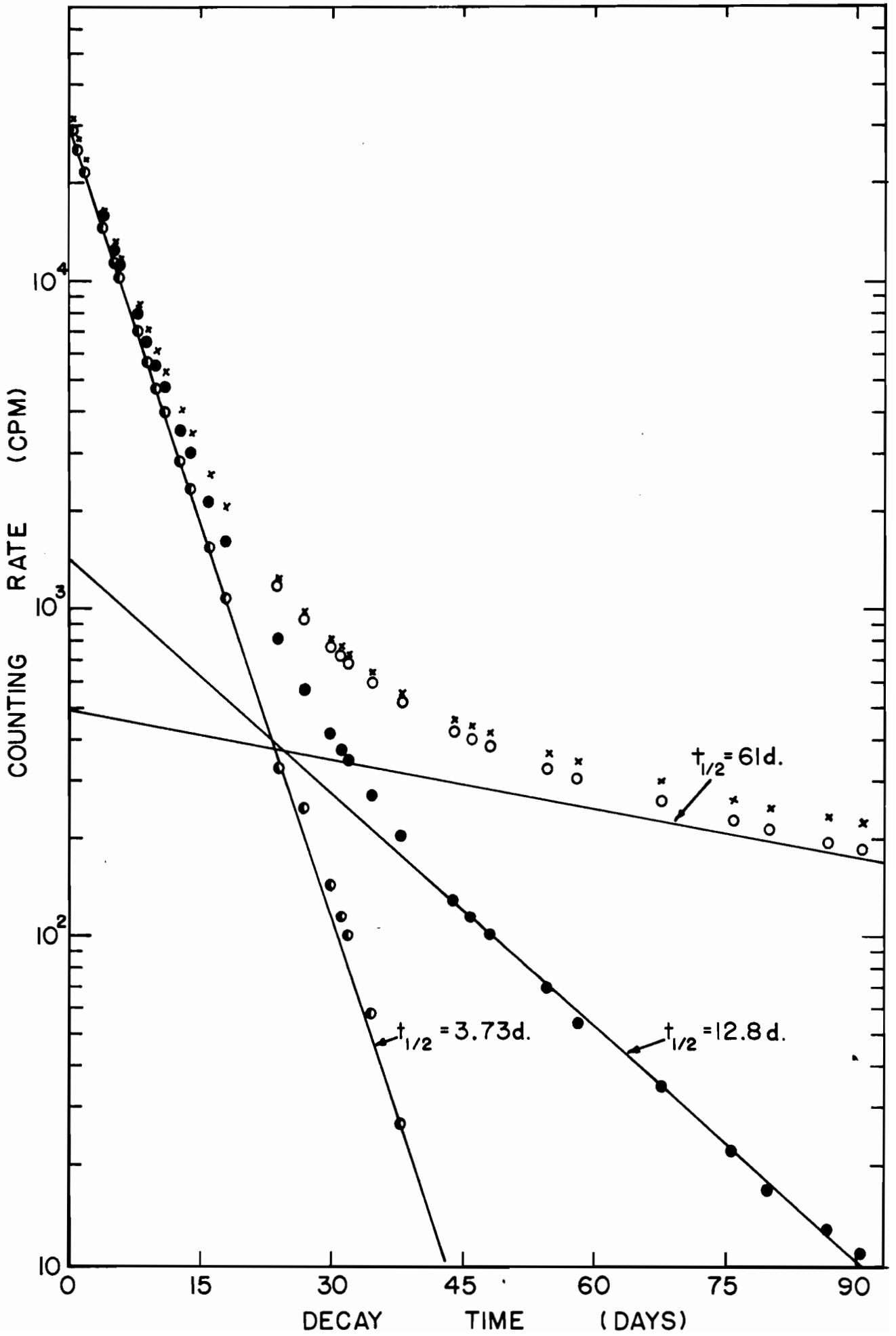
COUNTING RATE (CPM)
10^4
10^3
10^2
10
0
15
30
45
60
75
90
DECAY TIME (DAYS)
$t_{1/2}$ = 61d.
$t_{1/2}$ = 3.73d.
$t_{1/2}$ = 12.8 d.

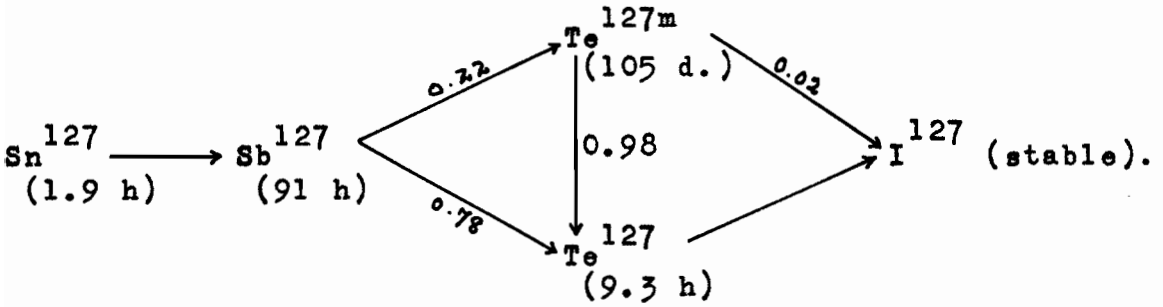

A gamma-ray spectrum of the antimony fraction, shown in Fig. 55, gives photopeaks at 215 kev, 461 kev, 677 kev, and 775 kev. Sb^{127} decays with a half-life of 91 hours[54] by the emission of β^- rays with energies of 800 kev (35%), 860 kev (10%), 1.11 Mev (35%), and 1.50 Mev (20%). Coincident gamma rays have energies of 58 kev, 240 kev, 456 kev, and 764 kev. Twenty percent of the decays lead to metastable Te^{127m} which has a half-life of 105 days, while the remainder lead to Te^{127} with a half-life of 9.3 hours. The metastable state decays 98.5% by isomeric transition and 1.5% by emission of a 730 kev β ray. Te^{126} decays by β^- emission of energies 270 kev (1%) and 695 kev (99%) with coincident gamma-ray energies of 58, 215, 360, and 418 kev respectively. Sb^{126} is a shielded nuclide since its parent Sn^{126} has a half-life of 2×10^{15} years. It decays 100% by the emission of a 1.9 Mev beta ray with a half-life of 60 days[54]. Coincident gamma rays have energies of 415 kev, 665 kev, and 695 kev. Sb^{124} is a shielded nuclide which decays with a half-life of 12.5 days[54] by β^- emission with energies of 51 kev (2%), 225 kev (11%), 621 kev (51%),

Figure 55

GAMMA SPECTRUM OF ANTIMONY FRACTION

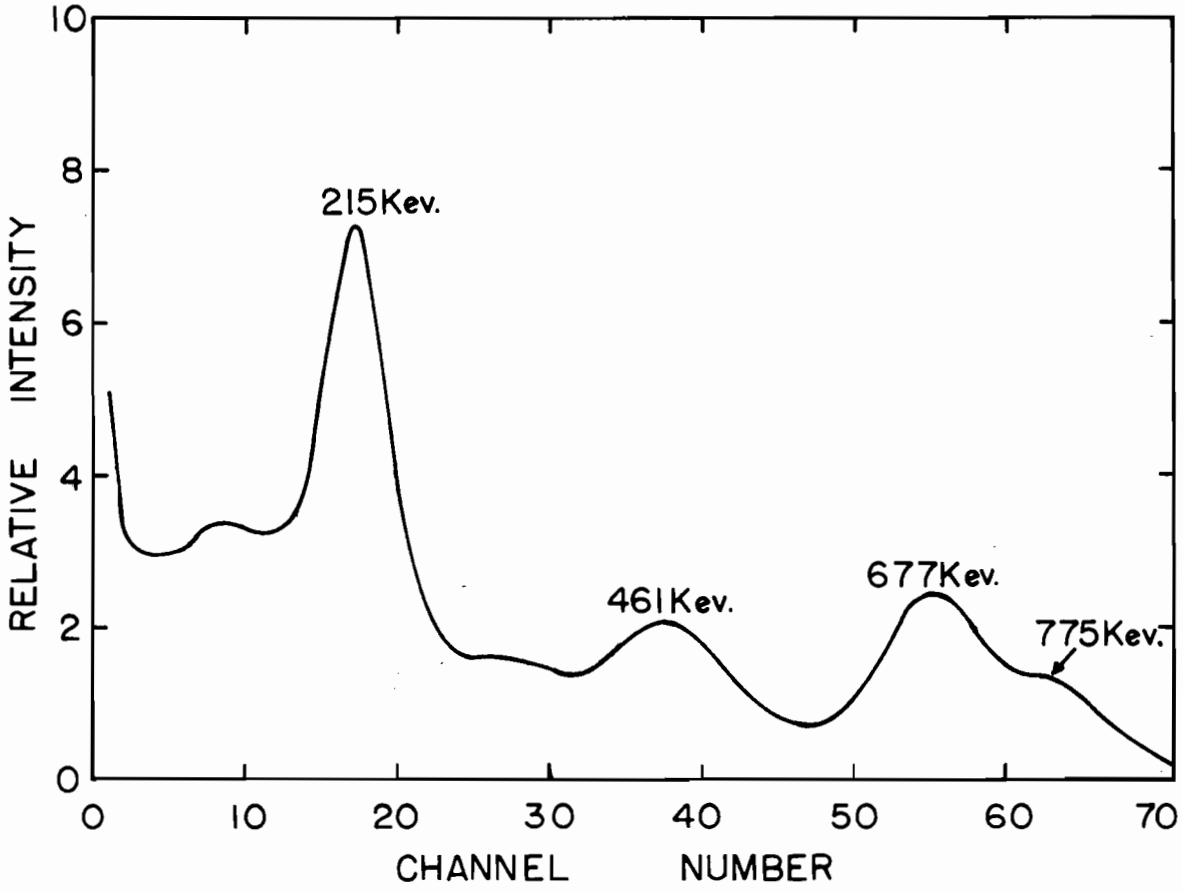
10
8
6
4
2
0
RELATIVE INTENSITY
215Kev.
461Kev.
677Kev.
775Kev.
0
10
20
30
40
50
60
70
CHANNEL NUMBER

954 kev (5%), 1.016 Mev (1.5%), 1.59 Mev (5%), and 2.313 Mev (23%). As would be expected, the gamma spectrum is quite complex, but its most intense gamma ray has an energy of 603 kev.

Disintegration rate determinations for Sb^{124} and Sb^{126} are not complicated. Fission yield data for these nuclides are given in Table XVII. For Sb^{127} it was necessary to take into account the amount of the Te^{127} activity which would be in equilibrium with its parent. From growth and decay considerations

$$\frac{N\lambda_{Te^{127}}}{N\lambda_{Sb^{127}}} = \frac{\lambda_{Te^{127}}}{\lambda_{Te^{127}} - \lambda_{Sb^{127}}} = 1.116.$$

From a consideration of actual activities measured on the 4π counter

$$\frac{A_1 + A_2}{A_1} = \frac{c_1 N_1 \lambda_1 + c_2 N_2 \lambda_2}{c_1 N_1 \lambda_1}$$

where subscripts 1 and 2 refer to Sb^{127} and Te^{127} respectively, A is the observed activity and c the detection efficiency, so that

$$\frac{A_1 + A_2}{A_1} = 1 + \left(\frac{c_2}{c_1} \times 1.116\right).$$

Since only 80% of the Te^{127} activity assumes equilibrium with Sb^{127} - the other 20% results from the isomeric transition

Table XVII

FISSION YIELD DATA FOR ANTIMONY ACTIVITIES

Irradiation	Sb^{124} (61 d.) F	Sb^{126} (12.8 d.) F	Sb^{127} (3.73 d.) F
Observed activity	4.90×10^2 c/m	1.40×10^3 c/m	1.585×10^4 c/m
Source-mount absorption factor	1.00	1.00	1.00
Self-absorption factor	0.991	1.00	1.00
Aliquot factor	2000	2000	2000
Chemical yield	93.0%	93.0%	93.0%
Time after irradiation	5.671 d.	5.671 d.	5.671 d.
Decay factor	0.9376	0.7357	0.3487
Time in reactor	1.998 d.	1.998 d.	1.998 d.
Saturation factor	0.0224	0.1026	0.3101
Activity at saturation	8.438×10^5 d/s	6.632×10^5 d/s	5.254×10^6 d/s
Fission rate	9.610×10^8 f/s	9.610×10^8 f/s	9.610×10^8 f/s
Fission yield	8.78×10^{-2}%	6.90×10^{-2}%	0.55%

from Te^{127m} (105 days) - and both Sb^{127} and Te^{127} activities are negligibly absorbed in the source mount and the source material, then

$$\frac{A_1 + A_2}{A_1} = 1 + (0.80 \times 1.116)$$

$$= 1.893.$$

The observed counting rate of the combined activities was divided by this factor to give the counting rate of Sb^{127}. Fission yield data for Sb^{127} are given in Table XVII.

(m) Tellurium

Tellurium was recovered from a fission product aliquot by precipitating tellurium metal with SO_2 in acid solution(79). A preliminary removal of selenium was effected by adding Te^{+4} carrier and fuming with HBr. Further decontamination was achieved by scavenging with ferric hydroxide. The tellurium was finally recovered as the metal, dissolved in nitric acid and made up to volume. Chemical yields were determined by precipitating the metal and weighing.

The tellurium activities expected to be present occur in the following mass chains

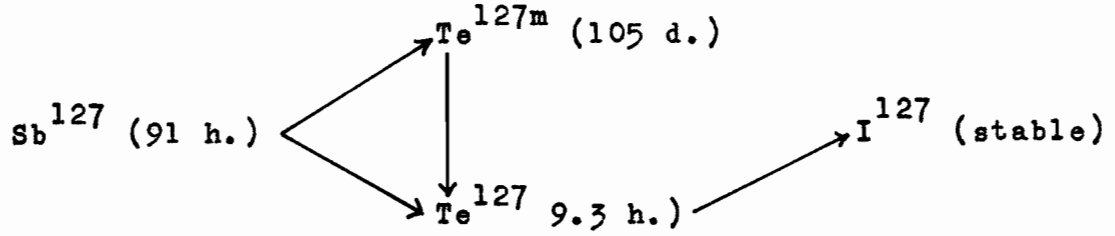

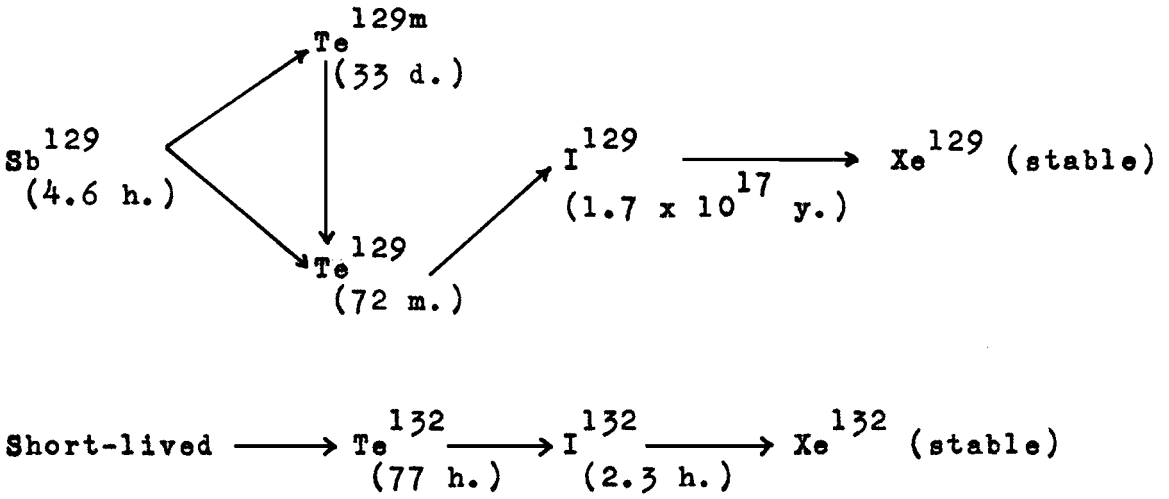

The gross β^- decay curve, as shown in Fig. 56, was resolved by estimating the 105-day tail and subtracting this from the experimentally determined counting rates. A 33-day component appeared which was taken to be Te^{129m}. On subtracting the longer-lived activities, as shown in Fig. 57, a 3.27-day activity remained which was assumed to be Te^{132} and I^{132} in equilibrium. The amount of Te^{132} in this equilibrium mixture was calculated from the growth and decay equations as discussed before, and the Te^{132} disintegration rate was determined from this. A gamma-ray spectrum of the tellurium fraction is given in Fig. 58. An X-ray and prominent photopeaks with 231 and 675 kev energies could be discerned with less intense gamma peaks at 513, 788, 963, and 1156 kev respectively. The 231 kev peak was seen to decay with a half-life of 3.4 days, while the 675 kev peak showed an initial growth followed by decay with a similar half-life (Fig. 59).

Figure 56

β^- DECAY OF TELLURIUM FRACTION

x - Experimental points

0 - 105-day activity subtracted

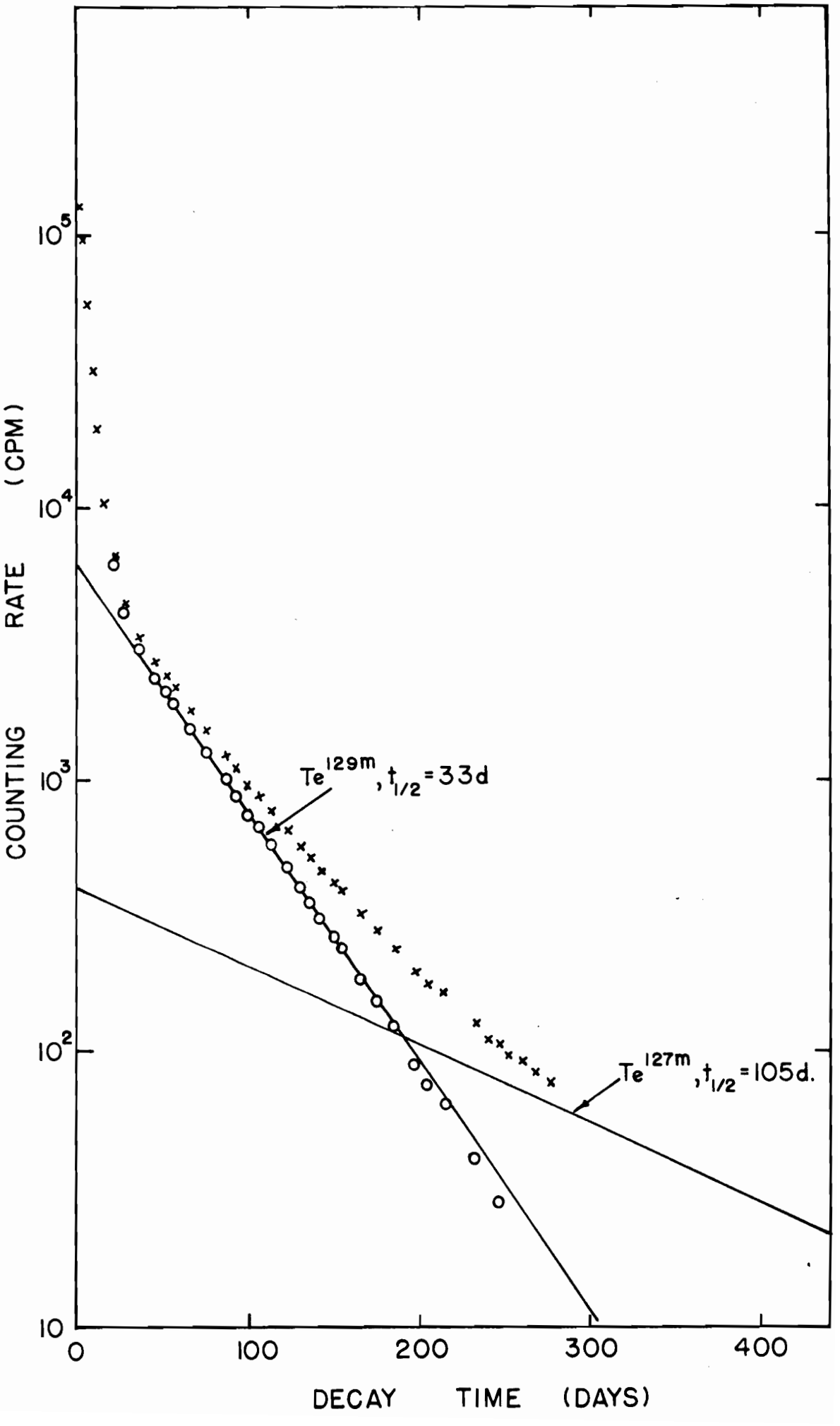
COUNTING RATE (CPM)
10^5
10^4
10^3
10^2
10
0
100
200
300
400
DECAY TIME (DAYS)
Te^{129m}, $t_{1/2}$ = 33d
Te^{127m}, $t_{1/2}$ = 105d.

Figure 57

β^- DECAY CURVE FOR Te^{132} (3.27 DAYS)

O - Experimental points

● - Longer-lived components subtracted

- - - - Calculated Te^{132} decay

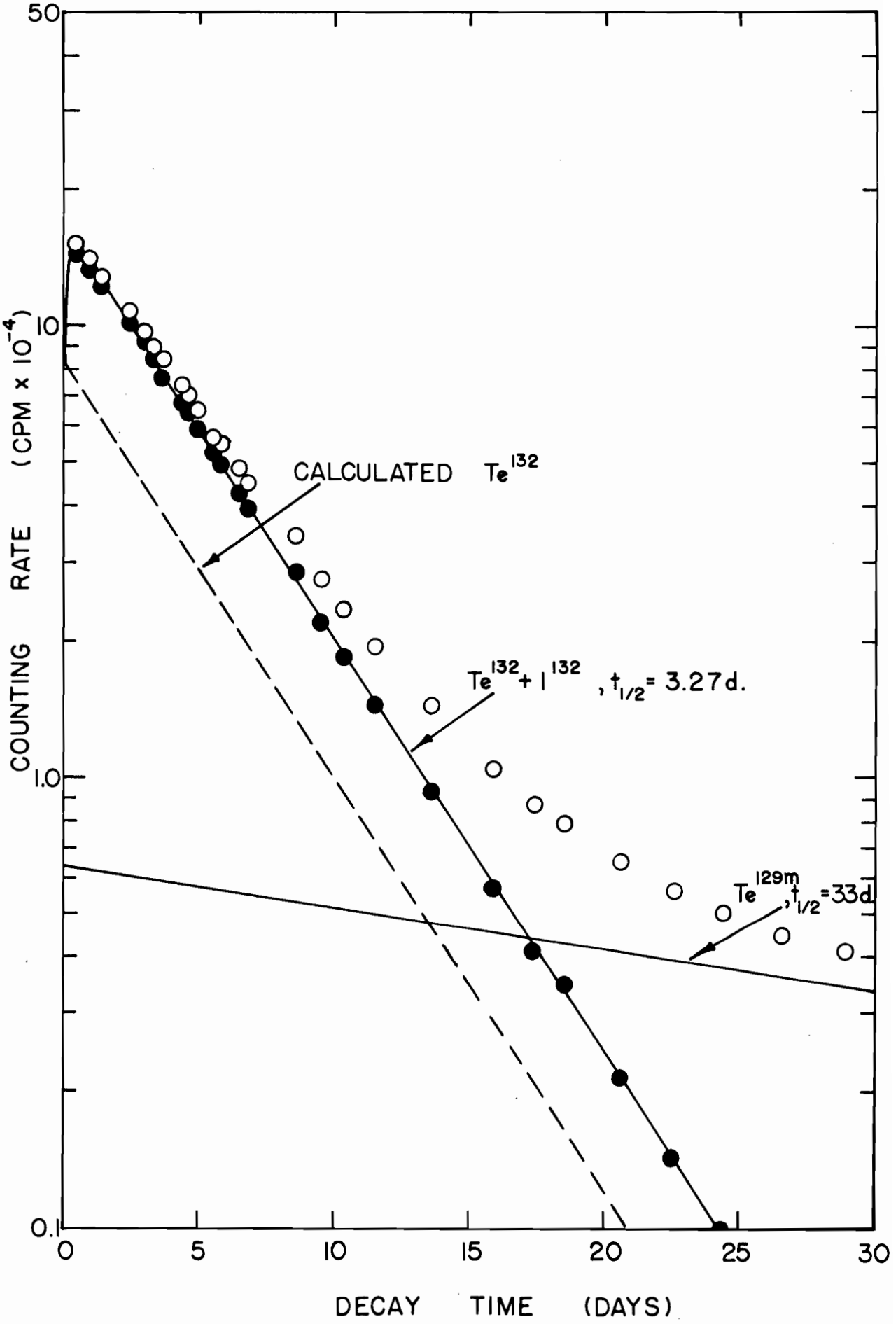
50
10
1.0
0.1
COUNTING RATE (CPM x 10^{-4})
CALCULATED Te^{132}
$Te^{132} + I^{132}$, $t_{1/2}$ = 3.27 d.
Te^{129m}, $t_{1/2}$ = 33 d.
0
5
10
15
20
25
30
DECAY TIME (DAYS)

Figure 58

GAMMA-RAY SPECTRUM OF TELLURIUM FRACTION

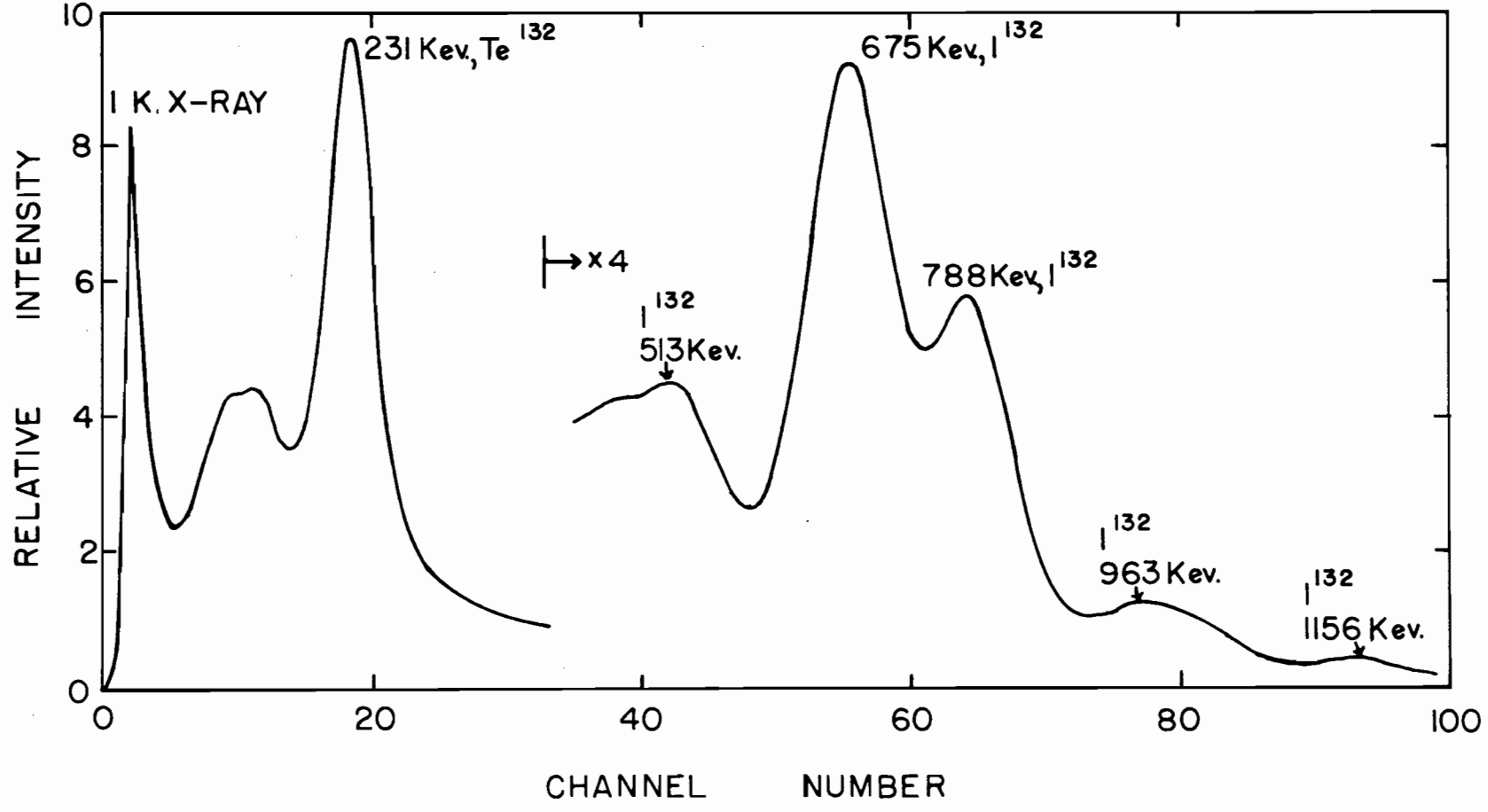
10
8
6
4
2
0
RELATIVE INTENSITY
I K. X-RAY
231 Kev., Te 132
675 Kev., I 132
x4
I 132
513 Kev.
788 Kev., I 132
I 132
963 Kev.
I 132
1156 Kev.
0
20
40
60
80
100
CHANNEL NUMBER

Figure 59

DECAY OF 230 AND 675 KEV GAMMA RAYS FROM SEPARATED TELLURIUM SAMPLE

($t_{\frac{1}{2}}$ = 3.4 days)

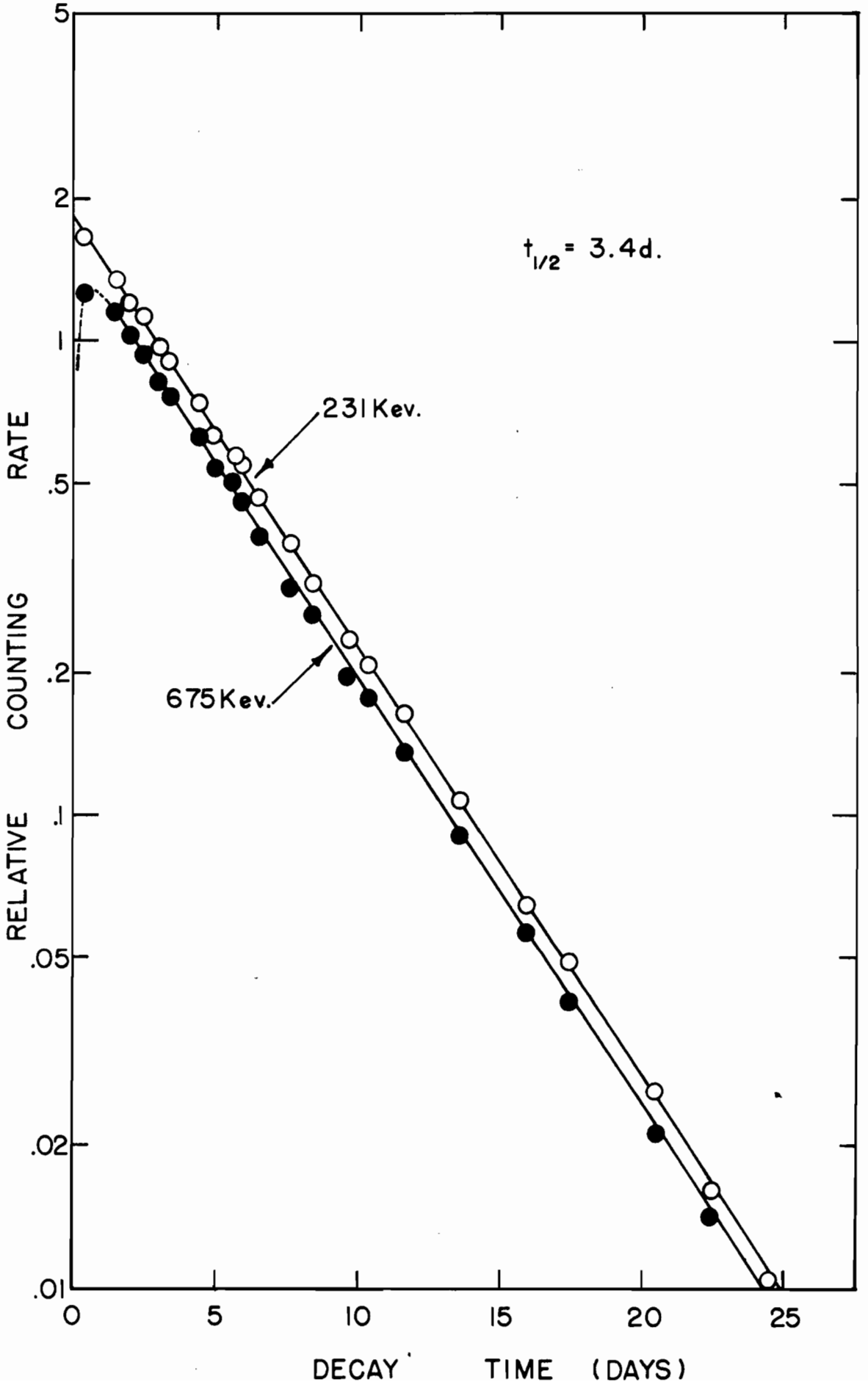
5
2
1
.5
.2
.1
.05
.02
.01
RELATIVE COUNTING RATE
$t_{1/2}$ = 3.4d.
231 Kev.
675 Kev.
0
5
10
15
20
25
DECAY TIME (DAYS)

Te^{132} decays to I^{132} with a half-life of 78 hours[54] by the emission of a 220 kev (100%) beta ray which has a 230 kev gamma ray in coincidence with it. I^{132} decays with a half-life of 2.4 hours by β^- emission (discussed under iodine) with coincident gamma-ray emission of which the more intense rays have energies of 520, 670, 777, 960, and 1160 kev respectively.

Fission yield data for Te^{132} are given in Table XVIII.

(n) Iodine

Iodine was separated from the other fission products by the solvent extraction method of Glendenin and Metcalf[80]. Iodide carrier was added and a preliminary oxidation of I^- to IO_4^- (periodate) was performed by NaClO in alkaline solution. Exchange between active iodine and the carrier is ensured by heating or allowing oxidation to proceed at room temperature followed by reduction to I_2 with hydroxylamine hydrochloride in acid solution. The iodine is then extracted with carbon tetrachloride followed by extraction with water containing $NaHSO_3$. Another oxidation-reduction cycle followed in which $NaNO_2$ was used to oxidize I^- to I_2 and SO_2 for the reduction of I_2 to I^-. The solution was then boiled to remove excess sulphur dioxide after which the I^- was neutralized with a dilute lithium hydroxide solution and made up to a volume of 10 mls.

Table XVIII

FISSION YIELD DATA FOR Te^{132} (78.5 HOURS)

Irradiation	H	J	Calculated from I^{132} (2.4 h.) B	D
Observed activity (c/m)	8.31×10^4	3.125×10^5	3.79×10^5	1.553×10^5
Source-mount absorption factor	0.992	0.992	1.00	1.00
Self-absorption factor	0.990	0.960	1.00	0.998
Aliquot factor	5000	2000	5000	2000
Chemical yield (%)	51.93	85.25	93.44	89.21
Time after irradiation (days)	6.973	8.027	6.159	8.382
Decay factor	0.2281	0.1825	0.2644	0.1636
Time in reactor (days)	2.133	2.056	2.005	1.994
Saturation factor	0.3636	0.3531	0.3515	0.3500
Activity at saturation (d/s)	1.636×10^8	1.988×10^8	3.625×10^8	1.015×10^8
Fission rate (f/s)	2.854×10^9	3.724×10^9	6.300×10^9	1.9431×10^9
Fission yield (%)	5.73	5.34	5.75	5.22

Chemical yield was determined by oxidizing the I^- to I_2 from an aliquot of the solution, extracting with a fixed volume of CCl_4 and measuring the absorbance at 517 m [81]. The standardization curve for this method is given in Fig. 60.

Sources for beta disintegration determinations were prepared by pipetting aliquots of the lithium iodide solution on to gold-coated VYNS films and drying them under an infra-red lamp. Kjelberg et al.[82] have used this technique in preparing iodide sources for 4 π counting. The lithium iodide continuously released the xenon formed by the decay of iodine activity and no measurable evaporation losses of iodine activity were found. The decay curve was resolved graphically into an 8.05-day component, a 23-hour component, and a 2.4-hour component, as shown in Figs. 61 and 62. These were taken to be 8.05-day I^{131}, 21-hour I^{133}, and 2.4-hour I^{132}. The decay chains for these masses are

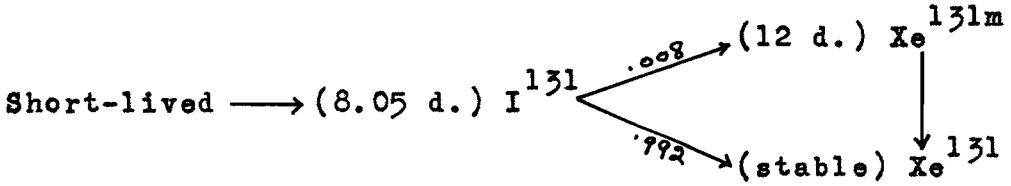

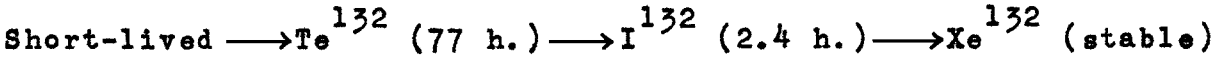

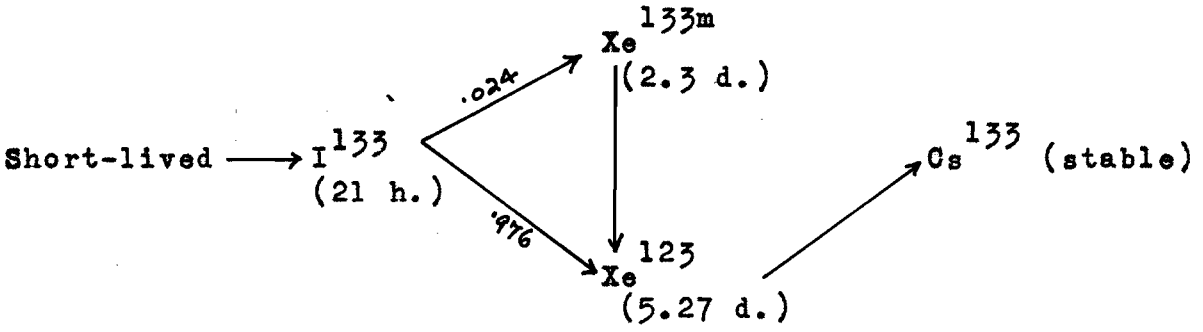

Figure 60

STANDARD ABSORBANCE CURVE FOR IODINE

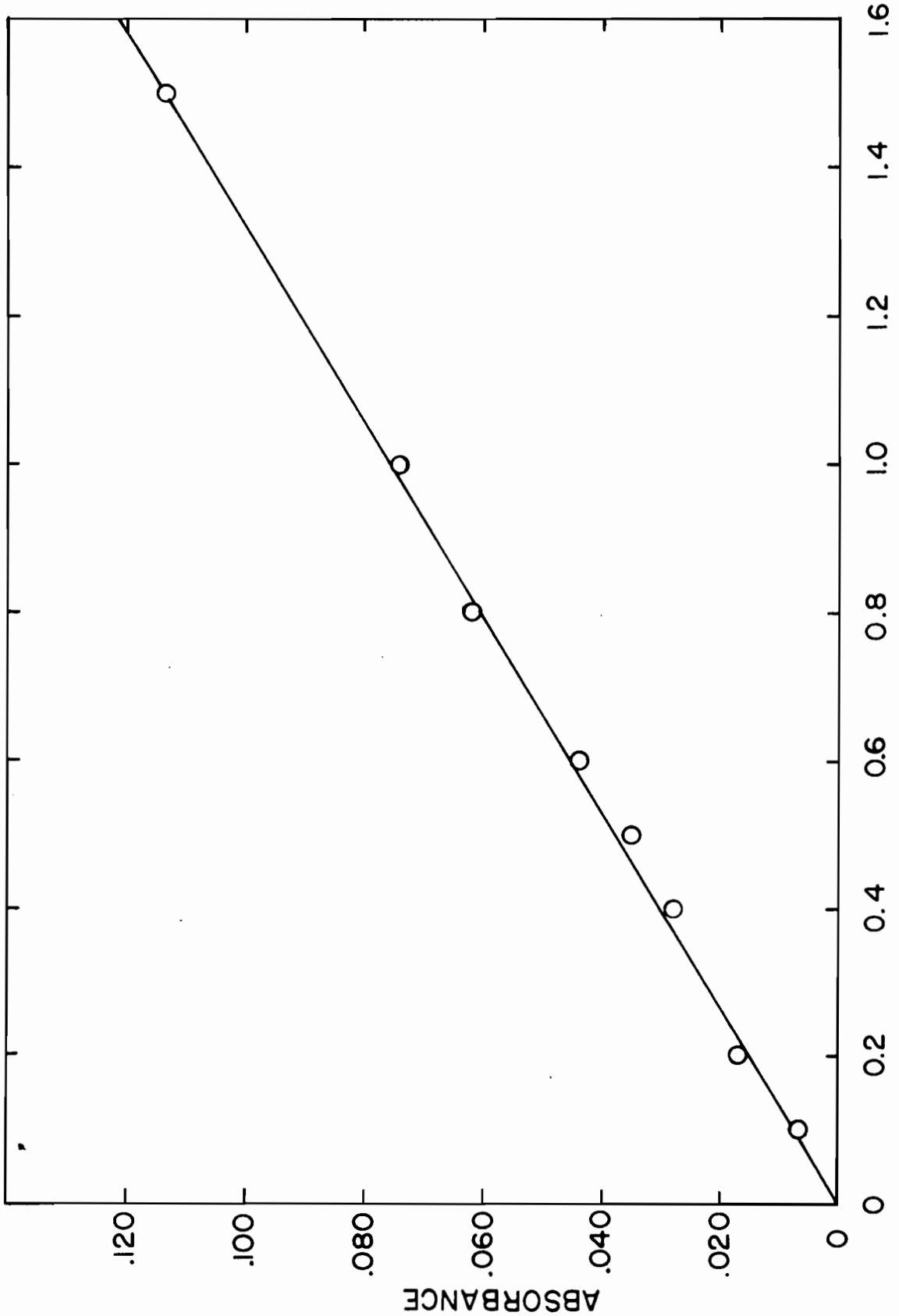
ABSORBANCE
.120
.100
.080
.060
.040
.020
0
0
0.2
0.4
0.6
0.8
1.0
1.2
1.4
1.6
mg. I_2 per 50 ml.

Figure 61

β^- DECAY OF I^{131}

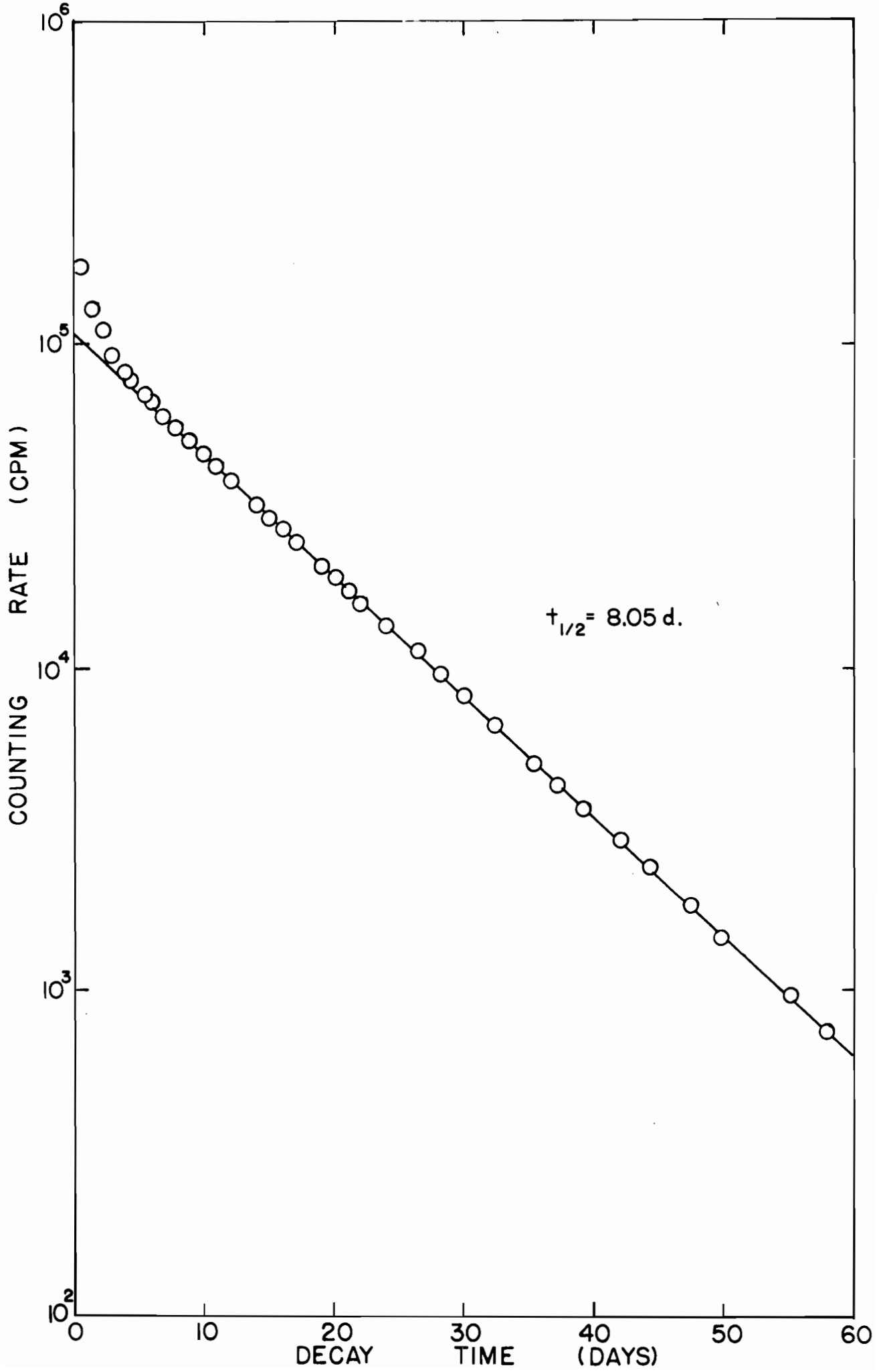
10^6
10^5
10^4
10^3
10^2
COUNTING RATE (CPM)
$t_{1/2}$= 8.05 d.
0
10
20
30
40
50
60
DECAY TIME (DAYS)

Figure 62

β^- DECAY OF I^{132} AND I^{133}

x - Experimental points

0 - 8.05-day activity subtracted

● - 23-hour activity subtracted

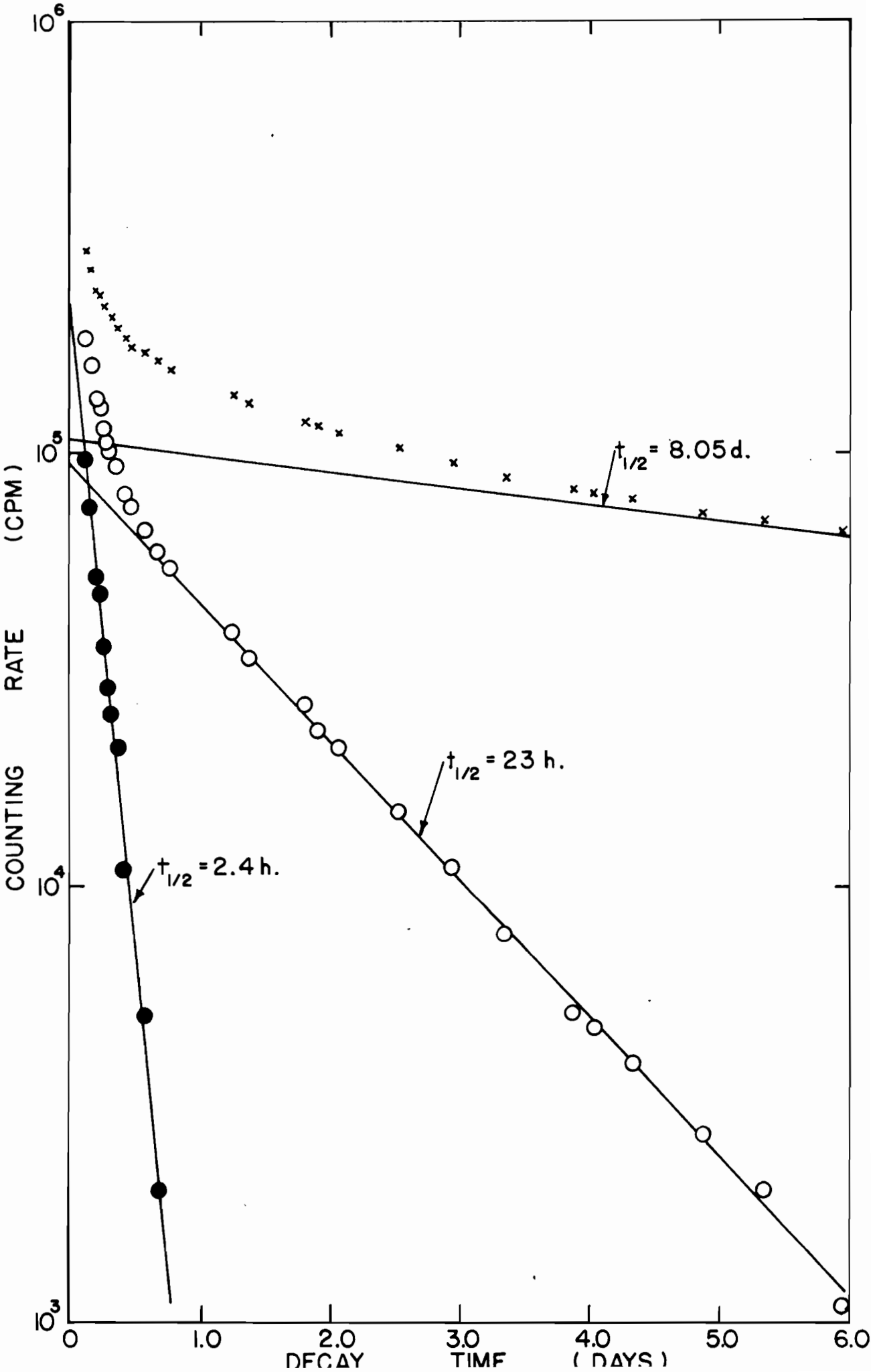
10^6
10^5
10^4
10^3
COUNTING RATE (CPM)
$t_{1/2}$ = 8.05 d.
$t_{1/2}$ = 23 h.
$t_{1/2}$ = 2.4 h.
0
1.0
2.0
3.0
4.0
5.0
6.0
DECAY TIME (DAYS)

I^{131} decays with a half-life of 8.05 days[54] by β^- emission of maximum energies 250 kev (2.8%), 330 kev (9.1%), 608 kev (87.5%), and 810 kev (0.7%). Its more intense gamma rays have energies of 284, 364, 638, and 724 kev respectively. I^{132} decays with a half-life of 2.4 hours by emission of β^- rays with maximum energies of 800 kev (21%), 1.04 Mev (15%), 1.22 Mev (12%), 1.49 Mev (12%), 1.61 Mev (21%), and 2.14 Mev (18%). Twenty-seven gamma rays are listed for I^{132}, but the more intense have energies of 520, 670, 777, and 960 kev. I^{133} decays with a half-life of 21 hours[54] by the emission of β^- rays with maximum energies of 650 kev (9%) and 1.4 Mev (91%). Its most intense gamma ray has an energy of 530 kev. A gamma spectrum of the iodine fraction, taken $\sim$ 6 hours after separation, showed gamma peaks at 350, 530, and 678 kev [Fig. 63(a)]. Thirteen days later only a 360 and a 655 kev gamma peak could be seen [Fig. 63(b)]. The 360 kev peak was observed to decay with a half-life of 8.00 days (Fig. 64) while the 530 and the 678 kev peaks decayed with half-lives of 21 hours and 2.4 hours respectively (Fig. 65). Fission yield data for I^{131} are given in Table XIX and for I^{133} in Table XX. Since the independently formed I^{132} (2.4 hours) had decayed away when the iodine separations were performed, this activity results from the decay of Te^{132} (77 hours) and was used to calculate the fission yield of Te^{132} (reported in Table XVIII).

Figure 63

GAMMA SPECTRUM OF IODINE FRACTION

(a) 6 hours after separation

(b) 13 days after separation

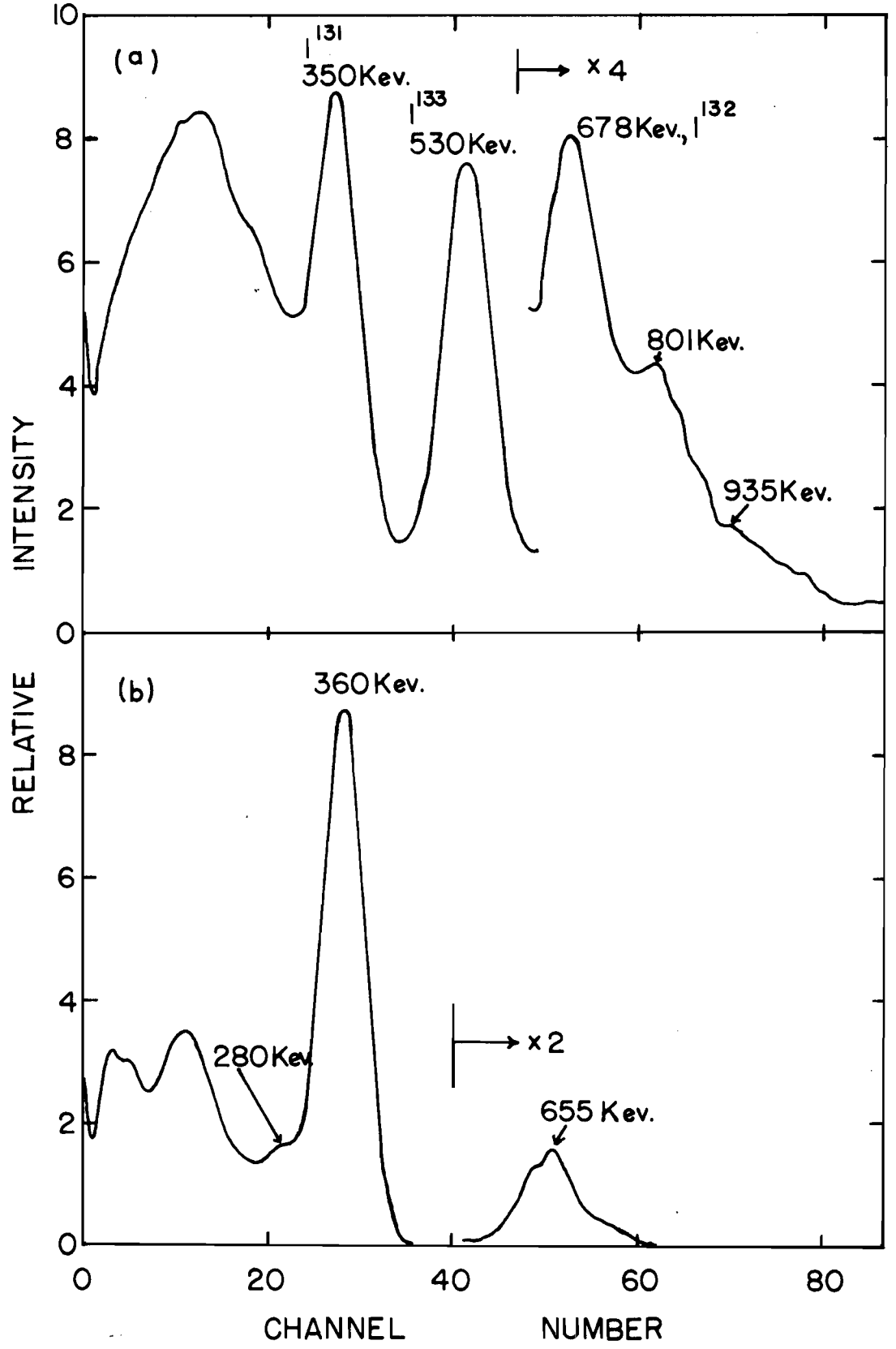
(a)
I^{131}
350Kev.
I^{133}
530Kev.
678Kev., I^{132}
801Kev.
935Kev.
× 4
INTENSITY
(b)
360Kev.
280Kev.
× 2
655 Kev.
RELATIVE
0
2
4
6
8
10
0
20
40
60
80
CHANNEL NUMBER

Figure 64

DECAY OF 360 KEV GAMMA RAY OF I^{131}

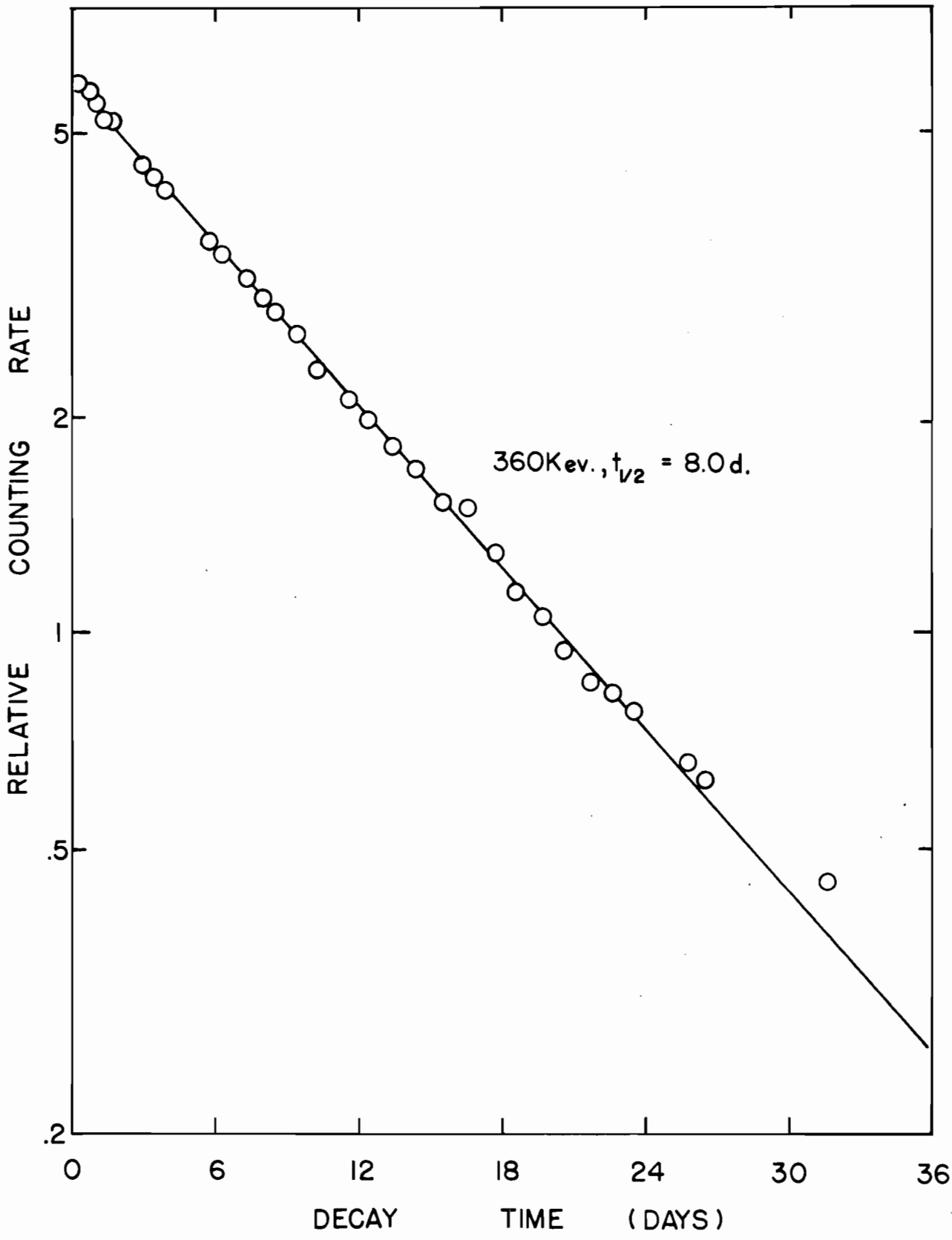
RELATIVE COUNTING RATE
5
2
1
.5
.2
360Kev., $t_{1/2}$ = 8.0 d.
0
6
12
18
24
30
36
DECAY TIME (DAYS)

Figure 65

DECAY OF 530 KEV AND 678 KEV GAMMA RAYS

OF IODINE FRACTION

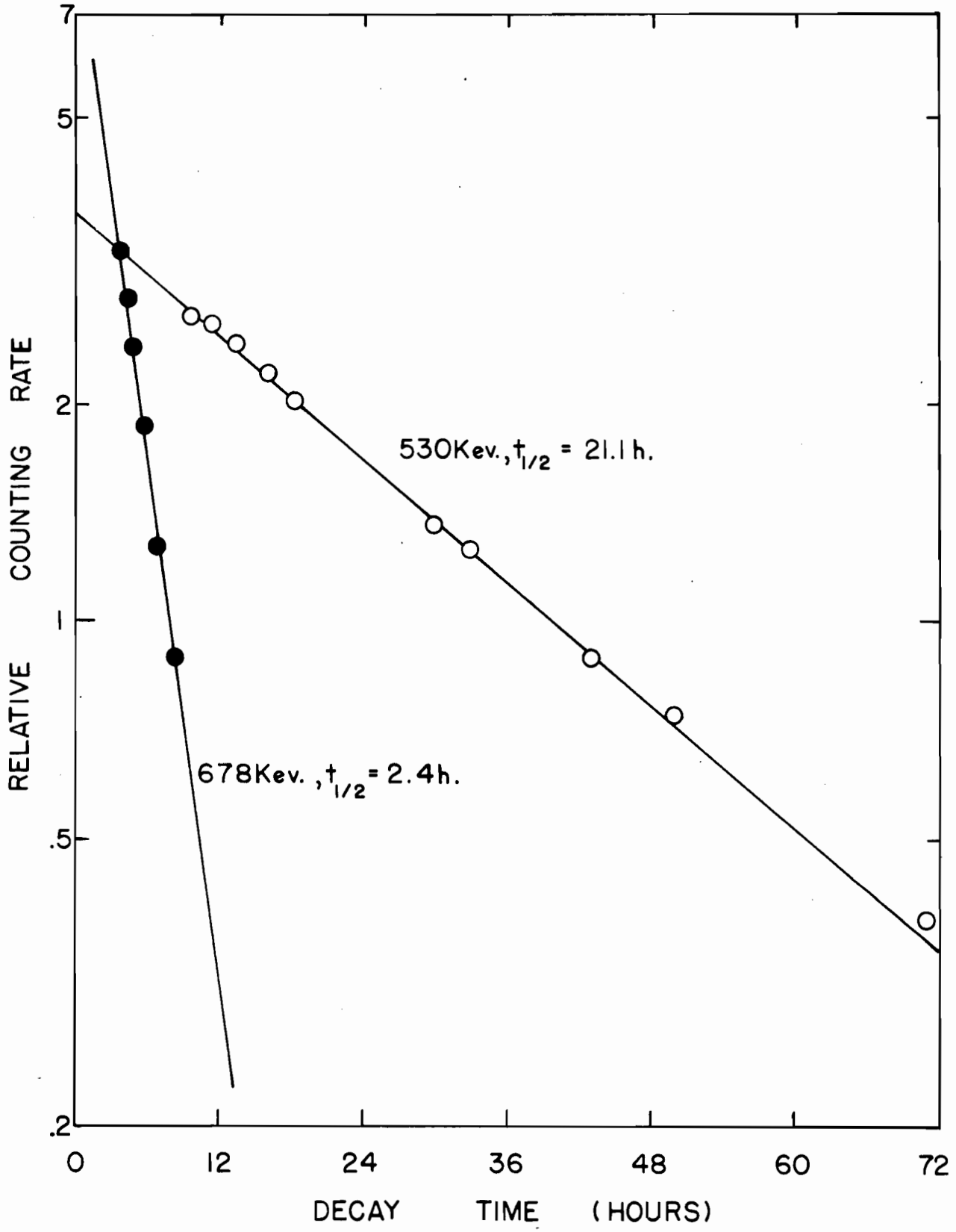
7
5
2
1
.5
.2
RELATIVE COUNTING RATE
530Kev., $t_{1/2}$ = 21.1 h.
678Kev., $t_{1/2}$ = 2.4h.
0
12
24
36
48
60
72
DECAY TIME (HOURS)

Table XIX

FISSION YIELD DATA FOR I^{131} (8.05 DAYS)

Irradiation	B	D	E	F
Observed activity (c/m)	2.50×10^5	1.575×10^5	1.08×10^5	1.30×10^5
Source-mount absorption factor	0.998	0.998	0.998	0.998
Self-absorption factor	0.993	0.991	0.997	0.991
Aliquot factor	5000	2000	5000	2000
Chemical yield (%)	93.44	89.21	94.08	96.26
Time after irradiation (days)	6.159	8.382	3.337	2.318
Decay factor	0.5885	0.4860	0.7503	0.8191
Time in reactor (days)	2.005	1.994	2.007	1.998
Saturation factor	0.1585	0.1578	0.1587	0.1580
Activity at saturation (d/s)	2.412×10^8	7.757×10^7	8.072×10^7	3.516×10^7
Fission rate (f/s)	6.300×10^9	1.9431×10^9	2.1633×10^9	9.610×10^8
Fission yield (%)	3.83	3.99	3.73	3.66

Table XX

FISSION YIELD DATA FOR I^{133} (23 HOURS)

Irradiation	E	F
Observed activity	9.4×10^4 c/m	2.25×10^5 c/m
Source-mount absorption factor	1.00	1.00
Self-absorption factor	1.00	0.998
Aliquot factor	5000	2000
Chemical yield	94.08%	96.26%
Time after irradiation	3.337 d.	2.318 d.
Decay factor	0.0924	0.1912
Time in reactor	2.007 d.	1.998 d.
Saturation factor	0.7613	0.7598
Activity at saturation	1.184×10^8 d/s	5.372×10^7 d/s
Fission rate	2.1633×10^9 f/s	9.6100×10^8 f/s
Fission yield	5.47%	5.59%

(o) Cesium

Cesium activity was separated from an aliquot of the fission product mixture by the method of Glendenin and Nelson[83]. After adding inactive cesium carrier, a silico-tungstate precipitation was performed which was specific for cesium. The precipitate was dissolved in sodium hydroxide and the cesium converted to the perchlorate by boiling the solution with 70% $HClO_4$. Upon diluting the resulting solution, silica and tungstic acid were precipitated and removed by centrifugation. The supernate was again fumed with perchloric acid from which, after cooling, the cesium perchlorate was precipitated by the addition of absolute alcohol. The cesium perchlorate was dissolved in water and the resulting solution scavenged by precipitating ferric hydroxide with NH_4OH from the heated solution. After removing the ferric hydroxide, the supernate was boiled with a small amount of sodium hydroxide to remove ammonia completely. From this solution the cesium was precipitated as perchlorate. The precipitate was washed several times with absolute alcohol, dissolved in water, and made up to volume.

From this solution, 100 λ aliquots were removed for $4\pi\beta^-$ counting and a 1 ml aliquot was used for analysis on the multichannel pulse height analyser. The remainder of the solution was used for chemical yield determination. This was done by precipitating the cesium as the chloroplatinate

and weighing.

The cesium activities expected to be present arise from the following decay chains:

136. $_{55}Cs^{136} \xrightarrow{13\ d.} {}_{56}Ba^{136}$ (stable)

137. Short-lived $\longrightarrow {}_{54}Xe^{137}$ (3.9 m) $\longrightarrow {}_{55}Cs^{136}$ (30 y.) $\xrightarrow{.95} {}_{56}Ba^{137m}$ (2.6 m) $\longrightarrow {}_{56}Ba^{137}$ (stable); $Cs^{136} \xrightarrow{.05} {}_{56}Ba^{137}$ (stable)

The gross β^- decay of the cesium activity is shown in Fig. 66. The curve was resolved graphically into two components:

(1) a long-lived component which had a counting rate considerably above background, and

(2) a 12.9-day component.

The latter activity was assumed to be Cs^{136} which has a reported half-life of 12.9 days[84], while the former was assumed to be Cs^{137} in equilibrium with Ba^{137m}. Cs^{137} has a reported half-life of 29.68 years[47]. A gamma-ray spectrum of the cesium activity taken 8 hours after separation is shown in Fig. 67(a). Gamma rays of energies 54, 135, 243, 324, 660, 848, 1088, 1270, 1456, and 1963 kev respectively characterized the gamma spectrum. A subsequent gamma

Figure 66

β^- DECAY OF CESIUM ACTIVITY

O - Experimental points

● - Long-lived activity subtracted

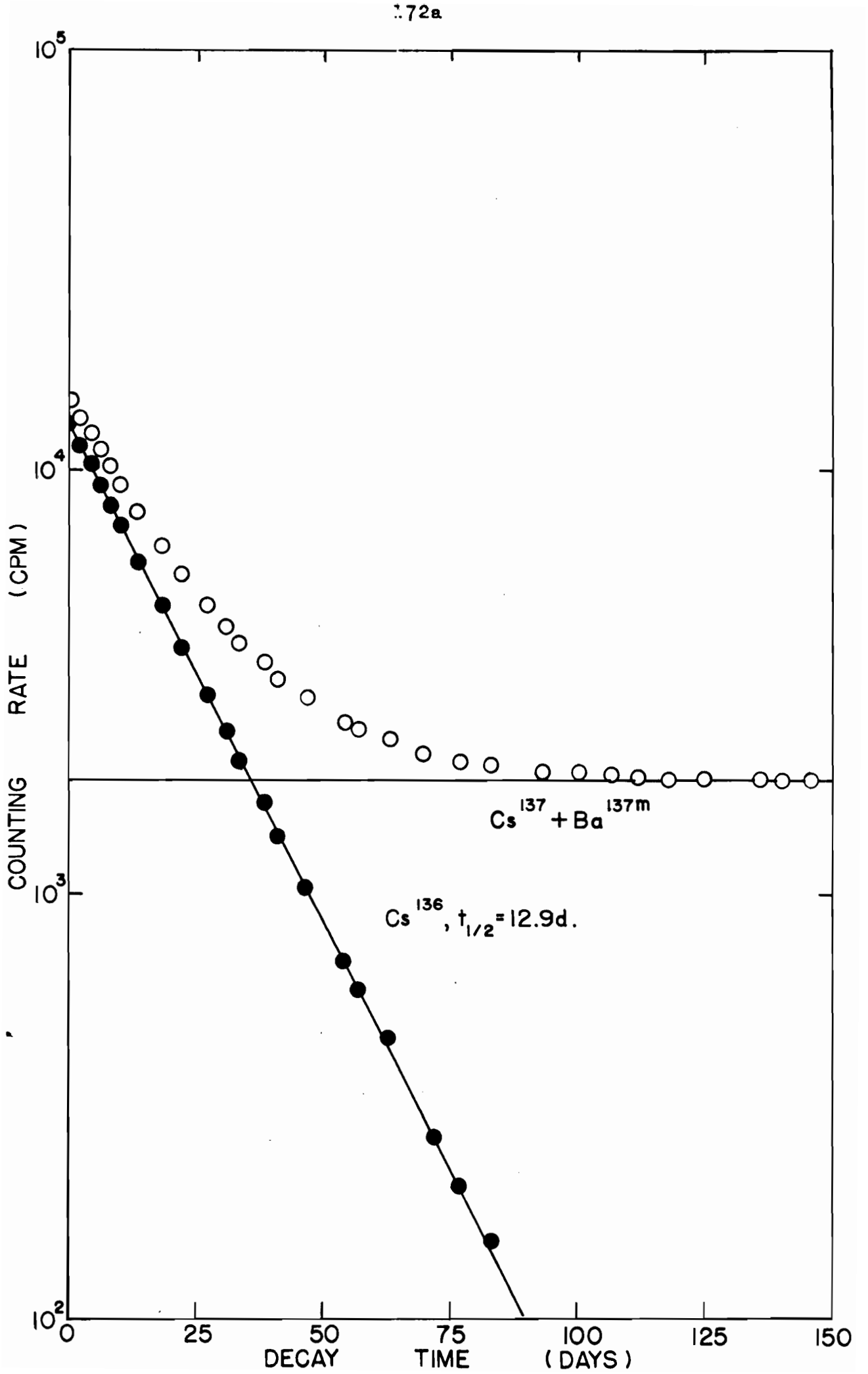
10^5
10^4
10^3
10^2
COUNTING RATE (CPM)
$Cs^{137} + Ba^{137m}$
Cs^{136}, $t_{1/2}$ = 12.9d.
0
25
50
75
100
125
150
DECAY TIME (DAYS)

Figure 67

GAMMA SPECTRUM OF CESIUM

(a) 8 hours after separation

(b) 100 days after separation

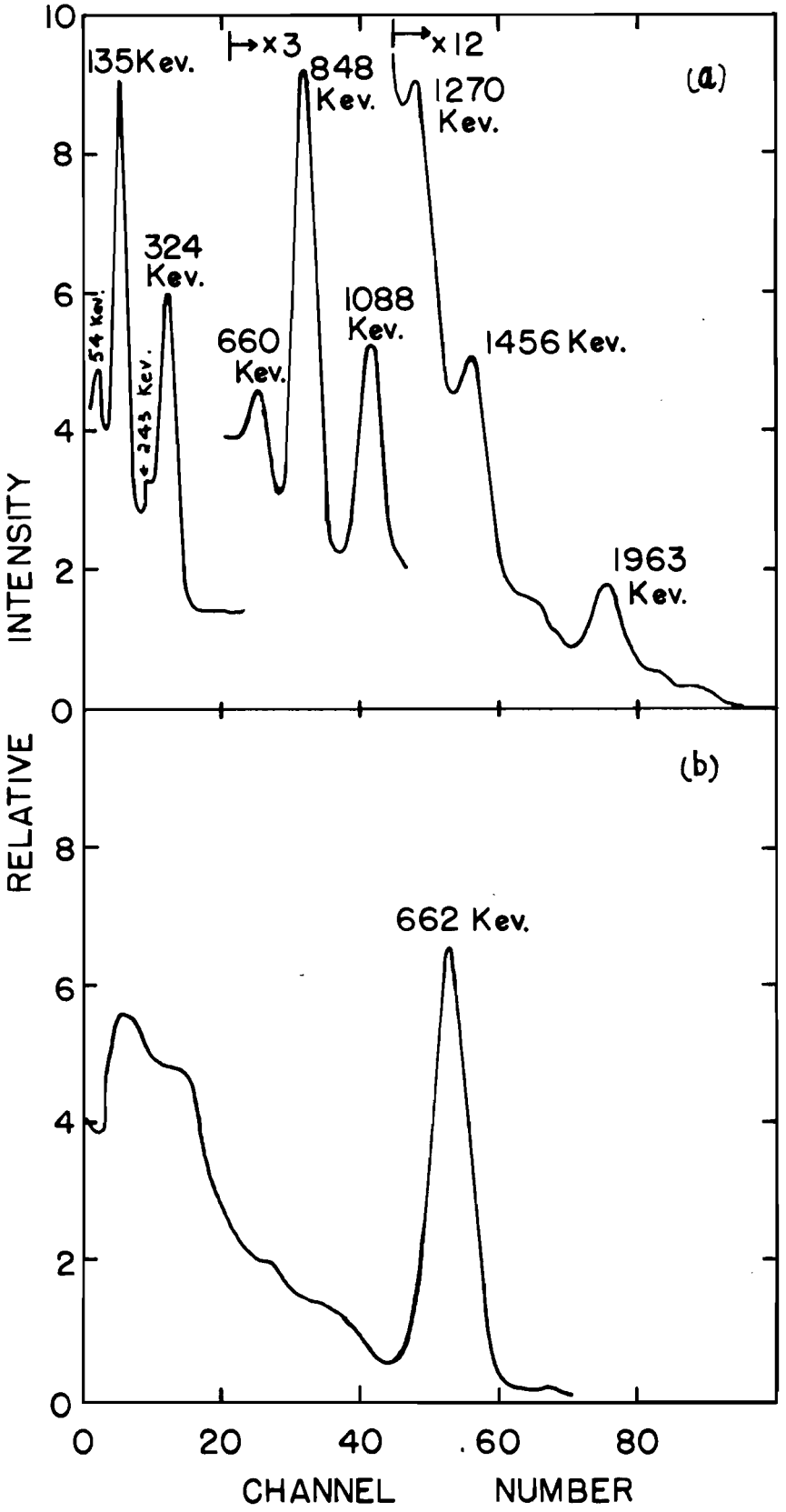
10
8
6
4
2
0
INTENSITY
→x3
→x12
135Kev.
54 Kev.
324 Kev.
245 Kev.
660 Kev.
848 Kev.
1088 Kev.
1270 Kev.
1456 Kev.
1963 Kev.
(a)
(b)
RELATIVE
662 Kev.
0
20
40
60
80
CHANNEL NUMBER

spectrum [Fig. 67(b)], taken 100 days after separation, showed only a 662 kev gamma ray. A comparison of these gamma spectra with Cs^{136} and Cs^{137} gamma spectra given by Heath[65] and the Nuclear Data Sheets[54] is shown in Table XXI. The decay of the 135, 848, and 1088 kev gamma rays was followed on the multichannel analyser. These were observed to die away with a half-life of 12.3 days as shown in Fig. 68.

Cs^{136} decays to Ba^{136} by the emission of beta rays with maximum energies of 347 kev (92.6%) and 657 kev (7.4%). Gamma rays from excited levels of Ba^{136} are in coincidence with these β^- rays and with one another. Disintegration rate calculations are therefore straightforward. Details of the fission yield calculations are given in Table XXII.

Cs^{137} decays to a metastable state of Ba^{137} as illustrated in the decay scheme below:

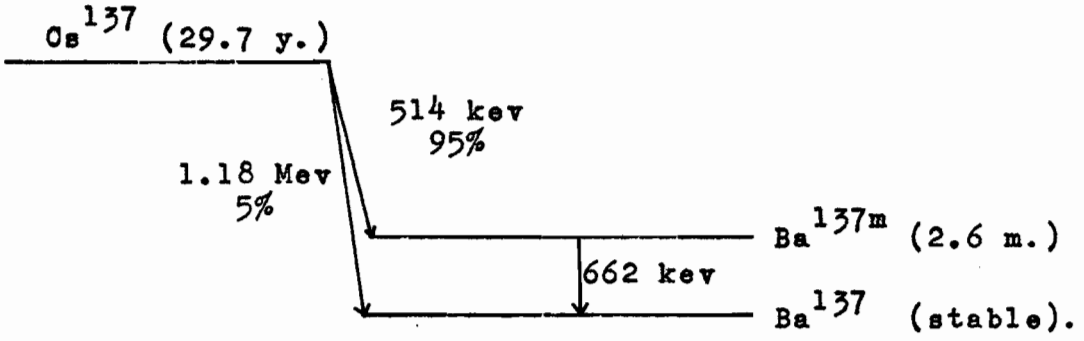

The 662 kev gamma ray is internally converted and a correction has therefore to be applied for the conversion electrons and the delayed gamma rays of this isomeric transition. The

Table XXI

COMPARISON BETWEEN GAMMA RAYS OF Cs^{136} AND Cs^{137} OBSERVED AND FROM THE LITERATURE

	Gamma-ray energies (kev)			
Nuclide	Observed	Heath[65]	Nuclear Data Sheets[54]	
Cs^{136}		30 (X-ray)		
	54	67	67	-
		87	86	88
	135	160 (+ 170)	152	153
			170	162
			200	-
	243		230	-
		270	270	265
	324	340	337	335
	848	820	830	822
	1088	1040	1065	1041
	1270	1230	1255	1245
			Sum Peaks	
	1456	1400	1410	1410
	1963	1860	1900	-
			2090	-
			2240	-
			2430	2350
			2490	2490
Cs^{137}		32 Ba K X-ray	K X-ray	
	662	662	662	

Figure 68

DECAY OF GAMMA PEAKS OF CESIUM ACTIVITY

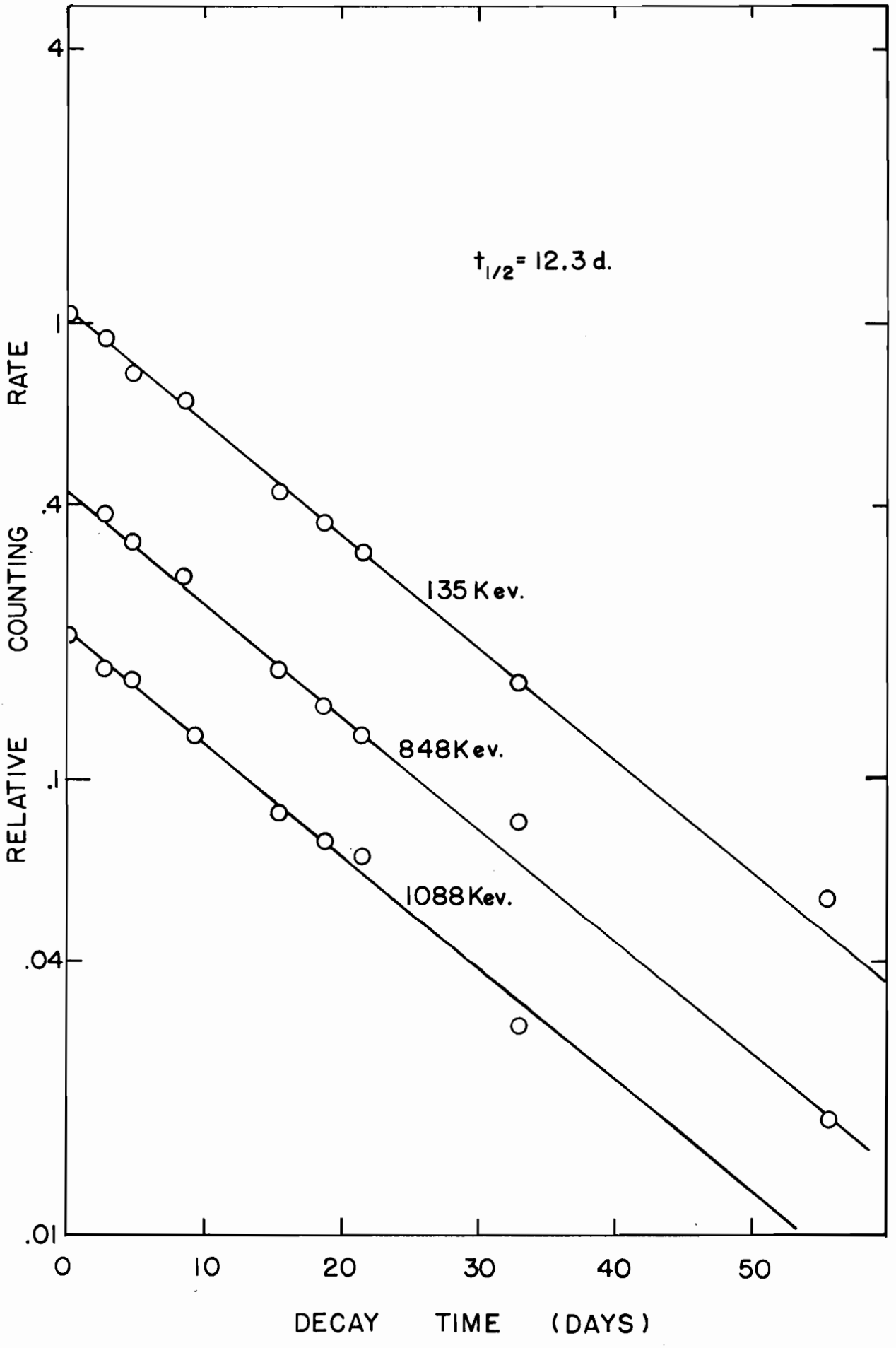
4
1
.4
.1
.04
.01
RELATIVE COUNTING RATE
$t_{1/2}$ = 12.3 d.
135 Kev.
848 Kev.
1088 Kev.
0
10
20
30
40
50
DECAY TIME (DAYS)

Table XXII

FISSION YIELD DATA FOR Cs^{136} (12.9 DAYS)

Irradiation	J	KB
Observed activity	1.30×10^4 c/m	4.946×10^3 c/m
Source-mount absorption factor	0.995	0.995
Self-absorption factor	0.965	0.960
Aliquot factor	333	125
Chemical yield	34.2%	39.8%
Time after irradiation	8.656 d.	25.004 d.
Decay factor	0.6281	0.2610
Time in reactor	2.056 d.	2.079 d.
Saturation factor	0.1046	0.1117
Activity at saturation	3.345×10^6 d/s	9.828×10^5 d/s
Fission rate	3.724×10^9 f/s	1.277×10^9 f/s
Fission yield	8.98×10^{-2} %	7.70×10^{-2} %

number of conversion electrons per disintegration of Cs^{137} is given by $\alpha_T/(1 + \alpha_T)$ which is calculated to be 0.1066 from $\alpha_K = 0.0976$, $\alpha_K/\alpha_L = 5.66$, $\alpha_L/\alpha_{M,N} = 3.85$ [85] and $\alpha_T = \alpha_K + \alpha_L + \alpha_{M,N}$. From this the number of unconverted gammas is 0.8934. The disintegration rate of Cs^{137} is then given by

$$\text{Observed D.R.} = Cs^{137}\text{D.R.}\left[1 + (0.1066 \times 0.95) + (0.8934 \times 0.95 \times 0.0018)\right]$$

where 0.95 is the branching ratio and 0.0018 is the estimated detection efficiency of the 4 π counter for the unconverted gamma rays.

$$\text{Thus} \quad \text{Observed D.R.} = 1.1028 \times Cs^{137}\text{ D.R.}$$

Since the observed disintegration rate is the sum of the Cs^{137} and the Ba^{137m} disintegration rates, then

$$N\lambda_{Ba^{137m}} = 0.1028\, N\lambda_{Cs^{137}} .$$

But
$$\frac{A_1 + A_2}{A_1} = 1 + \frac{c_2}{c_1}\frac{N_2\lambda_2}{N_1\lambda_1}$$

where the subscripts 1,2 refer to Cs^{137} and Ba^{137m} respectively, the A's are the observed counting rates, and the c's the detection efficiencies of the 4 π counter determined from the total absorption in the source-mount and the source itself.

Therefore
$$\frac{A_1 + A_2}{A_1} = 1 + \frac{0.1028\, c_2}{c_1}$$

and the Cs^{137} counting rate is given by

$$A_1 = \frac{\text{Observed counting rate}}{1 + \frac{0.1028\ c_2}{c_1}}$$

hence the Cs^{137} disintegration rate is given by

$$N_1 \lambda_1 = \frac{A_1}{c_1} = \frac{\text{Observed counting rate}}{c_1 + 0.1028\ c_2}$$

The disintegration rate for Cs^{137} was determined in this way and fission yields calculated as shown in Table XXIII.

Table XXIII

FISSION YIELD DATA FOR Cs^{137} (29.7 YEARS)

Irradiation	J	KB
Observed activity	1.700×10^3 c/m	1.573×10^3 c/m
Source-mount absorption factor	0.998	0.998
Self-absorption factor	0.975	0.972
Aliquot factor	333	125
Chemical yield	34.2%	39.8%
Time after irradiation	8.656 d.	25.004 d.
Decay factor	0.9995	0.9985
Time in reactor	2.056 d.	2.079 d.
Saturation factor	1.315×10^{-4}	1.3291×10^{-4}
Activity at saturation	2.157×10^8 d/s	6.396×10^7 d/s
Fission rate	3.724×10^9 f/s	1.277×10^9 f/s
Fission yield	5.79%	5.01%

(p) Barium

Barium was separated from the fission product mixture by the method of Glendenin[55]. After the addition of carriers, barium and strontium were isolated by precipitation of the nitrates with fuming nitric acid. The barium was then separated from strontium by precipitating $BaCrO_4$ from a buffered solution of the mixed nitrates. Further purification is achieved by repeated precipitations of $BaCl_2$ with an HCl-ether mixture. The final $BaCl_2$ precipitate was dissolved in water and made up to a volume of 10 mls. Chemical yields were determined by titration with EDTA in a 50% alcoholic solution using o-cresolphthalein complexone as indicator[49].

The activity of the prepared sources was measured as soon as possible after a separation. The counting rates were seen to increase to a maximum at about four days then to decrease with a half-life of 12.8 days, as shown in Fig. 69. This indicated the presence of 12.8-day Ba^{140} activity. The mass 140 decay chain is

$$\text{short-lived} \longrightarrow Ba^{140}(12.8\ \text{d.}) \longrightarrow La^{140}(40\ \text{h.}) \longrightarrow Ce^{140}\ (\text{stable}).$$

From the standard growth and decay equations, it can be shown that the growth of the lanthanum daughter activity is linear with respect to time for the first few hours after a separation. This allows back extrapolation to the time of separation, of a plot of the barium and lanthanum counting

Figure 69

β^- DECAY OF Ba^{140} - La^{140}

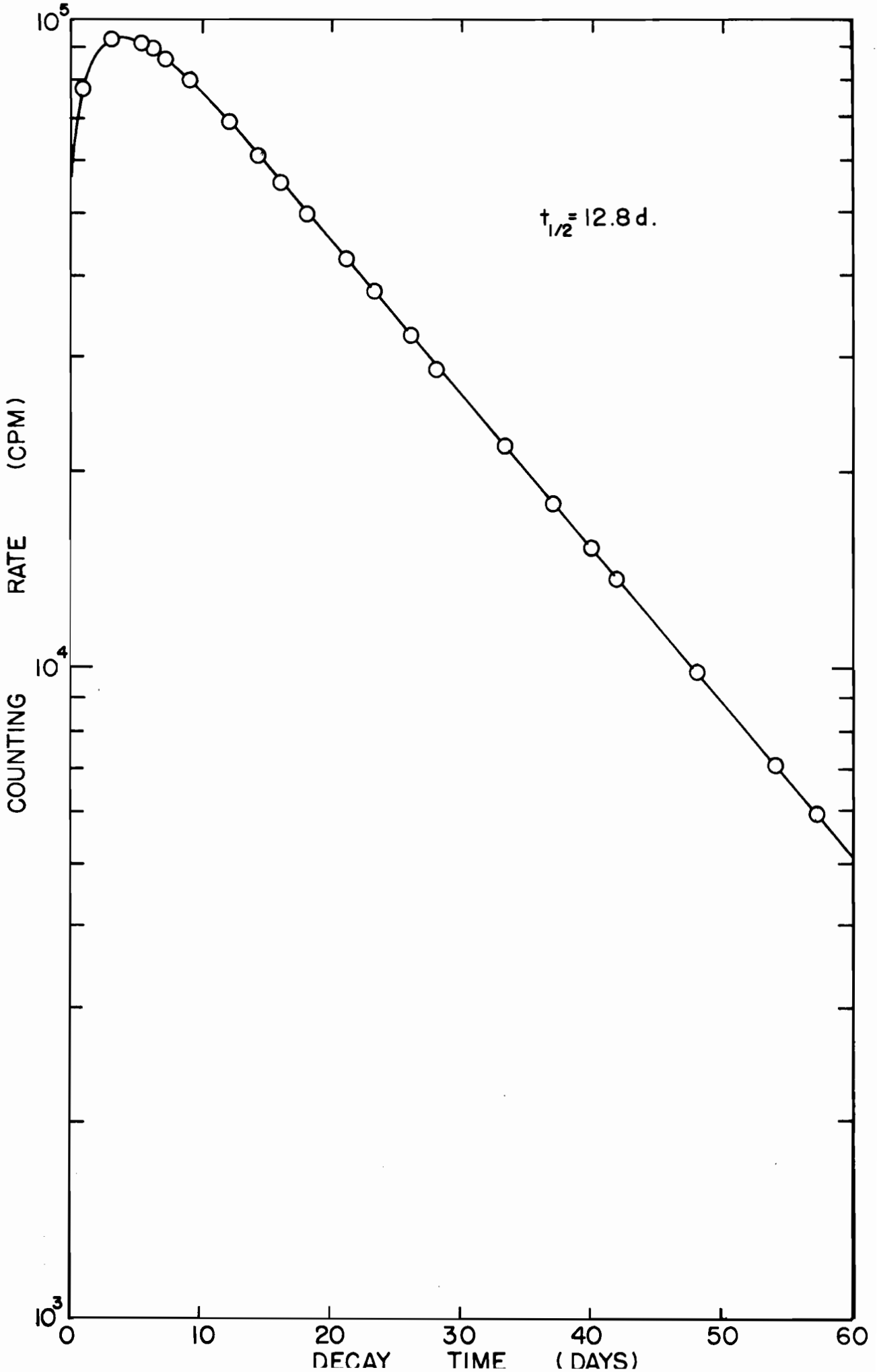
10^5
10^4
10^3
COUNTING RATE (CPM)
$t_{1/2}$ = 12.8 d.
0
10
20
30
40
50
60
DECAY TIME (DAYS)

rates versus time, when no lanthanum is present. As a check on this extrapolation, the initial Ba^{140} counting rates so obtained were used in growth and decay equations to calculate the barium and lanthanum counting rates at 1, 2, 3, and 4 hours after a separation. The calculated rates agree quite closely with the observed counting rates as shown in Fig. 70.

Ba^{140} decays with a half-life of 12.8 days[54] to La^{140} by the emission of β^- rays of maximum energies 480 kev (25%), 600 kev (10%), 900 kev (5%), and 1.01 Mev (61%). Gamma rays in coincidence with β^- emission have energies of 30, 118, 132, 162, 304, 422, 436, and 537 kev respectively. La^{140} also decays by β^- emission with maximum energies of 830(12%) kev, 1.10 (26%), 1.38 (45%), 1.71 (10%), and 2.20 (7%) Mev. There are 23 gamma rays in coincidence with β^- emission of which the more intense have energies of 329, 486, 816, 926 kev, 1.60 and 2.54 Mev respectively. A gamma-ray spectrum of the barium activity [Fig. 71(a)] about one hour after separation showed prominent peaks at 139, 290, 424, and 520 kev with less intense peaks at 847 and 1609 kev. In a second spectrum taken nine days after separation [Fig. 71(b)] the low energy peaks were seen to shift to 115, 280, and 485 kev; peaks at 828 and 1658 kev were more intense, and a prominent but low intensity peak showed up at 2588 kev. The decay of peaks at 115-139 kev, 280-290 kev, 485-524 kev, 828-847 kev, and 1609-1658 kev showed initial growths followed by decay with a half-life of 12.8 days, as shown in Fig. 72. Fission yield data for Ba^{140} are given in Table XXIV.

Figure 70

LINEAR GROWTH OF La^{140}

O Experimental points

● Averages

◐ Calculated from growth and decay equations

—— Least squares analysis

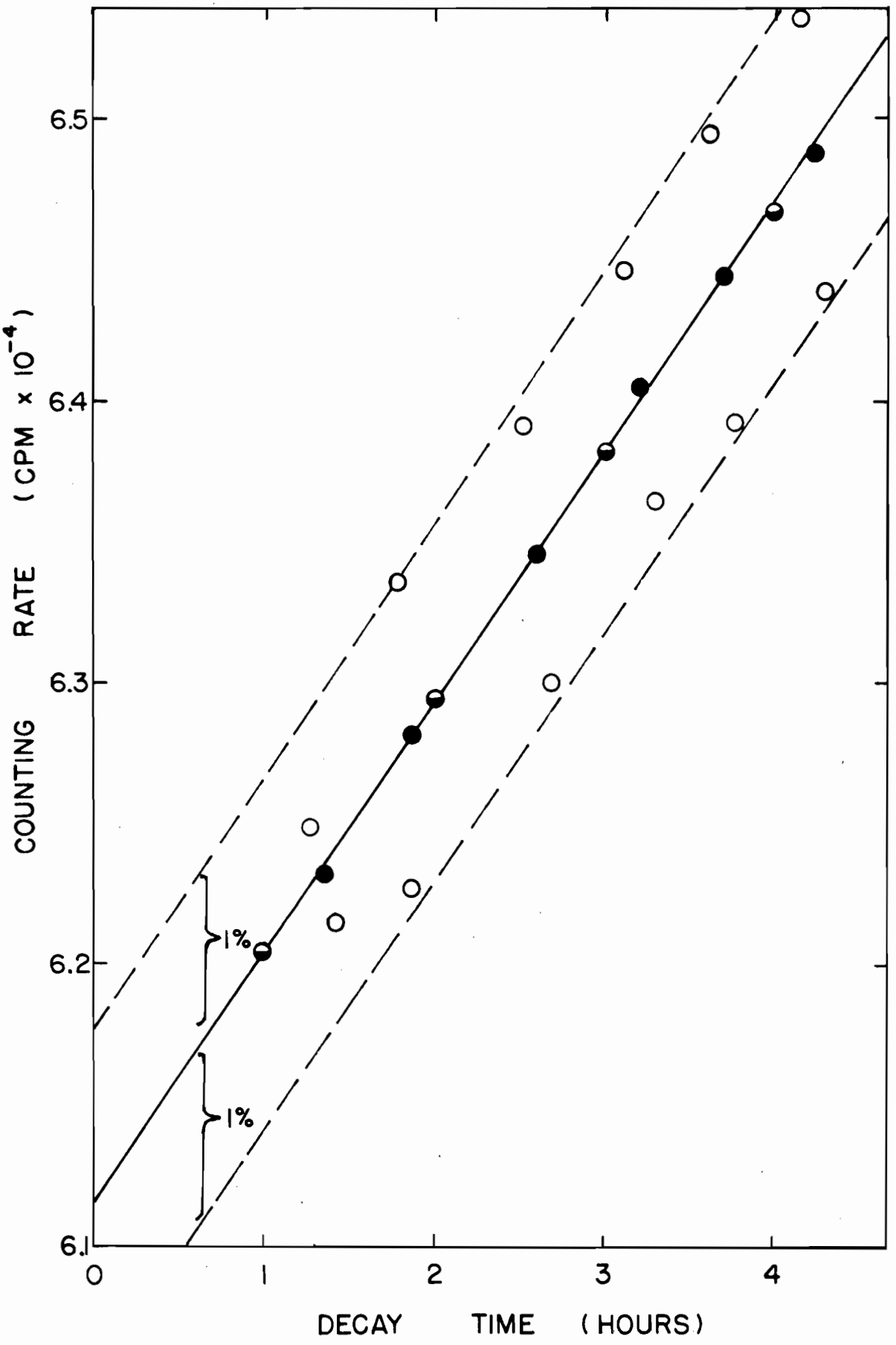
6.5
6.4
6.3
6.2
6.1
COUNTING RATE (CPM x 10^{-4})
1%
1%
0
1
2
3
4
DECAY TIME (HOURS)

Figure 71

Ba^{140} - La^{140} GAMMA SPECTRA

(a) One hour after separation

(b) Nine days after separation

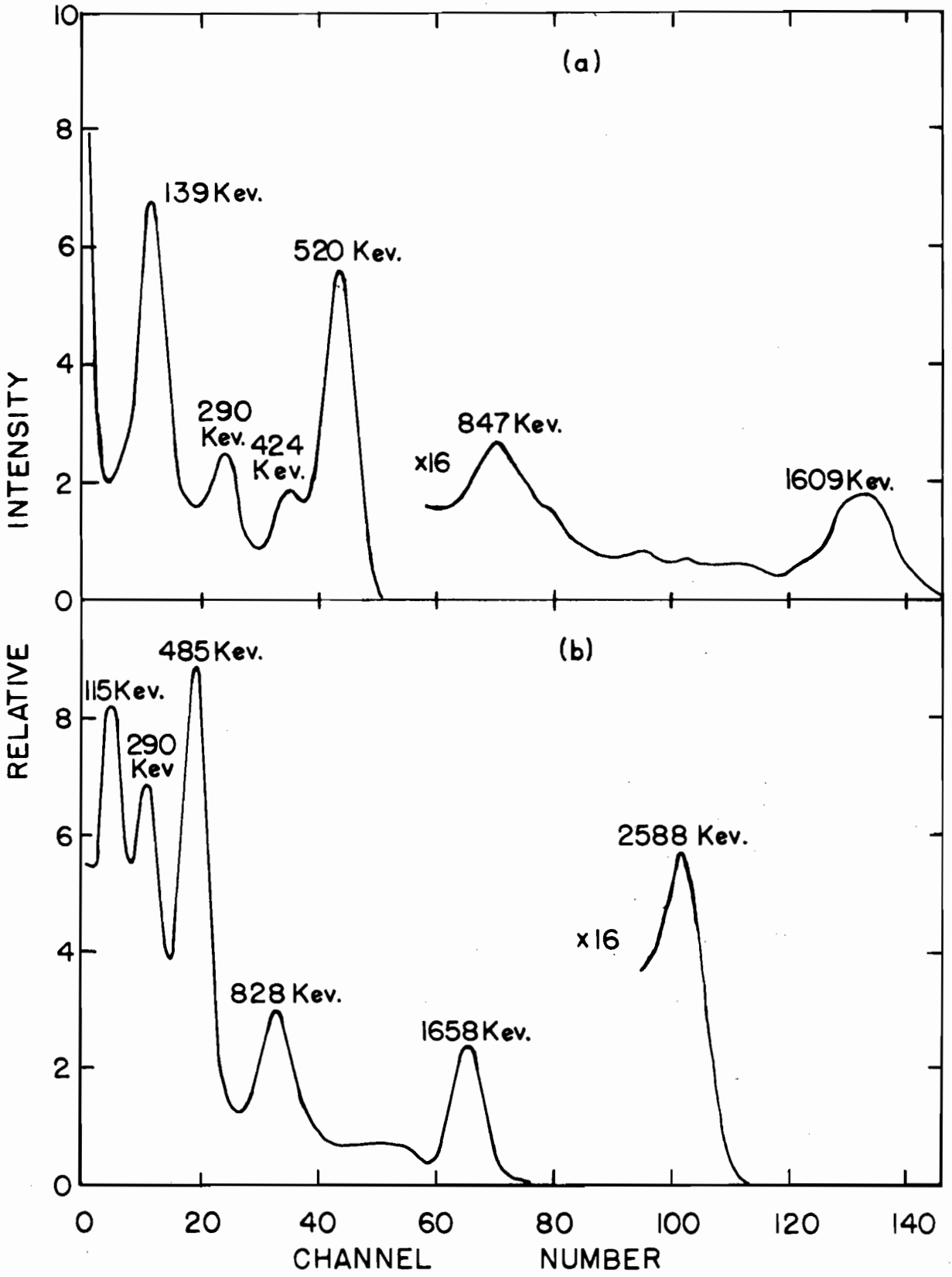
(a)
139 Kev.
520 Kev.
290 Kev.
424 Kev.
847 Kev.
x16
1609 Kev.
INTENSITY
(b)
485 Kev.
115 Kev.
290 Kev
2588 Kev.
x16
828 Kev.
1658 Kev.
RELATIVE
CHANNEL NUMBER
0
20
40
60
80
100
120
140
2
4
6
8
10

Figure 72

Ba^{140} - La^{140} GAMMA-RAY DECAY

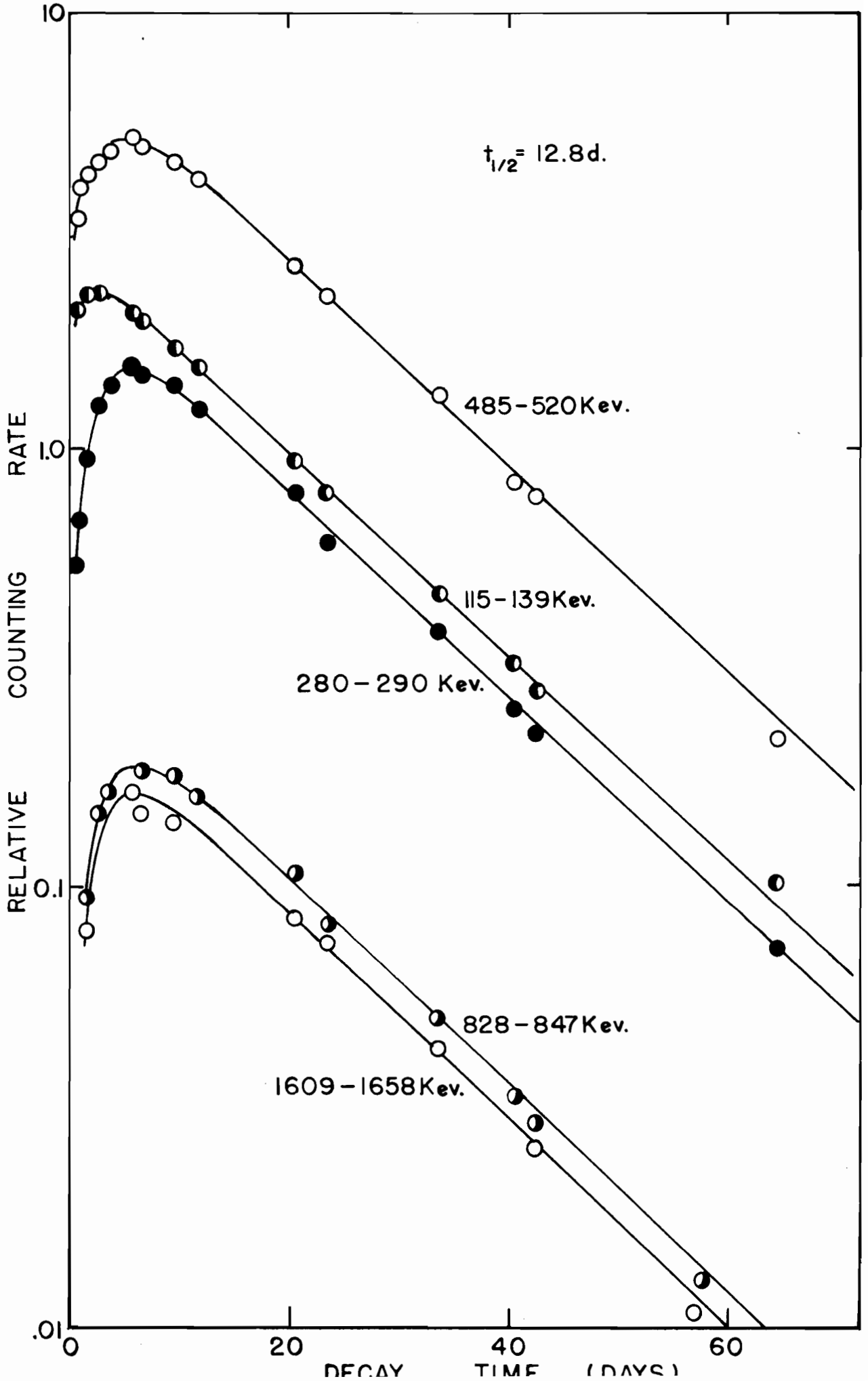
10
1.0
0.1
.01
RELATIVE COUNTING RATE
$t_{1/2}$= 12.8d.
485-520Kev.
115-139Kev.
280-290 Kev.
828-847Kev.
1609-1658Kev.
0
20
40
60
DECAY TIME (DAYS)

Table XXIV

FISSION YIELD DATA FOR Ba^{140} (12.8 DAYS)

Irradiation	A	B	D	E	F
Observed activity (c/m)	2.182×10^5	7.9499×10^4	4.2243×10^4	6.1151×10^4	3.8453×10^4
Source-mount absorption factor	1.00	1.00	1.00	1.00	1.00
Self-absorption factor	0.999	1.000	1.000	0.994	0.994
Aliquot factor	2500	5000	5000	1000	1000
Chemical yield (%)	62.36	42.45	40.72	32.01	38.41
Time after irradiation (days)	6.233	16.205	2.652	24.196	22.475
Decay factor	0.7136	0.4159	0.8662	0.2698	0.2962
Time in reactor (days)	2.033	2.005	1.994	2.007	1.998
Saturation factor	0.1043	0.1029	0.1024	0.1030	0.1026
Activity at saturation (d/s)	1.953×10^8	3.6467×10^8	9.7465×10^7	1.153×10^8	5.523×10^7
Fission rate (f/s)	3.567×10^9	6.300×10^9	1.9431×10^9	2.1633×10^9	9.610×10^8
Fission yield (%)	5.48	5.79	5.02	5.33	5.75

(q) Cerium

Cerium was isolated from the other fission products by oxidation with BrO_3^- in nitric acid and precipitating $Ce(IO_3)_4$ with HIO_3[59]. Repeated cycles of this operation were performed to separate cerium from the other rare earths. Further purification was achieved by reducing Ce^{+4} to Ce^{+3} and precipitating $Zr(IO_3)_4$. The cerium was finally precipitated as the hydroxide, dissolved in a minimum of HCl and made up to a volume of 10 mls. Chemical yields were determined by the alizarin sulphonate method[48] which gave a standardization curve as shown in Fig. 73.

The gross β^- decay curve (Fig. 74) was resolved by subtracting an estimated background activity from the experimental counting rates. A 33-day component and a 35.4-hour component appeared (Fig. 75). The background activity as drawn had a half-life of about two years and by trial and error was resolved into a long-lived activity considerably above background and a 285-day activity. The 33-day nuclide was assumed to be Ce^{141} and the 35.4-hour activity to be Ce^{143}. The estimated 285-day activity was taken to be Ce^{144}. The isobaric chains involved are:

Short-lived $\longrightarrow$ 3.8 h. $La^{141} \longrightarrow$ 33 d. $Ce^{141} \longrightarrow$ (stable) Pr^{141}

Short-lived $\longrightarrow$ 33 h. $Ce^{143} \longrightarrow$ 13.7 d. $Pr^{143} \longrightarrow$ (stable) Nd^{143}

Short-lived $\longrightarrow$ 280 d. $Ce^{144} \longrightarrow$ 17.4 m. $Pr^{144} \longrightarrow 5 \times 10^{15}$ y. Nd^{144}.

A gamma-ray spectrum (Fig. 76) of the cerium activities showed

Figure 73

STANDARD ABSORBANCE CURVE FOR CERIUM

(Sodium Alizarin Sulphonate method)

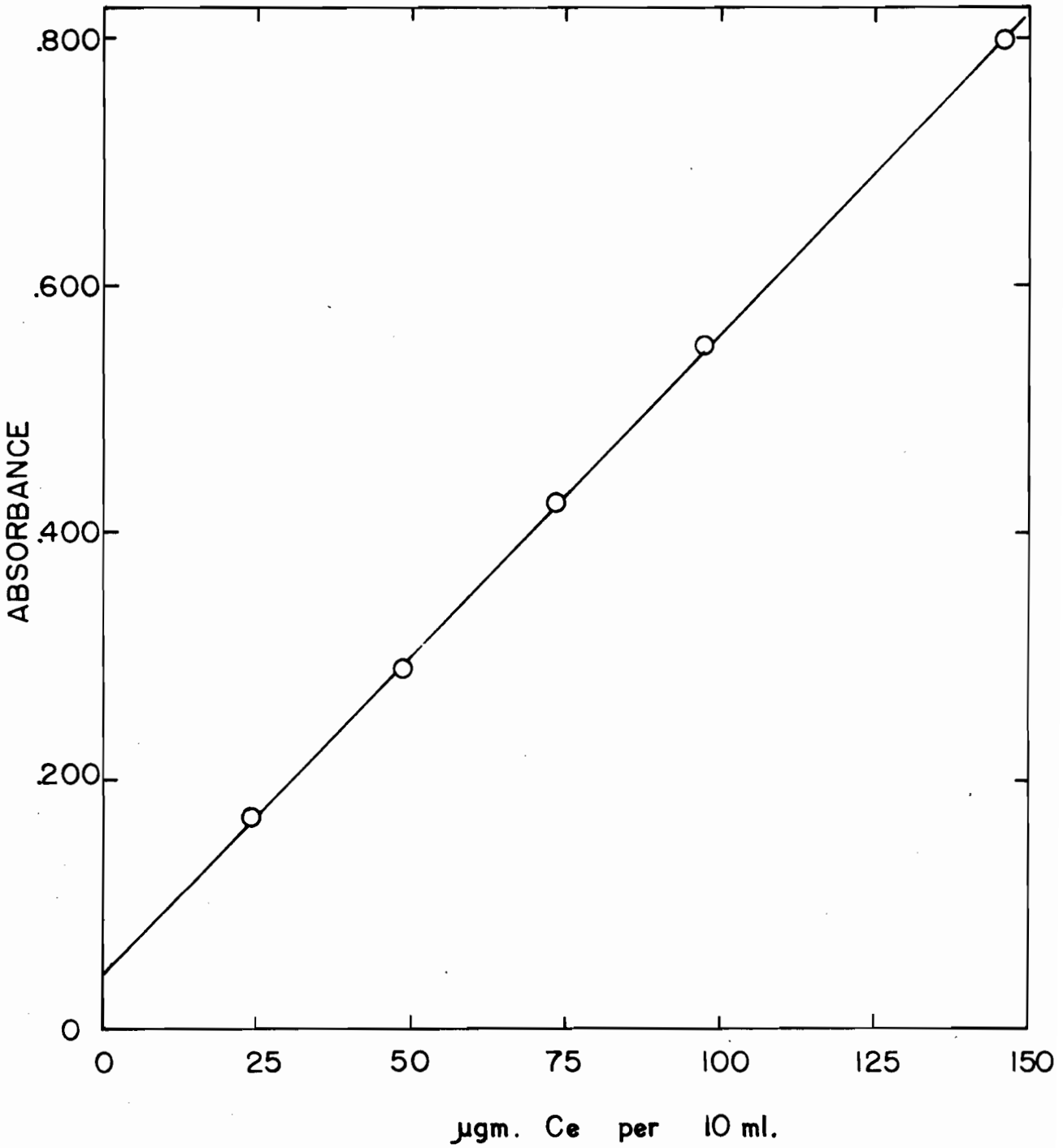
.800
.600
.400
.200
0
ABSORBANCE
0
25
50
75
100
125
150
µgm. Ce per 10 ml.

Figure 74

β^- DECAY OF CERIUM FRACTION

O - Experimental points

● - 'Background' activity subtracted

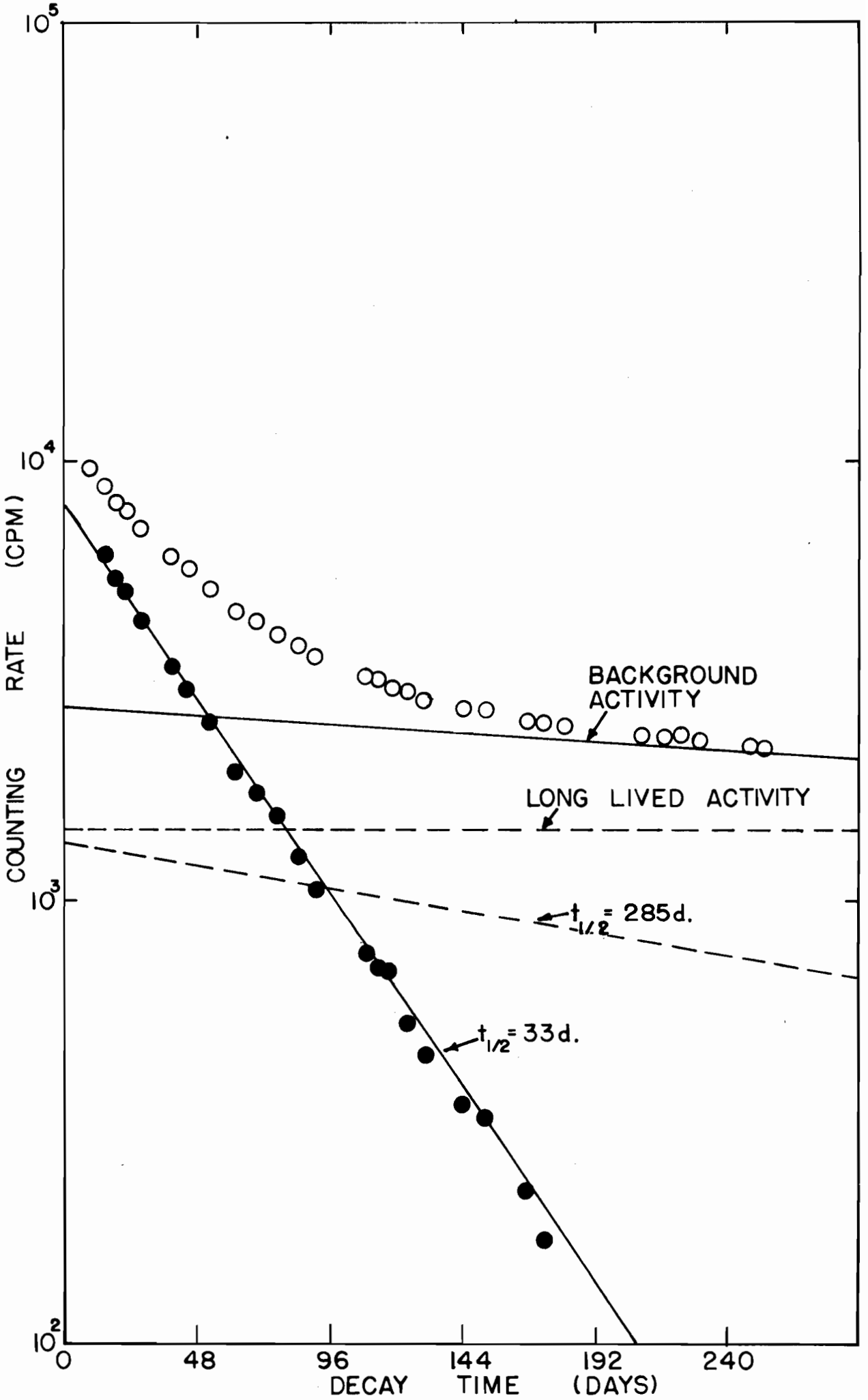
10^5
10^4
10^3
10^2
COUNTING RATE (CPM)
BACKGROUND ACTIVITY
LONG LIVED ACTIVITY
$t_{1/2}$ = 285d.
$t_{1/2}$ = 33d.
0
48
96
144
192
240
DECAY TIME (DAYS)

Figure 75

β^- DECAY OF Ce^{141} AND Ce^{143}

x - Experimental points

O - Long-lived activity subtracted

● - 33-day activity subtracted

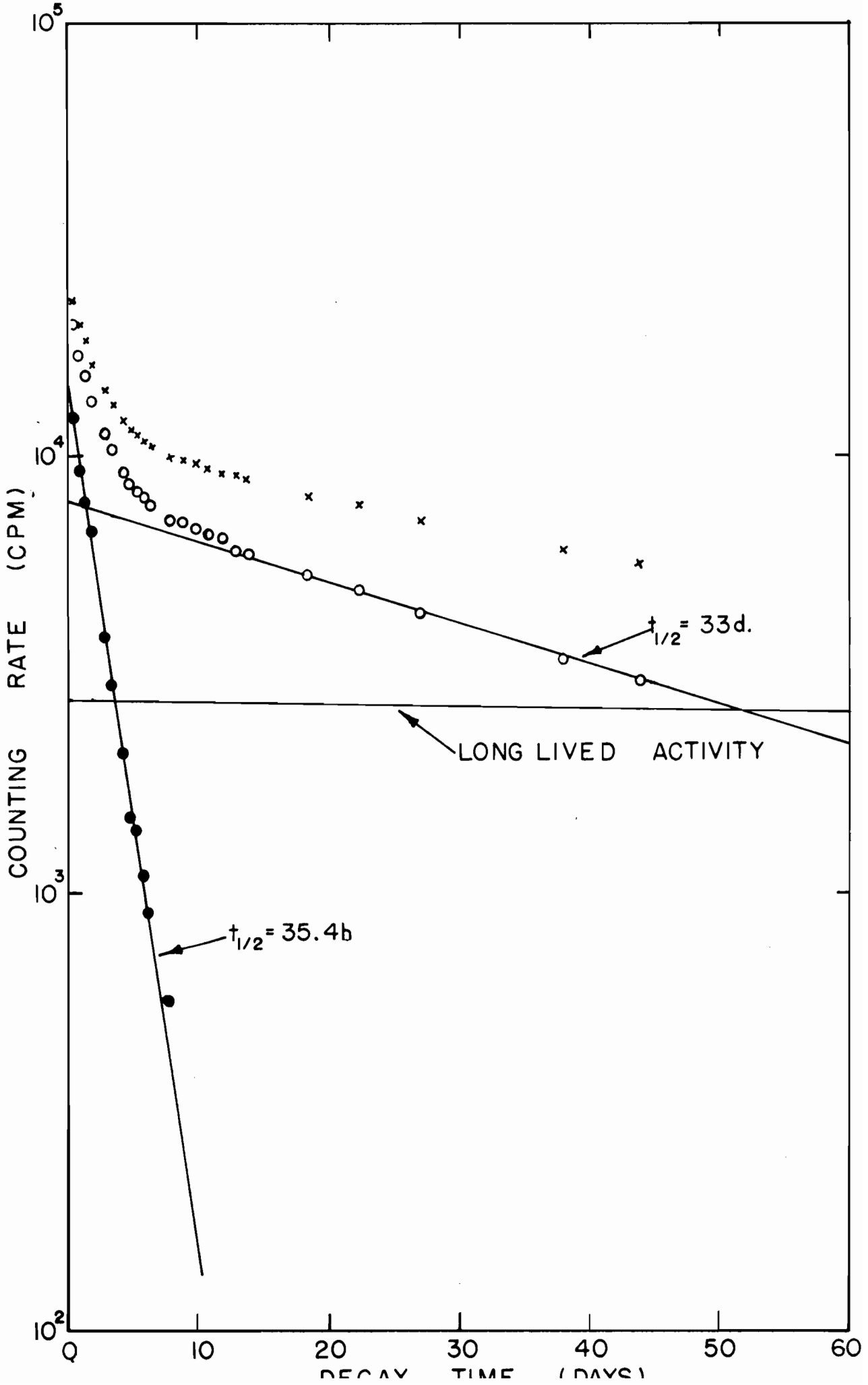
10^5
10^4
10^3
10^2
COUNTING RATE (CPM)
$t_{1/2}$ = 33d.
LONG LIVED ACTIVITY
$t_{1/2}$ = 35.4h
0
10
20
30
40
50
60
DECAY TIME (DAYS)

Figure 76

GAMMA SPECTRUM OF CERIUM FRACTION

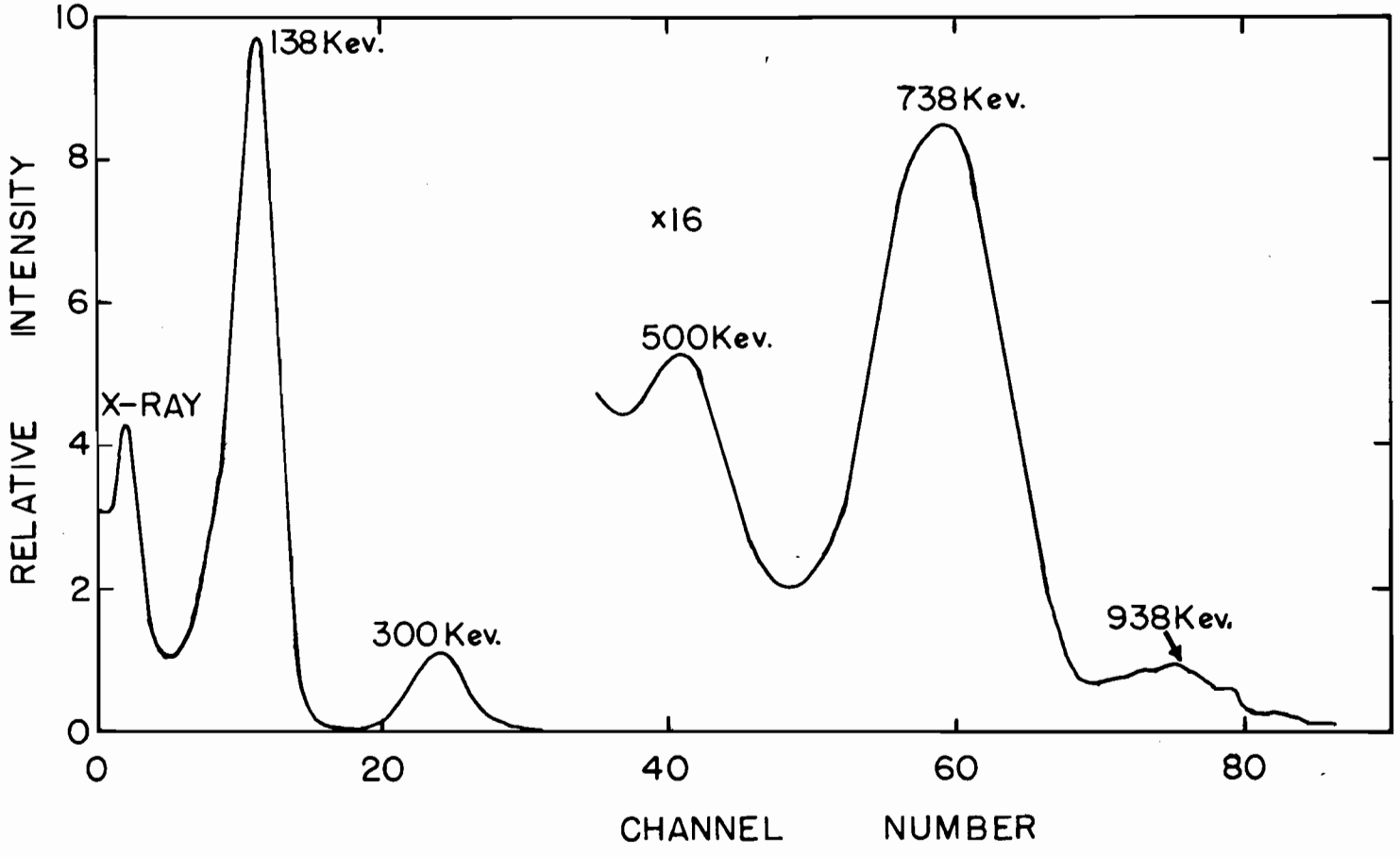
10
8
6
4
2
0
RELATIVE INTENSITY
138Kev.
738Kev.
x16
500Kev.
X-RAY
300Kev.
938Kev.
0
20
40
60
80
CHANNEL NUMBER

photopeaks at 138 kev, 300 kev, 500 kev, 738 kev, and 938 kev. The decay of the photopeaks was not followed.

Ce^{141} decays with a half-life of 33 days[54] by beta emission with maximum energies of 432 kev (70%) and 580 kev (30%). A 145 kev gamma ray is in coincidence with the 432 kev β^- ray. Ce^{143} decays with a reported half-life of 34 hours[54] by emitting β^- rays of energies 0.22 Mev (6%), 0.52 Mev (12%), 0.72 Mev (5%), 1.09 Mev (40%), and 1.38 Mev (37%). Gamma rays with energies of 290 kev, 350 kev, 660 kev, and 720 kev are the more abundant of the ten gamma rays reported. Ce^{144} has a reported half-life of 285 days[54], decaying by β^- emission with energies of 186 kev (20%), 240 kev (8%), and 320 kev (72%). The most intense coincident gamma ray has an energy of 134 kev. Pr^{144}, the daughter activity of Ce^{144}, decays with a half-life of 17 minutes by β^- emission with maximum energies of 800 kev (1%), 2.29 Mev (1.3%), and 2.98 Mev (97.7%). Fission yield calculations for Ce^{141} and Ce^{143} are straightforward and are given in Table XXV. For Ce^{144} it is necessary to take into account the contribution of the Nd^{144} (17 min.) daughter activity. Because $\lambda_{Ce^{144}} \ll \lambda_{Pr^{144}}$ at equilibrium, the disintegration rates are equal. Furthermore, since absorption into the source mount and source material was negligible, the observed counting rates are equal. The necessary correction was made in determining the Ce^{144} disintegration rate in order to calculate the fission yield (Table XXV).

Table XXV

FISSION YIELD DATA FOR CERIUM NUCLIDES

Irradiation	Ce^{141} (33 d.) J	Ce^{143} (35.4 h.) J	Ce^{144} (285 d.) J
Observed activity	7.90×10^3 c/m	1.50×10^4 c/m	6.70×10^2 c/m
Source-mount absorption factor	1.00	1.00	1.00
Self-absorption factor	1.00	1.00	1.00
Aliquot factor	5000	5000	5000
Chemical yield	7.4%	7.4%	7.4%
Time after irradiation	3.756 d.	3.756 d.	3.756 d.
Decay factor	0.9241	0.1712	0.9909
Time in reactor	2.056 d.	2.056 d.	2.056 d.
Saturation factor	0.0423	0.6194	0.0050
Activity at saturation	2.276×10^8 d/s	1.593×10^8 d/s	1.523×10^8 d/s
Fission rate	3.724×10^9 f/s	3.724×10^9 f/s	3.724×10^9 f/s
Fission yield	6.11%	4.28%	4.09%

(r) Rare Earths

The rare earth activities, europium and neodymium, were separated by a combination of the methods of Nervik[86] and Smith and Hoffmann[87]. Isolation and purification of the rare earths as a group was made after adding europium and neodymium carriers by precipitating the rare earth fluorides then, after dissolution, by eluting on a Dowex-1 anion exchange column with concentrated HCl. Prior to the elution, scavenging precipitations of $Zr_3(PO_4)_4$ and $BaSO_4$ were performed. After elution, the rare earth hydroxides were precipitated then dissolved in a small amount of concentrated HCl. Separation of europium from neodymium was achieved by elution at room temperature on a Dowex-50 cation exchange column with a 0.3 M α-hydroxy-isobutyric acid solution adjusted to pH 4.1 with concentrated NH_4OH. The individual rare earths were then precipitated as the hydroxides, dissolved in a minimum of dilute hydrochloric acid and made up to volume. Chemical yields were determined on the spectrophotometer by the sodium alizarin sulphonate method[48].

(i) Neodymium:

The β^- decay of the neodymium fraction, shown in Fig. 77, was seen to die away with an 11-day half-life, then to tail off into a long-lived activity. The neodymium activity expected to be present at the time of separation

Figure 77

β^- DECAY OF Nd^{147}

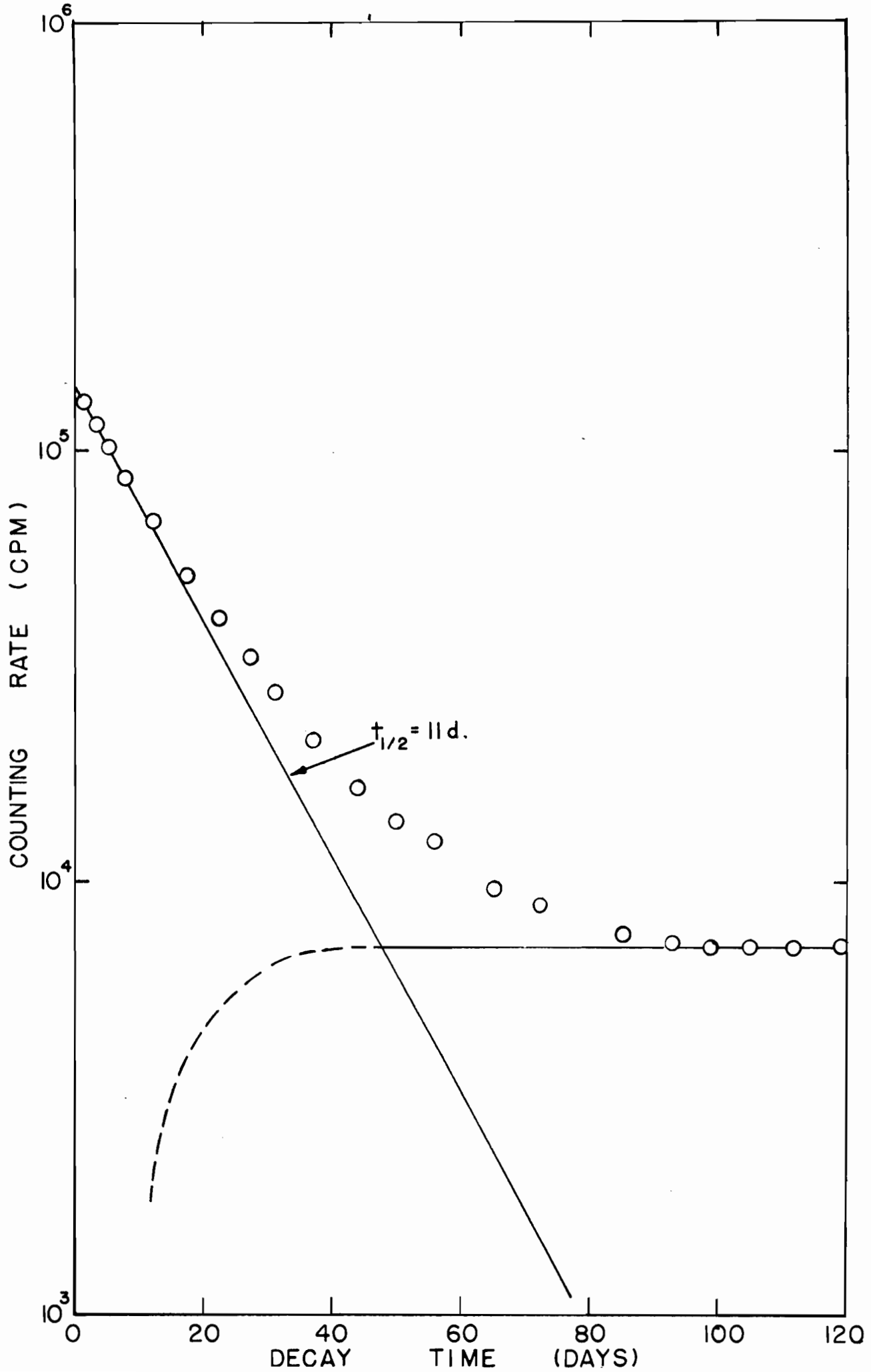
10^6
10^5
10^4
10^3
COUNTING RATE (CPM)
$t_{1/2}$ = 11 d.
0
20
40
60
80
100
120
DECAY TIME (DAYS)

occurs in the decay chain

$$\text{Short-lived} \longrightarrow Nd^{147}(11.1\ d.) \longrightarrow Pm^{147}(2.6\ y.) \longrightarrow Sm^{147}(1.3 \times 10^{11}\ y.)$$

The time required for the Pm^{147} daughter to reach maximum activity, calculated by the following equation[44]

$$t_m = \frac{2.303}{\lambda_2 - \lambda_1} \log \frac{\lambda_2}{\lambda_1} ,$$

is 72 days. From the decay curve this time was $\sim$ 44 days. It was therefore concluded that some other long-lived activity was present, in an amount estimated to be 4% of the counting rate of Nd^{147} at separation time. This was subtracted from the Nd^{147} counting rate for the disintegration rate determination. A gamma-ray spectrum of the neodymium fraction, shown in Fig. 78, showed photopeaks with 33, 93, 308, 416, 530, and 685 kev energies. This compared well with a gamma-ray spectrum given by Heath[65] for Nd^{147}. The 530 kev peak was seen to decay with a half-life of 11.5 days (Fig. 79). Nd^{147} decays with a half-life of 11.4 days[54] by β^- emission with maximum energies of 212 kev (3%), 368 kev (20%), and 810 kev (77%). The most intense gamma ray for Nd^{147} has an energy of 532 kev. Fission yield data for Nd^{147} are given in Table XXVI.

Figure 78

GAMMA-RAY SPECTRUM OF

NEODYMIUM ACTIVITY

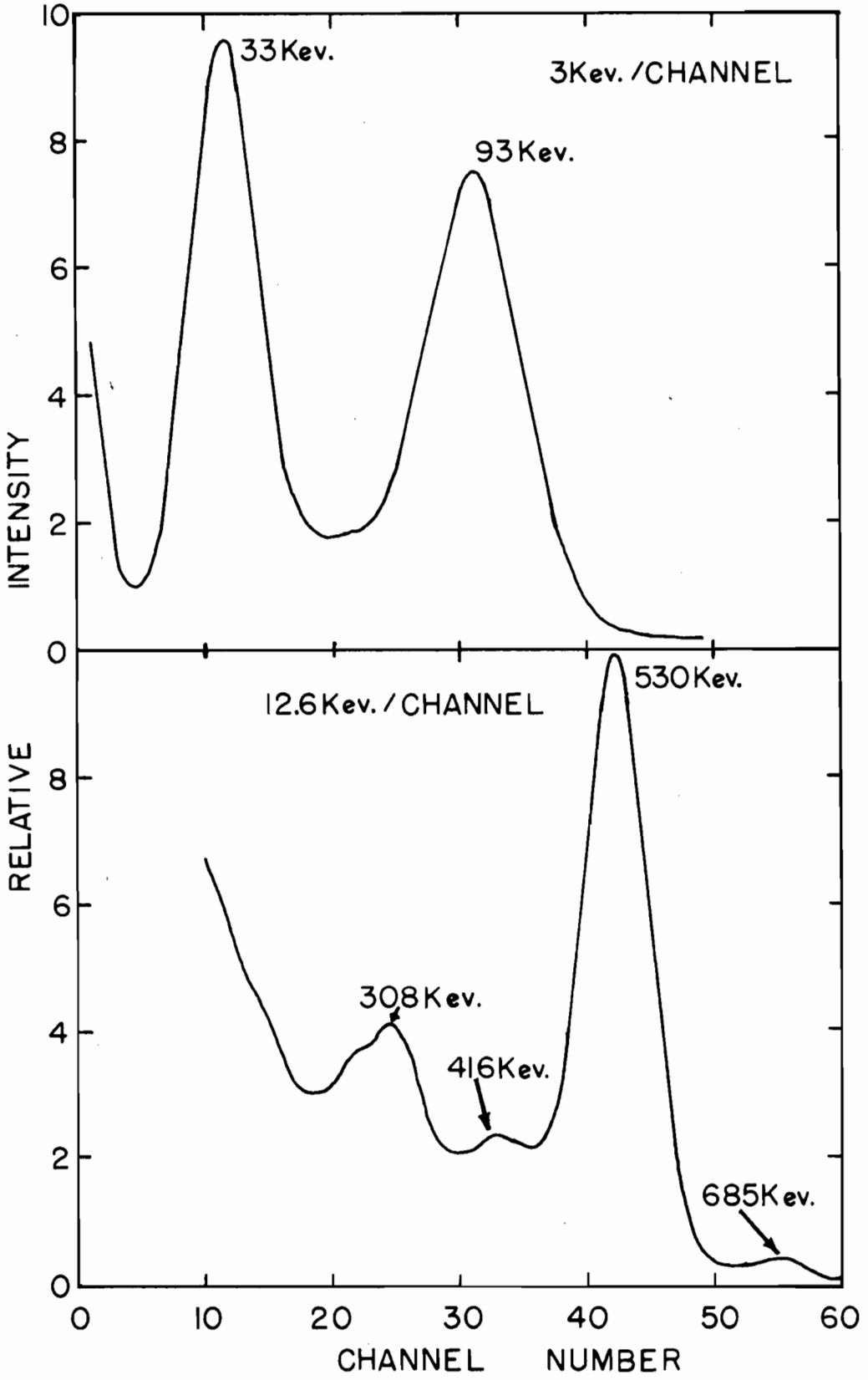
33Kev.
3Kev./CHANNEL
93Kev.
INTENSITY
12.6Kev./CHANNEL
530Kev.
RELATIVE
308Kev.
416Kev.
685Kev.
CHANNEL NUMBER

Figure 79

DECAY OF 530 KEV GAMMA RAY OF Nd^{147}

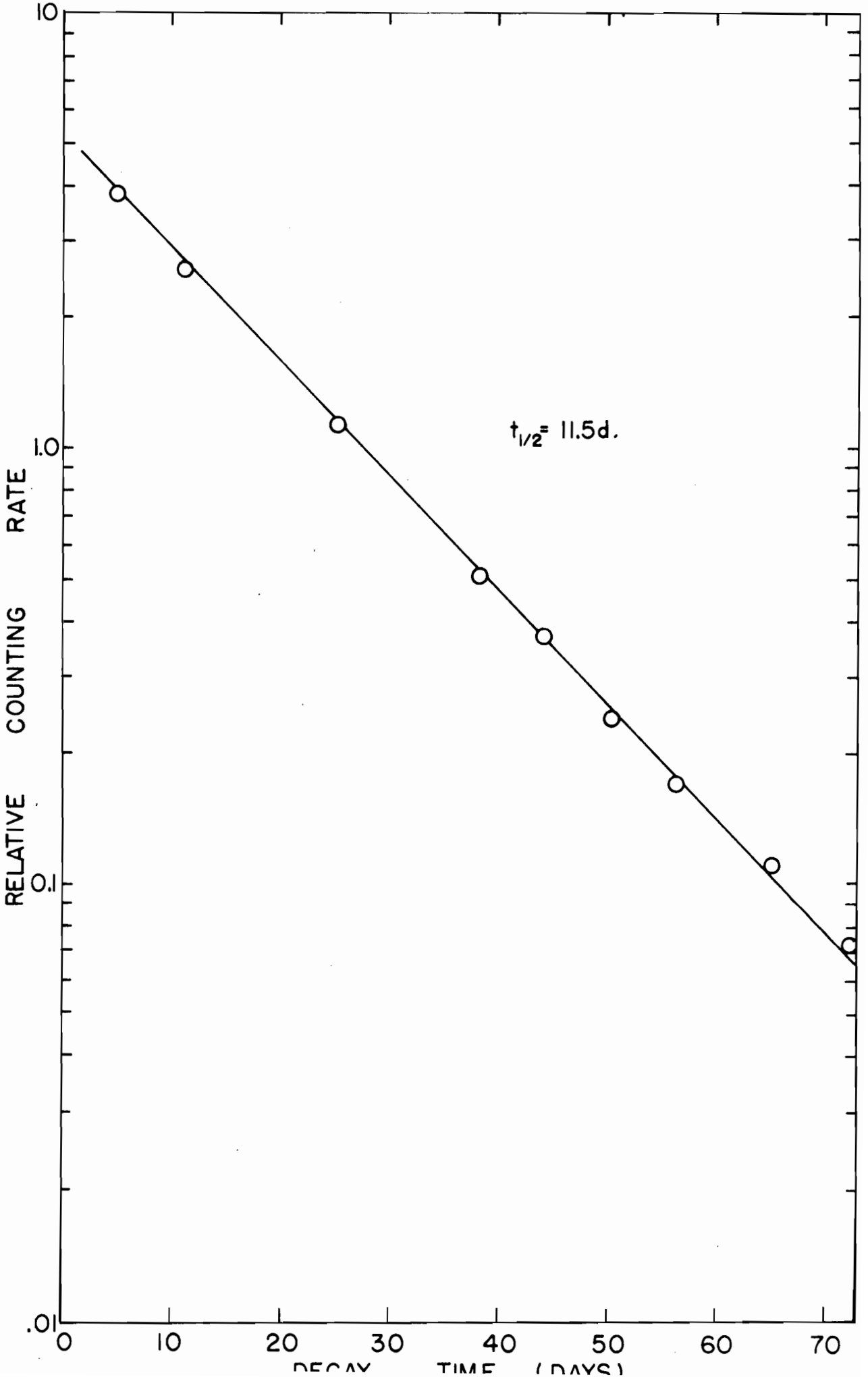
10
1.0
0.1
.01
RELATIVE COUNTING RATE
$t_{1/2}$= 11.5d.
0
10
20
30
40
50
60
70
DECAY TIME (DAYS)

Table XXVI

FISSION YIELD DATA FOR Nd^{147} (11 DAYS)

Irradiation	LA	LB
Observed activity	1.42×10^5 c/m	1.38×10^5 c/m
Source-mount absorption factor	0.997	0.997
Self-absorption factor	0.985	0.985
Aliquot factor	100	50
Chemical yield	58.56%	65.32%
Time after irradiation	42.414 d.	57.605 d.
Decay factor	0.0691	0.0265
Time in reactor	1.590 d.	1.590 d.
Saturation factor	0.0953	0.0953
Activity at saturation	6.207×10^7 d/s	7.101×10^7 d/s
Fission rate	4.483×10^9 f/s	4.631×10^9 f/s
Fission yield	1.38%	1.53%

(ii) Europium:

The β^- decay of the europium activity was resolved into a 71.5-day component and a 15.3-day component (Fig. 80). The activities expected to be present were Eu^{155} and Eu^{156} from the following isobaric chains:

$$\text{Short-lived} \longrightarrow Eu^{155}\ (1.7\ \text{y.}) \longrightarrow Gd^{155}\ (\text{stable})$$

$$Sm^{156}\ (9\ \text{h.}) \longrightarrow Eu^{156}\ (15.4\ \text{d.}) \longrightarrow Gd^{156}\ (\text{stable})$$

Since, at the end of the counting period, 120 days, the Eu^{156} activity would have decayed through ~ 8 half-lives, its contribution to the counting rate would be negligible. It would seem then that an activity with a half-life between 15 days and 1.7 years, in addition to the 1.7-year Eu^{155}, remains in the europium sample. A gamma-ray spectrum of the europium activities is shown in Fig. 81. Photopeaks with energies of 45, 93, 624, 806, 1160, and 1940 kev respectively are consistent with gamma-ray spectra of Eu^{155} and Eu^{156} shown by Heath[65]. Eu^{156} decays with a half-life of 15.4 days[54] by the emission of 500 kev (60%) and 2.4 Mev (40%) beta rays. Its gamma-ray spectrum is very complex. Fission yield data for Eu^{156} are given in Table XXVII.

Figure 80

DECAY OF EUROPIUM ACTIVITY

O - Experimental points

● - Long-lived activity subtracted

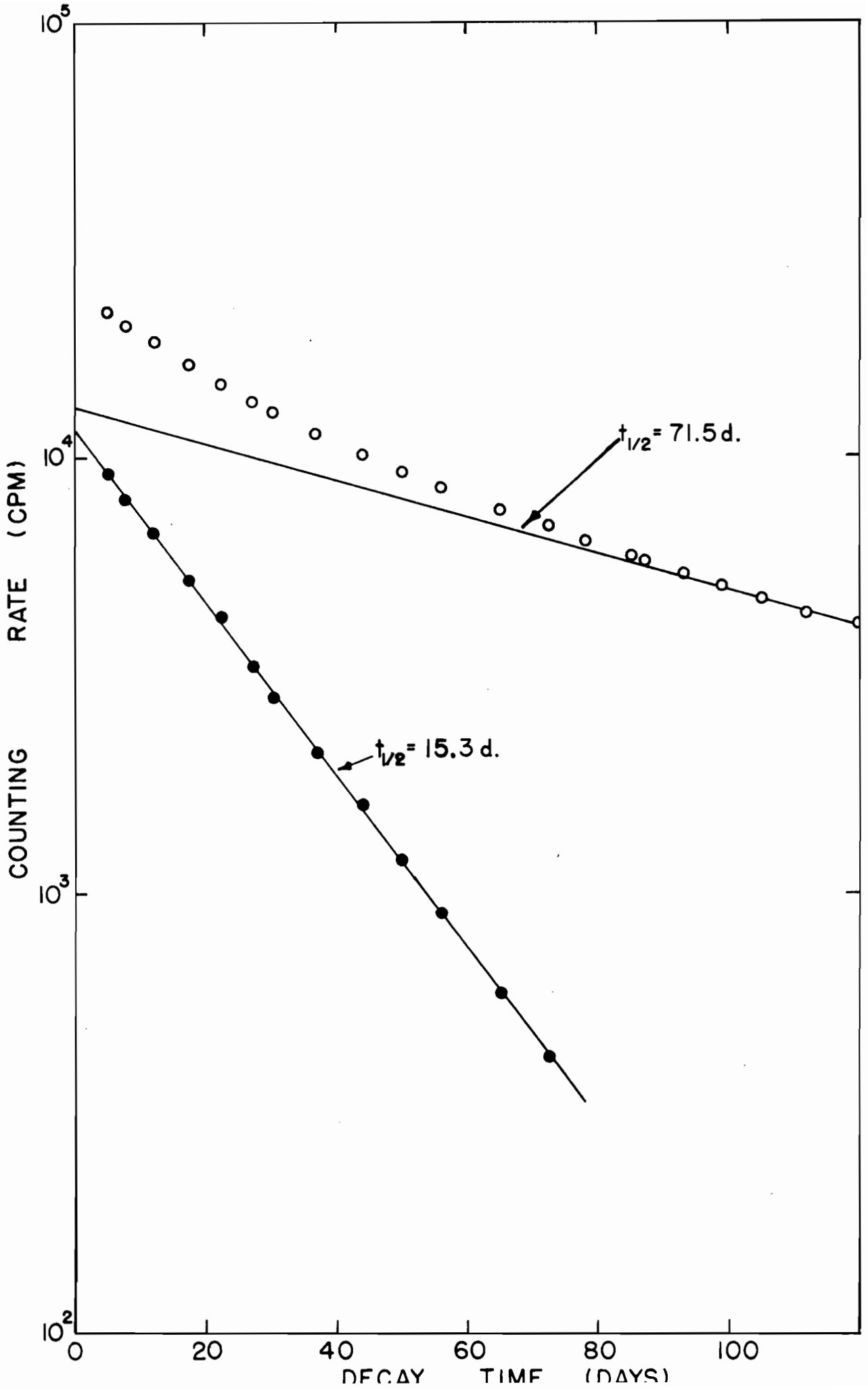
10^5
10^4
10^3
10^2
COUNTING RATE (CPM)
$t_{1/2}$= 71.5 d.
$t_{1/2}$= 15.3 d.
0
20
40
60
80
100
DECAY TIME (DAYS)

Figure 81

GAMMA SPECTRUM OF EUROPIUM ACTIVITY

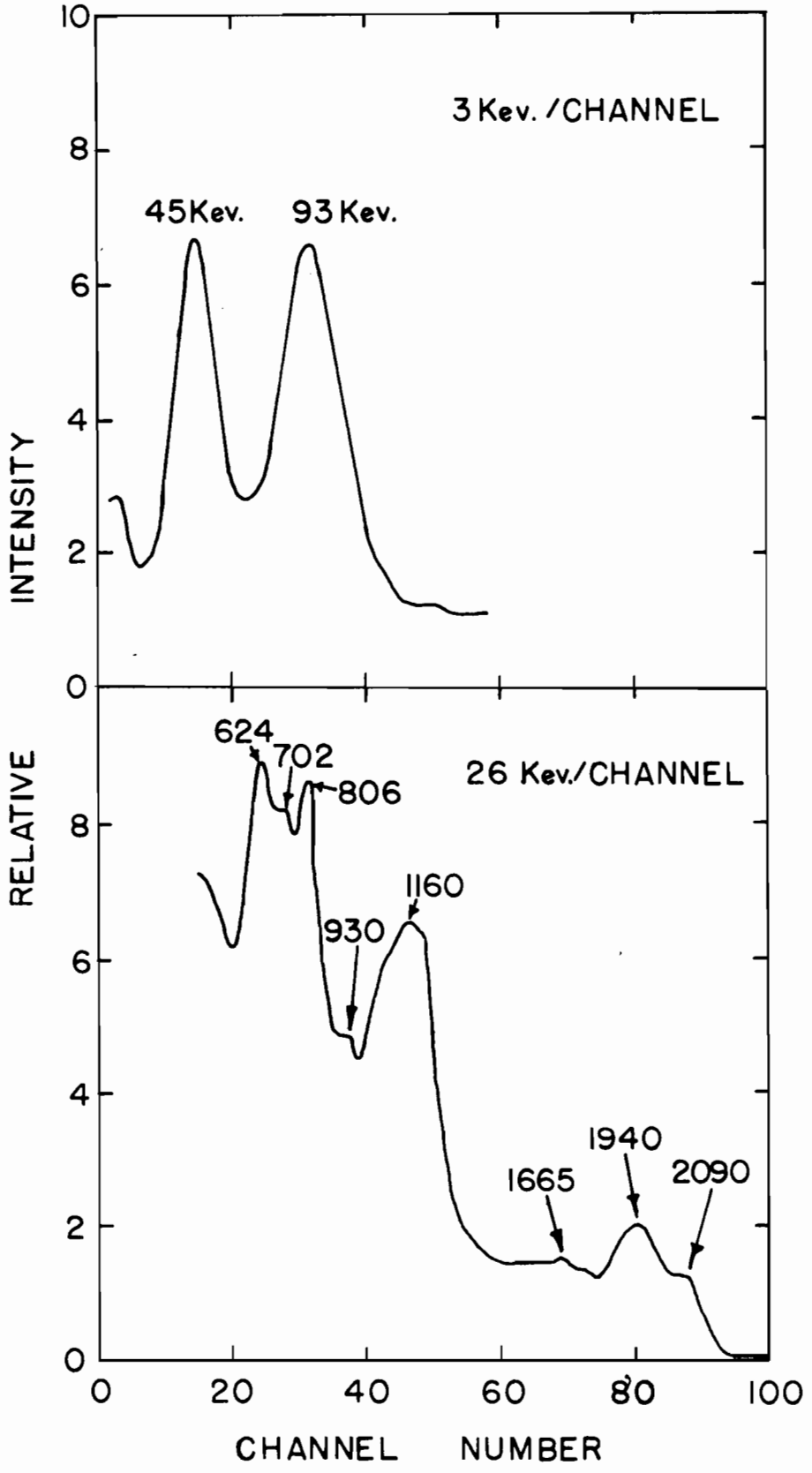
3 Kev. /CHANNEL
45Kev.
93 Kev.
INTENSITY
26 Kev./CHANNEL
624
702
806
1160
930
1665
1940
2090
RELATIVE
CHANNEL NUMBER
0
20
40
60
80
100
2
4
6
8
10

Table XXVII

FISSION YIELD DATA FOR Eu^{156} (15.3 DAYS)

Irradiation	LA	LB
Observed activity	1.16×10^{4} c/m	9.62×10^{3} c/m
Source-mount absorption factor	0.998	0.998
Self-absorption factor	0.998	0.996
Aliquot factor	100	50
Chemical yield	64.22%	57.34%
Time after irradiation	42.414 d.	57.605 d.
Decay factor	0.1483	0.0748
Time in reactor	1.590 d.	1.590 d.
Saturation factor	0.0691	0.0691
Activity at saturation	2.949×10^{6} d/s	2.721×10^{6} d/s
Fission rate	4.483×10^{9} f/s	4.631×10^{9} f/s
Fission yield	6.58×10^{-2} %	5.88×10^{-2} %

4. ERRORS

The errors in these experiments were as follows:

(a) Systematic errors

These errors arise in weighing, dilutions, pipetting and in chemical yield analyses. A sensitive microbalance was used for all weighings, while calibrated volumetric glassware and micropipettes were used for dilutions and pipetting. Chemical yield determinations were done either spectrophotometrically, by titration or by weighing. A Beckman DU spectrophotometer was used in making the absorbance measurements, while in the titrations calibrated pipettes and microburettes were used. The estimated errors from the above causes were less than $\pm$ 3%. By using very thin films the source-mount absorption errors were kept to $\pm$ 0.2%. In order to make self-absorption losses as small as possible, 5 to 10 milligrams of carrier were added before the chemical separations, the amount used depending upon the reported efficiency of the separation scheme employed. Errors associated with self-absorption losses were assessed at 0.1 to 2%, depending upon the energy of the β^- radiations. The loss of activity due to fission recoil was assumed to be negligible because of the low concentration of plutonium in the alloy used.

(b) Statistical errors

For all measurements on the 4 π proportional counter, more than 10^4 counts were recorded per counting

period, so that these errors were $\leq$ 1%. Only those prepared sources whose counting rates agreed within 1% were used for disintegration rate determinations.

(c) External errors

These arise in the decay schemes and decay constants of the nuclides of interest and influence the fission yields when used. Each fission yield was determined using the observed half-life and the decay scheme, as discussed.

In connection with saturation activity calculations, the pile power was constant during all the irradiations.

The calculated fission yields depend upon the ratio of the capture cross section for cobalt and the thermal neutron fission cross section for Pu^{239}. The values used for these were obtained from the literature. Where several values were obtained for a fission yield, an average value was calculated assuming equal statistical 'weights' for the individual values. The error quoted for the average fission yield is the standard deviation.

Where a single determination of a fission yield was made an error of $\pm$ 5% is quoted, while for two yield values the calculated average is given with the limits of the two values as the quoted error.

DISCUSSION

The absolute fission yields obtained in this work are presented in Table XXVIII, together with estimated isobaric yields and literature values for the masses measured. The isobaric yields were determined by calculating Z_p according to the equal charge displacement hypothesis for the mass numbers concerned, then by interpolation on the charge distribution curve (Fig. 3) of Glendenin et al.[12] to obtain the fractional cumulative yield. The fission yield was then corrected to give the isobaric yield. For the shielded nuclides, the same procedure applies except that the fractional chain yield is interpolated from the charge distribution curve. Corrections were only necessary for I^{133} in addition to the shielded nuclides.

The agreement with other radiochemically determined yields is in general good. The yield values in column 5 are good to $\pm$ 10 - 20%[25]. The agreement with mass spectrometric data is good on the rising and falling wings of each peak but very poor at the maxima of the peaks. The Mo^{99} yield of 5.61% is some 1% lower than the yield obtained by interpolation from the mass spectrometric data. This interpolated value is, however, a reflection of the very high yield, 7.05%, obtained for Mo^{100}. It was not possible in this work to determine radiochemically the yield at mass 100 since the isobaric chain is

Table XXVIII

ASBOLUTE THERMAL NEUTRON FISSION YIELDS FOR Pu^{239}

Nuclide	This work: Absolute yield %	This work: Estimated isobaric yield %	A (1) %	B (2) %	A (4) B (3)(5) %
Br^{82}	0.0036 ± 0.0002	0.36			
Sr^{89}	1.74 ± 0.05	1.74	1.71	1.8	1.71 (3)
Sr^{90}	2.05 ± 0.04	2.05	2.16		2.31 (4)
Y^{91}	2.41 ± 0.11	2.41	2.59 (Zr^{91})	2.8	2.45 (Sr^{91})(3)
Zr^{95}(Nb^{95})	5.06 ± 0.33	5.06	4.99 (Mo^{95})	5.6	
Mo^{99}	5.61 ± 0.33	5.61	6.44*	6.1	
Ru^{103}	5.79 ± 0.37	5.79	5.63	5.5	
Rh^{105}	5.47 ± 0.06	5.47	5.50*	3.7	
Ru^{106}	4.04 ± 0.22	4.04	4.53	4.7	
Pd^{109}	1.13 ± 0.06	1.13		1.0	
Ag^{111}	0.28 ± 0.04	0.28		0.27	
Pd^{112}(Ag^{112})	0.093 ± 0.003	0.093		0.10	
Cd^{115m}	0.003 ± 0.0006	0.003		0.003	
Cd^{115}	0.033 ± 0.002	0.033		0.045	
Total Cd^{115}	0.036	0.036	0.041*	0.048	
Sb^{124}	0.088 ± 0.004				
Sb^{126}	0.069 ± 0.003				
Sb^{127}	0.55 ± 0.03	0.55			
I^{131}	3.80 ± 0.14	3.80	3.77	3.6	
Te^{132}(I^{132})	5.51 ± 0.27	5.51	5.26	4.9	
I^{133}	5.53 ± 0.06	6.14	6.90	5.0	
Cs^{136}	0.083 ± 0.007	6.30	6.62		
Cs^{137}	5.40 ± 0.39	5.40	6.48	5.8	6.50 (4)
Ba^{140}	5.47 ± 0.32	5.47	5.58	5.36	
Ce^{141}	6.11 ± 0.31	6.11	5.23	4.9	
Ce^{143}	4.28 ± 0.21	4.28	4.56	5.1	
Ce^{144}	4.09 ± 0.20	4.09	3.84	3.7	3.6 (5)
Nd^{147}	1.46 ± 0.08	1.46	1.99		2.8(Pm^{147})(4); 2.2 (5)
Eu^{156}	0.062 ± 0.004	0.062	0.08	0.12	0.10 (5)

*Interpolated yields

A Mass spectrometrically determined yields

B Radiochemically determined yields

(1) Fickel and Tomlinson (35,36)

(2) Steinberg and Glendenin (25)

(3) Bartholomew, Martin and Baerg (27)

(4) Anikina et al. (37)

(5) Bunney et al. (26)

$$3\ \text{m.}\ Nb^{100} \longrightarrow \text{stable}\ Mo^{100}.$$

Discrepancies in the yields of I^{133}, Cs^{136}, Cs^{137}, and Ce^{141} occur in the heavy peak. The chain yield for masses 133 and 136 depend upon the fractional yields interpolated from the charge distribution hypothesis and would reflect the uncertainties involved in determining Z_p. The Cs^{137} yield of Fickel and Tomlinson[36] has been obtained using 26.6 years for the half-life of this nuclide. A recently reported value for this half-life is 29.68 years[47]. The Ce^{141} yield reported in this work is the result of a single determination and cannot be regarded as confirmed.

Independent yields for four shielded nuclides have been measured. These are for Br^{82}, Sb^{124}, Sb^{126}, and Cs^{136}. Of these, only the Cs^{136} yield has been measured previously. The value obtained, 0.083%, is in good agreement with a value of 0.089% obtained by Glendenin and reported by Steinberg and Glendenin[24] and a value of 0.0835 obtained by Grummitt and Milton[88]. When the independent yields for Sb^{124} and Sb^{126} are converted to chain yields according to the ECD hypothesis, the values obtained are several orders of magnitude too high when plotted on the mass distribution curve. This seems to be in accord with the proposal of Kennett and Thode[17] that, for masses A = 128 to A = 132, Z_p remained near 50. The influence of the 50 proton shell would be expected to be pronounced in the case of antimony which has Z = 51.

In Fig. 82 the mass distribution curve obtained in this work is shown in which the isobaric yields are plotted as a function of the mass number. Also included are the results of the mass spectrometric determinations[35,36] at masses where the yields differ. The mass distribution is seen to be symmetrical about mass 118 with the two maxima representative of asymmetric fission. The width at half height is approximately 16 mass units for both peaks. The peak to valley ratio is ~ 160. The sum of the yields in the light peak is 97%, while that of the heavy peak is 93%. The yields in each peak should sum up to 100%. The difference is seen to be mainly in the yields at the top of the peaks, which have not been measured radiochemically since the mass spectrometric data for either peak sum up to 100%.

The $4\pi\ \beta^-$ measurement technique was shown to be a very sensitive and accurate method for determining the absolute yields of the fission products. Nuclides which decay by β^- emission or coincident $\beta^- - \gamma$ emission were very accurately measured in this way. The strong absorption of very low energy β^- rays and conversion electrons place limitations, however, on the use of this technique when measuring nuclides which decay in these ways in that the corrections necessary are dependent upon decay scheme constants such as β^- branching ratios and internal conversion coefficients. These are seldom as accurate as one would desire.

The isobaric yields determined from the measured absolute yields are in the final analysis dependent upon charge distribution hypotheses which can hardly be said to be a consistent body of theory.

Figure 82

MASS DISTRIBUTION CURVE FOR Pu^{239}

● - this work

O - Fickel and Tomlinson

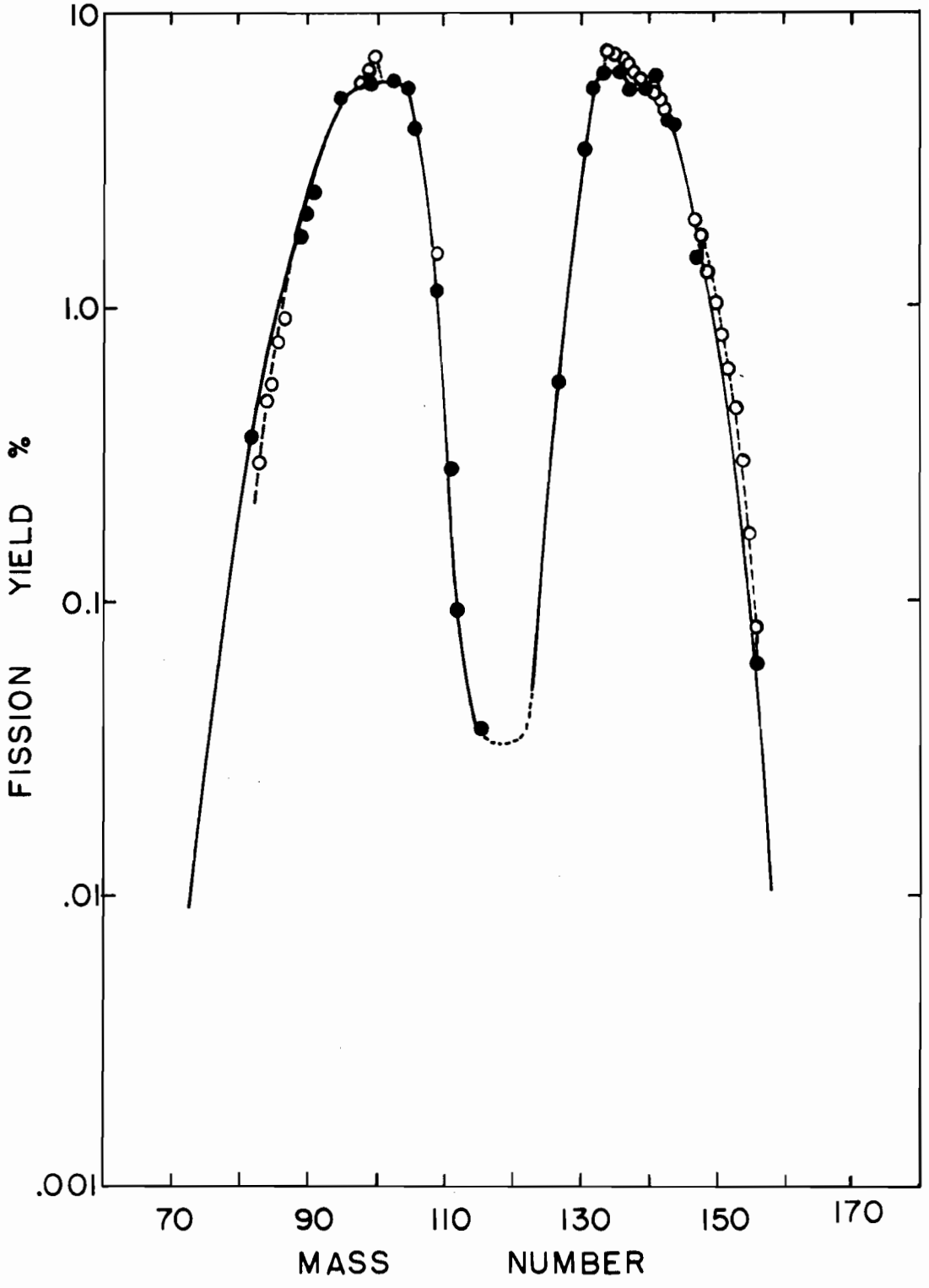
10
1.0
0.1
.01
.001
FISSION YIELD %
70
90
110
130
150
170
MASS NUMBER

SUMMARY

Radiochemical techniques have been used to measure the absolute yields for 24 nuclides and the independent yields for four shielded nuclides resulting from thermal neutron fission in Pu^{239}. Disintegration rates and half-lives were accurately determined by means of 4π beta proportional counting techniques. Further identification of the nuclides was obtained from gamma-ray scintillation spectrometry.

All irradiations were performed in a self-serve position at the NRX reactor at Chalk River, Ontario, where the neutron spectrum is predominantly thermal. The flux intensity was monitored by irradiating at the same time known weights of 'spec pure' very thin cobalt wire.

The fission yields measured were found to agree with other radiochemical data from the literature but to be lower, especially at the maxima of the mass distribution, than mass spectrometrically determined yields.

BIBLIOGRAPHY

1. E.F. Westrum, Jr., J.C. Hindman, and R. Greenlee, 'The Transuranium Elements', McGraw Hill Book Co., Inc., New York (1949).

2. D.J. Hughes, Nucleonics, 17, 132 (1959).

3. E.A. Eschbach and S. Goldsmith, Nucleonics, 21, 48 (1963).

4. E.K. Hyde, University of California Radiation Laboratory Report, UCRL - 9036 Rev. (1962) unpublished.

5. E. Fermi, E. Amaldi, O. d'Agostino, F. Rasetti, and E. Segre, Proc. Roy. Soc., A146, 483 (1934).

6. N. Bohr, Nature, 137, 344, 351 (1936).

7. N. Bohr and J. Wheeler, Phys. Rev., 56, 426 (1939).

8. J. Frenkel, Phys. Rev., 55, 987 (1939).

9. R.R. Wilson, Phys. Rev., 72, 189 (1947).

10. A.C. Pappas, Technical Report No. 63, Laboratory for Nuclear Science, Massachusetts Institute of Technology (1953).

11. A.C. Pappas, Proceedings of the Second United Nations Conference on the Peaceful Uses of Atomic Energy, P/583, Geneva, 1958.

12. L.E. Glendenin, C.D. Coryell, and R.R. Edwards, in 'Radiochemical Studies: The Fission Products', Edited by C.D. Coryell and N. Sugarman. National Nuclear Energy Series, Vol. 9, Div. IV, McGraw Hill Book Co., Inc., New York (1951), Paper 52, p. 489.

13. A.C. Wahl, R.L. Ferguson, D.R. Nethaway, D.E. Troutner, and K. Wolfsberg, Phys. Rev., 126, 1112 (1962).

14. H.G. Thode, C.C. McMullen, and K. Fritze, 'Advances in Inorganic and Radiochemistry', 2 (1960), Academic Press Inc., New York.

15. S. Katcoff, Nucleonics, 18, 201 (1960).

16. C.D. Coryell, R.A. Brightsen, and A.C. Pappas, Phys. Rev., 85, 732 (1952).

17. T.J. Kennett and H.G. Thode, Phys. Rev., 103, 323 (1956).

18. C.D. Coryell, M. Kaplan, and R.D. Fink, Can. J. Chem., 39, 646 (1961).

19. M.G. Mayer and J.H.D. Jensen, 'Elementary Theory of Nuclear Shell Structure', John Wiley and Sons, New York (1955).

20. L.E. Glendenin, Phys. Rev., 75, 337 (1949).

21. D.R. Wiles, M.Sc. Thesis, McMaster University (1950).

22. P. Fong, Phys. Rev., 89, 434 (1946).

23. R.B. Leachman, 'Some Recent Developments in Fission Physics', American Nuclear Society Meeting, Boston,1962.

24. E.P. Steinberg and M.S. Freedman, NNES, Vol. 9, Div. IV, Paper 219, p. 1378.

25. E.P. Steinberg and L.E. Glendenin, Proceedings of the International Conference on the Peaceful Uses of Atomic Energy, Geneva, 1955, P/614, Vol. 7, p. 3.

26. L.R. Bunney, E.M. Scadden, J.O. Abriam, and N.E. Ballou, Proceedings of the Second International Conference on the Peaceful Uses of Atomic Energy, Geneva, 1958, P/644.

27. R.M. Bartholomew, J.S. Martin, and A.P. Baerg, Can. J. Chem., 37, 660 (1959).

28. S. Katcoff, Nucleonics, 16, 78 (1958).

29. C.W. Stanley and S. Katcoff, J. Chem. Phys., 17, 653 (1949).

30. G.P. Ford et al., LA-1997 (1956), Quoted in S. Katcoff, Nucleonics, 18, 201 (1960).

31. D.M. Wiles, J.A. Petruska, and R.H. Tomlinson, Can. J. Chem., 34, 227 (1956).

32. W.H. Fleming and H.G. Thode, Can. J. Chem., 34, 193 (1956).

33. K. Fritze, C.C. McMullen, and H.G. Thode, Proceedings of the Second International Conference on the Peaceful Uses of Atomic Energy, Geneva, 1958, Paper 187.

34. D.B. Bidinosti, H.R. Fickel, and R.H. Tomlinson, Proceedings of the Second International Conference on the Peaceful Uses of Atomic Energy, Geneva, 1958, Paper 201.

35. H.R. Fickel and R.H. Tomlinson, Can. J. Phys., 37, 916 (1959).

36. H.R. Fickel and R.H. Tomlinson, Ibid. 37, 926 (1959).

37. M.P. Anikina, P.M. Aron, V.K. Gorshov, R.N. Ivanov, L.M. Krizhansky, G.M. Kukavadze, A.N. Mourin, I.A. Reformatsky, and B.V. Ershler, Proceedings of the Second International Conference on the Peaceful Uses of Atomic Energy, Geneva, 1958, Paper 2040.

38. B.D. Pate and L. Yaffe, Can. J. Chem., 33, 15 (1955).

39. B.D. Pate and L. Yaffe, Ibid. 33, 610 (1955).

40. B.D. Pate and L. Yaffe, Ibid. 33, 929 (1955).

41. B.D. Pate and L. Yaffe, Ibid. 33, 1656 (1955).

42. B.D. Pate and L. Yaffe, Ibid. 34, 265 (1956).

43. L. Yaffe and J.B. Fishman, Can. J. Chem., 38, 1113 (1960).

44. G. Friedlander and J.W. Kennedy, 'Nuclear and Radiochemistry', John Wiley and Sons, Inc., New York (1955).

45. H. Bateman, Proc. Cambridge Phil. Soc., 15, 423 (1910).

46. C.H. Westcott, Atomic Energy of Canada Ltd., Chalk River, Ontario, AECL - 1101 (1960).

47. S.G. Gobrics, W.E. Kunz, and A.E. Nash, Nucleonics, 21, 63 (1963).

48. E.B. Sandell, 'Colorimetric Determination of Traces of Metals', Interscience Publishers, Inc., New York, 1959 (Third Edition).

49. F.J. Welcher, 'The Analytical Uses of Ethylenediaminetetraacetic Acid', D. Van Nostrand Co., Inc., New York (1957).

50. L. Yaffe and J.B. Fishman, 'Metrology of Radionuclides', International Atomic Energy Agency, Vienna, 1960, p. 185.

51. D.C. Santry, Ph.D Thesis, McGill University (1958).

52. T.A. Eastwood and R.D. Werner, Nuc. Sci. and Eng., 13, 385 (1962).

53. L.E. Glendenin, R.R. Edwards, and H. Gest, NNES, 1951, Vol. 9, Div. IV, Paper 232.

54. Nuclear Data Sheets, National Academy of Sciences, National Research Council, Washington, D.C.

55. L.E. Glendenin, NNES, 1951, Vol. 9, Div. IV, Paper 236.

56. R.G. Osmond and M.J. Owers, J. Inorg. Nuclear Chem., 9, 96 (1959).

57. D.R. Wiles and R.H. Tomlinson, Can. J. Phys., 33, 133 (1955).

58. N.E. Ballou, NNES, 1951, Vol. 9, Div. IV, Paper 292.

59. W.F. Boldridge and D.N. Hume, NNES, 1951, Vol. 9, Div. IV, Paper 294.

60. F.L. Moore, Anal. Chem., 28, 997 (1956).

61. D.N. Hume, NNES, 1951, Vol. 9, Div. IV, Paper 245.

62. A.D. Horton, Anal. Chem., 25, 1331 (1953).

63. L.E. Glendenin, NNES, 1951, Vol. 9, Div. IV, Paper 253.

64. E.M. Scadden, Nucleonics, 15, 102 (1957).

65. R.L. Heath, IDO-16408 (U.S. Atomic Energy Commission Report, Idaho Falls, Idaho, 1957).

66. L.E. Glendenin, NNES, 1951, Vol. 9, Div. IV, Paper 260.

67. J.P. Cali and L.F. Lowe, Nucleonics, 17, 86 (1959).

68. P. Avignon, A. Michalowicz, and R. Bouchez, J. Phys. Radium, 16, 404 (1955).

69. AECL 1711 Progress Report, Atomic Energy of Canada Limited.

70. D. Strominger, J.M. Hollander, and G.T. Seaborg, Rev. Mod. Phys., 30, 585 (1958).

71. J.H. Davies and L. Yaffe, Can. J. Phys., 41, 762 (1963).

72. N.E. Ballou, NNES, 1951, Vol. 9, Div. IV, Paper 263.

73. J.O. Kartunen and H.B. Evans, Anal. Chem., 32, 917 (196

74. L.E. Glendenin, NNES, 1951, Vol. 9, Div. IV, Paper 267.

75. J.A. Seiler, NNES, 1951, Vol. 9, Div. IV, Paper 264.

76. L.E. Glendenin, NNES, 1951, Vol. 9, Div. IV, Paper 265.

77. J. Varma and C.E. Mandeville, Phys. Rev., 99, 977 (1955).

78. W.F. Boldridge and D.N. Hume, NNES, 1951, Vol. 9, Div. IV, Paper 272.

79. L.E. Glendenin, NNES, 1951, Vol. 9, Div. IV, Paper 274.

80. L.E. Glendenin and R.P. Metcalf, NNES, 1951, Vol. 9, Div. IV, Paper 278.

81. A.G. Collins and J.W. Watkins, Anal. Chem., 31, 1182 (1959).

82. A. Kjelberg, H. Taniguchi, and L. Yaffe, Can. J. Chem., 39, 635 (1961).

83. L.E. Glendenin and C.M. Nelson, NNES, 1951, Vol. 9, Div. IV, Paper 283.

84. J.L. Olsen and G.D. O'Kelley, Phys. Rev., 95, 1539 (1954).

85. Y. Yoshizawa, Nuclear Phys., 5, 122 (1958).

86. W.E. Nervik, in 'The Radiochemistry of the Rare Earths, Scandium, Yttrium and Actinium' by P.C. Stevenson and W.E. Nervik. Nuclear Science Series, National Research Council, U.S. Atomic Energy Commission, 1961, p. 186.

87. H.L. Smith and D.C. Hoffmann, J. Inorg. and Nuclear Chem., 3, 243 (1956).

88. W.E. Grummitt and G.M. Milton, J. Inorg. and Nuclear Chem., 20, 6 (1961).